UNIVERSITÀ
DEGLI STUDI
DI PADOVA

UNIVERSITY OF PADOVA

DEPARTMENT OF PHARMACEUTICAL
AND PHARMACOLOGICAL SCIENCES

DOCTORAL SCHOOL IN MOLECULAR SCIENCES
Curriculum in PHARMACEUTICAL SCIENCES
Cycle XXXI

DEVELOPMENT OF NOVEL SUPER STEALTH IMMUNOLIPOSOMES FOR ANTICANCER DRUG DELIVERY

Coordinator: *Prof. LEONARD JAN PRINS*
Supervisor: *Prof. GIANFRANCO PASUT*

Ph.D. student: *ELENA CANATO*

TABLE OF CONTENTS

1. ABBREVIATIONS

Abs	absorbance
ACN	acetonitrile
AUC	area under the curve
BCA	bicinchoninic acid
βGlu	β-Glutamic acid
BMPS	N-(ß-maleimidopropyloxy)succinimide ester
Boc	*tert*-butyloxycarbonyl
CHOL	cholesterol
Da	daltons
DCC	N,N'-dicyclohexylcarbodiimide
DDSs	drug delivery systems
DLS	dynamic light scattering
DMSO	dimethylsulfoxyde
DNA	desossiribonucleic acid
DSPE	distearoylphosphatidylethanolamine
DXR	doxorubicin
EDTA	ethylenediaminetetraacetic acid
equiv.	equivalents
EtOH	ethanol
Fab’	fragment, antigen binding
$F(ab')_2$	fragment, antigen binding
FBS	fetal bovine serum
Fc	fragment, crystallizable
FDA	Food and Drug Administration
FITC	fluorescein isothiocyanate
Gly-gly	glycyl-glycine
H&E	haematoxylin and eosin
^{1}H NMR	nuclear magnetic resonance spectroscopy of hydrogen
HER 2	human epidermal growth factor receptor 2
HSPC	hydrogenated soybean phosphatidylcholine
IC50	half maximal inhibitory concentration
IL-1β	interleukin 1β
IL-6	Interleukin 6
kDa	kilodalton
mAb	monoclonal antibody
MAL	maleimide

ABBREVIATIONS

MALDI	matrix-assisted laser desorption/ionization
MeOH	methanol
mM	milli-molar
MW	molecular weight
MWCO	molecular weight cut-off
mol/mol	moles/moles
NHS	N-Hydroxysuccinimide
nm	nanometers
o/n	overnight
PBS	phosphate-buffered saline
PBST	phosphate buffered saline with Tween-20
PdI	polydispersity index
PEG	polyethylen glycol
PES concentrator	polyethersulfone membrane concentrator
PK	Pharmacokinetic
PMSF	phenylmethylsulfonyl fluoride
RNA	ribonucleic acid
rt	room temperature
SDS-PAGE	Sodium Dodecyl Sulphate - PolyAcrylamide Gel Electrophoresis
SL	stealth liposomes
SIL	stealth immunoliposomes
SSL_n	super stealth liposomes (n = molecules of DSPE)
$SSIL_n$	super stealth immunoliposomes (n = molecules of DSPE)
SPDP	N-succinimidyl 3-[2-pyridyldithio]-propionate ester
TEM	transmission electron microscopy
TNFα	tumor necrosis factor α
TFA	trifluoroacetic acid
TLC	thin layer chromatography
TNBS	2,4,6-trinitrobenzenesulfonic acid
Vd	volume of distribution
v/v	volume/volume
w/w	weight/weight

2. ABSTRACT

Nowadays, liposomes play an important role in the field of drug delivery since they are biocompatible and versatile carriers. Their surface modification with hydrophilic polymers, usually polyethylene glycol (PEG), confers "stealth" properties, thus avoiding the fast clearance by the reticuloendothelial system and thereby increasing their circulation half-life *in vivo*. In such way, passive accumulation in the tumor site, exploiting the enhanced vascular permeability and lack of lymphatic drainage (EPR effect [1]) typically found in tumor tissues, is favoured.

The present work aimed at formulating new *Super Stealth Immunoliposomes* (SSILs), which should be both stable in the bloodstream and able to reach selectively the tumor site. The enhanced stability was achieved by using PEG dendron molecules conjugated to 2 or 4 molecules of distearoylphosphatidylethanolamine (DSPE) [2]. This allowed to increase the hydrophobic interactions with the phospholipid bilayer with respect to the classical PEG-single phospholipid derivatives, thus avoiding the polymer detachment. Active targeting, instead, was obtained by conjugation of these PEG dendron-lipids derivatives to a targeting moiety. In this case, the Fab' (fragment, antigen-binding) derived from Trastuzumab is used to target with high affinity HER-2 (human epidermal growth factor receptor 2), which is overexpressed on the surface of certain tumor cells. Doxorubicin, an antineoplastic drug commonly used in the treatment of a wide range of cancers (leukaemia, lymphoma, many types of carcinoma and soft tissue sarcomas), was chosen to be loaded into these nanocarriers. Since Doxyl®/Caelyx®, doxorubicin stealth liposomal formulation on the market, contains $mPEG_{2kDa}$-DSPE, it was initially decided to formulate SSILs using as well PEG_{2kDa} dendron-lipids derivatives. Preliminary *in vitro* and *in vivo* experiments on super stealth liposomes (SSL_n, n=2 or 4 DSPE), including either 5% or 10% mol of $mPEG_{2kda}$-$(DSPE)_n$ and formulated without the targeting ligand, evidenced a negative trend of stability with the increase of the hydrophobic anchor (PEG-DSPE > PEG-$DSPE_2$ > PEG-$DSPE_4$). This behavior was confirmed by *in vivo* pharmacokinetics since stealth liposomes (SL) presented a prolonged half-life ($t_{½}$ ~22h) compared to super stealth liposomes (SSL_2 $t_{½}$ ~8h and SSL_4 $t_{½}$ ~7h), which were eliminated even faster from the bloodstream than naked liposomes ($t_{½}$ ~10h). For this reason, it was decided to formulate super stealth immunoliposomes using a higher MW polymer, namely PEG 5kDa. $mPEG_{5kDa}$-$(DSPE)_n$ and Boc-NH-PEG_{5kDa}-$(DSPE)_n$ derivatives were successfully synthesized, purified and characterized by ^1H NMR spectroscopy. The Fab' fragment of Trastuzumab, chosen as targeting agent. Functionalization of NH_2-PEG-phopsholipids derivatives with N-(ß-maleimidopropyloxy)succinimide ester (BMPS) provided the best yields of monoPEGylated Fab'- PEG_{5kDa}-DSPE, Fab'-PEG_{5kDa}-$(DSPE)_2$ and PEG_{5kDa}-$(DSPE)_4$, as evidenced by SDS-PAGE analysis. Post-insertion of mPEG-lipid(s) derivatives or/and ligand-coupled PEG-lipid(s) derivatives into drug-loaded pre-formed naked liposomes either failed or caused aggregation of the liposomal vesicles. TEM analysis evidenced jagged and discontinuous surfaces, justifying the physical instability of the formulated vesicles.

ABSTRACT

Post-insertion of Fab'-PEG dendron-lipids derivatives on doxorubicin-loaded pre-formed stealth (SL) and super stealth liposomes (SSL_n) to obtain the corresponding super stealth immunoliposomes ($SSIL_n$) provided stable and homogeneous $SSIL_2$ (102.11 ± 3.68 nm) and SIL (128.23 ± 1.02 nm) with low polydispersity index (PdI <0.1). Post-insertion of ligand-coupled PEG-lipid(s) derivatives resulted in 79.8 µg Fab'/µmol HSPC for SIL and 23.63 µg Fab'/µmol HSPC for $SSIL_2$. $SSIL_4$ formulation evidenced problems of aggregation also with this post-insertion approach. *In vitro* stability studies over time revealed that after 2 months of incubation at 4°C and 25 °C all tested formulations were still stable and homogeneous (PdI <0.1), proving the stabilizing effect provided by PEG by steric hindrance. At 37°C, instead, all liposomal formulations started to aggregate after 14 days, showing also increased PdI (> 0.1). According to drug release experiments doxorubicin was efficiently entrapped inside the nanocarrier and drug leakage was not observed within the 16 h of incubation in all tested formulations. Preliminary *in vitro* cytotoxicity studies were performed on human breast ductal carcinoma cell line (BT-474) overexpressing HER-2, evidenced that SL-DXR could not reduce the cell viability below 50% after a 24 h-treatment with 10 µM DXR, whereas both SIL-DXR and $SSIL_2$-DXR reduced cell viability to about 40% in the same experimental conditions. Preliminary IC50 calculation evidenced that, at the tested conditions, all the doxorubicin-loaded liposomal formulations possessed the same potency in inducing cell death, whereas small differences were observed taking into consideration the efficacy of each formulation (SL-DXR < SIL-DXR < $SSIL_2$-DXR). Interestingly, $SSIL_2$-DXR possessed the same efficacy of free doxorubicin. *In vivo* pharmacokinetic studies in rats evidenced the prolonged half-life of $SSIL_2$ ($t_{½}$ = 37.80 h) compare to SL ($t_{½}$ = 10.77 h), confirming the stabilizing effect of PEG dendron-lipids derivatives over mPEG-DSPE. Accordingly, a reduction in the clearance rate of $SSIL_2$ (~0.2 ml/h) was observed with respect to SL (~0.5 ml/h), resulting in increased bioavailability (AUC) and distribution volume (Vd), also compared to all the other tested formulations. *In vivo* organ toxicity evaluation after single dose administration of 2.5 mg/kg in DXR evidenced that the gene expression of the three pro-inflammatory cytokines interleukin β1 (IL-1β), interleukin 6 (IL-6) and tumor necrosis factor α (TNFα) was enhanced in rats treated with SL-DXR and SIL-DXR, especially in liver, spleen and heart tissues. Histological analyses performed on liver and spleen sections of rats treated with SL-DXR and SIL-DXR showed remarkable alterations (granulomatous lesions, apoptotic bodies, etc.), whereas those treated with free DXR and $SSIL_2$-DXR resulted generally healthy. Heart, lungs and brain didn't show any pathological alteration in all the groups of rats examined.

Overall, $SSIL_2$ proved to be the best and safest formulation both in terms of pharmacokinetic profile, cytokines expression and histological analysis of RES organs, thus representing a promising system to improve conventional cancer therapy by enhancing drug delivery and antitumor efficacy.

3. RIASSUNTO

Attualmente, i liposomi rivestono un ruolo importante nel campo del *drug delivery* per la loro biocompatibilità e versatilità. La modifica della superficie liposomiale con polimeri idrofilici, generalmente polietilenglicole (PEG), conferisce proprietà "*stealth*" consentendo di evitare la rapida eliminazione da parte del sistema reticoloendoteliale, aumentando così il tempo di emivita *in vivo*. In questo modo, è favorito l'accumulo passivo nel sito tumorale, sfruttando l'aumentata permeabilità vascolare e il ridotto drenaggio linfatico (effetto EPR [1]) tipici dei tessuti tumorali. Il presente lavoro è mirato alla formulazione di nuovi immunoliposomi super stealth (SSILs) dotati sia di maggiore stabilità nel circolo sanguigno sia di un targeting selettivo al sito tumorale. L'aumentata stabilità è stata ottenuta mediante l'uso di molecole di PEG dendrone coniugate a 2 o 4 molecole di distearoilfosfoetanolamina (DSPE) [2]. Questo ha consentito di aumentare le interazioni idrofobiche con il doppio strato fosfolipidico rispetto al classico derivato PEG-fosfolipide ed evitare il distacco del polimero durante il circolo ematico. Il *targeting* attivo, invece, è stato ottenuto mediante coniugazione di questi derivati PEG dendrone-lipidi ad un agente di *targeting*. In questo caso, il Fab' (*fragment, antigen-binding*) del Trastuzumab che ha una elevata affinità verso il recettore HER-2 (*human epidermal growth factor receptor 2*), sovraespresso sulla superficie di alcune cellule tumorali. La doxorubicina, agente antineoplastico comunemente utilizzato nel trattamento di una grande varietà di tumori (lucemie, linfomi, vari tipi di carcinoma e sarcomi), è stata scelta per essere incapsulata all'interno di questi *nanocarriers*. Dal momento che Doxyl®/Caelyx®, formulazione liposomiale *stealth* contenente doxorubicina presente in commercio, contiene $mPEG_{2kDa}$-DSPE, è stato inizialmente deciso di formulare gli SSILs usando dei derivati PEG_{2kDa}-dendrone-lipidi. Studi preliminari *in vitro* e *in vivo* effettuati su liposomi super stealth (SSL_n, n=2 o 4 DSPE) contenenti il 5% o 10% mol di $mPEG_{2kda}$-$(DSPE)_n$ e privi di agente di *targeting*, hanno evidenziato un trend negativo di stabilità all'aumentare dell'ancoraggio idrofobico (PEG-DSPE > PEG-$DSPE_2$ > PEG-$DSPE_4$). Questo comportamento è stato confermato dagli studi di farmacocinetica *in vivo* poiché i liposomi stealth (SL) presentavano un'emivita prolungata ($t_{½}$ ~22h) rispetto ai liposomi super stealth (SSL_2 $t_{½}$ ~8h e SSL_4 $t_{½}$ ~7h), i quali venivano eliminati dal circolo sanguigno anche più rapidamente dei liposomi convenzionali ($t_{½}$ ~10h). Per questo motivo è stato deciso di formulare gli immunoliposomi super stealth usando un polimero a maggior peso molecolare (PEG 5kDa).

I derivati $mPEG_{5kDa}$-$(DSPE)_n$ e Boc-NH-PEG_{5kDa}-$(DSPE)_n$ sono stati sintetizzati, purificati e caratterizzati con successo mediante spettroscopia ^{1}H NMR. La funzionalizzazione dei derivati H_2N-PEG-lipidi con il cross-linker BMPS (estere N-(ß-maleimidopropilossi)succinimide) ha fornito rese migliori ottenendo i monoPEGhilati Fab'-PEG_{5kDa}-DSPE, Fab'-PEG_{5kDa}-$(DSPE)_2$ and PEG_{5kDa}-$(DSPE)_4$, come dimostrato dalla caratterizzazione mediante SDS-PAGE. La *post-insertion* dei derivati mPEG-$(DSPE)_n$ e/o Fab'-PEG-$(DSPE)_n$ in liposomi convenzionali preformati contenenti il farmaco non è avvenuta con successo o ha portato all'aggregazione delle vescicole liposomiali.

Le immagini acquisite mediante TEM hanno evidenziato superfici discontinue, motivando l'instabilità delle vescicole formulate. La *post-insertion* dei derivati Fab'-PEG dendrone-lipidi su liposomi stealth (SL) e super stealth (SSL_n) preformati contenenti doxorubicina, per ottenere i corrispondenti immunoliposomi super stealth ($SSIL_n$), ha fornito formulazioni stabili ed omogenee di $SSIL_2$ (102.11 ± 3.68 nm) e SIL (128.23 ± 1.02 nm) con basso indice di polidispersività (PdI <0.1). La post-insertion è risultata in 79.8 μg Fab'/μmol HSPC negli SIL e 23.63 μg Fab'/μmol HSPC negli $SSIL_2$. La formulazione $SSIL_4$ ha riportato problemi di aggregazione anche con quest'ultimo approccio di post-insertion. Studi di stabilità *in vitro* a lungo termine hanno evidenziato che le tutte le formulazioni testate erano stabili ed omogenee (PdI <0.1) dopo 2 mesi di incubazione a 4°C e 25°C, dimostrando l'effetto stabilizzante del PEG che previene l'aggregazione per ingombro sterico. Incubando a 37°C, invece, le formulazioni iniziavano ad aggregare dopo 14 giorni, mostrando anche un aumento della polidispersività (PdI >0.1). Studi di rilascio *in vitro* hanno confermato che tutte le formulazioni testate sono in grado di trattenere efficacemente la doxorubicina incapsulata, la quale non viene rilasciata durante le 16 ore di incubazione. Studi preliminari *in vitro* di citotossicità, eseguiti su cellule umane di carcinoma mammario (BT-474) che sovraesprimono HER-2, hanno dimostrato che SL-DXR non sono in grado di ridurre la vitalità cellulare al di sotto del 50% dopo un trattamento di 24 ore con DXR 10 μM, mentre risulta ridotta al 40% dopo trattamento con SIL-DXR e $SSIL_2$-DXR nelle stesse condizioni sperimentali. Un calcolo preliminare dell'IC50 ha dimostrato che tutte le formulazioni liposomiali possiedono la stessa potenza nell'indurre la morte cellulare, mentre minime differenze sono state osservate prendendo in considerazione l'efficacia di ciascuna formulazione (SL-DXR < SIL-DXR < $SSIL_2$-DXR). È interessante notare che $SSIL_2$-DXR dimostrano la stessa efficacia della DXR libera. Studi di farmacocinetica *in vivo* hanno evidenziato la prolungata emivita di $SSIL_2$ ($t_{½}$ = 37.80 h), confermando l'effetto stabilizzante dei derivati PEG dendrone-lipidi rispetto a mPEG-DSPE. Di conseguenza, una riduzione della *clearance* plasmatica di $SSIL_2$ (~0.2 ml/h) è stata osservata rispetto a SL (~0.5 ml/h), con aumento della biodisponibilità (AUC) e del volume di biodistribuzione (Vd) rispetto alle altre formulazioni testate. La valutazione della tossicità d'organo *in vivo* dopo una singola somministrazione di 2.5 mg/kg in DXR ha messo in evidenza che l'espressione genica delle tre citochine proinfiammatorie interleukina β1 (IL-1β), interleukina 6 (IL-6) e tumor necrosis factor α (TNFα) è aumentata nei ratti trattati con SL-DXR e SIL-DXR, specialmente nel fegato, nella milza e nel cuore. L'analisi istologica effettuata su sezioni di tessuto di fegato e milza di ratti trattati con SL-DXR e SIL-DXR ha dimostrato la presenza di notevoli alterazioni patologiche (lesioni granulomatose, corpi apoptotici, ecc), mentre gli organi dei ratti trattati con DXR e $SSIL_2$-DXR sono risultati complessivamente sani. Nel cuore, nei polmoni e nel cervello non è stata evidenziata alcuna alterazione patologica in tutti i gruppi di animali esaminati.

In generale, $SSIL_2$ sono emersi come la formulazione migliore e più sicura in termini di profilo farmacocinetico, espressione di citochine infiammatorie e analisi istologica degli organi del sistema reticolo endoteliale (RES), rappresentando perciò un promettente sistema per migliorare il veicolamento di farmaci antitumorali convenzionali.

4. INTRODUCTION

4.1 CANCER: A WORLDWIDE BURDEN

Cancer over the years has become a growing worldwide public health issue and nowadays according to the *World Health Organization* (WHO) it is the second leading cause of death globally. In 2015 it was responsible for 8.8 million deaths, 70% of which occurring in low- and middle-income countries [3]. Cancer treatment has also a great and increasing economic impact, with a total annual economic cost that in 2010 was amounting to US$ 1.16 trillion [4].
The American Cancer Society estimates 1.735,350 new cancer cases and 609,640 cancer deaths for the United States in 2018, mainly due to breast, prostate, lung, stomach and colorectal malignancies (Figure 4.1) [5].

Estimated New Cases

Males				Females		
Prostate	164,690	19%		Breast	266,120	30%
Lung & bronchus	121,680	14%		Lung & bronchus	112,350	13%
Colon & rectum	75,610	9%		Colon & rectum	64,640	7%
Urinary bladder	62,380	7%		Uterine corpus	63,230	7%
Melanoma of the skin	55,150	6%		Thyroid	40,900	5%
Kidney & renal pelvis	42,680	5%		Melanoma of the skin	36,120	4%
Non-Hodgkin lymphoma	41,730	5%		Non-Hodgkin lymphoma	32,950	4%
Oral cavity & pharynx	37,160	4%		Pancreas	26,240	3%
Leukemia	35,030	4%		Leukemia	25,270	3%
Liver & intrahepatic bile duct	30,610	4%		Kidney & renal pelvis	22,660	3%
All Sites	**856,370**	**100%**		**All Sites**	**878,980**	**100%**

Estimated Deaths

Males				Females		
Lung & bronchus	83,550	26%		Lung & bronchus	70,500	25%
Prostate	29,430	9%		Breast	40,920	14%
Colon & rectum	27,390	8%		Colon & rectum	23,240	8%
Pancreas	23,020	7%		Pancreas	21,310	7%
Liver & intrahepatic bile duct	20,540	6%		Ovary	14,070	5%
Leukemia	14,270	4%		Uterine corpus	11,350	4%
Esophagus	12,850	4%		Leukemia	10,100	4%
Urinary bladder	12,520	4%		Liver & intrahepatic bile duct	9,660	3%
Non-Hodgkin lymphoma	11,510	4%		Non-Hodgkin lymphoma	8,400	3%
Kidney & renal pelvis	10,010	3%		Brain & other nervous system	7,340	3%
All Sites	**323,630**	**100%**		**All Sites**	**286,010**	**100%**

Figure 4.1: Ten leading cancer types for the estimated new cancer cases and deaths by sex, United States, 2018.

Despite these trends of incidence and mortality, according to the most recent review by the National Cancer Institute (NCI) [6] the overall cancer death rate in the United States has fortunately declined by 1.4-1.8% per year since the early 1990s. Progress is therefore being made against the disease, though much more effort is still required in prevention and treatment.

"Cancer" is a generic term used to define a large group of diseases involving an unregulated and excessive cell growth (*neoplasia*, i.e. "new growth"), which persist and is uncoordinated with that of the normal neighboring tissue and it might have the potential to invade or spread to other parts of the body [7]. This process may lead to the formation of a mass or a lump, called "tumor", and it can be distinguished in *benign* or *malignant* depending on the degree of differentiation, growth rate and invasiveness. In benign tumors the neoplastic cells are well differentiated (resembling the tissue of origin), their growth is usually slow and, therefore, they remain localized to the site in which they originated.
Malignant tumors, instead, are completely undifferentiated, their growth is generally faster, locally invasive and they acquire the capability of spreading to other organs (*metastasis*) through the blood or the lymph system, with high probability of causing death (Figure 4.2) [8].

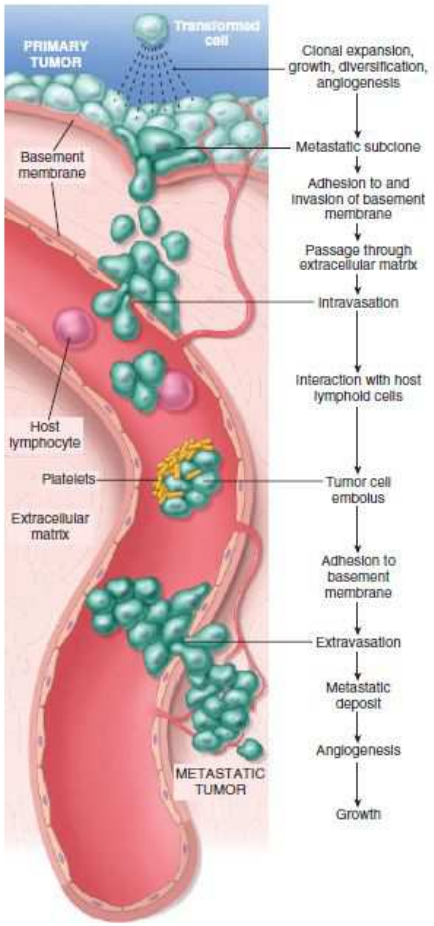

Figure 4.2: The metastatic cascade: the sequential steps involved in the hematogenous spread of a tumor.

Carcinogenesis is thus a multistep process (Figure 4.3) resulting from the accumulation of multiple genetic alterations (DNA mutations), starting from a single normal cell, that combined give rise to the transformed phenotype and all its associated features (known as *cancer hallmarks*):

- self-sufficiency in growth signals;
- insensitivity to growth-inhibitory signals;
- altered cellular metabolism;
- evasion of apoptosis (programmed cell death);
- limitless replicative potential (immortality);
- sustained angiogenesis (promotion of new blood vessels creation);
- invasion and metastasis;
- evasion of immune surveillance.

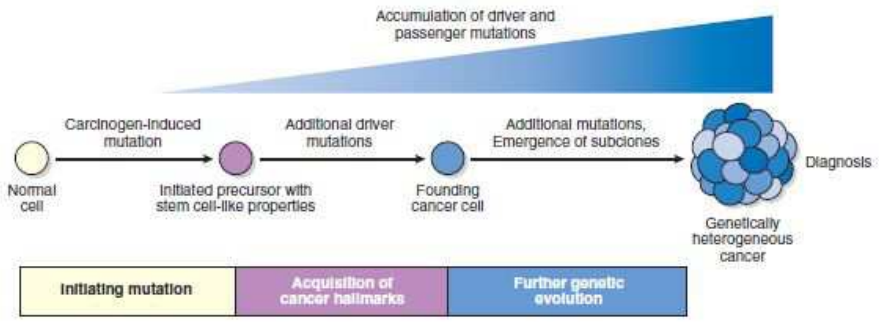

Figure 4.3: Development of cancer through stepwise accumulation of complementary driver mutations.

The risk for developing cancer strongly depends on the interactions between environmental exposures and genetic variants (inherited genetic defects). Indeed, 90-95% of cancer cases are due to genetic mutations from external factors, contributing also to cancer-related death, like tobacco (25-30%), diet and obesity (30-35%), infections (15-20%), radiation (10%), alcohol consumption, stress, lack of physical activity and pollution [9]. Besides, ageing is another significant factor affecting cancer frequency and mortality, with most cancer-related deaths occurring between 55 and 75 years of age [8].

4.2 FIGHTING CANCER: STRATEGIES AND THERAPIES

Prevention and early detection are the first fundamental steps to oppose the increasing cancer incidence and mortality. Good opportunities for intervention might arise since a considerably high percentage of tumors (30–50%) can be prevented by reducing or avoiding environmental risk factors (paragraph 1.1) and implementing existing evidence-based prevention strategies [7, 10, 11]. Once cancer is diagnosed, though, different treatment options are available according to the tumor nature (type, location, stage and grade). Solid and localized primary tumors can be removed by surgery, but this approach alone may not be resolutive and radiotherapy or chemotherapy might be required, especially in presence of *metastasis*. Palliative care treatment is usually combined to relieve cancer-associated symptoms and side effects, thus improving the quality of life of patients. Unfortunately, despite their high cytotoxic activity, most of the classical anticancer chemotherapeutics (alkylating agents, antimetabolites, antitumor antibiotics, etc.) are endowed with several limitations: poor water solubility, low therapeutic index, lack of selectivity towards cancer cells, rapid drug metabolism and drug-resistance development [12]. Therefore, the effectiveness of chemotherapy is so far limited by its toxicity to other tissues in the body which leads to harmful side effects. On top of that, considering the variability and heterogeneity of both tumors and patients it would be impossible to resort to a universal treatment, so the necessity of more selective and targeted approaches is arising.

Nowadays researchers are focused on developing *targeted cancer therapies* based on drugs or other substances which are able to interfere with and block the growth of tumors (*cytostatic*

effect) by interacting with specific molecules, called “molecular targets”, involved in the growth and progression of cancer [13]. These entities are usually proteins which are mutated or overexpressed on the surface of cancer cells but not in normal cells, providing the possibility to discriminate between normal tissues and tumors.
The Food and Drug Administration (FDA) has already approved many targeted cancer therapies, whereas other are under clinical and preclinical trials. These approaches include:

- hormone therapy;
- gene therapy;
- immunotherapy;
- cancer vaccines;
- combination therapy [14];
- use of *antibody-drug conjugates* (ADCs);
- design of innovative *drug delivery systems* (DDSs).

4.3 A FOCUS ON BREAST CANCER

Breast cancer is a disease in which malignant (cancer) cells develop from breast tissue. The most common types originate from the cells of the milk ducts (*ductal carcinoma*) and from the cells of the lobes or lobules (*lobular carcinoma*). Signs of breast cancer may include lumps, changes in breast shape, dimpling of the skin, fluid coming from the nipple, a newly inverted nipple, or a red or scaly patch of skin [15]. In case of metastasis there may be bone pain, swollen lymph nodes, shortness of breath or yellow skin.
The number of breast cancer cases worldwide has significantly increased over the years, affecting mostly women but in a small percentage (less than 1% of all cases [16]) also males. As reported by the WHO in the *World Cancer Report* 2014 [4], breast cancer is so far the most frequently diagnosed type of cancer and cause of cancer death among women, responsible for 1.7 million new cases (25% of all cancers in women) and 0.5 million cancer deaths (15% of all cancer deaths in women) in 2012. The biggest burden is attributable to high-income countries like western Europe and North America, where about 43% of estimated new cases and 34% of cancer deaths occurred in 2012. However, because of the combination of improved detection, earlier diagnosis (through population-based screening) and more effective treatment regimens, breast cancer incidence has been declining since the late 1980s over the past decade. Conversely, in developing countries the incidence is generally rising due to increased life expectancy, urbanization and adoption of western lifestyles, as well as breast cancer-related deaths are rising because most of cases are diagnosed in very late stages.
Several risk factors have been documented, even though for most women suffering from breast cancer it is not possible to identify specific risk factors [17]. The risk of developing breast cancer for long-term smokers is increased by 35% to 50% [18]. Alcohol abuse, dietary factors (overweight and obesity) and physical inactivity are responsible for 21% of all breast cancer deaths worldwide [10]. The NCI reported that other significant risk factors may be [15]:

- a familiar history of breast cancer in a first-degree relative (mother, daughter or sister);
- a personal history of either benign or malignant breast disease;
- inherited gene mutations (*BRCA1*, *BRCA2*, *p53*, etc.);
- exposure of breast tissue to estrogen made by the body (menstruating at an early age, first birth at older age or never having given birth, starting menopause at a later age);
- hormone therapy;
- radiotherapy;
- aging.

Even though some genetic modifications provide enhanced risk for developing breast cancer (such as *BRCA1* or *BRCA2*), genetic susceptibility (i.e. inherited gene mutations) plays just a minor role and accounts for only 5-10% of all cases [19].

Early detection is the key factor to improve breast cancer outcomes and survival [20]. The screening tests employed include clinical and breast self- examinations, mammography, genetic screening, biopsy, ultrasound and magnetic resonance imaging. So far, mammography screening is the only method that has proved to be efficient, but is very costly and cost-effective, thus less feasible in middle- and low-income countries. However, there are also discordant opinions based on the evidence that screening led to 30% overdiagnosis and overtreatment [21].

Once breast cancer is diagnosed, it is fundamental to assess the best treatment regimen according to the histopathology (microscopic examination of the tissue), grade (appearance of cancer cells compared to normal tissue), stage (growth and spread) and receptor status (presence of certain receptors on the surface, cytoplasm and nucleus of cancer cells) of the tumor.
Breast cancer cells may or may not express on their surface three important receptors: estrogen receptor (ER), progesterone receptor (PR) and human epidermal growth factor type 2 receptor (HER2). Upon the binding of chemical messengers, like hormones, to these receptors, cancer cells can undergo to changes that affect tumor growth and spread. Therefore, based on the receptor status we can distinguish different types of breast cancers: *hormone receptor positive* or *negative* (high and low levels of ER/PR, respectively); *HER2 positive* or *negative* (high and low levels of HER2, respectively); *triple negative* (low levels of both estrogen, progesterone and HER2/neu receptors). Currently, the main therapies available for adjuvant breast cancer treatment:

- *hormone-blocking agents*: drugs that block either the receptors (e.g. tamoxifen) or the production of estrogen with an aromatase inhibitor (e.g. anastrozole or letrozole; should be given only to postmenopausal women) [22];
- *chemotherapy*: usually a combination of classical anticancer drugs (e.g. methotrexate-fluorouracil-cyclophosphamide, doxorubicin-cyclophosphamide, etc.) that works by destroying fast-growing and/or fast-replicating cancer cells (either by causing DNA damage upon replication or by other mechanisms) but might also affect fast-growing normal tissues (hair matrix keratinocytes, intestinal epithelium, bone marrow) providing serious side-effects;
- *monoclonal antibodies*: entities that recognize with high specificity proteins overexpressed on the surface of tumor cells, called *antigens* (e.g. receptors), and upon binding they recruit other

components of the immune system with the aim of destroying the antigen-presenting target. The best-known example is *Trastuzumab* (*Herceptin®*), used to target HER2-positive breast cancer [23];

- *drug delivery systems* (DDSs): formulations or carrier systems designed to deliver the drug to the target site, improving its pharmacological and therapeutic properties, thus overcoming most of the limitations and side-effects correlated to classical anticancer therapy [24]. Examples of nanosize DDSs approved by FDA are liposomal formulations (e.g. *Doxil®/Caelix®, Myocet®)* and antibody-drug conjugates (e.g. *Trastuzumab emtansine*).

4.4 DRUG DELIVERY SYSTEMS (DDSs)

The development of new anticancer drugs is time-consuming and highly expensive. In addition, only a very small percentage of those new molecules that manage to enter the clinical trials actually reach the market. For this reason, considerable work has been done to create new chemical entities with improved features.

A *drug delivery system* (DDS) is defined as «a formulation or a device that enables the introduction of a therapeutic substance in the body and improves its efficacy and safety by controlling the rate, time, and place of release of the drug in the body. This process includes the administration of the therapeutic product, the release of the active ingredients by the product, and the subsequent transport of the active ingredients across the biological membranes to the site of action» [25].

The purpose is to overcome the multiple problems and limitations connected to the use of traditional anticancer drugs by exploiting the numerous advantages provided by DDSs [26, 27]:

- increased stability and water solubility of hydrophobic drugs;
- decreased toxicity;
- protection from chemical and enzymatic degradation;
- increased half-life (the higher hydrodynamic volume reduces renal excretion);
- reduced immunogenicity and antigenicity;
- selective drug accumulation at the tumor site (*passive* or *active targeting*);
- improved intracellular penetration (exploiting endocytosis mechanisms).

Great influence on drug delivery research derives from nanotechnology, leading to the development of systems on the nano-scale lenghth (10^{-9} m), thus endowed with such unique properties. These nanosize carriers (usually 1-100 nm), referred to as *nanocarriers*, are made of natural or synthetic materials and comprise different subclasses: bioconjugates, polymeric nanoparticles and nanocapsules, liposomes, micelles, dendrimers, nanotubes, nanogels and nanocrystals (Figure 4.4). It was estimated that in 2004 more than 200 companies were persuing nanomedicine development and 38 nanothechnology-enabled products reached the market, with a total sales amounting at $ 6.8 billion [28]. In 2012 a comprehensive analysis [29] of the worldwide state of investigational and approved nanomedicine products has identified 67

commercialized nanodevices and 33 marketed nanotherapeutics. A total of 25 devices and 122 therapeutics currently in development accounted for 789 ongoing clinical trials.

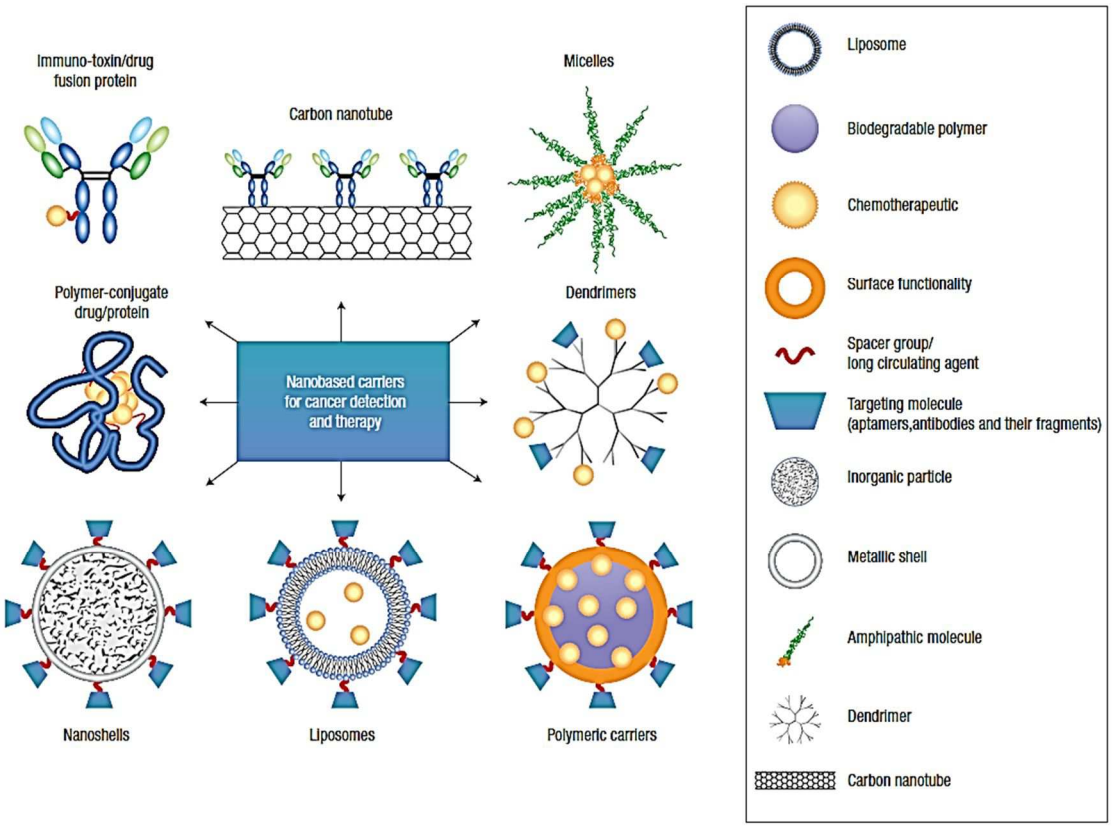

Figure 4.4: Examples of nanocarriers for targeting cancer.

An ideal nanocarrier should [25, 30, 31]:

- be biocompatible, non-toxic, non-immunogenic;
- be biodegradable through enzymatic or hydrolytic pathways or eliminated by renal excretion;
- homogeneous (low polydispersity);
- be either soluble or colloidal under aqueous conditions for increased effectiveness;
- exhibit significant differential uptake efficiency in the target cells over normal cells;
- improve intracellular penetration;
- have prolonged half-life, low aggregation rates and a long shelf-life;
- permit functionalization for cell-specific targeting moieties;
- be economic and available on large scale.

4.5 LIPOSOMES

The term "*liposome*" derives from the Greek words "*lipo*" (fat) and "*soma*" (body), defining a structure mainly composed by phospholipids. Liposomes were first discovered and described by Bangham in 1961, while adding a negative stain to dry phospholipids to test a new electron microscope [32]. He noticed the formation of a *bilayer* lipid structure, highly resembling the plasmalemma, thus providing the first evidence for the cell membrane being a lipid bilayer. For this reason, liposomes nowadays are largely employed as *in vitro* models to study the properties of biologic membranes.

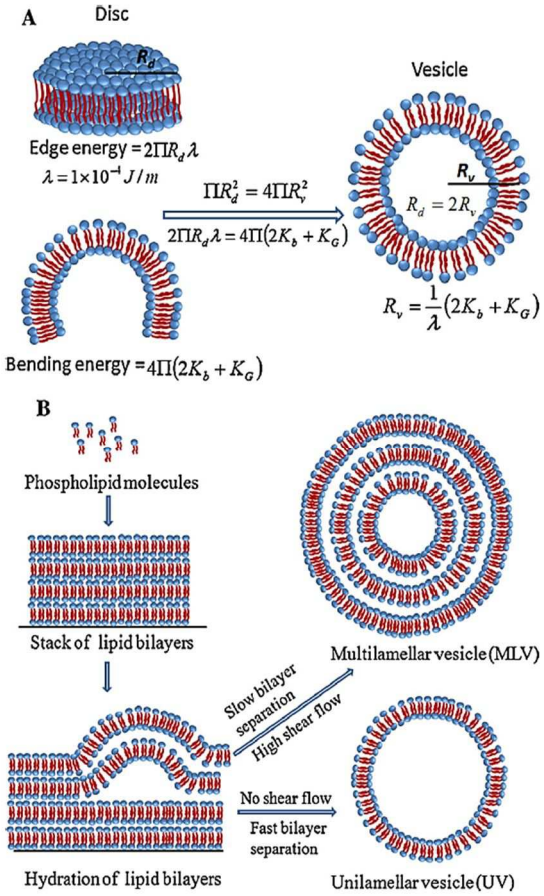

Figure 4.5: Schematic representation of phospholipids self-assembly involved in liposome formation. Liposomes are formed when the edge energy first exceeds the bending energy (A). The relative kinetics of bilayer folding due to hydrodynamic forces and bilayer separation under hydration forces dictates the size and lamellarity of vesicles formed (B).

The mechanism of liposome formation is a well-known and described thermodynamic process (figure 4.5) [33-36]. Phospholipids are amphiphilic molecules presenting a polar head (a phosphoric group which might be substituted with several organic groups, providing different charge properties) and two non-polar aliphatic chains, joint together by a glycerol moiety. In presence of aqueous media, they self-assemble forming highly ordered structures called *bilayers sheets*, which are thermodynamically unfavorable and tend to close, forming spherical vesicles (*lamellae*) with an empty aqueous hydrophilic core inside (figure 4.5). This feature is the discriminant factor between liposomes and micelles (figure 4.6), which instead are made of wedge-shaped phospholipids bearing only one acyl tail and upon self-assembling they form spherical structures with a filled hydrophobic core and a hydrophilic surface.

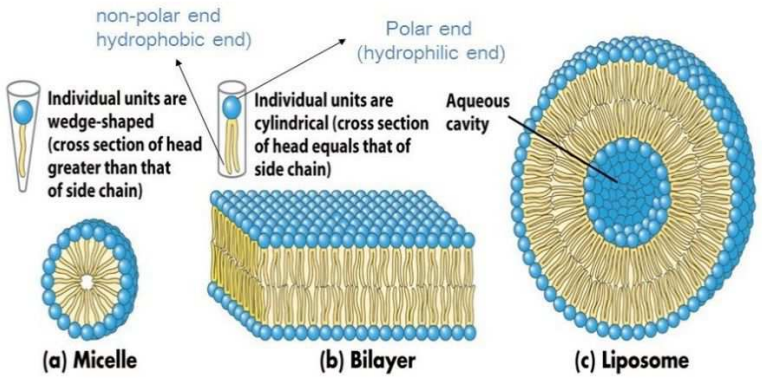

Figure 4.6: Schematic representation of a micelle (a), a lipid bilayer sheet (b) and a liposome (c).

According to the size and number of *lamellae* formed upon self-assembly in aqueous media, liposomes can be classified in two main categories: *Multi-Lamellar Vesicles* (MLVs) and *Unilamellar Vesicles* (UVs). MLVs comprise liposomes with a diameter ranging from 500 nm to 5 µm and formed by several concentric vesicles (onion-like structure) separated by aqueous media, thus permitting high payload of lipid-soluble molecules. Sometimes the multiple bilayers are not concentric and a *multivesicular* structure is created. MLVs are the liposomes of choice when a slow or sustained release of the drug is desired. On the other hand, UVs are liposomes formed by a single lipid bilayer and can be further subdivided, depending on their dimensions, in: *Small Unilamellar Vesicles* (SUVs), if the diameter is up to 100 nm; *Large Unilamellar Vesicles* (LUVs), ranging from 100 to 1000 nm; *Giant Unilamellar Vesicles* (GUVs) if the mean size exceeds 1 µm (Figure 4.7) [37]. GUVs are highly heterogeneous but permit high payload of water-soluble molecules, whereas SUVs are more homogeneous, but their loading efficiency is strongly decreased.

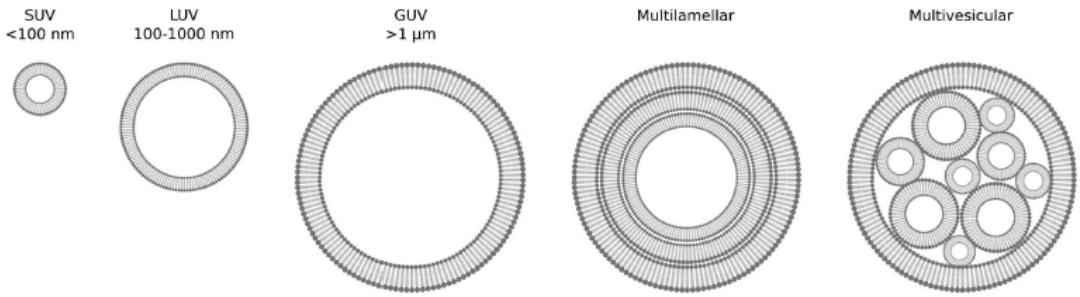

Figure 4.7: Liposome classification according to their morphological and structural features.

Great interest has been arising for liposomes as *nanocarriers* as they are biocompatible and biodegradable systems (same nature of biologic membranes), but also very versatile since they can be used for a large number of applications. In fact, they are extensively employed in cosmetic

and pharmaceutical industries and, additionally, they have been studied by food and farming industries to grow delivery systems able to entrap unstable compounds (e.g. antimicrobials, antioxidants, flavors and bioactive elements) and shield their functionality.

The great advantage with respect to the other DDSs is the ability to trap both hydrophobic and hydrophilic compounds, respectively within the bilayer and in the inner aqueous core, but also amphiphilic drugs (with intermediary *logP*) which partition between the aqueous core and lipid bilayer. Besides, it is also possible to exploit cationic liposomes (i.e. with a positively charged surface derived from the use of phospholipids with a cationic polar head group) to carry anionic molecules, e.g. nucleic acids, by means of formation of a stable neutral complex.

Many other advantages are [38]:

- being non-toxic and non-immunogenic;
- improved solubility of lipophilic and amphiphilic molecules;
- enhanced penetration of drugs into tissues (by adsorption, fusion, endocytosis or exchange of bilayer components between liposomes and cells);
- improved efficacy and therapeutic index of encapsulated drugs (shielding their toxicity towards sensitive tissues, thus reducing correlated side-effects);
- increased stability of the entrapped molecule (protection from degradation);
- possibility in cancer therapy to achieve specific delivery to the tumor site by means of passive accumulation (*passive targeting*) exploiting the *EPR effect* (*enhanced permeation and retention effect*) [39] (see paragraph 1.5.3);
- possibility of coupling with site-specific ligands (e.g. antibodies, peptides, nucleic acids, aptamers, carbohydrates) to achieve *active targeting* in cancer therapy, by addressing only tumor cells overexpressing the antigen [40];
- possibility to design either local or systemic sustained-release systems.

Nevertheless, liposomes also present some drawbacks [41]. The major problem is represented by *in vitro* instability, which may be induced by several factors. First, the possibility of oxidation and hydrolysis-like reactions of some phospholipids, favored by the exposure to oxygen, light, high pH and metal ions. This problem is easily solved by adding to the formulation stabilizing agents (e.g. antioxidants and chelators; cholesterol prevents hydrolysis by phospholipase). Then, the intrinsic tendency to aggregate, which might be solved either by using charged phospholipids or by coating liposome surface with hydrophilic polymers. Another matter of instability is given by the leakage of the loaded drug, sometimes happening right after the encapsulation process. Lyophilization can be a good strategy to prevent this inconvenient, otherwise synthetic phospholipids (e.g. diacethylenic phospholipids, able to form chemical bonds between the acyl chains, thus increasing the bilayer rigidity) can be exploited.
Finally, another great inconvenient of liposome formulation is the difficulty of scale-up and high costs production.

So far, several liposomal formulations have been introduced on the market and received FDA (or related foreign agency) approval for clinical use for a wide range of applications, as reported in Table 4.1 [42].

Table 4.1: List of approved liposomal drugs as of 2012.

Name	Description	Mechanism of action	Approval/indication
1) Liposomes			
AmBisome®	Amphotericin B encapsulated in liposomes (60–70 nm) composed of hydrogenated soy phosphatidylcholine, cholesterol, and distearoyl phosphatidylglycerol (2/0.8/1 molar)[15]	MPS targeting: Liposomes preferentially accumulate in organs of the MPS. Negative charge contributes to MPS targeting. Selective transfer of the drug from lipid complex to target fungal cell with minimal uptake into human cells has been postulated[16,17]	FDA 1997 Systemic fungal infections (IV)
DaunoXome®	Daunorubicin citrate encapsulated in liposomes (45 nm) composed of distearoyl phosphatidylcholine and cholesterol (2/1 molar)[18,19]	Passive targeting via EPR effect: Concentration of available liposomal drug in tumors exceeds that of free drug. Liposomal daunorubicin persists at high levels for several days[20]	FDA 1996 HIV-related KS (IV)
DepoCyt®	Cytarabine encapsulated in multivesicular liposomes (20 μm; classified as nanopharmaceutical based on its individual drug containing "chambers") made from dioleoyl lecithin, dipalmitoyl phosphatidylglycerol, cholesterol, and triolein[21]	Sustained release: This formulation of cytarabine maintains cytotoxic concentrations of the drug in the cerebrospinal fluid for more than 14 days after a single 50 mg injection[22]	FDA 1999/2007 Lymphomatous malignant meningitis (IV)
DepoDur®	Morphine sulfate encapsulated in multivesicular liposomes (17–23 μm; per se not a nanopharmaceutical – classified as such based only on its individual drug containing "nano-sized chambers") made from dioleoyl lecithin cholesterol, dipalmitoyl phosphatidylglycerol, tricaprylin, and triolein	Sustained release: After the administration into the epidural space, morphine sulfate is released from the multivesicular liposomes over an extended period of time[23,24]	FDA 2004 For treatment of chronic pain in patients requiring a long-term daily around-the-clock opioid analgesic (administered into the epidural space)
Doxil®	Doxorubicin hydrochloride encapsulated in Stealth® liposomes (100 nm) composed of N-(carbonyl-methoxypolyethylene glycol 2000)-1,2-distearoyl-sn-glycero3-phosphoethanolamine sodium, fully hydrogenated soy phosphatidylcholine, and cholesterol[9]	Passive targeting via EPR effect: Extravasation of liposomes by passage of the vesicles through endothelial cell gaps present in solid tumors. Enhanced accumulation of doxorubicin in lesions of AIDS-associated KS after administration of PEG-liposomal doxorubicin[25]	FDA 1995 AIDS-related KS, multiple myeloma, ovarian cancer (IV)
Inflexal® V	Influenza virus antigens (hemagglutinin, neuraminidase) on surface of 150 nm liposomes	Mimicking native antigen presentation: Liposomes mimic the native virus structure, thus allowing for cellular entry and membrane fusion.[26] Retention of the natural presentation of antigens on liposomal surface provides for high immunogenicity[27,28]	Switzerland 1997 Influenza vaccine
Marqibo®	Vincristine sulfate encapsulated in sphingomyelin/cholesterol (60/40, molar) 100 nm liposomes	Passive targeting via EPR effect: Extravasation of liposomes through fenestra in bone marrow endothelium	FDA 2012 Acute lymphoid leukemia, Philadelphia chromosome-negative, relapsed or progressed (IV)
Mepact™	Mifamurtide (synthetic muramyl tripeptide-phosphatidylethanolamine) incorporated into large multilamellar liposomes composed of 1-palmitoyl-2-oleoyl-sn-glycerol-3-phosphocholine and 1,2-dioleoyl-sn-glycero-3-phospho-L-serine[29]	MPS targeting: The drug, an immune stimulant, is anchored in negatively charged liposomal bilayer membrane	Europe 2009 Non-metastasizing resectable osteosarcoma (IV)
Myocet®	Doxorubicin encapsulated 180 nm oligolamellar liposomes composed of egg phosphatidylcholine/cholesterol (1/1, molar)	MPS targeting: Forms "MPS depot", slow release into blood circulation resembles prolonged infusion[30]	Europe 2000 Metastatic breast cancer (IV)
Visudyne®	Verteporfin in liposomes made of dimyristoyl-phosphatidylcholine and egg phosphatidylglycerol (negatively charged); lyophilized cake for reconstitution	Drug solubilization: Rendering drug biocompatible and enhancing ease of IV administration. No other apparent function of liposomes. Liposomal formulation instable in the presence of serum. Fast transfer of verteporfin from Visudyne® to lipoproteins[31]	FDA 2000 Photodynamic therapy of wet age-related macular degeneration, pathological myopia, ocular histoplasmosis syndrome (IV)

4.5.1 First-Generation Liposomes

Conventional or classical liposomes, also defined "first-generation" liposomes, consist only of natural phospholipids and eventually some modulating agents (e.g. cholesterol) or antioxidants (e.g. tocopherols). Among the conventional liposomal formulations on the market we recall, for example, AmBisome®, DaunoXome®, Marqibo® (reported in Table 4.1). Owing to their composition conventional liposomes suffer from several limitations, above all the physico-chemical instability (see paragraph 1.5) and the fast clearance from the bloodstream upon injection. Phagocytosis, indeed, consisting in the rapid uptake by the mononuclear phagocyte system (MPS), e.g. macrophages and monocytes, is known as the "natural fate" of liposomes and has been considered since the 1970s and 1980s a major obstacle for their use as drug carriers.

To overcome these drawbacks, liposomes have undergone extensive research on size and composition optimization. The appropriate choice of the formulation parameters is therefore fundamental to obtain a stable and efficient liposomal DDS. In fact, tuning the composition, surface charge, size and method of preparation considerably influences the physico-chemical properties of the final liposomal formulation and therefore its intrinsic stability, encapsulation efficiency and drug release profile, targeting mechanisms, biodistribution profile and so on.

For instance, the use of unsaturated phospholipids is responsible for the formation of more fluid and permeable bilayers, whereas a rigid and almost impermeable structure can be achieved with saturated phospholipids bearing long acyl moieties. Modulation of the bilayer permeability and fluidity, with the purpose of achieving an optimal release profile of the encapsulated molecules, is also obtained by addition of certain amounts of cholesterol (usually not more than 50%) in the lipid composition. In fact, cholesterol is an amphiphilic molecules which exerts a temperature-dependent fluidifying effect by intercalating among the acyl chains of the bilayer (Figure 4.8) [43]. Since the early 1980s cholesterol is also reported as a stabilizing agent against phospholipids transfer to serum high- and low-density lipoproteins (HDL and LDL), a phenomenon occurring during *in vivo* circulation of liposomes in the bloodstream and responsible for reduced stability, aggregation and drug release from the delivery system [44].

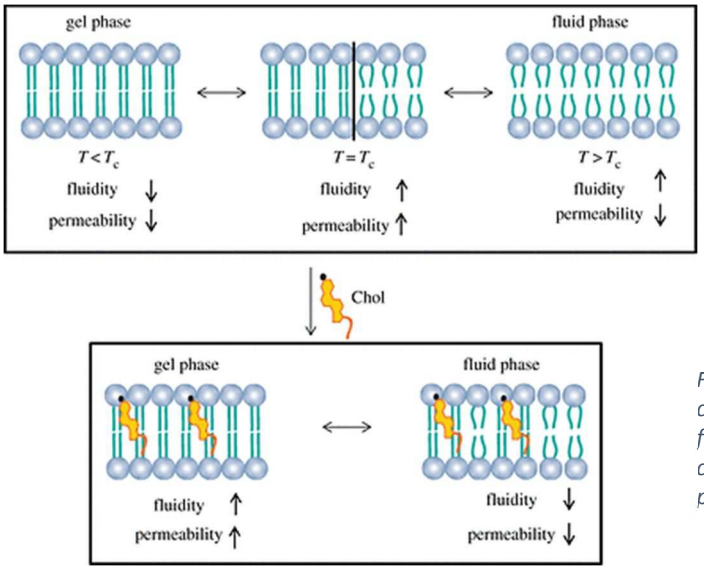

Figure 4.8: Temperature-dependent and cholesterol-dependent effect on membrane fluidity and permeability; T_c = temperature of crystalline-phase transition, from a solid-order phase (gel) to a liquid-disordered phase (fluid).

Liposomes charge and size can influence the *clearance* profile of the delivery system from the vasculature after intravenous administration. Positively charged liposomes are more toxic and eliminated faster than negative or neutral liposomes. Furthermore, SUVs can circulate longer in the bloodstream, whereas MLVs easily recognized by the immune system and readily eliminated. Indeed, for drug delivery purpose the desirable size of liposome is generally 50-200 nm, permitting an adequate residence time in the vasculature after intravenous administration and a preferential accumulation in tissues characterized by leaky blood vessels (e.g. with large fenestrations), like spleen and liver. This passive accumulation has been exploited for the treatment of tumor, infections or other pathologies concerning these organs. Here liposomes are recognized and destroyed by the mononuclear phagocyte system (MPS), thus releasing the drug. Nevertheless, liposomes can also directly interact with the targeted cells through different mechanisms (adsorption and extracellular content release, membrane fusion, internalization, transfer of lipophilic compounds) and release their payload.

If the target site is beyond the MPS, this efficient uptake by the macrophages and consequent removal from circulation is the main limiting factor against liposomes use as drug delivery systems. The adsorption of plasma proteins (*opsonins*) onto liposome surface (*opsinization*) triggers the macrophages or other cells of the immune system to easily recognize and remove the DDS from the bloodstream [45]. The MPS, indeed, is a defense mechanism of our organism against xenobiotics. Large pre-doses of empty liposomes are therefore required to block the MPS and increase circulation half-life of classical liposomes. For this reason, researchers focused their attention on identifying new methods to modify the surface of liposomes and create a sort of physical barrier to prevent opsonization. The first attempt aimed to mimic the membrane of erythrocytes (coated with a dense layer of carbohydrate groups), by addition of gangliosides and sialic acid derivatives, like the monosialoglyprotein GM1, to liposomes composed of egg phosphatidylcholine (egg PC) and cholesterol for membrane rigidity [46, 47]. The result was the achievement of the first sterically-stabilized long-circulating liposomal formulation that didn't require previous MPS blockade to exploit the therapeutic effect. The proposed mechanism was the enhancement of liposome surface hydrophilicity imparted by the gangliosides. Unfortunately, this behavior was observed only in animal models.

Afterwards, liposomes surface was variously decorated achieving more stable and efficient systems, thus creating different subclasses of liposomes which may be defined as “second-generation” liposomes.

4.5.2 Second-Generation Liposomes

To make up for the physico-chemical instability and fast clearance of conventional liposomes from the bloodstream, different approaches of surface modification were exploited, providing new liposomal formulations endowed with unique properties [48]. The so called “next-generation” or “second-generation” liposomes are indeed characterized by high mechanical stability, ability to

either induce or inhibit the immune system, prolonged circulation times, improved loading efficiency, enhanced penetration and target specificity.

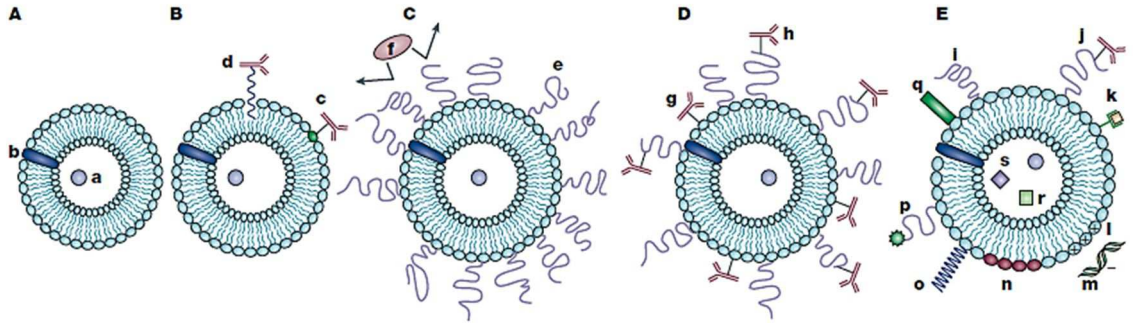

Figure 4.9: Evolution of liposomes. A) Conventional liposomes carrying either water-soluble (a) or lipid-soluble drugs (b). B) Antibody-targeted immunoliposome: the antibody can be covalently coupled to the phospholipids in the membrane (c) or hydrophobically anchored into the bilayer (d). C) Long-circulating "stealth" liposome: the polymer chains (e) shield the surface from opsonins binding (f). D) Long-circulating immunoliposome: PEG-coated liposomes bearing an antibody, either attached to the liposome surface (g) or to the distal end of PEG (h). E) New-generation liposomes: their surface can be differently modified by: attachment of a protective polymer coulped (j) or not (i) with a targeting ligand; attachment/incorporation of a diagnostic label (k), of positively charged lipids (l) for DNA complexation (m), of stimuli-sensitive lipids (n), of stimuli-sensitive polymer (o), of cell-penetrating peptides (p), of viral components (q), of magnetic particles (r) for magnetic targeting and/or colloidal gold or silver particles (s) for electron microscopy.

Long-circulating liposomes (Figure 4.9 C). Liposomes grafted with inert, biocompatible polymers, such as polyethylene glycol (PEG), which form a protective layer over the surface preventing the adsorption of opsonins and the subsequent clearance by the MPS. Owing to this property these liposomes are also referred to as "*stealth*" liposomes as they result invisible to the immune system. The most famous product on the market belonging to this category is Doxil®/Caelyx®, a Doxorubicin-loaded PEGylated liposomal formulation. Recent improvements were achieved with "*super stealth*" liposomes with enhanced *in vivo* stability provided by the use of PEG dendron-phospholipids constructs instead of PEG-single phospholipid derivatives typical of conventional stealth liposomes [2].

Immunoliposomes (Figure 4.9 B). Antibody-targeted liposomes with an antibody or its derivatives (e.g. Fab', scFv, etc.) either covalently coupled to reactive phospholipids in the membrane or hydrophobically anchored into the liposomal membrane after preliminary modification with a hydrophobic moiety. Immunoliposomes can be included into the wider class of *ligand-targeted liposomes*, i.e. liposomes whose surface has been modified for pharmaceutical purposes with site-specific ligands of different nature (antibody, peptides, nucleic acids, aptamers, carbohydrates, etc.) to achieve active targeting to the site of action.

Long-circulating immunoliposomes (Figure 4.9 D). Liposomes in which the "stealth" property provided by the surface modification with a protective polymer is combined to the presence of an antibody (or its derivatives), exploited for active targeting, that can be directly attached to the bilayer or linked through the grafted polymeric chains.

New-generation liposomes (Figure 4.9 E). This category includes a variety of most recent approaches to use liposomes as pharmaceuticals nanocarriers, usually combining different techniques of surface modifications:

- *stimuli-responsive liposomes* (e.g. temperature- or pH-sensitive liposomes, able to release their payload upon changes of pH or temperature) [49];

- *cationic liposomes* for *gene delivery* (use of positively charged phospholipids to allow the complexation with nucleic acids, forming an overall neutral system);

- *diagnostic liposomes* (bearing diagnostic labels either grafted on the surface or encapsulated);

- *virosomes* (liposome surface modified with fusogenic viral envelope proteins, i.e. with cell-penetrating properties);

- *magnetic liposomes* (loaded with the drug and a ferromagnetic material able to induce drug release when an external magnetic field is applied).

4.5.3 Stealth and Super stealth liposomes

Surface modification of conventional liposomes with polymers, such as polyethylene glycol (PEG), has provided long-circulating DDSs endowed with enhanced physical stability and reduced clearance. PEG is a non-ionic synthetic polymer of ethylene oxide, approved by Food and Drug Administration (FDA) owing to its useful properties, like biocompatibility, lack of toxicity, solubility in many aqueous and organic solvents, good excretion kinetics, low immunogenicity and antigenicity [50-52]. Moreover, the great advantage of using PEG is the wide range of molecular weights and structures available [53]. Different studies have demonstrated that the ability of PEG to prolong liposomes residence time in the bloodstream by preventing both aggregation (thus enhancing physical stability) and binding of plasma proteins (thus reducing the uptake by MPS) is due to its peculiar features. First, its high flexibility permit to shield the space adjacent to liposomes surface and just a small amount of PEG (5% molar ratio) is sufficient to provide a good surface coverage and create an adequate steric hindrance. Indeed, by using rigid polymers, such as dextran, it is not possible to obtain the same reduction of liposome-proteins interaction [53]. Furthermore, PEG hydrophilicity is responsible for the formation of a solvation shell on the surface of the nanocarrier that also play a role on preventing aggregation and opsonins binding.

Liposome surface decoration with PEG can be obtained either by physical absorption of the polymer onto the surface of the vesicles or by covalent attachment to reactive groups on the surface of preformed liposomes. Another option is to previously conjugate the polymer to a lipid molecule and add these PEG-lipid derivatives to the initial lipid mixture. In the present work mPEG-DSPE (methoxy-polyethylene glycol-distearoyl phosphoethanolamine) was used to produce stealth formulations. The graft density of the polymer, as well as its molecular weight, affects the degree of surface coverage and the distance between graft sites. Different polymer configuration

regimens are achieved: pancake-like (typical for PEG absorption), mushroom-like and brush-like, respectively corresponding to low, intermediate and high PEG density (Figure 4.10) [53, 54].

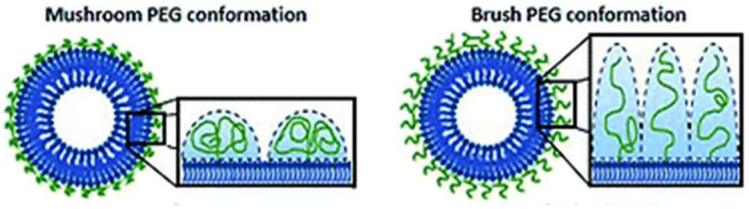

Figure 4.10: Conformations (brush or mushroom-like) of PEG grafted on the surface of liposomes.

PEG-coated liposomes are defined "*Stealth Liposomes*" (SL), according to the ability of PEG to make them "invisible" to the immune system. Prolonging the half-life of the nanocarrier, and consequently of the encapsulated drug, is crucial for drug delivery purpose, especially in anticancer therapy. The system can circulate longer in the bloodstream, enhancing the probability of reaching the tumor site and passively accumulate, allowing to reduce the dose and frequency of administration. The preferential accumulations of DDSs in cancer tissues is defined as *passive targeting* and it is most evident in solid tumors undergoing angiogenesis. The rapid formation of new blood vessels leads to the creation of a leaky and discontinuous endothelium which facilitate the extravasation of the nanocarriers into the interstitial space. In addition, the lack of an efficient lymphatic drainage system enables the accumulation of the extravasated DDS in proximity of the tumor area, working as a sustained drug-release system. In normal tissues, instead, the presence of tight junctions between capillary endothelial cells does not allow the nanocarriers to extravasate. This phenomenon is known as EPR effect (*Enhanced Permeability and Retention effect*) and was first described by Maeda et al. [1], which is thus responsible for the improved therapeutic effects of liposomal anticancer drugs compared to the free drugs.

Even though it is generally believed that stealth liposomes are inert systems, able to prevent or reduce immunogenicity, nevertheless it is reported that they can possibly induce idiosyncratic reactions through complement activation, classified as pseudoallergies, both in animals and humans. These reactions may lead to cardiopulmonary disturbance and other related symptoms of anaphylaxis. However, clinical evidence clearly demonstrates that complement activation alone cannot be the rate limiting factor in provocking hypersensitivity reactions upon liposomes administration. Therefore, many other factors may be involved, such as genomic differences between sensitive and non-sensitive individuals [55].
Ishida et al. [56] reported that PEGylated liposomes may be subjected to the *Accelerated Blood Clearance* (ABC) phenomenon, thus displaying unexpected pharmacokinetic behavior upon repeated injections. Specifically, a first dose of empty PEGylated liposomes administered by intravenous injection may induce anti-PEG IgM production. These immunoglobulins selectively bind to the surface of subsequently injected stealth liposomes, thus leading to complement

activation and fast clearance from the bloodstream. Ishida et al. also demonstrated that the magnitude of the ABC phenomenon depends on the physicochemical properties of the injected liposomes as a first dose, on the time interval between injections, and on the lipid dose and drug-encapsulation.

Another possible explanation for the rapid elimination of stealth liposomes from the bloodstream might be the loss of the protective polymer from the surface of the nanocarrier. The detachment of PEG-lipid molecules from the bilayer has been explained by the rapid removal of the hydrophilic coating *in vivo*, which may arise from exchange of the entire PEG-lipid conjugate from the liposomal membrane. In some cases also a chemical breakdown of the PEG-lipid conjugate is possible [57]. In other words, once in contact with the bodily fluids the polymer might detach from the surface if the hydrophobic interactions of the lipid anchor are not strong enough to evince the hydrophilic forces driving its solubilization in the surrounding aqueous media (Figure 4.11). As a result, the incomplete PEG coating of the surface leaves the carrier vulnerable to opsonization and enhances the elimination rate.

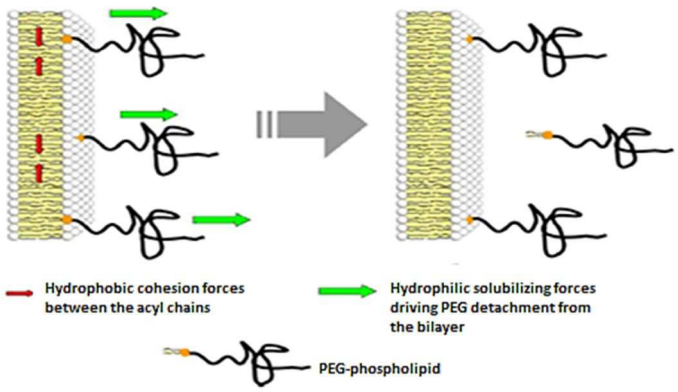

Figure 4.11: Forces involved in polymer binding and detachment from the bilayer.

To overcome the problem of PEG-lipid rapid detachment from the bilayer in the circulatory system and, thus, the incomplete surface shielding effect, improved PEG dendron-lipids derivatives were synthetized and incorporated into the bilayer providing new *Super Stealth Liposomes* (SSL). The PEG dendron-lipids derivatives were obtained by linking 2 or 4 molecules of distearoyl phosphatidylethanolamine (DSPE) to a molecule of mPEG 5 kDa, using β-glutamic acid as branching agent [2] (Figure 4.12 and Figure 4.13).

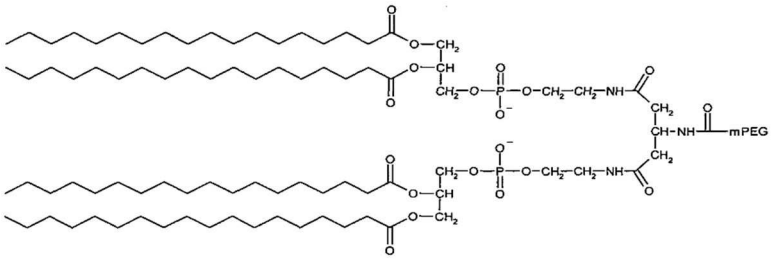

Figure 4.12: Structure of mPEG-β-Glu-(DSPE)$_2$.

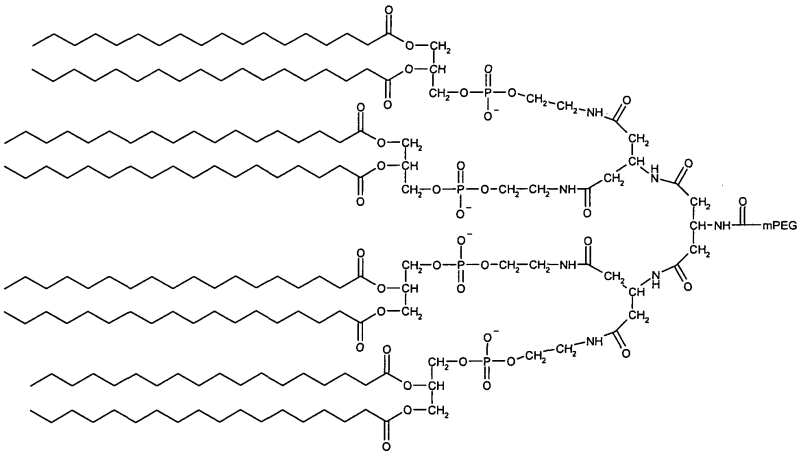

Figure 4.13: Structure of mPEG-β-Glu-(DSPE)$_4$.

The presence of an increased number of lipid molecules conjugated to a single polymer chain allows to enhance the hydrophobic interactions with the phospholipids of the liposome's bilayer, thereby reducing the probability of detachment. Therefore, SSLs showed enhanced stability, prolonged circulation half-life and lower uptake by MPS in comparison to stealth liposomes. Furthermore, *in vitro studies* suggested a low toxicity and high intracellular uptake of SSLs with respect to SLs. Overall, SSLs may have the potential to greatly improve conventional cancer treatment by enhancing drug delivery and antitumor efficacy [2].

4.5.4 Evolution from Immunoliposomes to Super stealth immunoliposomes

Although several liposomal formulations of classical chemotherapeutic drugs have already been approved for cancer therapy and reached the market, in all cases the drug delivery to the tumor site is achieved by means of passive accumulation through EPR effect. The functionalization of liposomes with targeting moieties, i.e. ligands of various nature (antibody, peptides, nucleic acids, aptamers, carbohydrates, etc.), has emerged over the years as a promising strategy for achieving a targeted drug delivery system. The most exploited approach relays on the coupling of antibodies to the surface of liposomes, thus providing the so called immunoliposomes. The rationale behind this idea is to enhance the amount of anticancer drug reaching the tumor cells and minimize the

accumulation in other healthy tissues, by means of antibody-mediated recognition of specific antigens overexpressed on the surface of cancer cells.

Depending on the coupling strategy immunoliposomes can be classified as (Figure 4.14):

- *type I*, whether the antibody is directly conjugated to the lipid bilayer (either in presence or absence of PEG coating);
- *type II*, whether the conjugation occurs at the distal end of the PEG chain [58].

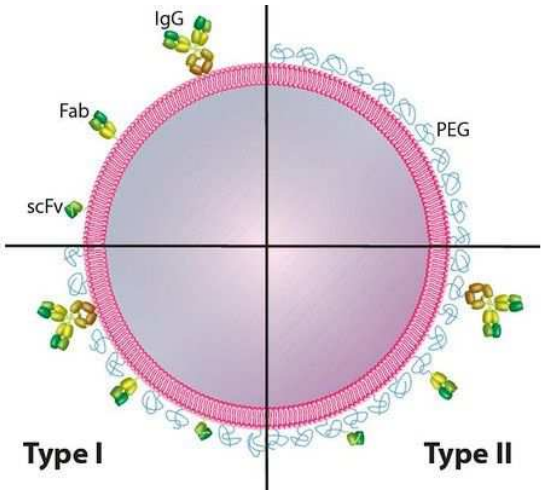

Figure 4.14: Generations of immunoliposomes.

Early attempts to couple antibodies on the surface of liposomes go back to around the 1980s, when several approaches were analyzed to attach antibody molecules or protein models to the surface of naked liposomes [59, 60]. One conjugation strategy included the use of bifunctional reagents to couple the protein to reactive groups on liposome surface [61, 62]. Introduction of hydrophobic residues to the protein structure also enabled its effective incorporation into the lipid bilayer [63]. Another possibility was antibody coupling by means of activated sugar moieties either in the protein structure or incorporated in the liposome membrane and exposed on the outer surface [64]. Overall, surface adsorption (non-covalent conjugation) of antibodies on liposome membrane proved to be not efficient enough since they suffered destabilization after serum proteins exposure *in vivo*. This approach led also to relatively low attachment efficiency and liposomes aggregation. Moreover, the amount of adsorbed antibody was difficult to control, as well as its correct orientation. The further addition of PEG-coating allowed at the same time to exploit the advantage of achieving a sterically stabilized long-circulating formulation with improved pharmacokinetic properties. However, in some cases the steric hindrance provided by PEG also affected antibody-antigen recognition, which resulted in either reduced or prevented binding, based on the amount of polymer and its length [65]. To avoid this problem and restore

the efficacy of antigen-antibody binding, several techniques were developed to consent the conjugation of the targeting agent to the distal end of the polymer [66]. A crucial factor, though, is the orientation of the antibody covalently attached onto the surface of the PEG layer, since it strongly influences the association of the nanocarrier with tumor cells overexpressing the specific antigen. Depending on the coupling chemistry, indeed, PEGylation may occur at different sites of the antibody structure, resulting in a random orientation of the targeting moiety. Nevertheless, site-specific conjugation is preferable because the antigen-binding site is equally exposed and protruding from liposome surface [67].

In the last 20 years, a new interesting approach to couple different kind of ligands (including antibodies) to either naked or PEG-coated liposomes was introduced. According to this method, known as *post-insertion technique* [68], ligands are first coupled to the distal terminus of PEG-lipids derivatives, forming an unstable micellar suspension which is subsequently co-incubated with preformed liposomes. Spontaneous transfer and incorporation of modified ligand take place, from their micellar state into the more thermodynamically favorable bilayer of liposomes, in a temperature- and time-dependent manner (Figure 4.15).

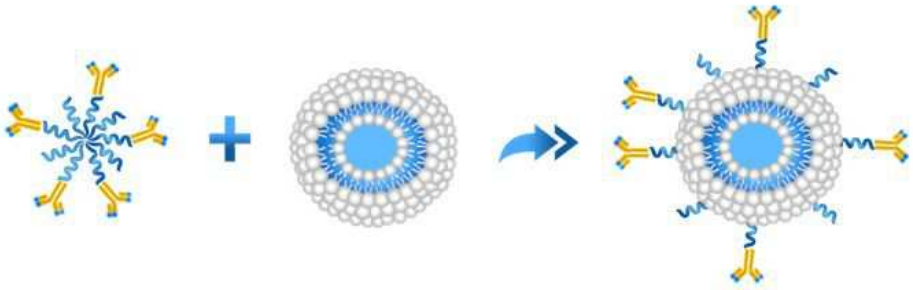

Figure 4.15: Schematic representation of the post-insertion technique.

It was reported that the coupling of the whole antibody to liposomes resulted highly immunogenic, leading to reduced residence time of the drug delivery system in the bloodstream [69]. Several mechanisms may contribute to immunoliposomes depletion: Fc-mediated phagocytosis by circulating or liver and spleen macrophages, opsonization of the coupled antibodies, activation of complement-mediated cytotoxicity and antibody-dependent cellular cytotoxicity (ADCC). Accordingly, the progresses in monoclonal antibody engineering allowed the development of less immunogenic fragments (still bearing the antigen-binding site), such as *fragment antigen-binding* (Fab') and *single chain fragment variable* (scFv) fragments, which are lately being employed instead of the whole antibody structure. The use of antibody fragments can indeed prolong the circulation time with respect to full antibody-targeted liposomes, even though at some level they still accelerate the clearance [70]. Interestingly, it has been shown [71] that in some tumors the accumulation of long-circulating immunoliposomes and non-targeted stealth liposomes is somehow comparable. The great difference, though, stands on the enhanced therapeutic activity of stealth immunoliposomes, as they bind with high affinity to tumor-associated internalizing agents overexpressed on the surface of cancer cells. The better

internalization allows higher amounts of chemotherapeutic drug to accumulate inside the tumor cells, thus explicating its cytotoxic effect. On the contrary, the accumulation of conventional stealth liposomes is usually confined to the interstitial space in proximity of tumor site. The targeting efficacy of immunoliposomes is also strictly influenced by antigen density on the surface of target tumor cells, which unfortunately is often low [72]. Generally, the higher the antigen density the higher the selectivity towards cancer cells and the more intense the antitumor activity.

The present work aims at combining PEG dendron-lipids derivatives with the Fab' fragment derived from Trastuzumab (Herceptin®), a monoclonal antibody (mAb), by coupling it to the free end of PEG, to obtain new *Super Stealth Immunoliposomes* (SSILs). Trastuzumab is used to target with high affinity the HER2 (human epidermal growth factor receptor 2), which is overexpressed on the surface of certain tumor cells. These novel formulations, therefore, should possess both the enhanced stability in the bloodstream provided by PEG and the ability to reach selectively the tumor site. The post-insertion approach is exploited to incorporate Fab'-PEG dendron-lipids derivatives into preformed PEG-coated liposomes.

4.6 ANTIBODIES AND THEIR FRAGMENTS AS TARGETING TOOLS FOR DRUG DELIVERY

During the last decades, the interest on antibodies for commercial development has been strongly increasing for several reasons [73]:

- their specific action, generally inducing less side-effects;
- the possibility to be coupled to other therapeutic entities providing efficient delivery to the target site, thereby reducing potential side effects;
- they may be exploited for diagnostic purposes by conjugation to radioisotopes;
- technology improvements led to the achievement of complete human monoclonal antibodies, which are less immunogenic.

Antibodies or immunoglobulins are large glycoproteins (82–96% protein, 4–18% carbohydrate) [74] secreted by plasma B cells (B lymphocytes) of the adaptive immune system in two physical forms: as soluble proteins freely circulating in the bloodstream or as membrane-bound proteins on the surface of B-cells. Immunoglobulins consist of three equal-sized globular portions, loosely connected by a flexible stretch of polypeptide chain, known as the *hinge region*, forming a roughly Y-shaped macromolecule (or combination of such macromolecule). Two main regions can be distinguished [73]: the variable region (V), consisting in the two "arms" of the Y and defining the antigen-binding region; the constant region (C), represented by the "stem" of the Y and responsible for the interactions with effector cells of the immune system and other molecules. Five different isotypes of immunoglobulins are recognized in humans, namely IgA, IgD, IgE, IgM, and IgG, based on their C region. IgGs are usually present as monomers, whereas IgAs and IgMs generally associate respectively as dimers and pentamers. The most abundant in human serum,

accounting for 10-20% of plasma proteins, and widely used for therapeutic purposes are the IgGs (Figure 4.16 and Figure 4.17).

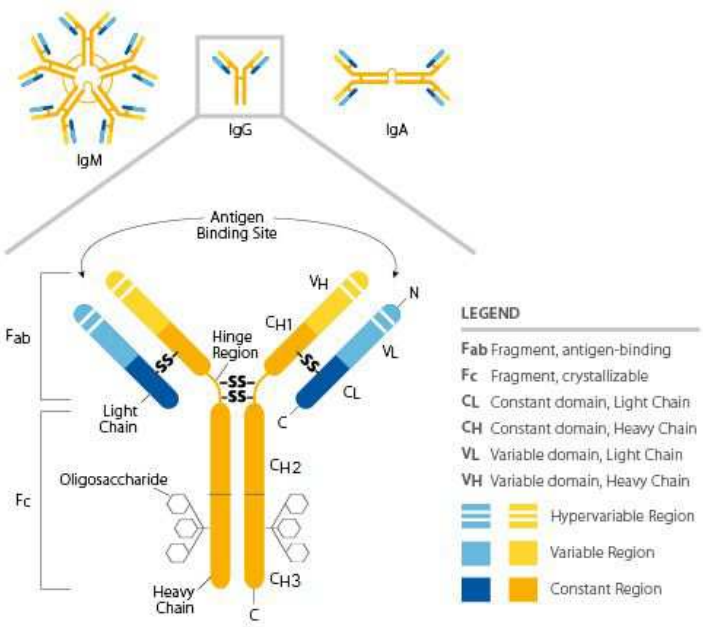

Figure 4.16: Schematic representation of IgG.

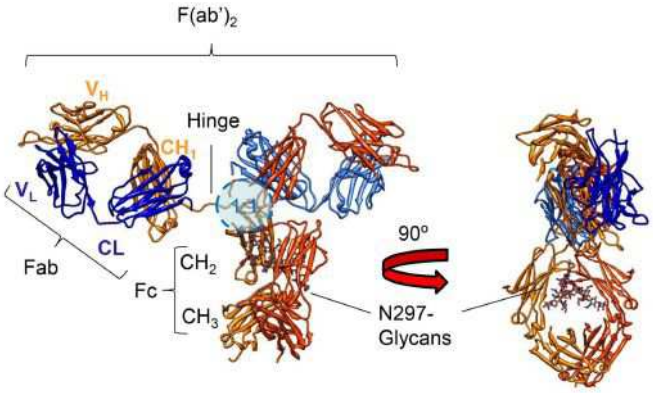

Figure 4.17: Crystal structure of a human IgG1 molecule.

IgGs have a molecular weight of about 150 kDa, since they are composed of two identical heavy chains (H) of 50 kDa and two identical light chains (L) of 25 kDa, held together by inter-chain disulphide bonds as well as non-covalent interactions. Each heavy chain consists of an N-terminal variable domain (VH) and three constant domains (CH1, CH2, CH3), with a hinge region between CH1 and CH2, whereas each light chain is made of one N-terminal variable domain (VL) and one

constant domain (CL). Two types of light chains exist, lambda (λ) and kappa (κ), and the average of κ to λ ratio in humans is 2:1. The association of the light chain with the VH and CH1 domains of the heavy chain forms the Fab fragment (fragment, antigen-binding) of the antibody. Instead, the combination of the lower hinge region and the CH2 and CH3 domains of the heavy chains represents the Fc fragment (fragment, crystallizable), which is responsible for effector recognition and binding. In addition, a highly conserved N-linked glycosylation site (Asn297) is located between the two CH2/CH3 domains forming the Fc.
IgGs can be further divided in four subclasses, based on the heavy chain type, in order of decreasing relative abundance: IgG1, IgG2, IgG3 and IgG4. The main structural differences reside in the number and location of interchain disulfide bonds and the length of the hinge region. Most IgGs present four interchain disulfide bonds, two connecting the H chains at the hinge region and other two connecting the L chains to the H chains. The subtypes show over 90% homology in amino acid sequence, but great variability is observed in the N-terminal sequences of both the heavy and light chains between different antibodies. It was suggested that the conserved sequences in human IgG1 antibodies are approximately 95% and the remaining 5% is variable, creating the antigen-binding specificity [75]. The V regions are further classified into three hypervariable sequences (HV1, HV2, HV3), which are also defined as complementarity determining regions (CDR1, CDR2, CDR3). This variability is due to a recombinational process following the exposure to an antigen, which leads to stimulation, diversification, and propagation of many genetically distinct B-cells producing millions of antibodies (*polyclonal antibodies*) with slightly different antigen-binding sites, thus with different affinities and specificities.

Technology advancement led to the generation of *monoclonal antibodies* (mAbs), obtained from a single clone of B cells and characterized by unique structure and high affinity for a single specific epitope of an antigen. The first murine mAbs were produced in 1975 by Köhler and Milstein, who developed the *hybridoma technology* [76]. This approach is based on the fusion of a B lymphocyte cell clone with a myeloma cell, resulting in a hybrid cell line with both limitless replicative potential and ability to produce antibodies. Unfortunately, the therapeutic use of murine antibodies is strongly limited by their high immunogenicity, because they elicit the formation of human anti-mouse antibodies (HAMAs) responsible for the short serum half-life. Therefore, humanized chimeric antibodies were generated by means of genetic engineering approaches, with the purpose of further reducing the immunogenicity, in which the C region is human (60-70% of the protein structure), whereas the V region is murine [77]. Chimeric antibodies, though, could still induce the secretion of human anti-chimeric antibodies (HACA). Subsequently, highly humanized antibodies (90–95% human) were developed by engrafting only murine-sequence derived CDR regions into human sequence-derived V regions. Though, a similar immunogenic potential with respect to fully human antibodies was observed, as these mAbs could still evoke the formation of human anti-human antibodies (HAHA).

The introduction of novel technologies, such as the use of transgenic mice and phage display platforms, allowed the production of fully human mAbs (Figure 4.18) whose sequence is entirely human.

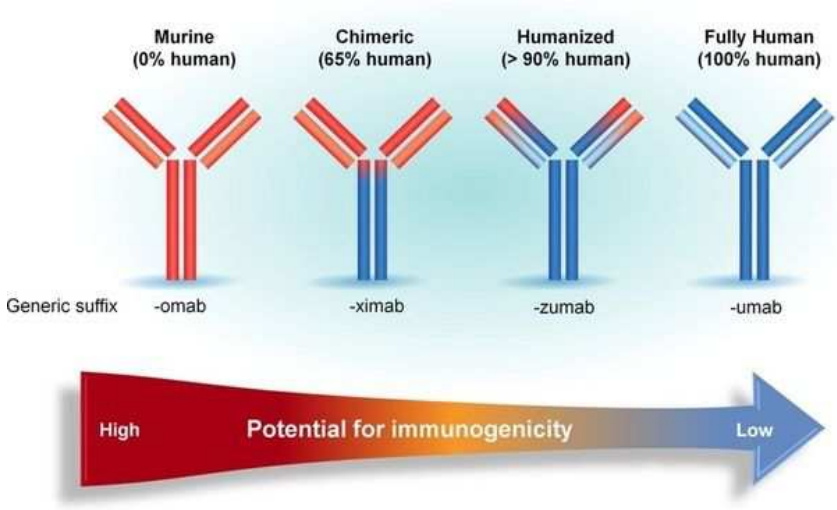

Figure 4.18: Evolution of monoclonal antibodies (mAbs) and their correlated potential for immunogenicity.

Thanks to their unique affinity and specificity, mAbs have acquired great interest in the field of anticancer drug delivery as efficient tools to achieve a targeted delivery to cancer cells. As already mentioned, the use of full antibodies coupled to liposomal nanocarriers may result in fast clearance from the bloodstream as they are potentially highly immunogenic.

With the aim of achieving a stable, efficient targeted drug delivery system, other alternative forms of antibodies (still retaining the antigen-binding site) have been generated through enzymatic digestion and reduction. The two most widely exploited pathways contemplate the use of two different proteolytic enzymes, thus providing different outcomes (Figure 4.19) [78-80].
In the first approach, treatment with papain cleaves the N-terminal side of the disulfide bonds of the hinge region and generate two identical Fab fragments and one Fc fragment. Fab fragments are 50 kDa (VH-CH1)/(VL-CL) heterodimers linked by a single disulfide bond.
The other approach, instead, involves the treatment with pepsin which cleaves at the C-terminal side of the disulfide bonds of the hinge region and produces one large fragment with two antigen-binding sites, namely $F(ab')_2$, and many smaller peptides deriving from the degradation of the Fc portion. Further selective reduction of $F(ab')_2$ at the disulfide bonds of the hinge region generates two identical F(ab') fragments, each bearing one antigen-binding site. Well-established protocols of reduction are based on the use of mild reducing agents, like β-mercaptoethylamine (β-MEA), β-mercaptoethanol (β-ME), dithiothreitol (DTT), tris(2-carboxyethyl)phosphine (TCEP), glutathione or cysteine [80].

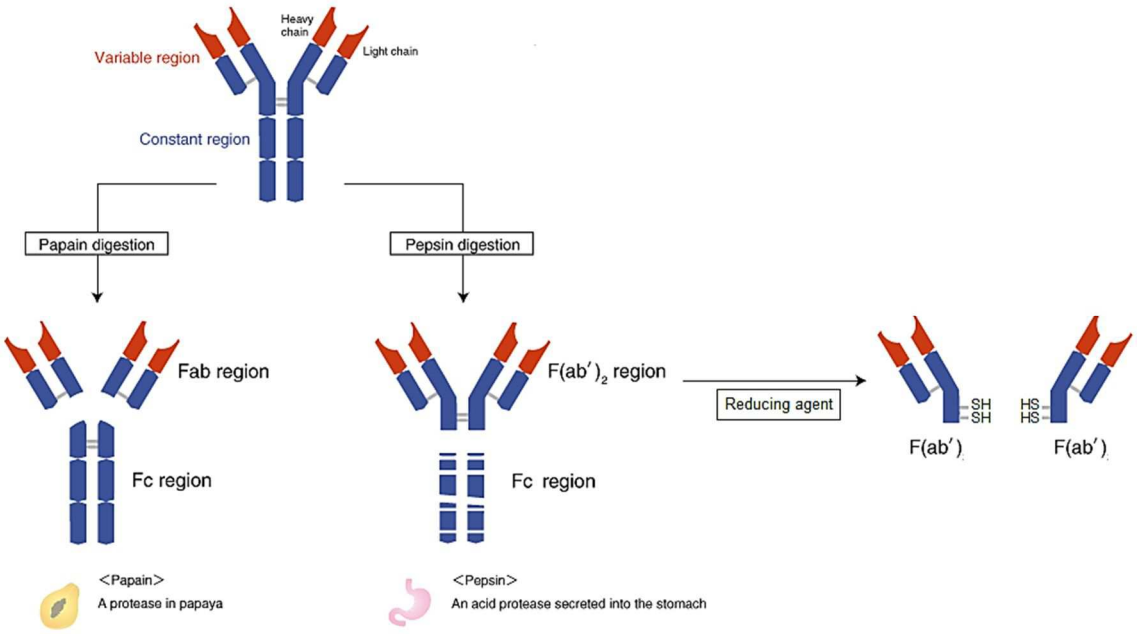

Figure 4.19: Proteolytic fragments obtained from papain- and pepsin-mediated IgG digestion.

Another common antibody fragment is the single chain fragment variable (scFv), which contains recombinant VL and VH regions joined by a short hydrophilic and flexible peptide sequence of at least 12 residues. Shorter linkers (5–10 residues) do not allow the pairing of the variable domains but allow the association with another scFv to form a bivalent dimer, e.g. diabody (60 kDa) or trimer, e.g. triabody (90 kDa) (Figure 4.20). ScFv (25-30 kDa) are commonly expressed in bacterial culture and can be engineered with various tags (e.g. poly-His) or amino acids sequences (e.g. terminal Cys, thus providing a free sulfhydryl group for coupling to other entities) [81].

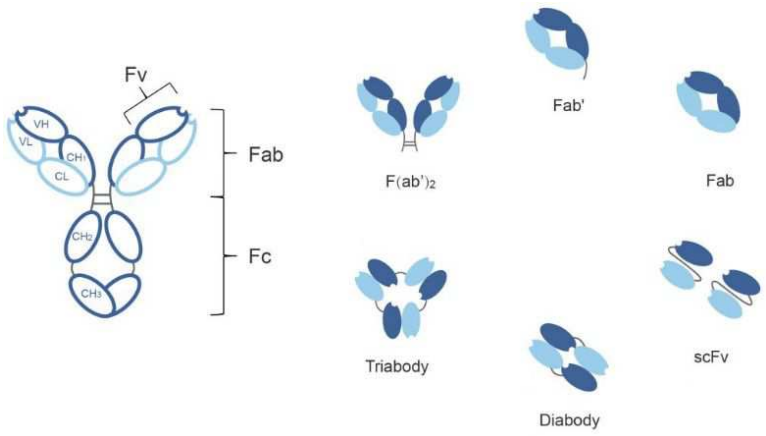

Figure 4.20: Schematic representation of various antibody constructs.

When all factors are taken together, the choice of the most suitable targeting agent for immunoliposomes formulation rely not only on the therapeutic outcome, but also on other criteria: stability, production yields, affinity and specificity of binding, immunogenicity and toxicity. In this context, mAbs are generally more expensive and inconvenient to produce, whereas smaller fragments can be produced in bacteria or in other expression systems, but also engineered and selected for optimal stability and affinity [81].
The potential immunogenicity arising from the use of the whole antibody derives from the presence of Fc domain, against which most HAMA response is directed and responsible for increased MPS clearance through specific recognition by phagocytic cells carrying Fc receptors. It is reported that liposomes coupled with antibody fragments preserving the antigen-binding site but lacking the Fc domain (e.g. Fab', scFv, etc.) showed considerably improved pharmacokinetic and pharmacodynamic profiles over full antibody targeted liposomes in various animal models. In addition, the clearance was comparable to that of non-targeted liposomes, resulting in increased therapeutic effects [82, 83].
Moreover, antibody fragments also allow easier conjugation to liposomes containing functionalized PEG-lipid derivatives, exploiting the thiol groups of Cys in the hinge region. Full antibody structure, instead, often requires modification of existing functional groups which are usually abundant and non-homogeneous orientation of the antibody on the surface of the nanocarrier might be achieved (see paragraph 1.6.1).

4.6.1 Coupling strategies

Several chemical strategies have been thoroughly described [78] to conjugate antibodies or their fragments to liposomes, either by covalent or non-covalent bonds. Most approaches involve conjugation to the distal end of PEG-lipids components, on which the inert methoxy group has been replaced with reactive moieties.

Overall, these coupling methods are based on:

a) use of free amino and carboxylic groups present in the antibody molecule (Figure 4.21).

These functionalities, however, are relatively abundant in the protein, thus undesired random orientation of the antibody on the surface of liposomes might be achieved.

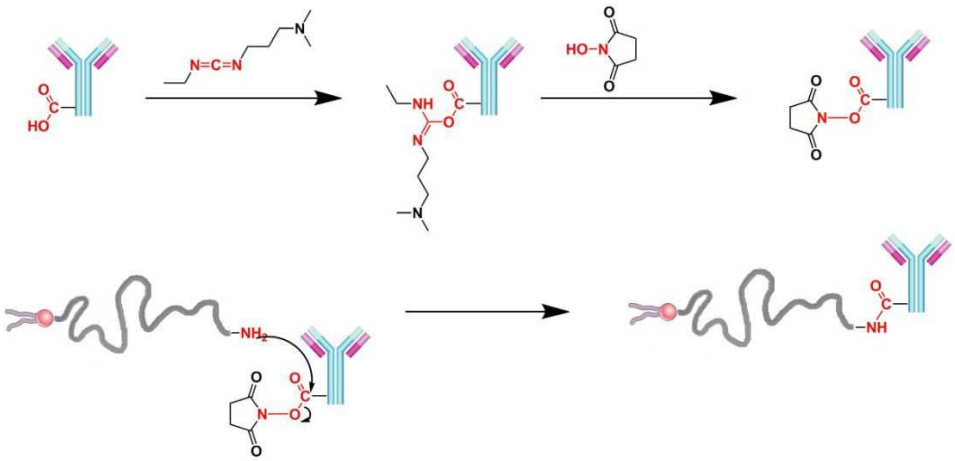

Figure 4.21:Example of conjugation of EDC/NHS activated -COOH group of the antibody to amine-PEG-lipids.

b) Site-directed conjugation to the carbohydrate chains in the Fc region.

This approach requires prior mild oxidation of the sugar residues with sodium periodate to obtain aldehyde groups and subsequent coupling to hydrazide-containing crosslinking agent or PEG chain on liposome surface (Figure 4.22). Care should be taken as some antibodies may be glycosylated in proximity of the antigen-binding site.

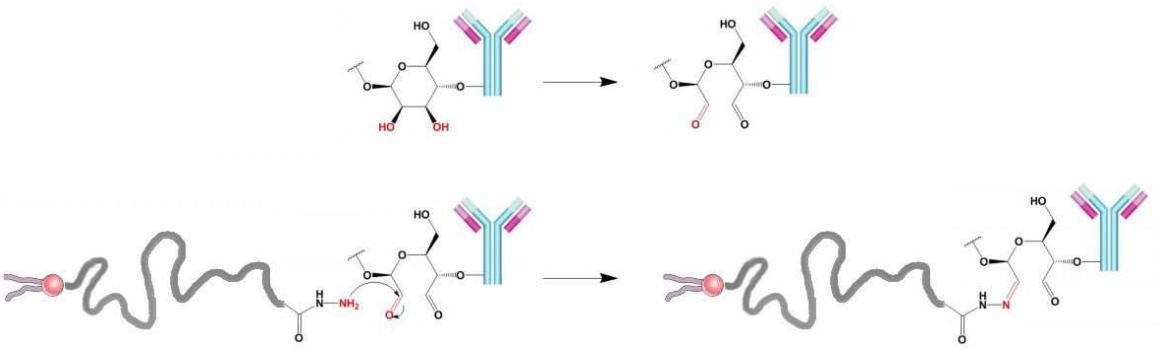

Figure 4.22: Conjugation of aldehyde modified antibody to a hydrazide modified lipid.

c) Modification of existing functional groups (disulfide, amine, carboxylic and carbohydrate groups) present in the antibody with cross-linking agents containing reactive functionalities.

For instance, 2-Iminothiolane (Traut's reagent) is a cyclic imidothioester used to introduce free sulfhydryl group in the antibody structure, upon ring opening, after reaction with primary amines. Other commonly employed cross-linking agents are: succinimidyl 3-(2-pyridyldithio)propionate (SPDP); N-succinimidyl S-acetylthioacetate (SATA); 4-succinimidyloxycarbonyl-alpha-methyl-α(2-pyridyldithio)toluene (SMTP); etc. Thiolated antibodies can be reacted with maleimide-containing PEG-lipid derivatives to form a stable non-cleavable thioether bond (Figure 4.23).

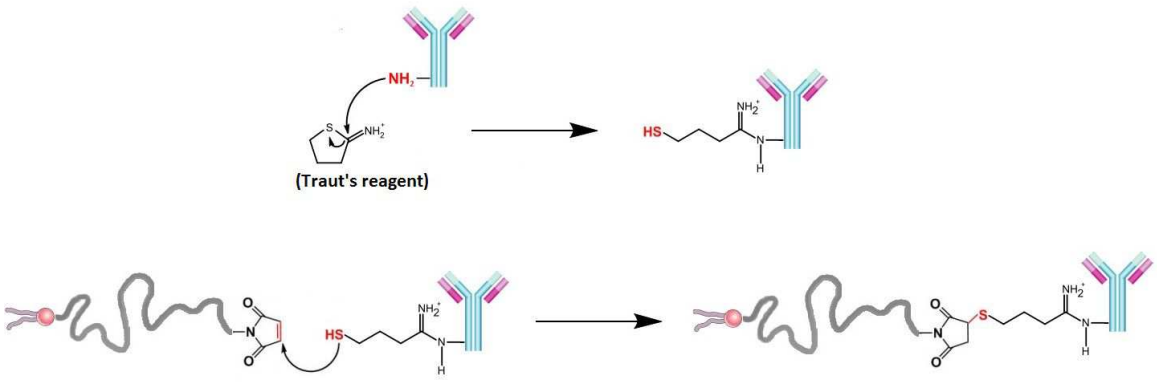

Figure 4.23: Thiolation of an antibody introduces a reactive thiol group which can further react with maleimide-derivatized PEG-lipids.

d) Use of free functional groups of phospholipids, e.g. amine and hydroxyl groups, or their modification with cross-linking agents containing reactive moieties. For example, phospholipids containing amine groups can be modified with SPDP cross-linking agent to introduce a disulfide group which is later exploited to couple antibodies by means of reversible disulfide bond formation (Figure 4.24).

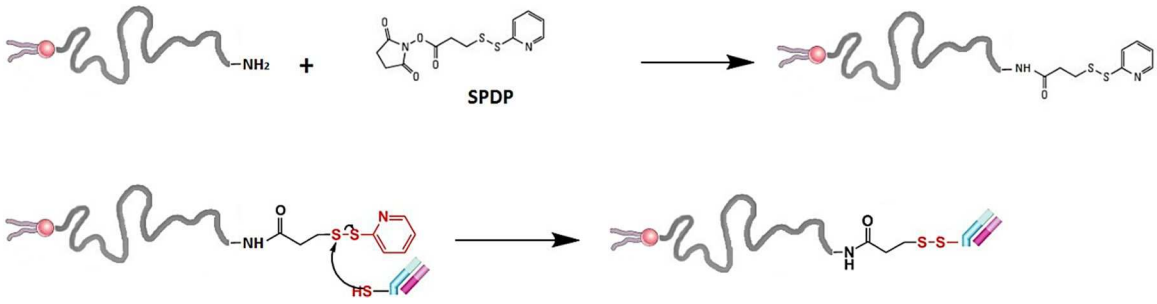

Figure 4.24: Example of phospholipids modification to introduce reactive functionalities to couple antibodies or antibody fragments. In this case, modification with SPDP allows to form a reversible disulfide bond with a Fab' fragment.

e) Use of a wide range of functionalized PEG-lipid derivatives working as linker between the antibodies and liposomes. This also includes antibody and PEG-lipids functionalization with proteins or small molecules with strong affinity for each other (e.g. biotin and avidin; folate and folate-binding protein; poly-His and Ni-NTA), thus generating a non-covalent coupling (Figure 4.25).

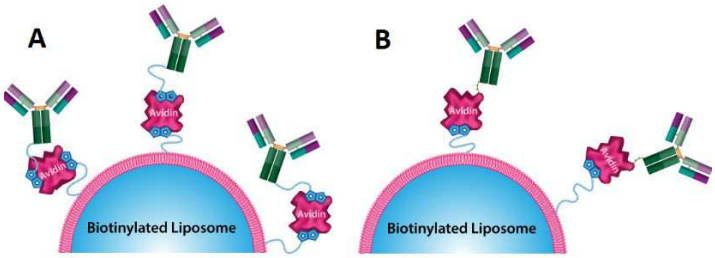

Figure 4.25: Antibody-liposome association using avidin-biotin binding. A) The quadrivalent avidin molecule bridges the two biotinylated components; B) the antibody is covalently bonded to the avidin which binds the biotin on the surface of biotinylated liposomes.

Antibody fragments usually allow easier conjugation to liposomes containing functionalized PEG-derivatives, providing homogeneous coupling and fragment orientation, whereas full antibodies may display random orientation depending on the coupling chemical approach. This relies on the fact that antibody fragments present sulfhydryl group in hinge region readily available for coupling, instead the whole antibody often requires previous modifications.

In the present work, Fab' of Trastuzumab (Herceptin®) was chosen as targeting agent of doxorubicin-loaded stealth and super stealth liposomes. Digestion with pepsin and further reduction with a reducing agent provided the desired Fab' fragment, which was conjugated to PEG-lipid and PEG dendron-lipids derivatives through the maleimide method. This approach is based on the reaction between a maleimide-containing molecule and a free thiol moiety of another molecule to form an irreversible thioether bond. For this purpose, N-(β-maleimidopropyloxy)succinimide ester (BMPS) was exploited, which is a heterobifunctional cross-linking agent bearing a NHS group, for the coupling to the terminal amino group of PEG-lipids derivatives, and a maleimide reactive group which can react with the sulfhydryl moiety of Fab' (Figure 4.26).

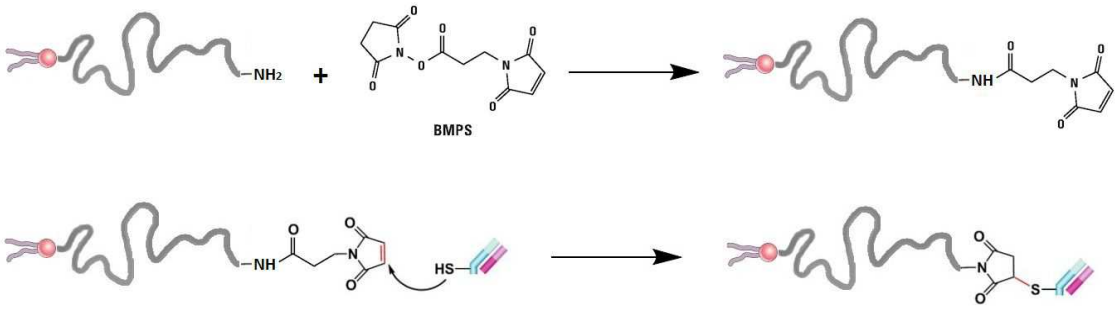

Figure 4.26: Schematic representation of Fab' coupling to a PEG-lipid derivative, after derivatization with N-(β-maleimidopropyloxy)succinimide ester (BMPS), exploiting the maleimide method.

4.6.2 Trastuzumab (Herceptin®)

Trastuzumab, sold under the brand name Herceptin®, is a recombinant humanized IgG1-κ mAb in which murine CDRs that bind with high affinity human epidermal growth factor receptor type 2 (HER-2) were grafted to human antibody framework regions by means of genetic engineering [84]. First developed by Genentech jointly with the University of California, Los Angeles, Trastuzumab received FDA approval in 1998 for the therapy against metastatic breast cancer overexpressing HER2, becoming the first mAb in clinical use for the treatment of solid tumors. Since then, many other mAbs have been clinically approved for cancer therapy, including antibody fragments (mostly Fabs) [85].

Overexpression of HER2 (also referred to as HER2/neu or ErbB2), a 185 kDa oncogene receptor, occurs in 20-30% of invasive breast and ovarian carcinomas, as well as some other adenocarcinomas, whereas its expression in normal tissues is generally low. High expression levels of HER2 are usually associated with poor prognosis in patients, since it is involved in the stimulation of cell proliferation and angiogenesis, inhibition of apoptosis and development of metastasis [86]. Therefore, nowadays it is widely exploited as biomarker and therapeutic target in HER2 positive breast cancer. HER2 belongs to the tyrosine-specific protein kinase family, the epidermal growth factor receptor (EGFR) family, represented by four EGF receptors: ErbB1, ErbB2, ErbB3 and ErbB4, also called HER1, HER2, HER3 and HER4, respectively [87]. HER receptors are transmembrane proteins with partial homology that normally regulate several cellular responses, like normal cell growth and survival, as well as adhesion, migration, differentiation. They are composed of an extracellular ligand-binding domain and a cytoplasmic region with enzymatic activity (except for HER3), joint by a transmembrane domain. Such structure enables the transmission of signals across the plasma membrane with subsequent activation of gene expression, leading to various cellular responses. Specifically, in HER2 the extracellular region is composed by 630 amino acids and is divided in four domains (I-IV) [88].

When HER receptors are isolated as monomers they are “inactive”, which means that there is not signal-transducing tyrosine kinase activity, whilst upon ligand binding they activate and associate in either homodimers (e.g. HER3-HER3) or heterodimers (e.g. HER2-HER3). The tendency of forming dimers is due to the higher stability of the complex between a ligand and two receptors. Once activated, phosphorylation of the tyrosine kinase domain occurs, inducing signal-transduction cascades which promote cellular proliferation and survival. Several different ligands have been described, including EGF-like molecules, transforming growth factor (TGF)-α and neuregulins, but none is specific for HER2. In contrast to the other HER receptors, the extracellular domain of HER2 can assume a fixed conformation resembling a ligand-activated state, permitting the dimerization even in absence of a ligand. Receptor overexpression or mutation can also induce dimerization of HER2 [89]. In addition, HER2 has the capability of reducing the rate of ligand dissociation from the other EGFR of the pair and therefore is responsible for stronger and more prolonged activation of the signalling network. For these reasons, HER2 is the major partner for EGFRs dimers formation [87] because it provides more stable and potent heterodimeric complexes with respect to those involving other EGFRs. The most potent and predominant

combination in carcinoma cells is HER2-HER3. HER2 heterodimers undergo endocytosis at a lower rate than EGFR homodimers, remaining for a longer time at the cell surface and once internalized the complex is targeted for recycling, whereas EGFR homodimers are destined for degradation.

Trastuzumab can bind with high affinity to HER2, even though the overall mechanism behind its therapeutic effect is still not completely understood, but multiple processes seem to be involved. Trastuzumab binding site is located in the extracellular portion of HER2, specifically in a region of domain IV that is occupied by the domain II finger-like projection in the other HER receptor of the complex [88]. The antigen-antibody interactions involved are mainly electrostatic and hydrophobic. Recently, De et al. reviewed Tastuzumab mechanism of action, reporting three direct effects mediated by its interaction with HER2 [90]. First, it inhibits the ligand-independent HER2–HER3 heterodimerization occurring under conditions of HER2 over-expression, whereas it has little impact on the ligand-inducible association of these receptors. Moreover, it prevents the proteolytic cleavage of the HER2 extracellular domain and thereby the formation of the active $p95_{HER2}$ fragment (membrane-bound phosphorylated remnant fragment, still able to activate signal-transduction pathways). Additionally, Trastuzumab drives the antibody-dependent cellular cytotoxicity (ADCC) toward HER2-positive tumors by Fc-mediated recruitment of immune effector cells that express Fc receptors (FcRs) on their surface. The combination of these effects triggers the down-regulation of the signaling pathways related to HER2 dimerization.

The ability of Trastuzumab to bind with high affinity to HER2 is strongly correlated with its therapeutic efficacy. Even small changes in the antigen structure can have a great impact on the strength of interaction. It is reported that the loss of a single hydrogen-bond at the interface between the antibody and the receptor is responsible for a 1000-fold reduction of the binding efficiency. Thus, HER2 structure may play an important role on the development of acquired resistance to Trastuzumab treatment [88].

In the present work, the Fab' fragment of Trastuzumab was employed as specific ligand for actively targeting doxorubicin, a chemotherapeutic agent, encapsulated inside PEGylated liposomes to cancer cells overexpressing HER2 receptor.

4.7 DOXORUBICIN

Doxorubicin (DXR), sold under the trade name of Adriamycin, is an anticancer drug that belongs to the anthracycline antibiotics class and is a 14-hydroxylated derivative of daunorubicin, the most abundantly natural product isolated from *Streptomyces peucetius* (var. *caesius*). In the 1970s it was introduced into the clinic use and since then has proved to be among the most effective anticancer drugs used to treat a wide range of solid tumors and hematopoietic malignancies, receiving FDA approval in 1974. Doxorubicin, indeed, is indicated in the treatment of many human cancers, including breast, ovarian, lung, bladder, thyroid, liver, and gastric cancers; Hodgkin's and non-Hodgkin's lymphomas; Wilm's tumor; soft-tissue sarcoma; neuroblastoma; acute lymphoblastic leukemia [91].

The drug molecule possesses a planar aglyconic structure, comprised of a tetracyclic ring with quinine-hydroquinone adjacent groups, attached by a glycosidic bond to a 3-amino-2,3,4–trideoxy-L-fucosyl sugar residue, known as daunosamine (Figure 4.27).

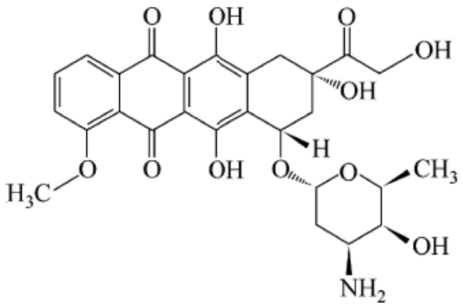

Figure 4.27: The chemical structure of doxorubicin.

Anthracycline antibiotics exert their cytotoxic effects through several proposed mechanisms [92] (Figure 4.28), mainly interfering with enzymes involved in DNA replication and inflicting their action regardless of what cell cycle phase the cell is in, though preferring mitotic cells. First, DXR is known to intercalate the DNA due to its planar aglyconic structure which allows for drug accommodation between DNA base pairs, thereby inhibiting both DNA and RNA polymerase and ultimately ceasing DNA replication and RNA transcription. This process occurs as DXR enters the cell through diffusion using its high binding affinity to the cytoplasm's proteasome (20S subunit). Once the complex is translocated into the nucleus, the drug dissociates from the proteasome and binds to the DNA, thanks to its higher affinity for nuclear DNA over the proteasome. The amount of DXR within the nucleus can reach a saturation level of 340 µm, roughly corresponding to one molecule of drug being intercalated at every fifth base pair on the DNA strand. The free intracellular doxorubicin left (2% of total intracellular drug) is equally distributed indiscriminately among the other organelles (Golgi apparatus, lysosomes and mitochondria). Recently it was reported that doxorubicin can intercalate also mitochondrial DNA.

Another proposed mechanism is DXR binding to DNA-associated enzymes, such as topoisomerase I and II, resulting in double-strand DNA breaks during DNA replication and therefore stimulation of a range of cytotoxic and antiproliferative effects. The apoptosis pathway is triggered when the attempts to repair the DNA fail and cellular growth is inhibited at phases G1 and G2. Another mechanism attributed to doxorubicin action includes the generation of free radicals, which further provokes DNA damage, inhibition of macromolecule production, DNA unwinding/separation and increase in alkylation. Finally, doxorubicin can affect and interact with the cell and mitochondrial membrane by binding to proteins responsible for enzymatic electron reduction of DXR, with subsequent formation of highly reactive species of hydroxyl free radicals. The effect of these free radicals makes doxorubicin a potent anticancer drug, efficacious against various forms of cancer, though these same mechanisms are responsible for the dangerous side effects and toxicity elicited by the drug's use, due to the lack of specificity against tumor cells.

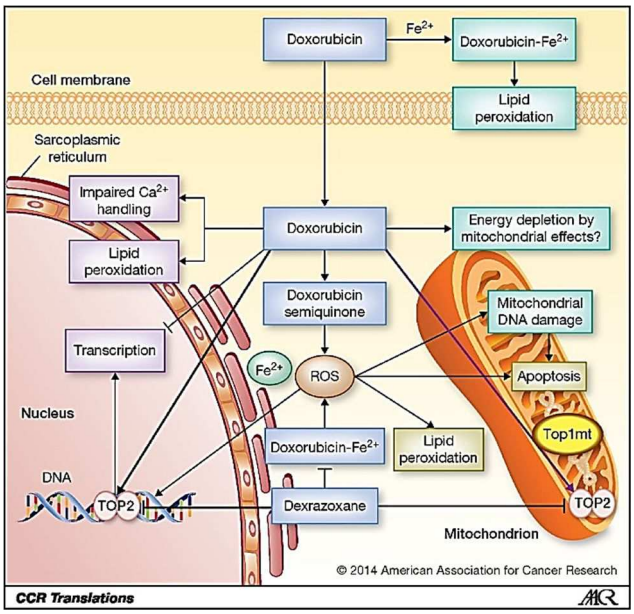

Figure 4.28: Proposed mechanisms of action od doxorubicin.

In cancer treatment doxorubicin is administered intravenously as single agent (60-75 mg/m^2) every 3 weeks, or in combination with other chemotherapeutic agents (40-60 mg/m^2) every 3-4 weeks. Upon injection the drug shows a triphasic plasma clearance, comprising a rapid initial phase of distribution (3-5 min), in which doxorubicin is readily taken up by tissues, and a terminal half-life of 24–36 h. Accumulation occurs mostly in the liver, likely due to the organ's role in metabolism. The major metabolite of doxorubicin is doxorubicinol, obtained from a two-electron stereospecific reduction of the ketone in C-13, forming a secondary alcohol. Both doxorubicin and doxorubicinol (74-76% bound to plasma proteins) can undergo different metabolic reactions (e.g. hydrolytic glycosidic and reductive cleavage, O-sulfation, O-demethylation and O-glucuronidation), leading to the formation of additional metabolites. Despite its high penetrating power into tissues, DXR cannot pass through the blood–brain barrier; furthermore, its concentration in bone marrow and white blood cells is 200–500 times higher than in the plasma. The excretion of the drug is mediated by the hepatobiliary pathway and is normally in the range of 324–809 ml/min/m^2: 50% of the drug is excreted in the bile, usually within 5-7 days after treatment, whilst only 5-12% in the urine (3% as doxorubicinol). After 24 h, instead, 10-20 % of the drug is eliminated through the faeces, reaching the 50% after 150 h.

Anthracyclines are associated with several multidirectional cytotoxic effects, the most prominent being cardiotoxicity. During the 1970s, early clinical trials showed in phase II and III studies common side effects of acute vomiting and nausea, mucositis, gastrointestinal problems, alopecia, urine discoloration, and disturbances to the neurological system (e.g. hallucinations and light-headedness). The reason behind these side effects resides in the lack of specificity of the drug against cancer cells, causing other cell types in the body being affected. The severity and occurrence of these effects depends on the dosage, like cumulative dose-dependent cardiotoxicity

as well as other tissue toxicities such as nephropathy, tissue extravasation, and t-AML (therapy-related acute myeloid leukemia).

The most important side-effect of DXR therapy is cardiotoxicity, which can be either acute, occurring during or shortly after the treatment, or chronic, developing within a year (early-onset) or even several years after the completion of the therapy (late-onset) [93]. Acute cardiotoxicity is usually reversible and manageable, frequently associated with arrhythmias. Chronic cardiotoxicity, instead, is represented by cardiomyopathy and congestive heart failure (CHF), with 20% of incidence when the cumulative dose is 550 mg/m^2, reaching 50% at the cumulative dose of 1000 mg/m^2. The main pathologic manifestation associated to chronic cardiotoxicity are cardiomyocyte degeneration (hypertrophy), interstitial fibrosis and left ventricular contractile dysfunction. Several hypotheses on the mechanisms leading to cardiotoxicity, including doxorubicin-mediated generation of reactive oxygen species (ROS), altered calcium homeostasis, impaired gene and protein expression and mitochondria dysfunction, have been formulated. Presumably, these conditions might result in cardiomyocyte depletion through apoptosis or necrosis.

It is reported that resistance mechanisms might onset upon doxorubicin treatment, including gp170-dependent MDR, decreased expression or mutations of topoisomerase II, and increased expression of sulfhydryl enzymes (e.g., glutathione and glutathione-dependent enzymes) [91].

4.7.1 Doxorubicin formulations on the market and in clinical development

Drug delivery systems loaded with anthracyclines already present on the market, as well as those under clinical development, aim at reducing the well-known side effects correlated to their use as anticancer agents, particularly the cardiotoxicity.

Myocet® is a DXR-loaded non-PEGylated liposomal formulation manufactured by Elan Pharmaceuticals (Princeton, New Jersey), approved in 2000 in Europe for the management of metastatic breast cancer in combination with cyclophosphamide. The particle size of liposomes is about 190 nm and they could provide longer circulating half-life in blood as compared with the free drug. Pharmacokinetic studies proved that free doxorubicin had an elimination half-life ($t_{½}\beta$) of 0.2 h and an area under the plasma concentration-time curve (AUC) of 3.81 mg h/ml, compared to the 2-3 h and 46 mg h/ml for Myocet®. This formulation, though, tends to reduce drug-related toxicity (e.g. cardiotoxicity) rather than to enhance antitumor efficacy. In a phase III comparison study of free DXR with Myocet®, patients treated with Myocet® had low incidence of cardiac events (13% vs 29%), mucositis/stomatitis (8.6% vs 11.9%), and nausea/vomiting (12.3% vs 20.3%) [94, 95].

The introduction of liposome PEG coating significantly improved the pharmacokinetic profile, prolonging the *in vivo* circulation time and the tumor delivery. PEGylated liposomal doxorubicin, sold under the trade name *Doxil®* (USA) or *Caelyx®* (Canada, Europe), was approved in 1995 by FDA and in 2000 by EMA for the treatment of ovarian and breast cancer, multiple myeloma and

AIDS-related Kaposi's sarcoma after the failure or intolerance to prior systemic chemotherapy. Doxil® is characterized by an elimination half-life of 41-70 h and an AUC of 902 mg h/ml. A Phase III trial of Doxil® demonstrated a reduction of cardiotoxicity (3.9% vs 18.8%), neutropenia (4% vs 10%), vomiting (19% vs 31%), and alopecia (20% vs 66%) [94, 96]. Doxil® liposomes (80-100 nm) are composed of high phase-transition-temperature (Tm) phospholipid hydrogenated soy phosphatidylcholine (HSPC), cholesterol and N-(carbonyl-methoxypolyethylene glycol 2000)-1,2-distearoyl-sn-glycero-3-phosphoethanolamine sodium salt ($mPEG_{2000}$-DSPE) in a molar ratio of 56:38:5. Optimum proportion of cholesterol and HSPC provides a non-flexible bilayer at 37°C and below. Like in Myocet®, the encapsulation of the anticancer drug within the nanocarrier prevents its bioavailability at cardiac muscle cells and the myocardium, thus reducing cardiotoxicity.

Lipo-dox® (TTY Biopharm Company Ltd, Taipei Taiwan) is the second generation of PEGylated liposomal doxorubicin, composed of distearoylphosphatidylcholine (DSPC) and cholesterol. DSPC, which has two completely saturated fatty acids (both stearic acids), is characterized by high phase-transition temperature (Tm=55°C), providing higher stability compared with other phospholipids containing unsaturated fatty acid (e.g. egg phosphatidycholine, PC) or fatty acids of shorter or not uniform carbon chains, like HSPC. A phase I clinical study, revealed that Lipo-dox® achieved the most prolonged circulation half-life (65 hours). However, no differences in survival between free DXR and Lipo-dox® in a murine B-cell lymphoma model were observed. Neutropenia, stomatitis and skin toxicity were reported in many cases of Lipo-dox® administration. Moreover, stomatitis became the new dose-limiting toxicity of PEGylated liposomal doxorubicin, appearing at doses of 30 mg/m^2 and reaching dose limit at 50 mg/m^2, whereas Doxil reached dose limit at 80 mg/m^2.

Several doxorubicin liposomal formulations are currently under clinical trials [97]:

- *Thermodox®* (Celsion Corporation): thermosensitive liposomes which exhibit temperature-dependent release of encapsulated drug(s), once the local tissue temperature is elevated to 42 °C by radiofrequency ablation. Application of local hyperthermia also causes leakage of blood vessels within tumours, thereby increasing accumulation of liposomes in the tumour. This formulation (phase III clinical trial) uses lysolipid thermally sensitive liposome (LTSL) technology to encapsulate doxorubicin for the treatment of various solid tumours, allowing 25 times greater concentration of the drug in the target area than i.v. treatment of free or encapsulated-DXR. Thermodox® is mainly indicated for the treatment of hepatocellular carcinoma and recurring chest wall breast cancer.
- *MCC-465*: immunoliposomes for the treatment of metastatic stomach cancer, composed of DPPC, cholesterol and maleimidated palmitoyl phosphatidyl ethanolamine and tagged with PEG and the $F(ab')_2$ fragment of human monoclonal antibody GAH.
- *2B3-101*, PEGylated doxorubicin liposomes that targets patients with brain metastases and developed based on glutathione PEGylation. Glutathione enhances the delivery of encapsulated moiety across the blood brain barrier (BBB). The technology behind the development of 2B3-101 is termed G-technology, which allows the encapsulation of various molecules (i.e. high and low MW drugs, hydrophilic and lipophilic compounds) without any modifications of the payload.

5. MATERIALS AND METHODS

5.1 MATERIALS AND INSTRUMENTS

$mPEG_{2kDa}$-DSPE, $mPEG_{2kDa}$-$(DSPE)_2$ and $mPEG_{2kDa}$-$(DSPE)_4$ were previously synthesized in-house. $mPEG_{5kDa}$-NHS and Boc-PEG_{5kDa}-NHS were obtained from Iris Biotech Gmbh (Marktredwitz, Germany), whereas MAL-PEG_{5kDa}-DSPE, hydrogenated soybean phosphatidylcholine (HSPC) and 1,2-Distearoyl-sn-glycero-3-phosphoethanolamine (DSPE) from Nof Corporation (Tokyo, Japan). Cholesterol, instead, was provided by Sigma-Aldrich s.r.l. (Milan, Italy).
N-succinimidyl-3-(2-pyridyldithio)-propionate (SPDP) and N-(β-maleimidopropyloxy)succinimide ester (BMPS) were purchased from Proteochem (Loves Park, IL, USA). Doxorubicin was acquired by 21CEC PX Pharm Ltd. (Eastbourne, East Sussex, United Kingdom) and Trastuzumab was bought as commercial formulation Herceptin available in the pharmacy distribution.
All reagents including salts and solvents were acquired from Sigma-Aldrich s.r.l. (Milan, Italy), like iron(III) chloride hexahydrate and ammonium thiocyanate used for lipid content quantification, trifluoroacetic acid, sinapinic acid, D_2O, $CDCl_3$, isopropanol, chloroform, methanol, ammonium sulfate, sodium azide, triton X-100 for liposome disruption, triethylamine, cysteamine, etc.

Aqueous solutions were filtered with Millipore 0.22 µm cellulose acetate filter (Billerica, MA USA). Metrhom (Herisau, Svizzera) 794 Basic Titrino was used for pH measurements. Solvents and buffers were sonicated in a Branson-Emerson 5210 Ultrasonic Cleaner (Danbury, CT, USA).
Organic solvents were removed under vacuum using a Buchi R II Rotavapor (Flawil, Switzerland). Samples were lyophilized either using a Hetossic HETO lyophilizator (Allerød, Denmark) or a CentriVap Benchtop Vacuum Concentrators (Labconco, Kansas City, MO, USA) connected to a Heto cooling trap.
Mass spectra were obtained with an Ab Sciex 4800 Plus MALDI TOF/TOF instrument (Framingham, MA, USA), an Applied Biosystems Mariner ESI–TOF instrument (Monza, MI, Italy) or a Xevo G2-S Q-Tof instrument (Waters Corporation, Milford, MA, USA). NMR spectra were acquired using a Brüker Avance 400 spectrometer (Rheinstetten, Germany) operating at 400 MHz.
AKTA purifier (GE Healthcare, Uppsala, Sweden) was used for chromatographic purifications by gel filtration on a Superose® 12 10/300 GL column provided by GE Healthcare (USA). Micro-BCA and BCA Protein Assay Kit for protein quantification were purchased from Sigma-Aldrich s.r.l. (Milan, Italy). Precast gels for SDS-PAGE were obtained from Thermo Fisher Scientific (Waltham, MA, USA) and Bio-Rad (Milan, Italy).

Liposomes were extruded using a LiposoFast Basic extruder purchased from Avestin Europe GmbH (Manheim, Germany) through Whatman® Nuclepore Track-Etched Membranes made of polycarbonate (400-200-100-50 nm pore size) acquired from Sigma-Aldrich s.r.l. (Milan, Italy). Liposomes hydrodynamic volume was assessed by Malvern Instrument Ltd. Zetasizer Nano ZS

apparatus (Worcestershire, United Kingdom). Liposomal formulations were chromatographed on PD-10 Desalting Columns containing Sephadex G-25 resin, obtained from Thermo Fisher Scientific (Waltham, MA, USA), or on columns containing Sepharose CL-4B cross-linked resin acquired from Sigma-Aldrich s.r.l. (Milan, Italy). Liposomes were observed on a Tecnai G^2 (FEI) transmission electron microscope operating at 100 kV and images were captured with a Veleta (Olympus Soft Imaging System) digital camera.
Protein solutions and liposomes suspensions were concentrated upon centrifugation on Amicon Ultra-15 centrifugal devices or Pierce Protein Concentrators PES purchased by ThermoFisher Scientific (Waltham, MA, USA) and Sigma-Aldrich s.r.l. (Milan, Italy). Samples were centrifuged using a D3024 High Speed Micro-Centrifuge (Scilogex LLC, Rocky Hill, CT, USA) or a Sorvall™ ST 16 Centrifuge (Thermo Scientific). Spectrophotometric UV-Vis determinations were made on a Thermo Scientific Evolution 201 spectrophotometer (Waltham, MA, USA), whereas fluorescence measurements were performed on a FP-6500 Jasco spectrofluorometer.
Female Sprague Dawley rats for pharmacokinetics were obtained from Charles River Laboratories International (Wilgminton, MA, USA).

SV Total RNA Isolation System kit by Promega Corporation (Madison, USA) and One Step Solution SYBR PrimeScript RT-PCR kit II (Takara, Japan) were used for RNA extraction and amplification. The gene expression quantification was performed on a Eco™ Real-Time PCR system.
D-MEM and the other cell culture reagents were obtained from Gibco-ThermoFisher Scientific (Waltham, MA, USA). Nonfat dry milk, rabbit polyclonal Caspase 3 antibody (#9662), rabbit polyclonal Cleaved Caspase 3 (Asp175) antibody (#9661) for western blot analyses were purchased from Cell Signaling Technology (Danvers, Massachusetts, USA), whereas monoclonal beta-Actin antibody from Sigma-Aldrich s.r.l. (Milan, Italy). Amersham ECL Plus Western Blotting Detection System (GE Healthcare Europe GmbH, Milan, Italy) was used for protein staining and the chemiluminescence was measured with Fusion Solo S instrument (Vilber Lourmat).

5.2 PRELIMINARY STUDIES

Preliminary studies were performed on super stealth liposomes formulated with $mPEG_{2kda}$ dendron derivatives, previously synthesized in-home and conjugated to either 2 or 4 molecules of distearoylphosphatidylethanolamine (DSPE). The aim was to assess whether the obtained sterically stabilized liposomes were endowed with the best features in term of physical stability and residence time in the bloodstream.

5.2.1 Liposome preparation

Liposomes were prepared by thin layer evaporation (TLE) technique. Briefly, the lipid mixture was dissolved in 2 ml of $CHCl_3$:MeOH 3:1 v/v in a round-bottom flask, followed by removal of the organic solvents by rotary evaporation, with formation of a lipid film, and o/n drying under vacuum. The lipid mixture of conventional liposomes (CL) was composed of hydrogenated soybean phosphatidylcholine (HSPC, MW 785 Da) and cholesterol (CHOL, MW 387 Da) in a 2:1 HSPC:CHOL molar ratio. PEGylated formulations included 5% or 10% mol of $mPEG_{2kDa}$-$(DSPE)_n$, providing either stealth liposomes (SL) or super stealth liposomes (SSL_n, n= n° of DSPE molecules (2 or 4) attached to PEG). The lipid film was rehydrated for 1 hour at 60-65°C using Rotavapor® (without vacuum) with 1-2 ml of 250 mM ammonium sulphate pH 5.0. The obtained liposomal suspension was homogenized by repeated freeze and thaw cycles, followed by storage at 4°C for 45 minutes, sonication at 4°C for 15 minutes and subsequent hot extrusion (65°C) through polycarbonate filters of decreasing pore size (400-200-100-50 nm). Liposomes mean size was assessed by dynamic light scattering (DLS) measurements as reported in section 5.2.2.
The external buffer was exchanged with PBS pH 7.4 by gel filtration on PD-10 desalting columns (containing Sephadex® G-25 medium), thus creating a pH gradient across the bilayer.
Liposomes concentration was determined by Stewart assay, described in section 5.2.3.

5.2.2 Dynamic Light Scattering (DLS) measurements

DLS was used to assess liposomes mean size and polydispersity index (PdI).
Samples of each liposomal formulation were appropriately diluted and analyzed setting the instrument as follows:

- *method*: manual measurement;
- *material*: liposomes;
- *disperdant*: water a 25°C;
- *equilibration time*: 60 sec;
- *backscatter angle*: 173°;
- *analysis mode:* 3 measurements (15 runs each with a duration of 10 seconds).

The vesicles mean hydrodynamic volume and the formulation polydispersity were determined based on the average of the 3 measurements.

5.2.3 Stewart assay for the quantification of lipid content

The quantification of the lipid content of each liposomal formulation was performed according to Stewart assay [98], which is based on the ability of phospholipids to form a colored complex with ammonium ferrothiocyanate. Specifically, when a chloroform solution of phospholipids is mixed with an aqueous solution of ammonium ferrothiocyanate two phases are generated, with the colored complex forming in the organic phase. The color intensity of the complex is proportional to the lipid content in the solution. The advantage of this method is that, unlike Bartlett assay, the presence of inorganic phosphate does not interfere with this assay and therefore PBS buffer or other phosphate-based buffers can be used.
The reagent is obtained by mixing 27.03 g of $FeCl_3 \cdot 6\ H_2O$ and 30.4 g of NH_4SCN up to 1 L of milliQ water and this solution is stable for several months.
The assay was carried out diluting a small aliquot of liposomes into 2 ml of $CHCl_3$ in 15 ml tubes and adding 2 ml of reagent ammonium ferrothiocyanate. After mixing for 20 seconds each tube and centrifuging 10 minutes at 1000 rpm, the lower organic phase was subjected to UV-Vis spectrophotometric measurement at 485 nm. The lipid concentration of each sample was extrapolated using a calibration curve prepared starting from a standard solution of 0.2 mg/ml HSPC in chloroform, as reported in Table 5.1.

Table 5.1: Preparation of the calibration curve. (*) calculated with respect to the organic phase.

Standard solution (0.2 mg/ml)	Chloroform	Reagent (ferrothiocyanate)	Final concentration (*)
0 ml	2 ml	2 ml	0 mg/ml
0.1 ml	1.9 ml	2 ml	0.01 mg/ml
0.2 ml	1.8 ml	2 ml	0.02 mg/ml
0.3 ml	1.7 ml	2 ml	0.03 mg/ml
0.4 ml	1.6 ml	2 ml	0.04 mg/ml
0.5 ml	1.5 ml	2 ml	0.05 mg/ml
0.6 ml	1.4 ml	2 ml	0.06 mg/ml

5.2.4 Long-term stability studies

In vitro stability studies were performed by evaluating the homogeneity of the liposomal suspensions over time, both in term of vesicles mean size and polydispersity.

Samples of each empty liposomal formulation (170 µl, 3 mM) containing 0.05% w/v NaN_3 were stored at 4°C for 5 months. DLS measurements were performed at fixed time points, as reported in section 5.2.2, to assess liposomes mean size (hydrodynamic volume) and polydispersity index (PdI) and evaluate the overall physical stability of the formulation.

5.2.5 *In vitro* stability experiments in presence of a detergent

In vitro stability was also assessed performing a titration with Triton X-100 (Figure 5.1), a non-ionic surfactant composed of a hydrophilic polyethylene oxide chain and an aromatic hydrocarbon lipophilic group. Thanks to its amphiphilic nature it is able to interact with the liposome bilayer, by altering its structure and causing, above a certain concentration, its disruption with formation of aggregates and mixed micelles.

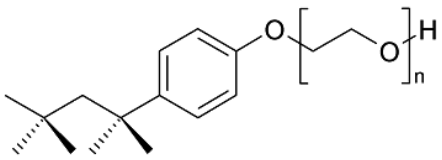

Figure 5.1: Structure of Triton X-100.

The experiments were carried out on empty liposomal formulations, by addition of 2.5 µl of Triton X-100 (300 mM) to samples of each liposomal suspension (3 mM) every 10 minutes. The dimensions of liposomes were evaluated by DLS measurements over the time as in section 5.2.2.

5.2.6 Doxorubicin loading

Liposomes collected after buffer exchange through PD-10 desalting column presented acidic aqueous medium inside (ammonium sulfate pH 5.0) and neutral external medium (PBS pH 7.4). This transmembrane pH gradient was exploited to encapsulate the model drug, doxorubicin (DXR, MW 580 Da), following the remote loading technique [99-101], as illustrated in Figure 5.2.

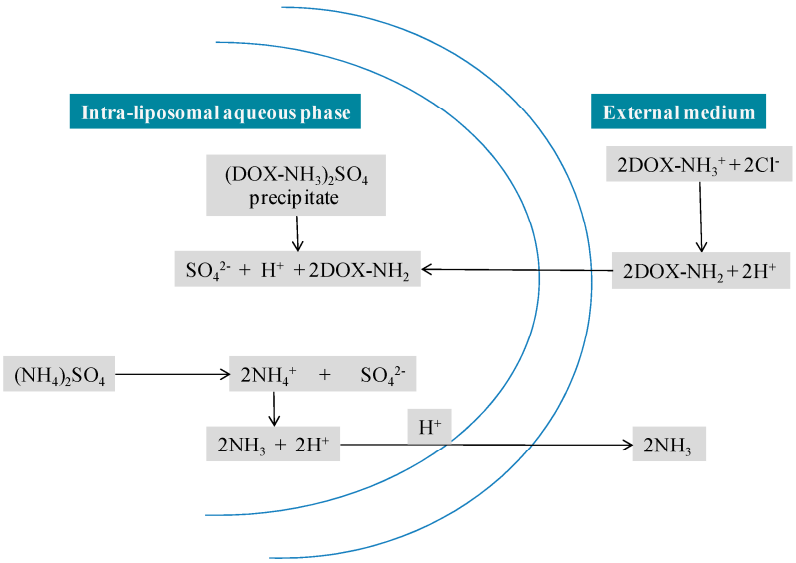

Figure 5.2: Remote loading of doxorubicin.

Briefly, the total amount of DXR was previously dissolved in 0.9% w/v NaCl by stirring at 60°C, followed by incubation with empty liposomes using 1 mg of DXR every 10 µmol of HSPC and stirring for 30 minutes at 60°C. Free doxorubicin was then removed by gel-filtration on a PD-10 desalting column, eluting in PBS pH 7.4 and the integrity of the vesicles was assessed by DLS measurements as reported in section 5.2.2. All these steps were performed in dark conditions in order to avoid degradation of light-sensitive DXR.
The concentration of the encapsulated DXR was determined by spectrophotometry. An aliquot of drug-loaded liposomal suspension was properly diluted in methanol, vesicles were disrupted by addition of 5% v/v of detergent Triton X-100 and subsequent absorbance measurement was performed at 477 nm (ε_{477} = 13050 $M^{-1} \cdot cm^{-1}$ in methanol).

The encapsulation efficiency (EE%) was calculated as:

$$EE\% = \frac{\text{amount of entrapped DXR}}{\text{amount of total DXR}} \cdot 100$$

5.2.7 Drug release experiments

The liposomal release of DXR was quantified by the fluorescence dequenching of self-associated DXR in liposomes upon dilution outside the liposomes [100].
500 µl of each liposomal formulation (1 mM) were incubated for 2 hours at 37°C, during which the leakage of DXR was investigated by measuring the increase of fluorescence intensity every 15 min, using a fluorometer (λ_{ex}= 470nm; λ_{em}= 584nm). At the end of each analysis liposomes were

disrupted by addition of 5% v/v of 1 M Triton X-100 to calculate the 100% dequenched DXR (total DXR). The experiments were performed on a Jasco FP-6500 fluorometer, setting the analysis conditions as reported in Table 5.2.

Table 5.2: Spectrofluorometer settings.

Analysis	→	Long time-course measurement
Duration	→	120 minutes
Data pitch	→	3 minutes
$\lambda_{excitation}$	→	470 nm
$\lambda_{emission}$	→	584 nm
Band with (excitation)	→	5 nm
Band with (emission)	→	10 nm
Sensitivity	→	Medium
Response	→	0.5 sec
Internal temperature (peltier)	→	37°C

5.2.8 *In vivo* studies

5.2.8.1 Ethics statement

The study protocol was approved by the Ethics Committee of the University of Padova and the Italian Ministry of Health (Authorization no. 938/2016-PR obtained on October 10, 2016), and animals were handled in compliance with national (Italian) Legislative Decree 26/2014 guidelines and according to the "Guide for the Care and Use of Laboratory Animals" by the National Research Council of the National Academies.

5.2.8.2 Pharmacokinetics in rats

In vivo pharmacokinetic studies were performed using the liposomal formulations with 5% mol of $mPEG_{2kda}$-lipid(s) derivatives and were carried out in female Sprague Dawley rats (200-250 g), randomly divided in groups of 3 rats each. A dose of 1.74 mg/kg in DXR of each drug-loaded liposomal formulation (CL, SL, SSL_2, SSL_4) was administered via tail vein to the rats previously anesthetized with isoflurane gas (mixed with O_2 in enclosed cages). At scheduled time points blood samples (~200 µl) were withdrawn from the tail, collected into heparin treated tubes and

thereafter immediately centrifuged 15 min x 1500 g for plasma separation. DXR was extracted by treating 50 µl of plasma with 1.2 ml of 81 mM HCl in isopropanol to allow plasma proteins precipitation, including a 5% v/v of 1M Triton X-100 for liposomes disruption. After o/n incubation at 4°C, samples were centrifuged 3 min at 3000 rpm and the supernatants were analyzed by fluorometric measurements (λ_{ex}= 470nm; λ_{em}= 584nm). The concentration of DXR in each plasma sample was extrapolated through a calibration curve of standards solutions of DXR-loaded stealth liposomes. The data were analyzed by applying a bicompartmental model using PKSolver 2.0 software.

5.3 SYNTHESIS OF PEG DENDRON-LIPIDS DERIVATIVES

Two different series of PEG dendron-lipids derivatives were synthetized starting either from a linear $mPEG_{5kDa}$-NHS or a heterobifunctional Boc-NH-PEG_{5kDa}-NHS (Figure 5.3).

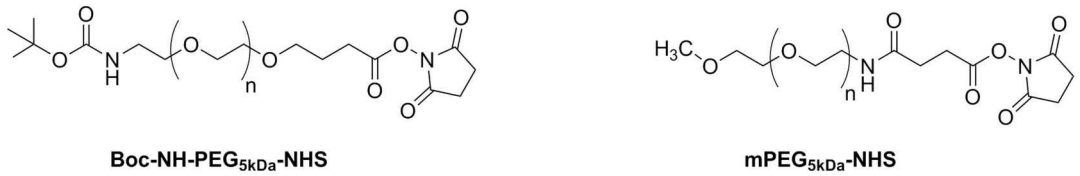

Figure 5.3: Chemical structure of the starting polymers $mPEG_{5kDa}$-NHS and Boc-NH-PEG_{5kDa}-NHS.

The *N*-Hydroxysuccinimide (NHS) activated carbonyl group was exploited for the derivatization with a branching agent, beta-glutamic acid (β-Glu), to achieve a PEG dendron structure and further conjugate 2 or 4 molecules of distearoylphosphatidylethanolamine (DSPE).
Repeated steps of β-Glutamic acid derivatization and carboxyl groups activation were performed until the achieved branching degree consented the coupling with 2 or 4 molecules of DSPE.
Since the synthesis steps were the same for each series of compounds, the backbone polymer was addressed as X-PEG_{5kDa}-NHS, where X referred to either the terminal methoxy moiety or *tert*-butyloxycarbonyl (Boc)-protected primary amino group of PEG.

5.3.1 Determination of the activation degree of X-PEG_{5k}-NHS

Firstly, the degree of activation of the starting polymer was assessed by using a spectroscopic assay based on the so-called Glycyl-Glycine (Gly-Gly) test. According to this assay the activated PEG was reacted with an equimolar amount of 0.285 mg/ml Gly-Gly (MW 132.12 Da) for 30

minutes at room temperature in 0.2 M borate pH 8. Snyder and Sobocinski colorimetric assay [102] was then performed on the reaction mixture to evaluate the percentage of unreacted dipeptide and, therefore, to derive the corresponding polymer activation degree. This assay is based on the use of 2,4,6-trinitrobenzenesulfonic acid (TNBS), which reacts stoichiometrically with primary amino groups in alkaline conditions to give a trinitrophenyl derivative chromophore with maximum absorption at 420 nm (Figure 5.4).

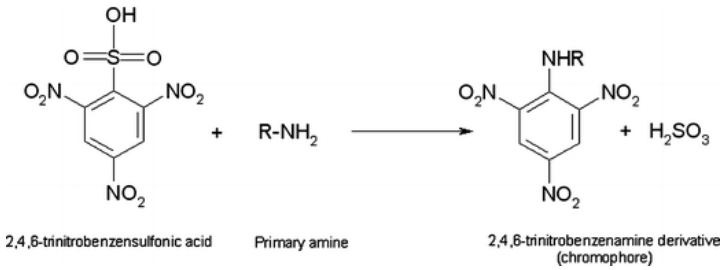

Figure 5.4: Reaction between 2,4,6-trinitrobenzensulfonic acid and a free primary amine group.

The samples were prepared in triplicate according to Table 5.3 and the reactions were incubated for 30 min at room temperature before reading the absorbance at λ = 420 nm using a UV–visible spectrophotometer.

Table 5.3: Samples solutions for TNBS assay.

	Blank	**PEG reaction mixture (P)**	**Gly-Gly standard solution (G)**
955 µl	0.2 M borate pH 9.3	0.2 M borate pH 9.3	0.2 M borate pH 9.3
25 µl	0.2 M borate pH 8.0	sample P	sample G
20 µl	TNBS	TNBS	TNBS

The percentage of free amino groups was calculated as:

$$Abs_{420}\ P : Abs_{420}\ G = X : 100$$

where Abs_{420} G is the absorbance of Gly-Gly reference solution and Abs_{420} P is the absorbance of PEG reaction mixture. The percentage of activation of X-PEG_{5kDa}-NHS was calculated as:

$$\% \text{ activation} = 100 - X$$

5.3.2 Synthesis of X-PEG-βGlu

X-PEG_{5kDa}-βGlu was obtained through the reaction between the activated carboxyl group of PEG and the amino group of β-glutamic acid, leading to the formation of an amide bond (Figure 5.5Figure 5.5).

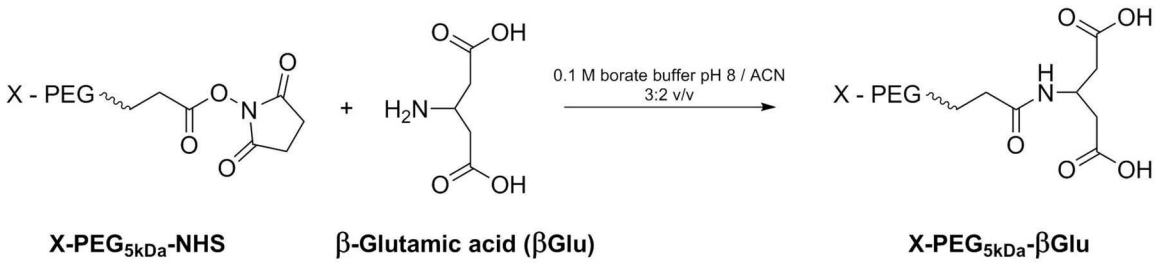

Figure 5.5: Synthesis of X-PEG_{5kDa}- βGlu.

X-PEG_{5kDa}-NHS was reacted as reported in Table 5.4 with 3 equivalents (in excess to activated -COOH groups of PEG) of β-Glutamic acid (βGlu, MW 147.13 Da), previously dissolved in 0.1 M borate buffer pH 8.0/ACN 3:2 v/v, at a final polymer concentration of 10% w/v. The reaction mixture was adjusted at pH 8.0 with triethylamine (TEA) and left stirring o/n at room temperature. After acidification at pH 5.0 with HCl and removal of ACN under vacuum, the product was purified by extractions with CH_2Cl_2. The organic phase, dried over anhydrous Na_2SO_4, was concentrated by rotary evaporation and precipitated in cold diethyl ether under stirring. After 1-2 h at -20°C, the precipitate was filtered and dried under vacuum o/n. The final product was characterized by ^1H NMR spectroscopy to assess the degree of βGlu coupling.

Table 5.4: Reagents amount and yield (% w/w) of βGlu coupling to X-PEG_{5kDa}-NHS. (a) PEG activation degree.

PEG dendron-lipids derivatives	*mPEG-NHS* (81%)[a] [5056 Da]	*β-Glutamic acid* [147.13 Da]	Yield (% w/w) of *mPEG-βGlu* [5088 Da]
mPEG-DSPE₂	1 g	87 mg	98% (0.98 g)
mPEG-DSPE₄	2 g	175 mg	96% (1.92 g)
	Boc-NH-PEG-NHS (78%)[a] [4790 Da]	*β-Glutamic acid* [147.13 Da]	Yield % (w/w) of *Boc-NH-PEG-βGlu* [4822 Da]
Boc-NH-PEG-DSPE₂	4.5 g	415 mg	98% (4.4 g)
Boc-NH-PEG-DSPE₄			

5.3.3 Activation of the carboxyl groups of X-PEG$_{5kDa}$-βGlu via NHS/DCC

The activation to succinimide ester of the carboxyl groups of X-PEG$_{5kDa}$-βGlu was achieved by addition of 3 equiv. of N,N'-dicychlohexylcarbodiimide (DCC, MW 206.33 Da) and 1.5 equiv. of NHS (MW 115.09 Da), both in excess for each carboxyl group (Figure 5.6).

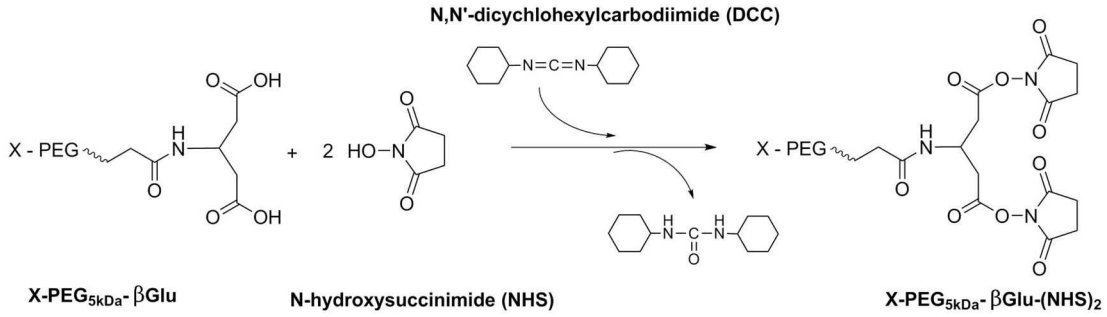

Figure 5.6: Activation via NHS/DCC of the carboxyl groups of X-PEG$_{5kDa}$-βGlu to succinimide ester.

The reaction was carried out in anhydrous CH_2Cl_2, according to Table 5.5, at a final polymer concentration of 10% w/v and stirred at room temperature o/n. The reaction mixture was filtered to remove the by-product dicyclohexylurea (DCU) and directly dropped into cold diethyl ether under stirring. After 1-2 h storage at -20°C, the precipitate was filtered and dried under vacuum o/n. The recovered product, X-PEG$_{5kDa}$-βGlu-(NHS)$_2$, was tested by Snyder and Sobocinsky assay to assess the final degree of activation.

Table 5.5: Reagents amount and yield (% w/w) of the carboxyl groups activation of X-PEG$_{5kDa}$-βGlu.

PEG dendron-lipids derivatives	*mPEG-βGlu* [5088 Da]	*DCC* [206.33 Da] *NHS* [115.09 Da]	Yield (% w/w) of *mPEG-βGlu-(NHS)$_2$* [5282 Da]
mPEG-DSPE$_2$	0.98 g	238 mg DCC 67 mg NHS	93% (0.91 g)
mPEG-DSPE$_4$	1.92 g	467 mg DCC 130 mg NHS	84% (1.62 g)
	Boc-NH-PEG-βGlu [4822 Da]	*DCC* [206.33 Da] *NHS* [115.09 Da]	Yield % (w/w) of *Boc-NH-PEG-βGlu*-(NHS)$_2$ [5016 Da]
Boc-NH-PEG-DSPE$_2$	1.97 g	506 mg DCC 141 mg NHS	95% (1.88 g)
Boc-NH-PEG-DSPE$_4$	2.43 g	624 mg DCC 174 mg NHS	97% (2.36 g)

5.3.4 Synthesis of X-PEG-βGlu-(βGlu)$_2$

X-PEG$_{5kDa}$-βGlu-(NHS)$_2$ was further reacted with 3 equiv. of β-Glutamic acid (βGlu, MW 147.1 Da) with respect to activated -COOH groups of PEG, according to Table 5.6 and as reported in section 5.3.2, with the purpose of increasing the polymer branching (Figure 5.7). The final product was characterized by ^{1}H NMR spectroscopy to assess the degree of βGlu conjugation.

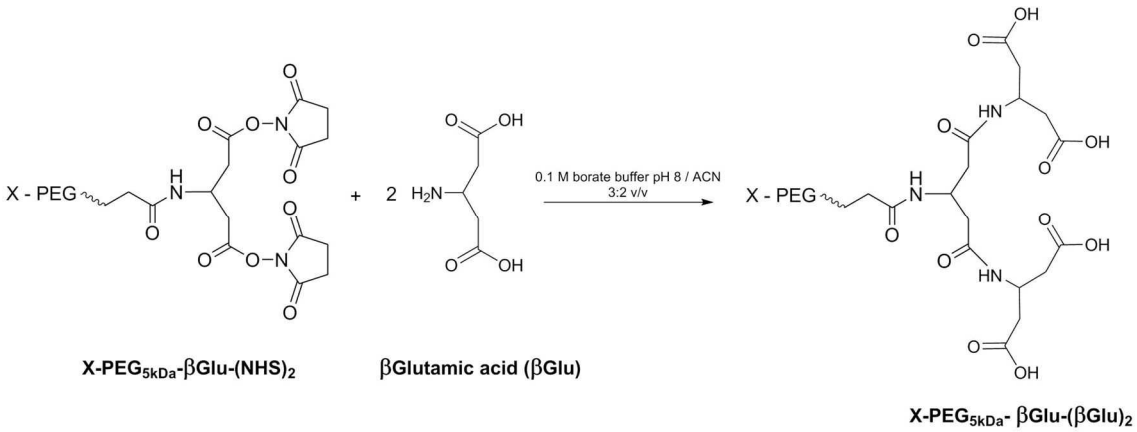

Figure 5.7: Synthesis of X-PEG$_{5kDa}$-βGlu-(βGlu)$_2$.

Table 5.6: Reagents amount and yield (% w/w) of βGlu coupling to X-PEG$_{5kDa}$- βGlu-(NHS)$_2$. (a) PEG activation degree.

PEG dendron-lipids derivatives	*mPEG-βGlu-(NHS)$_2$* [5282 Da]	*β-Glutamic acid* [147.13 Da]	Yield (% w/w) of *mPEG-βGlu-(βGlu)$_2$* [5346 Da]
mPEG-DSPE$_2$	0.91 g (76%)[a]	116 mg	93% (0.85 g)
mPEG-DSPE$_4$	1.62 g (67%)[a]	181 mg	96% (1.56 g)
	Boc-NH-PEG-βGlu-(NHS)$_2$ [5016 Da]	*β-Glutamic acid* [147.13 Da]	Yield % (w/w) of *Boc-NH-PEG-βGlu-(βGlu)$_2$* [5080 Da]
Boc-NH-PEG-DSPE$_2$	1.88 g (71%)[a]	235 mg	85% (1.59 g)
Boc-NH-PEG-DSPE$_4$	2.36 g (74%)[a]	307 mg	92% (2.19 g)

5.3.5 Activation of the carboxyl groups of X-PEG$_{5kDa}$-βGlu-(βGlu)$_2$ via NHS/DCC

The carboxyl groups of X-PEG$_{5kDa}$-βGlu-(βGlu)$_2$ were activated to succinimide ester (Figure 5.8) through the reaction with 3 equiv. of DCC and 1.5 equiv. of NHS, both in excess for each carboxyl group, according to Table 5.7. The reaction was conducted as explained in section 5.3.3 and the final degree of activation was tested by Snyder and Sobocinsky assay.

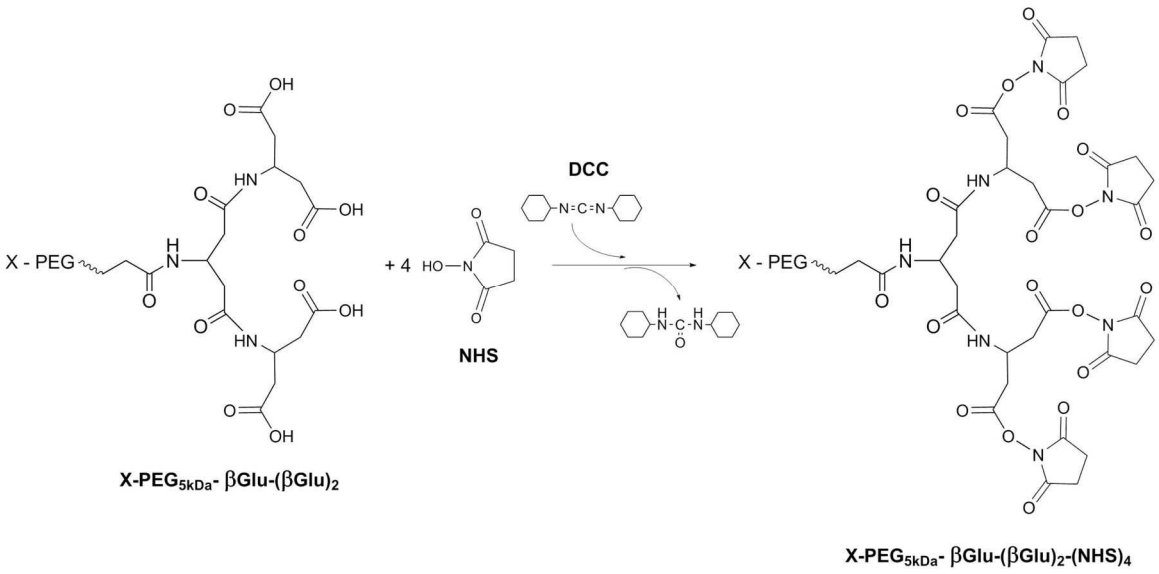

Figure 5.8: Activation via NHS/DCC of the carboxyl groups of X-PEG$_{5kDa}$-ßGlu-(ßGlu)$_2$.

Table 5.7: Reagents amount and yield (% w/w) of the carboxyl groups activation of X-PEG$_{5kDa}$-ßGlu-(ßGlu)$_2$.

PEG dendron-lipids derivatives	*mPEG-ßGlu-(ßGlu)$_2$* [5346 Da]	*DCC* [206.33 Da] *NHS* [115.09 Da]	Yield (% w/w) of *mPEG-ßGlu-(ßGlu)$_2$-(NHS)$_4$* [5734 Da]
mPEG-DSPE$_2$	0.85 g	394 mg DCC 110 mg NHS	66% (0.56 g)
mPEG-DSPE$_4$	1.56 g	723 mg DCC 202 mg NHS	87% (1.35g)
	Boc-NH-PEG-ßGlu-(ßGlu)$_2$ [5080 Da]	*DCC* [206.33 Da] *NHS* [115.09 Da]	Yield % (w/w) of *Boc-NH-PEG-ßGlu-(ßGlu)$_2$*-(NHS)$_4$ [5468 Da]
Boc-NH-PEG-DSPE$_2$	0.8 g	390 mg DCC 109 mg NHS	97% (774 mg)
Boc-NH-PEG-DSPE$_4$	2.19 g	1.07 g DCC 298 mg NHS	93% (2.04 g)

5.3.6 Synthesis of X-PEG-βGlu-(βGlu)$_2$-(βGlu)$_4$

The branching of the activated dendron X-*PEG-ßGlu-(ßGlu)$_2$*-(NHS)$_4$ was further increased to allow the following coupling with 4 molecules of phospholipid (Figure 5.9). The polymer, therefore, was reacted with 2.5 equiv. (total) of β-Glutamic acid (βGlu), according to Table 5.8Table 5.8, in the same conditions as reported in section 5.3.2. Finally, the degree of βGlu derivatization of the product was assessed by ^{1}H NMR spectroscopy.

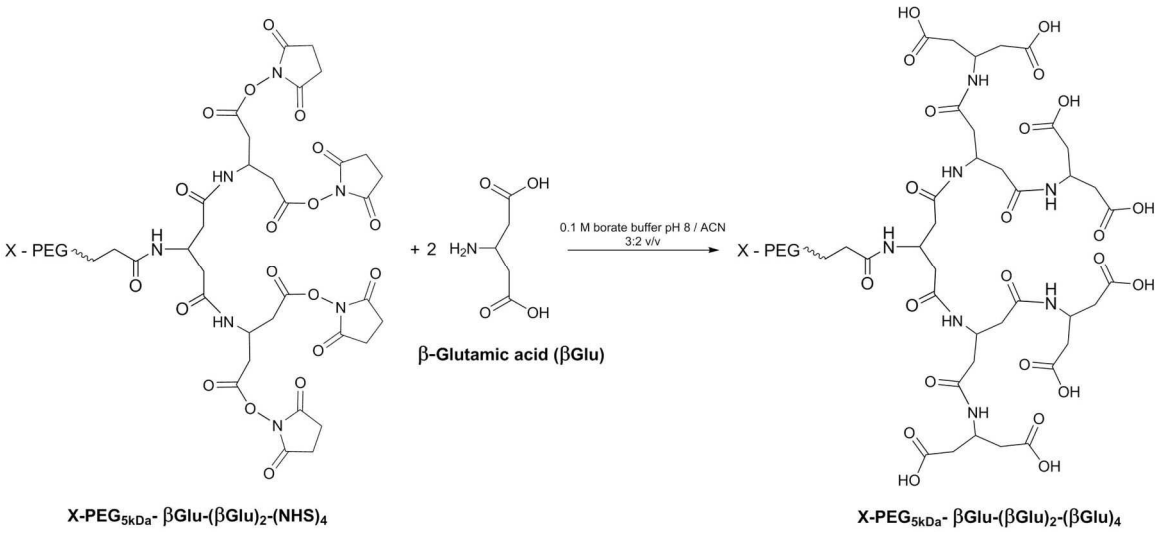

Figure 5.9: Synthesis of X-PEG$_{5kDa}$-ϐGlu-(ϐGlu)$_2$-(ϐGlu)$_4$.

Table 5.8: Reagents amount and yield (% w/w) of ϐGlu coupling to X-PEG$_{5kDa}$- ϐGlu-(ϐGlu)$_2$-(NHS)$_4$. (a) PEG activation degree.

PEG dendron-lipids derivatives	*mPEG-ϐGlu-(ϐGlu)$_2$-(NHS)$_4$* [5734 Da]	*ϐ-Glutamic acid* [147.13 Da]	Yield (% w/w) of *mPEG-ϐGlu-(ϐGlu)$_2$-(ϐGlu)$_4$* [5862 Da]
mPEG-DSPE$_4$	1.35 g (65%)[a]	346 mg	90% (1.22 g)
	Boc-NH-PEG-ϐGlu-(ϐGlu)$_2$-(NHS)$_4$ [5468 Da]	*ϐ-Glutamic acid* [147.13 Da]	Yield % (w/w) of *Boc-NH-PEG-ϐGlu-(ϐGlu)$_2$-(ϐGlu)$_4$* [5596 Da]
Boc-NH-PEG-DSPE$_4$	1.1 g (66%)[a]	296 mg	93% (1.02 g)

5.3.7 Activation of the carboxyl groups of X-PEG$_{5kDa}$-βGlu-(βGlu)$_2$-(βGlu)$_4$ via NHS/DCC

The carboxyl groups of X-*PEG-ϐGlu-(ϐGlu)$_2$-*(*ϐGlu*)$_4$ were activated to succinimide ester to yield the product X-*PEG-ϐGlu-(ϐGlu)$_2$-*(*ϐGlu*)$_4$-(NHS)$_8$ (Figure 5.10), by means of reaction with 3 equiv. of DCC and 1.5 equiv. of NHS, both in excess for each carboxyl group. The reaction was carried out as explained in section 5.3.3 and according to Table 5.9. The final degree of activation of the carboxyl groups was assessed by Snyder and Sobocinsky assay.

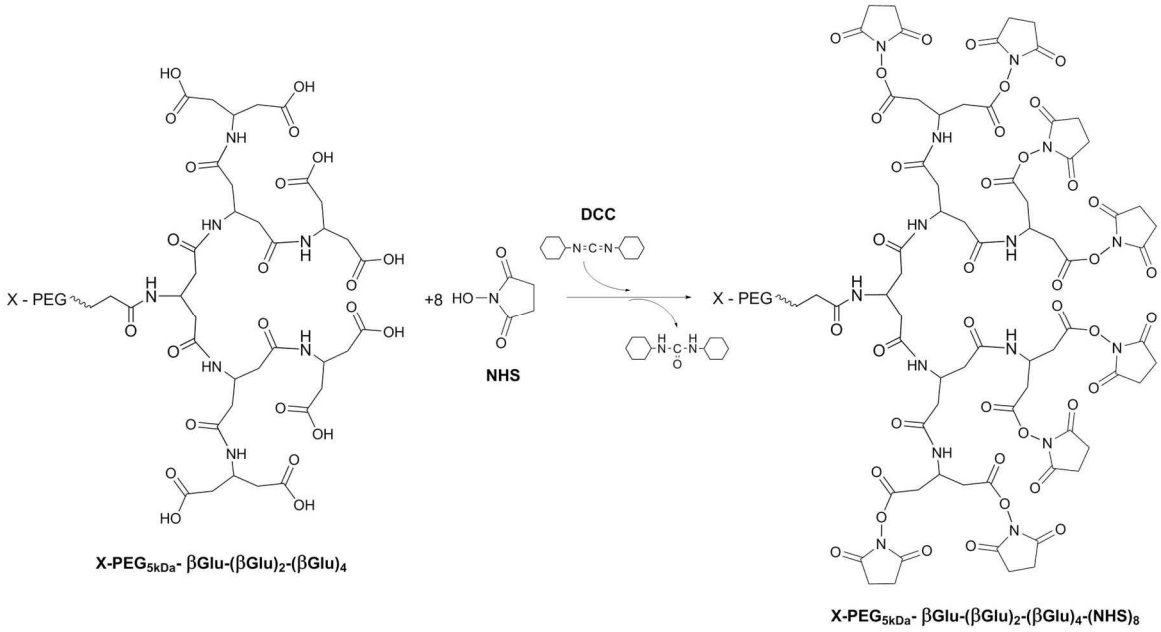

Figure 5.10: Activation via NHS/DCC of the carboxyl groups of X-PEG$_{5kDa}$-βGlu-(βGlu)$_2$-(βGlu)$_4$.

Table 5.9: Reagents amount and yield (% w/w) of the carboxyl groups activation of X-PEG$_{5kDa}$-βGlu-(βGlu)$_2$-(βGlu)$_4$.

PEG dendron-lipids derivatives	*mPEG-βGlu-(βGlu)$_2$-(βGlu)$_4$* [5862 Da]	*DCC* [206.33 Da] *NHS* [115.09 Da]	Yield (% w/w) of *mPEG-βGlu-(βGlu)$_2$-(βGlu)$_4$-(NHS)$_8$* [6638 Da]
mPEG-DSPE$_4$	1.22 g	1.03 g DCC 287 mg NHS	90% (1.1 g)
	Boc-NH-PEG-βGlu-(βGlu)$_2$-(βGlu)$_4$ [5596 Da]	*DCC* [206.33 Da] *NHS* [115.09 Da]	Yield % (w/w) of *Boc-NH-PEG-βGlu-(βGlu)$_2$-(βGlu)$_4$*-(NHS)$_8$ [6372 Da]
Boc-NH-PEG-DSPE$_4$	1.02 g	902 mg DCC 252 mg NHS	100% (1.03 g)

5.3.8 Distearoylphosphatidylethanolamine (DSPE) conjugation to the activated carboxyl groups of X-PEG$_{5kDa}$-βGlu-(βGlu)$_2$ or X-PEG$_{5kDa}$-βGlu-(βGlu)$_2$-(βGlu)$_4$

Firstly, the previously synthesized PEG dendons were characterized by MADI-TOF mass spectroscopy and then coupled to either 2 or 4 molecules of distearoylphosphatidylethanolamine (DSPE). The conjugation occurred by means of reaction between the activated carboxyl groups of PEG and the amino group of DSPE, leading to the formation of amide bonds (Figure 5.11 and Figure

5.12). Different molar excesses of DSPE (MW 748.1 Da) were exploited, depending on the final PEG dendron-lipids derivative that should be achieved.
1 equiv. of DSPE was used in excess for each activated carboxyl group toward which the coupling was addressed, according to Table 5.10Table 5.10. The only exception was the first synthesized derivative, Boc-NH-PEG_{5kDa}-$(DSPE)_2$, which was reacted with 1.1 equiv. of DSPE in excess for each activated carboxyl group of PEG.

DSPE was dissolved in $CHCl_3$ at 45°C, adjusting the pH between 8.0-9.0 with triethylamine (TEA). This solution was dropped into the solution of activated PEG dendron, previously dissolved in $CHCl_3$, at a final polymer concentration of 10% w/v. The reaction was stirred for 3 hours under reflux condition at 45°C (pH 8.0-9.0) and monitored by thin layer chromatography (TLC) to verify the decrease of free DSPE from the mixture reaction and the simultaneous formation of the product. The mixture reaction was eluted in 10 ml $CHCl_3$:MeOH 8:2 v/v (+20 µl H_2O) and stained with either iodine vapors (I_2) for PEG visualization or 0.2% w/v ninhydrin in EtOH solution for DSPE visualization. The reaction mixture was purified as reported in section 5.3.9.

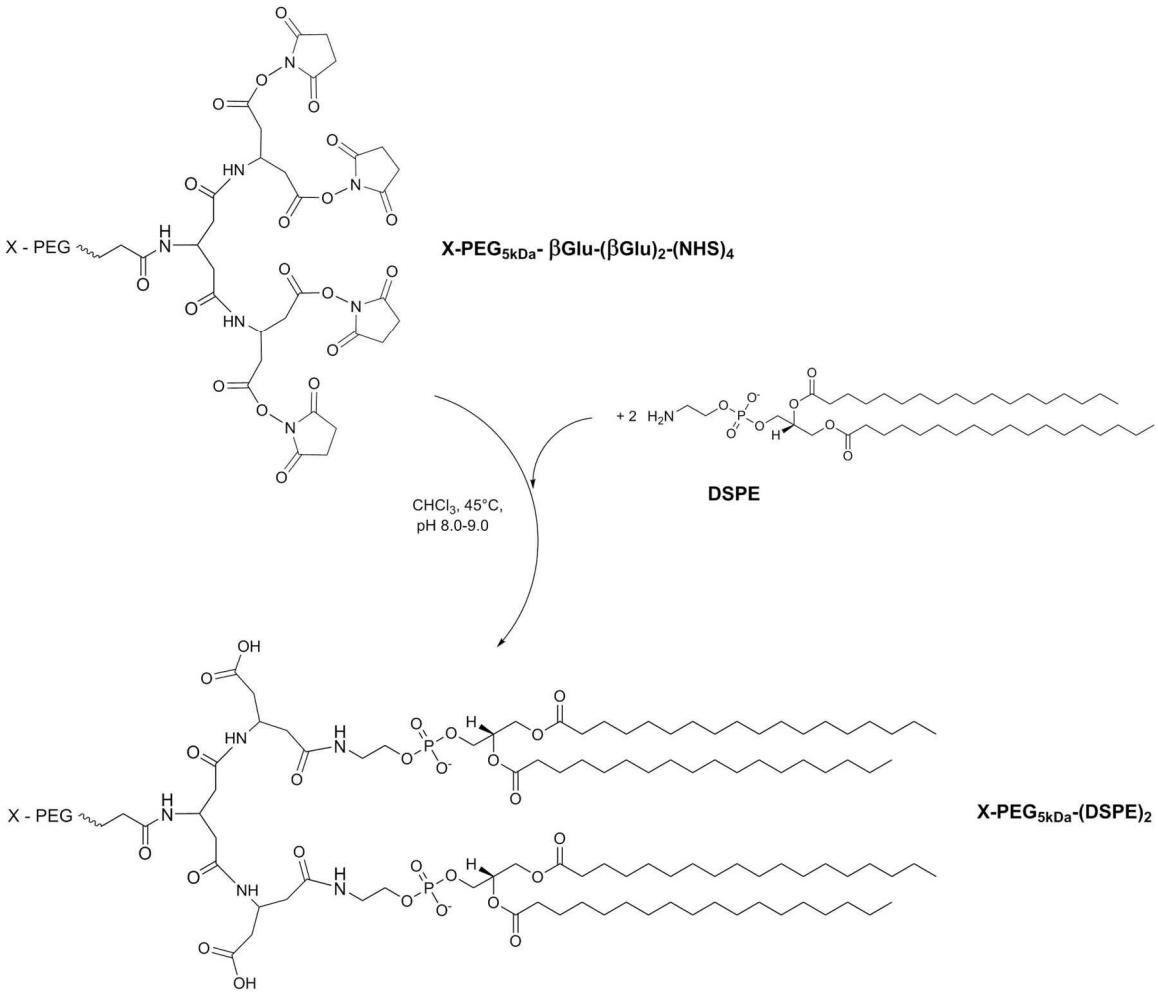

Figure 5.11: Synthesis of X-PEG_{5kDa}- $(DSPE)_2$.

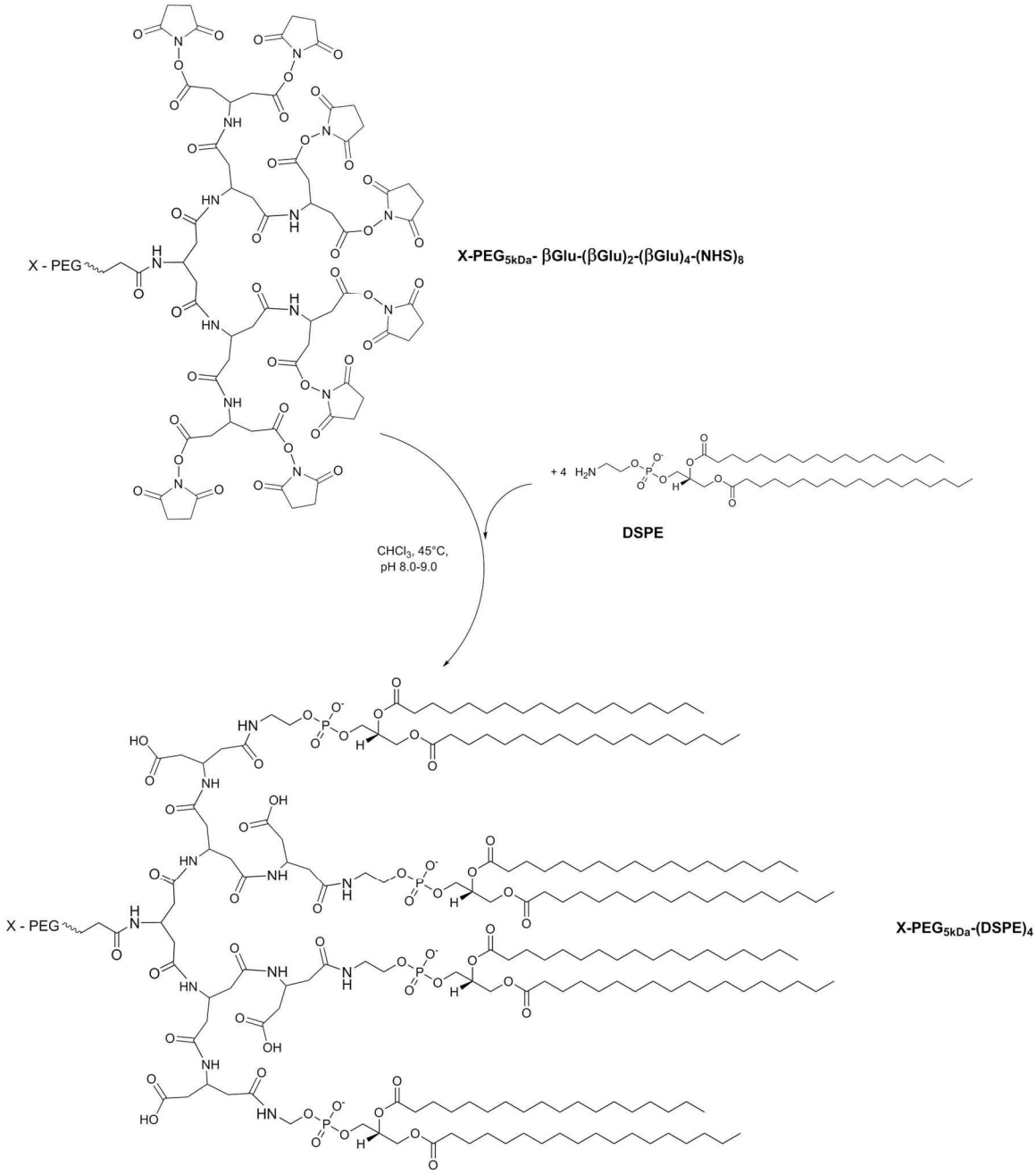

Figure 5.12: Synthesis of X-PEG$_{5kDa}$- (DSPE)$_4$.

Table 5.10: Reagents amount and yield (% w/w) of DSPE coupling. (a) PEG activation degree.

PEG dendron-lipids derivatives	*mPEG-βGlu-(βGlu)$_2$-(NHS)$_4$* [5734Da] *Boc-NH-PEG-βGlu-(βGlu)$_2$-(NHS)$_4$* [5468 Da]	*DSPE* [748.1 Da]	Yield (% w/w) of *X-PEG-(DSPE)$_2$*
mPEG-DSPE$_2$	558 mg (62%)[a]	146 mg	118% (658 mg)
Boc-PEG-DSPE$_2$	774 mg (63%)[a]	233 mg	99% (770 mg)
	mPEG-βGlu-(βGlu)$_2$-(βGlu)$_4$-(NHS)$_8$ [6638 Da] *Boc-NH-PEG-βGlu-(βGlu)$_2$-(βGlu)$_4$-(NHS)$_8$* [6372 Da]	*DSPE* [748.1 Da]	Yield % (w/w) of *X-PEG-(DSPE)$_4$*
mPEG-DSPE$_4$	1.1 g (65%)[a]	496 mg	95% (1.05 g)
Boc-NH-PEG-DSPE$_4$	0.49 g (64%)[a]	230 mg	92% (0.45 g)

5.3.9 Removal of unconjugated DSPE

Several approaches were employed to purify the unreacted DSPE from the reaction mixture containing the previously synthesized PEG dendron-lipids derivatives.

a) *Purification by means of lauroyl chloride.*

This method exploits the conjugation of lauroyl chloride, a saturated fatty acid, to free unreacted DSPE to increase its apolar content over the PEG dendron-lipids derivative and, thus, achieve a selective separation upon precipitation in organic solvent. The reaction occurs by formation of an amide bond between the acyl chloride moiety of lauroyl chloride and the primary amino group of DSPE (Figure 5.13).

Figure 5.13: Coupling reaction between the primary amino group of unreacted DSPE and the acyl chloride moiety of lauroyl chloride.

A preliminary test was performed on a linear Boc-NH-PEG_{5kDa}-DSPE, previously synthesized. Briefly, Boc-NH-PEG_{5kDa}-NHS (MW 5000 Da) was reacted in reflux with 1.8 equiv. of DSPE (MW 748.1 Da) in $CHCl_3$ at 45°C at a final polymer concentration of 10% w/v, adjusting the pH at 8.0-9.0 with TEA. The purification was performed by addition of 1.5 equiv. (with respect to the total amount of DSPE) of lauroyl chloride (MW 218.76 Da, *d*=0.946 g/ml) to the reaction mixture, which was stirred o/n at 45°C and pH 8.0-9.0. The chloroform solution was dropped into cold diethyl ether and after 1-2 hours at -20°C the precipitate was recovered by filtration and dried under vacuum o/n. The product was further dialyzed in a 100k MWCO float-a-lyzer against 50 mM NaCl and then H_2O over weekend. The solution was freeze-dried and characterized by ^1H NMR spectroscopy and ^1H DOSY NMR spectroscopy.

b) *Purification by means of precipitation in acetonitrile.*

This approach exploits the low solubility of DSPE in acetonitrile to remove the unreacted amount by precipitation [103]. Firstly, an attempt was made on the reaction mixture of Boc-NH-PEG_{5kDa}-$(DSPE)_2$. Right after the conjugation of DSPE to Boc-NH-PEG-βGlu$(βGlu)_2(NHS)_4$ in $CHCl_3$, as reported in section 5.3.8, the organic solvent was removed by rotary evaporation and the obtained film was resuspended in ACN at final concentration of 15 mg/ml. After 4 hours at -4°C the precipitate was separated by centrifugation at 10ʹ000 rpm and the supernatant containing the product was collected. Cycles of washing with ACN, storage at -4°C and subsequent centrifugation were repeated at least 3 times to recover as much product as possible. The supernatants were gathered and dried under vacuum, followed by dissolution in $CHCl_3$ and precipitation in cold diethyl ether. After 1-2 hours at -20°C the product was recovered by filtration, dried under vacuum o/n and characterized by ^1H NMR spectroscopy.

c) *Purification by flash column chromatography.*

First, a thin layer chromatograph (TLC) was performed to optimize the separation of the compounds in the reaction mixture. The best separation conditions were achieved by elution with $CHCl_3$:MeOH 8:2 v/v (10 ml + 20 µl H_2O), assessed by staining with iodine vapors (I_2) for PEG visualization and, separately, with 0.2% w/v ninhydrin in EtOH solution for DSPE visualization. Therefore, the reaction mixture was purified by flash column chromatography, using silica gel (40-63 µm mean particle size) as stationary phase. The product was eluted using as mobile phase mixtures of $CHCl_3$ and MeOH at increasing polarity, starting with 100 ml of $CHCl_3$, followed by 100 ml of $CHCl_3$:MeOH 9:1 v/v and, finally, 100 ml of $CHCl_3$:MeOH 8:2 v/v. The eluate was collected into fractions and monitored by TLC to evaluate in which fractions the desired product is contained. These fractions were gathered, dried under vacuum, dissolved in $CHCl_3$ and precipitate in cold diethyl ether. After 1-2 hours at -20°C the product was filtered, dried o/n under vacuum and finally characterized by ^1H NMR spectroscopy.

d) *Purification by means of dialysis in 20% v/v MeOH.*

DSPE is almost insoluble in every aqueous and organic solvent but moderately soluble in MeOH and $CHCl_3$. Therefore, at the end of the coupling reaction with DSPE, the organic solvent was removed under vacuum and the mixture reaction was resuspended in 20% v/v MeOH and dialyzed (3.5k MWCO) 1-2 days against the same medium to remove unreacted DSPE. Then the medium was replaced by H_2O and the dialysis was performed for 2 other days, followed by freeze-drying to recover the purified product and ^1H NMR spectroscopy characterization.

5.4 BOC-PEG DENDRON-LIPIDS DERIVATIVES MODIFICATION FOR LIGAND COUPLING

Two different chemistries of coupling were taken into consideration, involving the use of two different cross-linking agents (Figure 5.14).

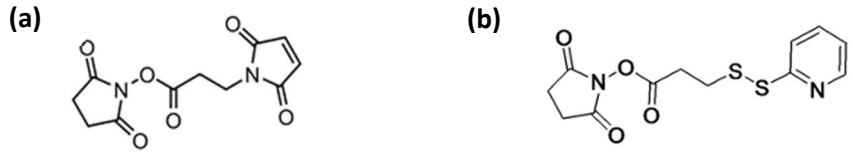

Figure 5.14: Chemical structure of the protein cross-linker employed to couple the Fab' of Trastuzumab to the synthetized PEG dendron-lipids derivatives: ***a)*** *BMPS and* ***b)*** *SPDP.*

The first one was N-Succinimidyl 3-[2-pyridyldithio]-propionate ester (SPDP), containing a NHS group that can react with PEG terminal amino group and a pyridinyldisulphide group, able instead to react with the sulfidryl group of Fab' with formation of a reversible disulphide bond. The second one was N-(β-maleimidopropyloxy)succinimide ester (BMPS), bearing a NHS group for the coupling to the PEG terminal amino group and a maleimide reactive group for the reaction with the sulfhydryl moiety of Fab', creating a non-cleavable thioether bond.

5.4.1 Removal of protecting group t-Boc from Boc-NH-PEG dendron-lipids derivatives

Firstly, the tert-butyloxycarbonyl protecting group (Boc) was cleaved from Boc-NH-PEG_{5kDa}-$(DSPE)_2$ (Figure 5.15Figure 5.15) and Boc-NH-PEG_{5kDa}-$(DSPE)_4$ (Figure 5.16) to free the primary amino group of PEG.

The polymer was dissolved in CH_2Cl_2:TFA 50:50 v/v at a final PEG concentration of 2% w/v and stirred for 20 minutes on ice bath (4°C). Next, TFA was removed by rotary evaporation washing at least 10 times with CH_2Cl_2. The product was dissolved in $CHCl_3$ and dropped into cold diethyl ether. After 1-2 hours the product was recovered by means of filtration and drying o/n under vacuum. The absence of the protecting group was assessed by ^1H NMR spectroscopy, whereas the percentage of free amino groups was calculated by Snyder and Sobocinski assay.

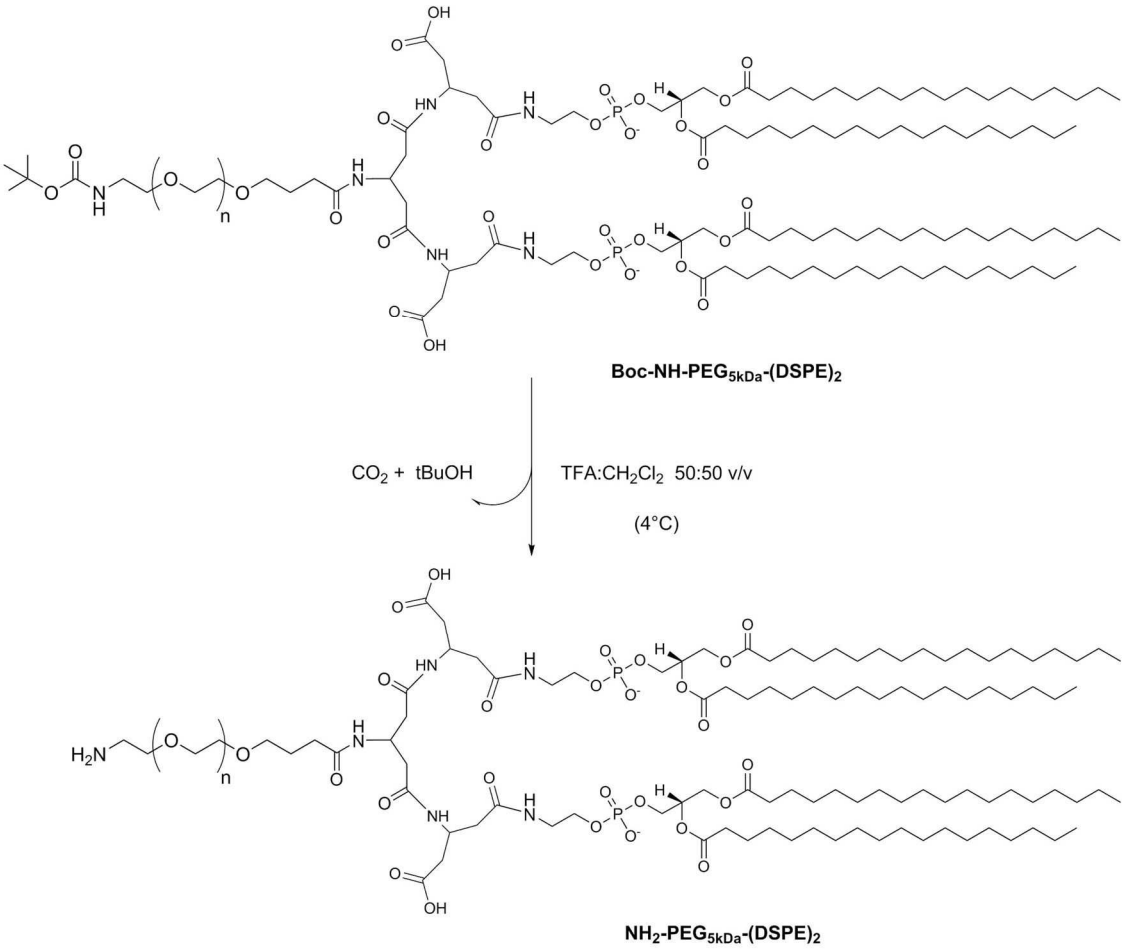

Figure 5.15: Removal of Boc protecting group from Boc-NH-PEG$_{5kDa}$-(DSPE)$_2$.

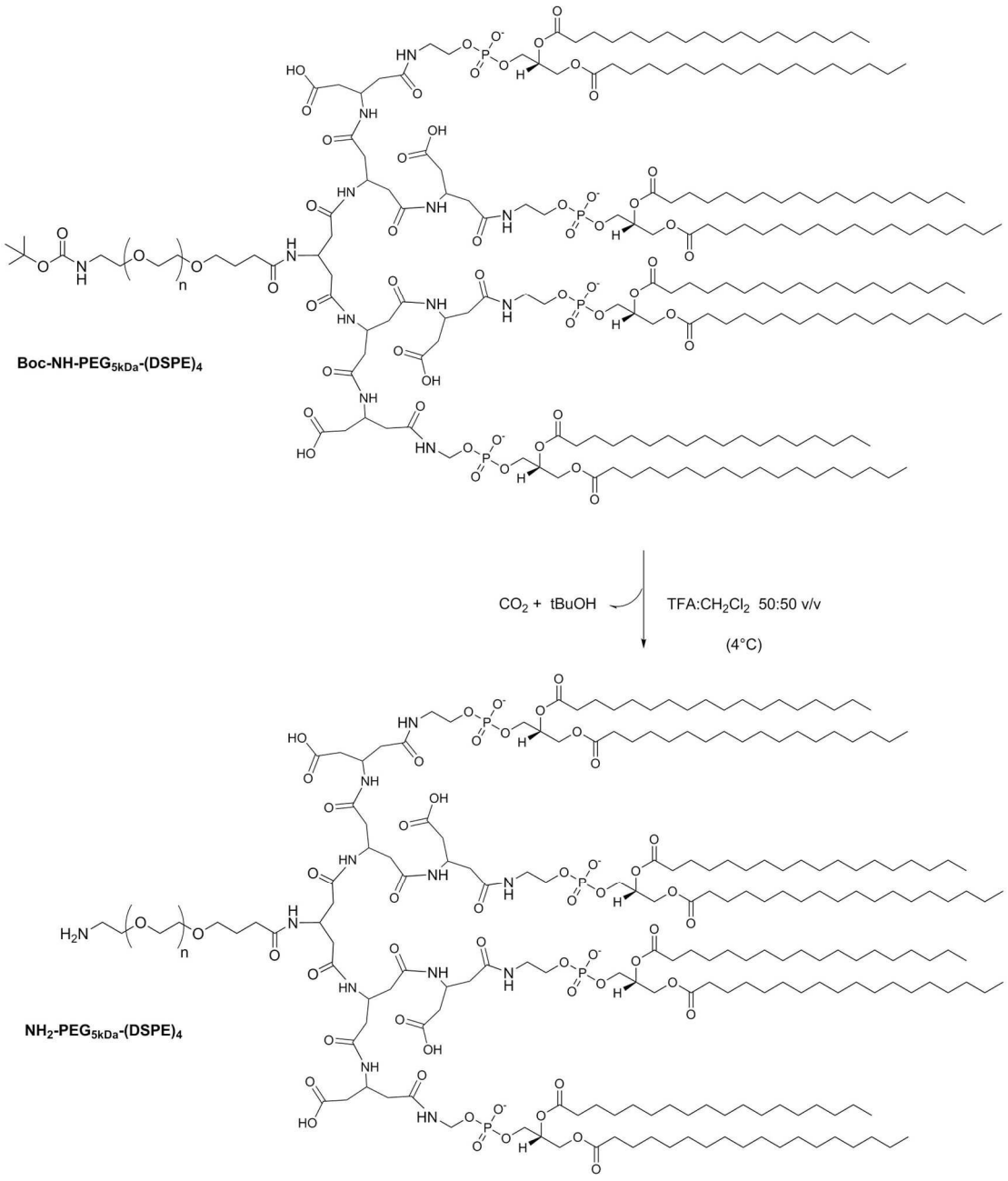

Figure 5.16: Removal of Boc protecting group from Boc-NH-PEG$_{5kDa}$-(DSPE)$_4$.

5.4.2 SPDP coupling to H_2N-PEG_{5kDa}-$(DSPE)_n$

H_2N-PEG_{5kDa}-$(DSPE)_2$ (7.6 µmol; MW 6542 Da) was reacted o/n at room temperature with 2 equiv. of SPDP (15.2 µmol; MW 312.36 Da) in borate 0.1 M/ACN 3:2 v/v, adjusting the final solution at pH 8.0 (Figure 5.17). Snyder and Sobocinski assay was performed to calculate the amount of free amino groups (unreacted PEG). ACN was evaporated under vacuum and the product was dialyzed against milliQ H_2O (3.5k MWCO) to remove unreacted SPDP, followed by recovery by freeze-drying

(44 mg, yield: 88% w/w). The lyophilized product was characterized by ^{1}H NMR spectroscopy by comparison with SPDP spectrum. Snyder and Sobocinski assay was repeated on the dried product as confirmation, to assess the amount of unreacted PEG (corresponding to the percentage of free primary amines).

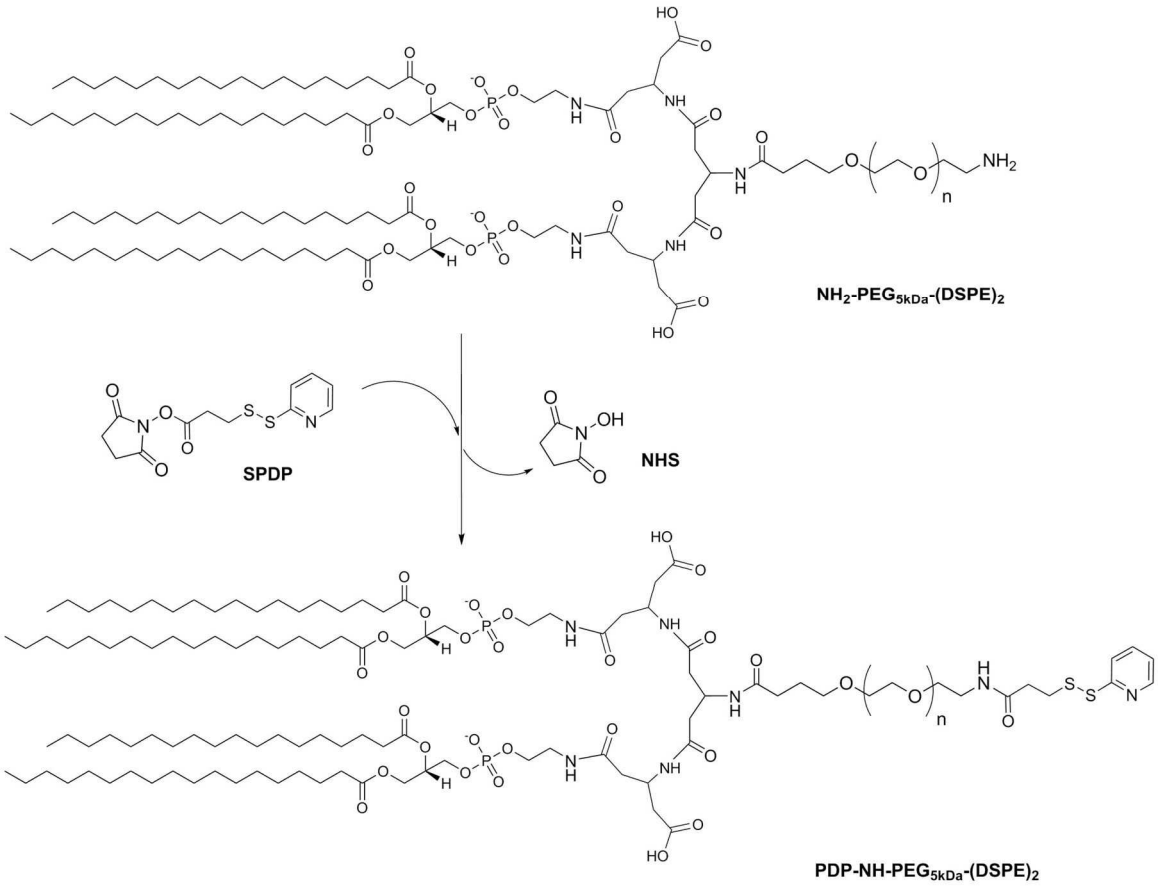

Figure 5.17: SPDP derivatization of H_2N-PEG_{5kDa}-$(DSPE)_2$.

5.4.3 BMPS coupling to H_2N-PEG_{5kDa}-$(DSPE)_n$

580 mg of H_2N-PEG_{5kDa}-$(DSPE)_2$ (MW 6542 Da) were reacted o/n in borate 0.1 M pH 8/ACN 2:3 v/v with 3 equiv. of BMPS (71 mg; MW 266.21 Da), previously dissolved in the smallest volume of DMSO, adjusting the reaction mixture at pH 8 (Figure 5.18). Snyder and Sobocinski assay was performed to evaluate the percentage of free amino groups. The product was dialyzed against milliQ H_2O (3.5k MWCO) to remove unreacted BMPS, followed by lyophilization. 531 mg of product were recovered (yield: 92% w/w) and characterized by ^{1}H NMR spectroscopy by comparison to BMPS spectrum. According to ^{1}H NMR spectroscopy BMPS coupling wasn't achieved in these conditions.

Successful coupling of the cross-linking agent was achieved by lowering the pH to 7.2.
Briefly, $H_2N\text{-}PEG_{5kDa}\text{-}(DSPE)_n$ was reacted for 45 minutes at room temperature with 8 equiv. of BMPS (MW 266.21 Da), previously dissolved in DMSO, in PBS pH 7.2/ACN 3:1 v/v adjusting the final solution at pH 7.2, according to Table 5.11.

Unreacted BMPS was removed by dialysis against milliQ H_2O (14k MWCO) at pH 6.0 to prevent maleimide hydrolysis. After lyophilization the recovered products were characterized by ^1H NMR spectroscopy and compared to BMPS spectrum. The final $BMP\text{-}NH\text{-}PEG_{5kDa}\text{-}(DSPE)_n$ derivatives were referred to as $MAL\text{-}PEG_{5kDa}\text{-}(DSPE)_n$ derivatives.

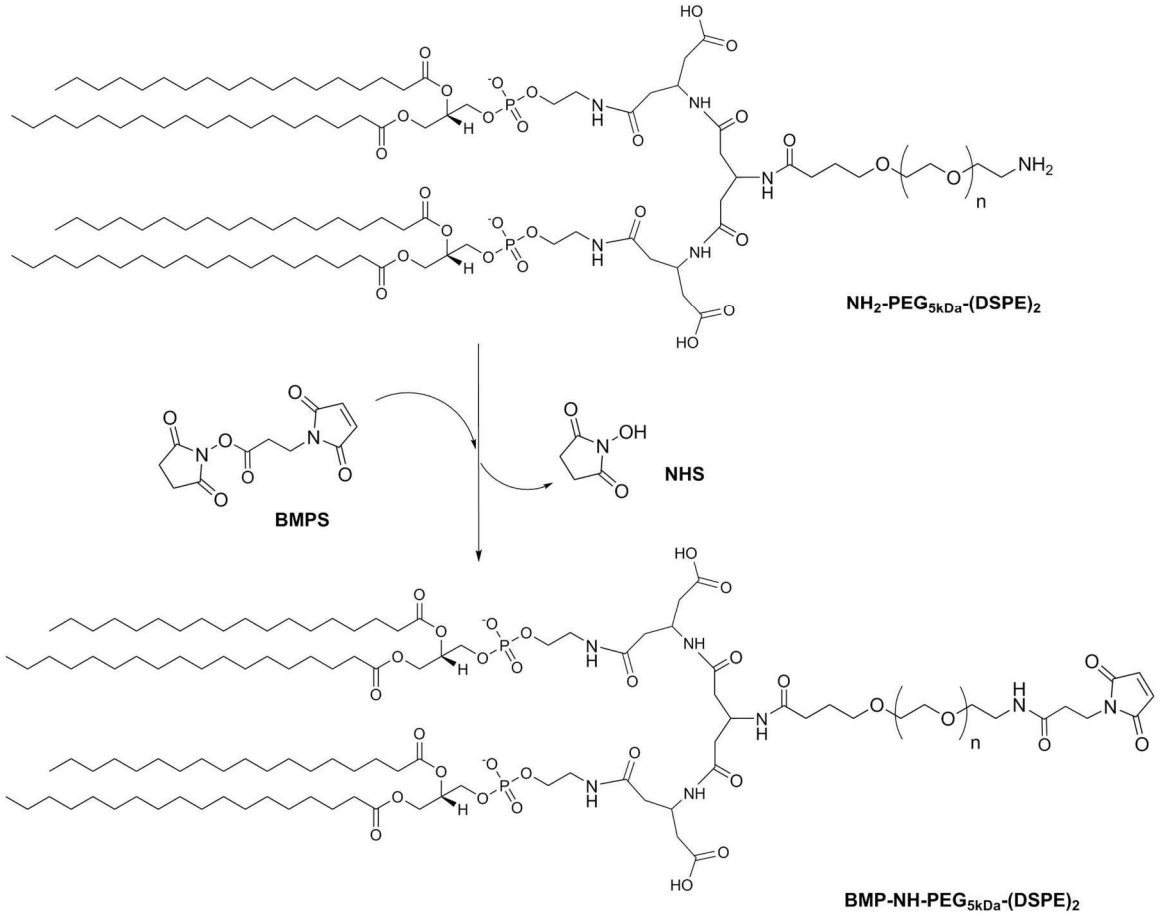

Figure 5.18: BMPS coupling to $H_2N\text{-}PEG_{5kDa}\text{-}(DSPE)_2$.

Table 5.11: Reagents amount and yield (% w/w) of BMPS coupling.

PEG dendron-lipids derivatives	*NH_2-PEG-(DSPE)$_2$* [6442 Da]	*BMPS* [266.21 Da]	Yield (% w/w) of *MAL-PEG-(DSPE)$_2$*
MAL-PEG-DSPE$_2$	168 mg	55.5 mg	90% (151 mg)
	NH_2-PEG-(DSPE)$_4$ [8420 Da]	*BMPS* [266.21 Da]	Yield % (w/w) of *MAL-PEG-(DSPE)$_4$*
MAL-PEG-DSPE$_4$	200 mg	50.6 mg	73% (145 mg)

5.5 PREPARATION OF Fab'

The fragment antigen-binding (Fab') is obtained starting from the whole antibody, through enzymatic digestion and following reduction of the disulphide bonds of the hinge region.

5.5.1 Proteolytic digestion of Trastuzumab by pepsin

Firstly, Trastuzumab was either dialyzed o/n (Slide-A-Lyzer G2 dialysis cassettes 3.5k MWCO, 500µl) against acetate buffer 0.1 M pH 3.8 or buffer exchanged with same buffer by means of 50k MWCO PES concentrators (3-4 centrifugations for 10 minutes x 10000 g). The mAb was then digested for 3 hours at 37°C by the proteolytic enzyme pepsin (Ɛ=1.47 $mL \cdot cm^{-1} \cdot mg^{-1}$), using an enzyme/substrate ratio of 1:50 w/w, yielding the $F(ab')_2$ fragment which corresponds to the antibody lacking the Fc (fragment, crystallizable) moiety (Figure 5.19). The reaction mixture was filtered for 1 min x 6000 rpm using Corning® Costar® Spin-X® centrifuge tube filters to remove any aggregate or particulate. $F(ab')_2$ was then purified by gel filtration though a Superose 12 10/300 GL column and eluting with PBS 1X pH 7.4, in isocratic conditions, at a flow rate of 0.5 ml/min (λ=280 nm). The collected purified peak was concentrated in Amicon® Ultra-15 centrifugal filter devices at 5000 g (4°C), quantified by BCA assay (as in section 5.5.3.2) and analysed by SDS-PAGE, ESI-TOF and MALDI-TOF.

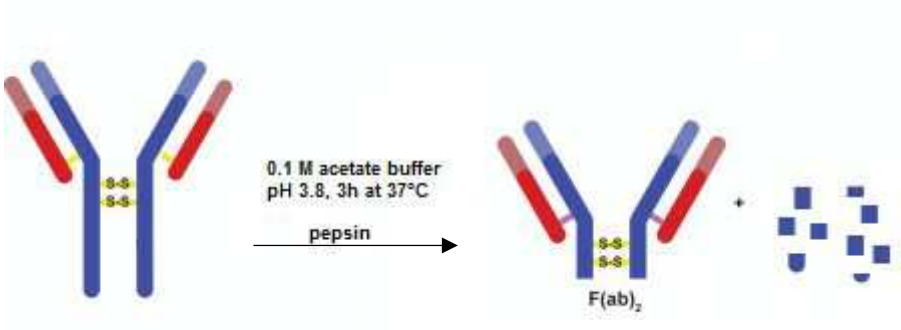

Figure 5.19: Trastuzumab proteolytic digestion by pepsin.

5.5.2 Reduction of F(ab')$_2$ to Fab'

The purified F(ab')$_2$ was treated with 10 mM cysteamine (MW 113.61 Da) for 30 minutes at room temperature to achieve selective partial reduction of the interchain disulphide bonds of the hinge region (joining the two Fab' fragments) as reported in Figure 5.20. Cysteamine removal was performed either by buffer exchanging on 30k MWCO PES concentrator or by gel filtration using a Superose 12 10/300 GL column and eluting at a flow rate of 0.5 ml/min, in isocratic conditions (λ=280 nm), with 50 mM sodium phosphate, 150 mM sodium chloride, 10 mM EDTA pH 5.0. The collected peaks were analyzed by SDS-PAGE, ESI-TOF and MALDI-TOF.

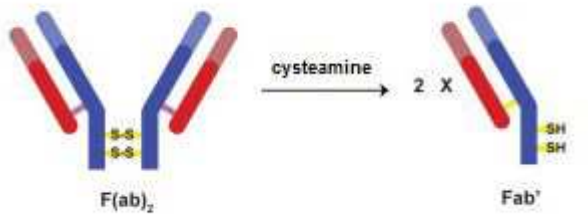

Figure 5.20: F(ab')$_2$ reduction to Fab' by means of cysteamine.

5.5.3 Determination of protein concentration

5.5.3.1 UV-Visible spectroscopy

Protein concentration was determined using a spectrophotometer and measuring the absorbance at 280 nm so far as the extinction coefficient was known: Trastuzumab Ɛ=1.43 ml·cm^{-1}·mg^{-1}; Trastuzumab Fab' Ɛ=1.35 ml·cm^{-1}·mg^{-1}. These coefficients were used also for the corresponding PEGylated proteins.

5.5.3.2 Bicinchoninic acid (BCA) assay

Protein concentration was assessed by a means of a colorimetric assay known as bicinchoninic acid (BCA) assay, based on the ability of protein's peptide bonds to reduce Cu^{2+} ions from the copper (II) sulfate (green solution) to Cu^{+}, in basic condition at 37°C. Upon copper reduction, two molecules of bicinchoninic acid chelate a Cu^{+} ion forming a purple-colored complex with a maximum absorbance at 562 nm (Figure 5.21). The degree of color shift from green to purple is proportional to the concentration of the protein in solution.

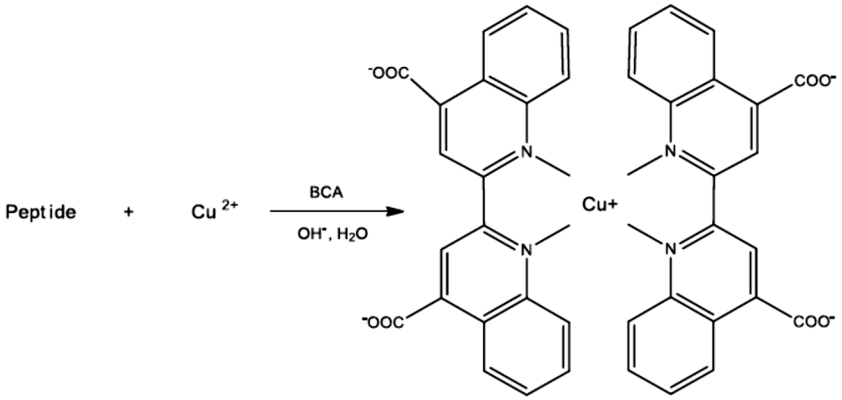

Figure 5.21: Complex formation between two molecules of bicinchoninic acid and a Cu^{+} ion.

Protein samples were prepared in triplicate, according to Table 5.12Table 5.12, and incubated with the working reagent for 30 minutes at 37°C, followed by absorbance measurement at λ = 562 nm using a UV–visible spectrophotometer. The working reagent (WR) is a solution of bicinchoninic acid solution and $CuSO_4$ 50:1 v/v, freshly prepared before incubation with the protein samples. Protein quantification is performed exploiting a calibration curve of bovine serum albumin (BSA, Ɛ=0.664 $ml \cdot cm^{-1} \cdot mg^{-1}$) at different concentrations, ranging from 0.1 to 1 mg/ml, previously prepared.

In case of $F(ab')_2$ the quantification was performed using a calibration curve prepared with Trastuzumab (Ɛ=1.43 $ml \cdot cm^{-1} \cdot mg^{-1}$) in the range of 0.1-0.6 mg/ml.

Table 5.12: Samples solutions for BCA assay.

	Blank	**Standards**	**Samples**
450 µl	WR	WR	WR
20 µl	H_2O	0.1-1 mg/ml BSA or 0.1-0.6 mg/ml Trastuzumab	Protein solution

5.5.4 Sodium dodecyl sulfate polyacrylamide gel electrophoresis (SDS-PAGE)

SDS-PAGE analysis was performed following the Laemmli method [104] using precast gels with a gradient of polyacrylamide percentage (4-15%). Protein samples were prepared by dissolving 5-10 µg of protein in non-reducing loading buffer, according to necessity, whereas PEG samples were prepared using 3-5 µg of polymer and the same amount of non-reducing loading buffer as the protein samples. Immunoliposomes samples, instead, where prepared using 10-20 µg of Fab'. Non-reducing loading buffer was composed of sodium dodecyl sulfate (SDS), glycerol,

bromophenol blue in TRIS-glycine buffer pH 6.8. All the samples were heated at 95°C for 5 minutes to favor protein denaturation. Once loaded into the wells of the gel, the electrophoretic run was performed setting a constant voltage of 200 V and decreasing the amperage during the run from 70 mA to 30 mA. After the run, the gel was first pre-treated with 0.1 M perchloric acid and then stained with iodine and barium chloride solution (in acidic conditions) for PEG visualization. Subsequently, iodine staining was removed using ascorbic acid, followed by proteins detection through Coomassie Brilliant Blue R250 staining. Unspecific staining of the polyacrylamide gel was removed using a de-staining solution composed of 40% MeOH and 7% acetic acid v/v.

5.5.5 Mass spectrometry

ESI–TOF mass spectrometry (ESI-MS) was performed using a Xevo G2-S Q-Tof (Waters Corporation, Milford, MA, USA) instrument, operating in positive ion mode (2.5 kV). Samples were dissolved in H_2O:ACN 50:50 v/v + 0.1% formic acid and 1-10 µg of sample were injected in the mass spectrometer by infusion at 0.05 ml/min.

MALDI TOF/TOF mass spectrometry was performed on a REFLEX time-of-flight (4800 Plus MALDI TOF/TOF, AB Sciex, Framingham, MA, USA) equipped with a SCOUT ion source, operating in positive linear mode. A pulsed UV laser beam (nitrogen laser, λ 337 nm) generates ions that are accelerated to 25 kV. A saturated solution of sinapinic acid in H_2O:ACN 50:50 v/v + 0.1% TFA v/v was used as solid matrix and mixed with an equal volume of sample. 1 µl of the resulting mixture was loaded on the plate and analyzed.

5.6 PEGYLATION OF Fab'

As soon as Fab' was prepared and purified as reported in section 5.5 it was immediately reacted with PEG, after protein concentration assessment by UV-Vis spectrophotometric measurement, to avoid as much as possible thiol oxidation, which might prevent the PEGylation.

5.6.1 Fab' PEGylation with MAL-PEG_{5kDa}-FITC

A preliminary Fab' PEGylation experiment was carried out using heterobifunctional MAL-PEG_{5kDa}-FITC, containing a maleimide group and labelled with fluorescein isothiocyanate (FITC).

Briefly, once Fab' was obtained, it was reacted o/n at 4°C with 8 equiv. of MAL-PEG_{5kDa}-FITC, adjusting the pH at 7.0. The reaction mixture was purified by gel filtration on a Superose 12 10/300

GL column eluting with PBS 1X pH 7.4, in isocratic conditions, at a flow rate of 0.5 ml/min. The collected peaks were characterized by SDS-PAGE.

5.6.2 Fab' PEGylation with PDP-NH-PEG$_{5kDa}$-(DSPE)$_n$

The reaction between the free sulfhydryl group of Fab' and PDP-NH-PEG$_{5kDa}$-(DSPE)$_n$ derivative led to the formation of a reversible disulphide bond (Figure 5.22Figure 5.22). Fab' was reacted o/n at 4°C with 9 equiv. of PDP-PEG$_{5kDa}$-(DSPE)$_2$ and the reaction mixture was purified by gel filtration on a Superose 12 10/300 GL column eluting with PBS 1X pH 7.4 (isocratic conditions) at a flow rate of 0.5 ml/min. Characterization of the collected peaks was performed by SDS-PAGE analysis.

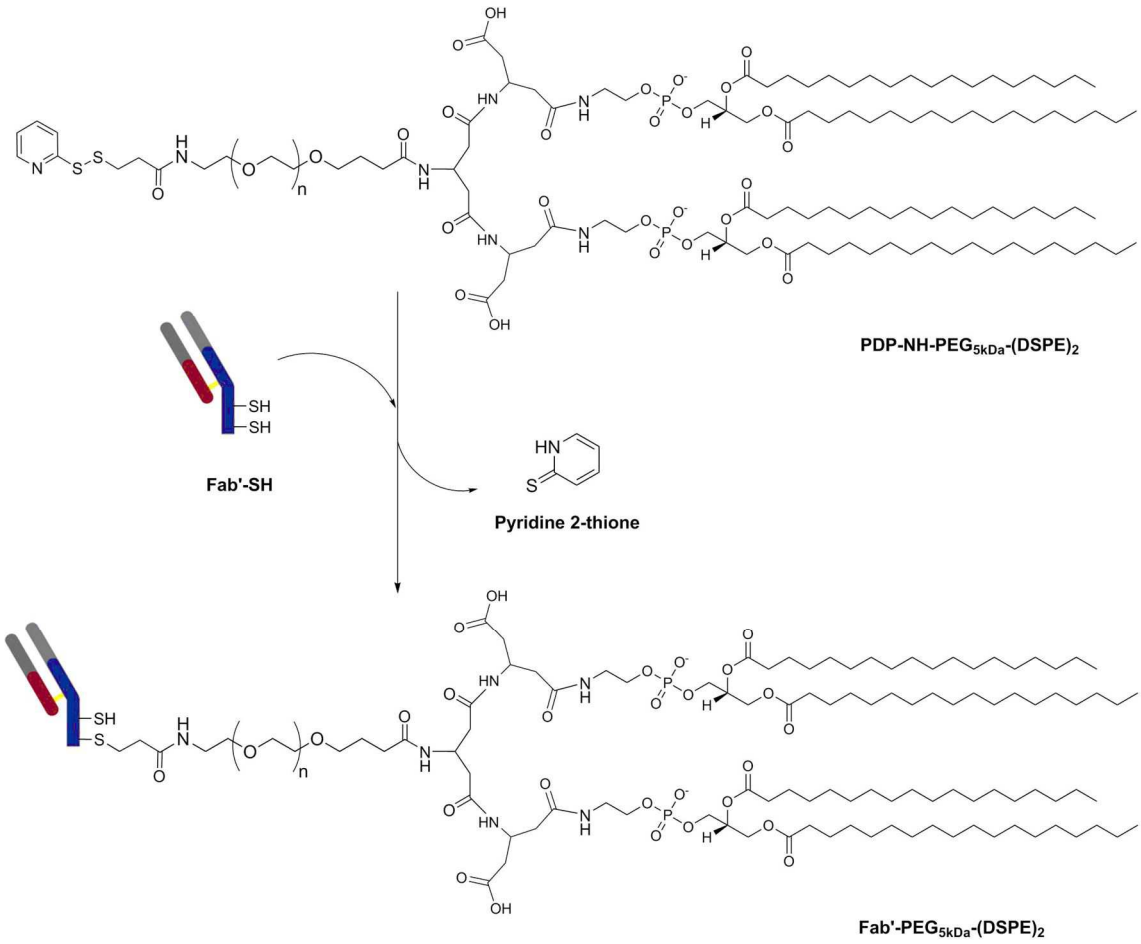

Figure 5.22: Coupling reaction of Fab' to PDP-NH-PEG$_{5kDa}$-(DSPE)$_2$.

To improve the yield of reaction Fab' was also reacted with a mixture of mPEG$_{5kDa}$-(DSPE)$_2$:PDP-PEG$_{5kDa}$-(DSPE)$_2$ 4:1 mol/mol. Briefly, mPEG$_{5kDa}$-(DSPE)$_2$ (2 µmol; MW 6808 Da) and PDP-PEG$_{5kDa}$-(DSPE)$_2$ (0.5 µmol; MW 6639 Da) were dissolved in $CHCl_3$ and dried under vacuum, followed by

rehydration in PBS pH 7.4 at 60-65 °C to achieve a 10 mM micellar solution. This mixture was immediately reacted o/n with the collected Fab' at a "PEG-PDP":"Fab'-SH" 10:1 molar ratio, adjusting the solution at pH 7.5-8.0. Protein samples were withdrawn at each reaction step and characterized together by SDS-PAGE analysis.

5.6.3 Fab' PEGylation with BMP-NH-PEG$_{5kDa}$-(DSPE)$_n$

The coupling was performed following the maleimide method [78], according to which the free sulfhydryl group of Fab' was reacted with the maleimide reactive moiety of BMP-NH-PEG$_{5kDa}$-(DSPE)$_n$ derivative, leading to the formation of a non-cleavable thioether bond (Figure 5.23).

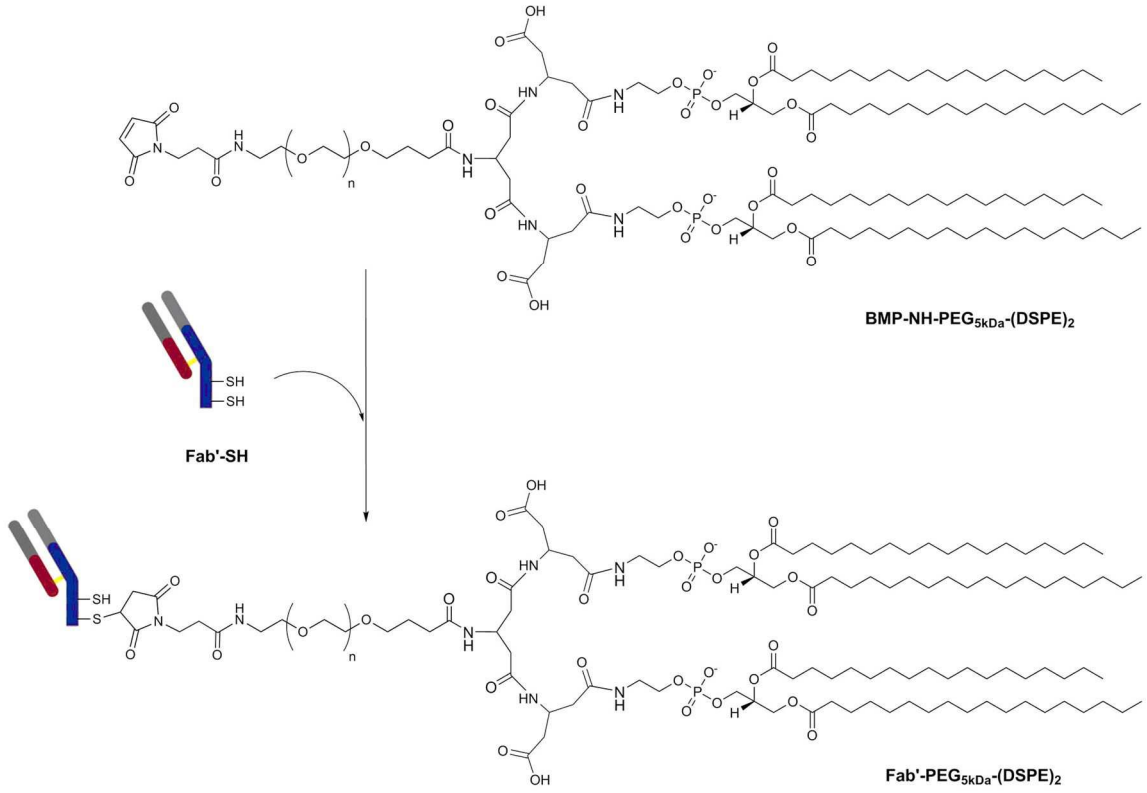

Figure 5.23: Example of Fab' coupling to BMP-NH-PEG$_{5kDa}$-(DSPE)$_2$ through maleimide method.

Since commercial MAL-PEG$_{5kDa}$-DSPE was used as reference for stealth immunoliposomes (SIL) formulation, for simplicity the polymers containing a reactive maleimide group were addressed as MAL-PEG$_{5kDa}$-(DSPE)$_n$. Fab' was reacted with MAL-PEG$_{5kDa}$-(DSPE)$_n$ at different "MAL-PEG":"Fab'-SH" molar ratio (with respect to the effective degree of maleimide derivatization of the polymer) depending on the derivative. 10 equiv. of MAL-PEG$_{5kDa}$-(DSPE), 12 equiv. of MAL-PEG$_{5kDa}$-(DSPE)$_2$

and 15 equiv. of MAL-PEG_{5kDa}-$(DSPE)_4$ were respectively reacted with Fab'. The polymer was dissolved in milliQ H_2O at 60-65°C right before the incubation with Fab' and the reaction was stirred o/n at room temperature, adjusting the solution at pH 7.0-7.5. The reaction output was characterized by SDS-PAGE analysis.

5.7 OPTIMIZATION Fab' PRODUCTION

Scale-up of Fab' production was required for immunoliposomes formulation.
Therefore, 17.3 mg/ml $F(ab')_2$ was reduced with 10 mM cysteamine (30 min, rt, 300 rpm) in PBS pH 7.4 and the resulting Fab' was purified by gel filtration on a Superose 12 10/300 GL column in isocratic conditions (flow rate of 0.5 ml/min) eluting with 150 mM NaCl, 50 mM NaH_2PO_4, 10 mM EDTA pH 5.0. The collected peaks were analysed by SDS-PAGE, showing excessive reduction of the interchain disulphide bond between heavy and light chains of Fab' (two bands at ~20-25 kDa).
With the aim of optimizing the yield of Fab' different reaction conditions were tested and characterized by SDS-PAGE analysis. Cysteamine removal was performed, unless otherwise specified, by buffer exchange through 10k MWCO PES concentrators using 150 mM NaCl, 50 mM NaH_2PO_4, 10 mM EDTA pH 5.0.

5.7.1 Fixed $F(ab')_2$ concentration

a) 0.5 mg of $F(ab')_2$, at a final concentration of 17.3 mg/ml in PBS pH 7.4, were reduced with different concentrations of cysteamine (50-25-10-5 mM). Each reaction was incubated for 30 min at room temperature.
   The reaction mixture with 10 mM cysteamine was performed in duplicate. The first reaction was purified by means of 10k MWCO PES concentrators, whilst the second one by gel filtration on a Superose 12 10/300 GL column in isocratic conditions, at a of flow rate of 0.5 ml/min, eluting with 150 mM NaCl, 50 mM NaH_2PO_4, 10 mM EDTA pH 5.0.

b) 0.35 mg of $F(ab')_2$, at a final concentration of 2 mg/ml in PBS pH 7.4, were reduced with 0.5-1-3 mM cysteamine at room temperature for 30 minutes. At fixed time points (15-30-60 minutes) protein samples of 0.11 mg were withdrawn from the reaction mixtures and purified from cysteamine.

5.7.2 Fixed cysteamine concentration

0.35 mg of $F(ab')_2$, at a final concentration of 2-5-10 mg/ml, were reduced with 10 mM cysteamine in PBS pH 7.4 by 30 minutes incubation at room temperature. The reactions were monitored after

10-20-30 minutes, by withdrawal of 0.11 mg of protein from the reaction mixtures and purification from cysteamine.

5.7.3 Other conditions

Some other reaction conditions were tested according to literature to assess whether and how the buffer, pH or temperature may influence the yield of reaction.

a) 0.5 mg of $F(ab')_2$ were reduced with 5 mM cysteamine at a final concentration of 2 mg/ml in 0.1 M phosphate buffer, 2 mM EDTA pH 6.0 at room temperature. 50 µg of protein were withdrawn after 15-30-60 minutes and 2-3-4-5-6 hours and purfied.

b) 0.1 mg of $F(ab')_2$ were reduced with 5 mM cysteamine at a final concentration of 2 mg/ml in 0.1 M phosphate buffer, 2 mM EDTA pH 6.0 at 20°C for 16 hours. Cysteamine removal was performed through 10k MWCO PES concentrators in 0.2 M acetate buffer including 1 mM EDTA, pH 4.5.

c) 0.1 mg of $F(ab')_2$ were reacted 30 minutes at room temperature with 10 mM cysteamine at a final concentration of 0.5 mg/ml in PBS pH 5.0 or in 20 mM sodium acetate, 100 mM Na_2SO_4 pH 5.0, both including 5 mM EDTA.

d) 0.5 mg $F(ab')_2$, at a final concentration of 10 mg/ml, were reduced with 50 mM cysteamine in 150 mM NaCl, 50 mM NaH_2PO_4, 10 mM EDTA pH 7.2, for 90 min at 37°C. 50 µg of protein were withdrawn after 30-60-90 minutes and purified.

5.8 SELECTIVE RE-OXIDATION Fab'

According to literature [105, 106], mild re-oxidation of the Fab' fragment, which underwent excessive reduction of the interchain disulphide bond between heavy and light chain, was attempted by means of $CuSO_4$.
Aliquots of $F(ab')_2$ were reduced with 10 mM cysteamine at a final concentration of 17.3 mg/ml in PBS pH 7.4 for 30 min at room temperature, followed by cysteamine purification through 10k MWCO PES concentrators. The reaction mixtures were then incubated with different amounts of $CuSO_4$ (0.001-0.01-0.1-1 mM). Protein samples of 10 µg were withdrawn at different time points and 0.1 M Na-EDTA pH 7.5 was added to stop the reaction.

5.8.1 Selective re-oxidation followed by Fab' PEGylation

Re-oxidized Fab' was reacted with MAL-PEG_{5kDa}-DSPE to check whether the reactivity of the thiol groups of the hinge region was preserved after the oxidation with $CuSO_4$, because the re-oxidation step might affect also the vicinal sulfhydryl groups used for PEG coupling.
17.3 mg/ml $F(ab')_2$ was reacted 30 min at room temperature with cysteamine 25 mM (for complete $F(ab')_2$ reduction) in PBS pH 7.4, followed by cysteamine removal through 10 MWCO PES concentrators using PBS pH 7.4. The protein solution was then incubated 3 hours at room temperature with 10 µM $CuSO_4$. Fab' purification was performed on a Superose 12 10/300 GL column equilibrated with 150 mM NaCl, 50 mM NaH_2PO_4, 10 mM EDTA pH 5.0 in isocratic conditions (flow rate: 0.5 ml/min). Fab' concentration was assessed through UV-VIS measurement at 280 nm, then Fab' was reacted o/n with 10 equiv. of MAL-PEG_{5kDa}-DSPE, adjusting the solution at pH 7.0. Each step was characterized by SDS-PAGE.

5.8.2 Fab' PEGylation followed by selective re-oxidation

Fab' was previously PEGylated with MAL-PEG_{5kDa}-DSPE and in a second step gently re-oxidized to recreate the disulphide bond between heavy and light chain.
17.3 mg/ml $F(ab')_2$ was incubated with 10 mM cysteamine, 30 min in PBS pH 7.4 at room temperature, followed by Fab' purification on a Superose 12 10/300 GL column equilibrated with 150 mM NaCl, 50 mM NaH_2PO_4, 10 mM EDTA pH 5.0 in isocratic conditions (flow rate: 0.5 ml/min). Protein concentration of the collected peak was assessed by absorbance measurement at 280 nm, followed by o/n incubation with 15 equiv. of MAL-PEG_{5kDa}-DSPE, adjusting the solution at pH 7.0. Subsequently, selective re-oxidation was performed for 3 hours using 10 µM $CuSO_4$, which was then removed by 10k MWCO PES concentrator. Each step was characterized by SDS-PAGE.

5.9 EVALUATION OF STORAGE CONDITIONS

$F(ab')_2$ at a final concentration of 17.3 mg/ml was reacted 30 min at rt with 10 mM cysteamine in PBS pH 7.4. It was decided to compare cysteamine purification by removal through PES 10k MWCO concentrators using either 150 mM NaCl, 50 mM NaH_2PO_4, 10 mM EDTA pH 5.0 or simple milliQ water. Furthermore, aliquots of purified Fab' were frozen with N_2 or kept at -20°C or at +4°C to verify if different storage conditions could affect the protein integrity.
Since excessive Fab' reduction after cysteamine purification with water wasn't evidenced it was decided to assess Fab' reactivity by o/n reaction at pH 7.0 (25°C) with 10 equiv. of MAL-PEG_{5kDa}-DSPE and characterization by SDS-PAGE analysis.

5.10 IMMUNOLIPOSOMES FORMULATION

Different approaches of liposomes preparation were exploited to assess the best formulation conditions. mPEG-lipid(s) derivatives or/and ligand-coupled PEG-lipid(s) derivatives were included in the formulation following the post-insertion method [68], either into drug-loaded pre-formed naked liposomes or into drug-loaded pre-formed stealth liposomes. According to literature, the transfer of PEG-lipids derivatives (micelles solution) to the liposomal vesicles occurs in a temperature- and time-dependent manner. Upon post-insertion stealth liposomes (SL), super stealth liposomes (SSL_n, n= n° of DSPE molecules (2 or 4) attached to PEG) and super stealth immunoliposomes ($SSIL_n$, n= n° of DSPE molecules (2 or 4) attached to PEG) were obtained.

5.10.1 Liposomes preparation

Liposomes were prepared by thin layer evaporation (TLE) technique. Briefly, the lipid mixture was dissolved in 2 ml of $CHCl_3$:MeOH 3:1 v/v in a round-bottom flask, followed by removal of the organic solvents by rotary evaporation, with formation of a lipid film, and o/n drying under vacuum. The lipid mixture was composed of hydrogenated soybean phosphatidylcholine (HSPC, MW 785 Da) and cholesterol (CHOL, MW 387 Da) in a 2:1 HSPC:CHOL molar ratio, either including or not 4% mol of $mPEG_{5kDa}$-$(DSPE)_n$ at a final molar ratio of 16:8:1 HSPC:CHOL:$mPEG_{5kDa}$-$(DSPE)_n$.

The lipid film was rehydrated for 1 hour at 60-65°C with 1-2 ml of 250 mM ammonium sulphate pH 5.0 using a rotary evaporator without vacuum. The obtained liposomal suspension was homogenized by repeated freeze and thaw cycles, followed by storage at 4°C for 45 minutes, sonication at 4°C for 15 minutes and subsequent hot extrusion (65°C) through polycarbonate filters of decreasing pore size (200-100-50nm). Liposomes mean size was assessed by dynamic light scattering (DLS) measurements as reported in section 5.2.2.
The external buffer was exchanged with PBS pH 7.4 by gel filtration on PD-10 desalting columns (containing Sephadex® G-25 medium), thus creating a pH gradient across the bilayer.
The final liposome concentration was determined by Stewart assay, described in section 5.2.3.

5.10.2 Doxorubicin loading

Liposomes collected after buffer exchange through PD-10 desalting column presented acidic aqueous medium inside (ammonium sulfate pH 5.0) and neutral external medium (PBS pH 7.4). This transmembrane pH gradient was exploited to encapsulate the model drug, doxorubicin (DXR, MW 580 Da), following the remote loading technique previously described in section 5.2.6.

Briefly, the total amount of DXR was previously dissolved in 0.9% w/v NaCl by stirring at 60°C, followed by incubation with the liposomal suspension at a ratio of 0.2:1 w/w DXR:HSPC for 1 hour at 60°C at 400 rpm. Free doxorubicin was then removed by gel-filtration on PD-10 desalting column (containing Sephadex® G-25 medium), eluting in PBS pH 7.4, and the integrity of the

vesicles was assessed by DLS measurements as reported in section 5.2.2. All these steps are performed in dark conditions to avoid degradation of DXR, which is a light-sensitive drug.

The concentration of the encapsulated DXR was determined by spectrophotometry, by proper dilution in methanol of an aliquot of drug-loaded liposomal suspension, vesicles disruption by addition of 5% v/v of 1M Triton X-100 and subsequent spectrophotometric absorbance measurement at 477 nm (ε_{477} = 13050 $M^{-1} \cdot cm^{-1}$ in methanol).

The encapsulation efficiency (EE%) was calculated as:

$$EE\% = \frac{\text{amount of entrapped DXR}}{\text{amount of total DXR}} \cdot 100$$

5.10.3 Post-insertion of PEG-lipid(s) derivatives

Two main post-insertional approaches were exploited to transfer mPEG-lipid(s) derivatives or/and ligand-coupled PEG-lipid(s) derivatives from a micellar solution of this compounds to the lipid bilayer of drug-loaded pre-formed liposomes. In the first approach the post-insertion was performed on naked liposomes, whereas in the second approach on PEG-coated liposomes. The thermodynamically favorable transfer to liposomes bilayer is driven by hydrophobic forces between lipid components.

5.10.3.1 1st approach

DXR-loaded liposomes composed of HSPC:CHOL 2:1 mol/mol were incubated for 1h at 60°C with a micelles solution of 2% mol $mPEG_{5kDa}$-$(DSPE)_n$ in PBS pH 7.4, thus providing stealth liposomes (SL). Subsequently, a micelles solution of Fab'-PEG_{5kDa}-$(DSPE)_n$ derivatives was incubated 1h at 60°C with SL in 0.05:1 PEG:HSPC molar ratio, thus providing stealth immunoliposomes (SIL) and super stealth immunoliposomes ($SSIL_2$ and $SSIL_4$ according to the number of DSPE molecules conjugated to PEG). Following transfer, the mixture was cooled and chromatographed over a Sepharose CL-4B column, equilibrated with PBS pH 7.4 buffer, to separate the liposomes from non-transferred micellar PEG-lipid(s) derivatives and free ligand. The purification and effective incorporation of Fab'-PEG_{5kDa}-$(DSPE)_n$ into the bilayer were assessed by SDS-PAGE, whereas the quantification of the incorporated ligand-coupled PEG-lipid(s) derivative was performed by micro-BCA assay, as described in section 5.10.4. The final liposomal suspension was concentrated upon centrifugation in 50k MWCO Amicon concentrator devices and the lipid concentration was determined by Stewart assay following the protocol reported in section 5.2.3. Further characterization was obtained by TEM analysis, as reported in section 5.10.5.

Alternatively, a similar approach was carried out involving the simultaneous post-insertion of both $mPEG_{5kDa}$-$(DSPE)_n$ and Fab'-PEG_{5kDa}-$(DSPE)_n$ micellar solutions, using the same molar amounts previously described and comparing the final outcome with respect to the sequential post-insertion approach.

5.10.3.2 2nd approach

The post-insertion was performed on DXR-loaded stealth (SL) or super stealth (SSL_n) liposomes composed of HSPC:CHOL:mPEG-$(DSPE)_n$ 16:8:1 molar ratio. The obtained liposomes were incubated for 1 hour at 60°C with a micelles solution of 2% mol Fab'-PEG-$(DSPE)_n$, previously reacted 15 min (25°C) with 2 equiv. of thioglycolic acid (MW 92.12 Da, *d*=1.325 g/ml) to block unreacted maleimide groups, thus providing SIL, $SSIL_2$ and $SSIL_4$. Reference stealth and super stealth liposomes (i.e. SL, SSL_2 and SSL_4) were instead obtained by incubation with 2% mol of the corresponding mPEG-$(DSPE)_n$. The liposomal suspension was cooled and subsequently purified by elution in a Sepharose CL-4B column, equilibrated with PBS pH 7.4 buffer, to separate non-transferred micellar PEG-lipid(s) derivatives and free ligand. Characterization by SDS-PAGE allowed to verify the effective incorporation of Fab'-PEG_{5kDa}-$(DSPE)_n$ into the bilayer. Micro-BCA assay was used to quantify the amount of transferred ligand-coupled PEG-lipid(s) derivative, as in section 5.10.4. Liposomes were additionally characterized by TEM, as reported in section 5.10.5.

5.10.4 Ligand quantification by micro-BCA assay

Micro-BCA assay is a high sensitivity test for protein quantification, which can be used to measure very dilute protein concentrations (ranging from 0.5 to 30 µg/ml) in very small sample volumes.
The assay works as the classical BCA assay reported in section 5.5.3.2, leading to the formation of a purple-colored complex with a maximum absorption at 562 nm and the coloration intensity is proportional to the protein concentration. This assay was used to quantify the amount of transferred ligand-coupled PEG-lipid(s) derivative into the liposome bilayer.

Samples were prepared in triplicate at different dilutions, following Table 5.13, and the blank was prepared for each dilution using a solution of DXR-loaded stealth liposomes (DXR-SL) at the same DXR concentration of the sample.
1 part (100 µl) of sample solution was mixed with 1 part (100 µl) of working reagent (WR) and after 1 hour of incubation at 60°C the absorbance at 562 nm was recorded and the protein concentration was determined by comparison to a standard curve.
The standard curve was obtained by serial dilution from a stock solution of bovine serum albumin (BSA, ε= 0.664 ml $\cdot$ cm^{-1} $\cdot$ mg^{-1}) and ranging from 30 µg/ml to 5 µg/ml.

The working reagent is obtained by mixing:

- solution A: sodium carbonate, sodium tartrate, sodium bicarbonate in 0.2 M NaOH, pH 11.25;

- solution B: 4% w/v bicinchoninic acid solution, pH 8.5;
- solution C: 4% w/v copper(II) sulfate, pentahydrate solution.

Working reagent is prepared by mixing 25 parts of A with 25 parts of B and subsequently by adding 1 part of C.

Table 5.13: Samples and calibration curve standards preparation.

	Blank (calibration curve)	BSA standards	Blank (samples)	Samples
100 µl	WR	WR	WR	WR
100 µl	H_2O	5-30 µg/ml BSA	DXR-SL	SIL/$SSIL_n$

The Fab' amount of each liposomal formulation was expressed as µg Fab'/µmol HSPC.

5.10.5 Transmission Electron Microscopy (TEM)

One drop of 0.2 mg/ml liposomal suspension (about 25µl) was placed on 400 mesh holey film grid. The samples were diluted with deionized water to avoid as much as possible salts interference. After staining with 1% uranyl acetate the sample was observed with a Tecnai G^2 (FEI) transmission electron microscope operating at 100 kV. Images were captured with a Veleta (Olympus Soft Imaging System) digital camera.

5.11 *IN VITRO* EXPERIMENTS

5.11.1 Long-term stability studies

In vitro stability studies were performed by evaluating the homogeneity of the liposomal suspensions over time, both in term of vesicles mean size and polydispersity.

Specifically, samples of each liposomal formulation (300 µl, 3 mM) containing 0.05% w/v NaN_3 were incubated over time at different temperatures (4-25-37°C). DLS measurements were performed at predetermined time points to assess the liposomes mean size (hydrodynamic volume) and polydispersity index (PdI) and, thus, evaluate the overall physical stability of the formulation.

5.11.2 Drug release experiments

The liposomal release of DXR was quantified by the fluorescence dequenching of self-associated DXR in liposomes upon dilution outside the liposomes [100].
500 µl of each liposomal formulation (1 mM) were incubated for 16 h at 37°C, during which the leakage of DXR was investigated by measuring the increase of fluorescence intensity every 30 min, using a spectrofluorometer (λ_{ex}= 470nm; λ_{em}= 584nm). At the end of each analysis liposomes were disrupted by addition of 5% v/v of 1 M Triton X-100 to calculate the 100% dequenched DXR (total DXR). The experiments were performed on a Jasco FP-6500 spectrofluorometer, setting the analysis conditions as reported in Table 5.14.

Table 5.14: Spectrofluorometer settings.

Analysis	→	Long time-course measurement
Duration	→	16 hours
Data pitch	→	30 minutes
$\lambda_{excitation}$	→	470 nm
$\lambda_{emission}$	→	584 nm
Band with (excitation)	→	5 nm
Band with (emission)	→	10 nm
Sensitivity	→	Medium
Response	→	0.5 sec
Internal temperature (peltier)	→	37°C

5.11.3 Cytotoxicity studies

The cytotoxic effect of targeted doxorubicin-loaded liposomal formulations (SIL-DXR and $SSIL_2$-DXR) was evaluated and compared to non-targeted doxorubicin-loaded liposomes (SL-DXR) with respect to empty stealth liposomes (SL) and free DXR (positive control). Human breast ductal carcinoma cell line (BT-474), overexpressing HER-2, were chosen to perform the studies.

5.11.3.1 Cell viability evaluation by Crystal Violet assay

BT-474 cells were cultured in high glucose D-MEM medium, enriched with 10% FBS (fetal bovine serum) and 1% Pen Strep (Penicillin-Streptomycin mixture), at 37°C and 5% CO_2. 4000 cells/well

in 100 µl were seeded in 96-well clear flat-bottom plates and let adhere overnight. The following day the cells were treated in triplicate by adding 100 µl of DXR, SL, SL-DXR, SIL-DXR and $SSIL_2$-DXR at a final doxorubicin concentration of 1 µM, 10 µM and 50 µM, including untreated cells as negative control. The plates were incubated at 37°C in a humidified incubator with 5% CO_2.

After 1 h, 12 h and 24 h of treatment, the culture medium was removed and replaced with complete fresh medium. Cells were incubated again at 37°C, up to 84 h (short incubation) or 132 h (long incubation). Next, cells were washed with PBS and eventually fixed with 100 µl of 10% formalin for 15 minutes and stored in PBS until analysis time. After PBS removal, cells were stained with 100 µl of crystal violet staining solution for 20 minutes at room temperature, followed by washing with water and air-drying of the plates. 100 µl of 10% acetic acid were added to each well and the plates were put on a shaker for 20 minutes at room temperature. Optical Density (OD) was measured at 590 nm using a microplate spectrophotometer. The assay relies on the affinity between the dye and the external surface of the DNA double helix, so the amount of dye absorbed depends on the total DNA content in the culture, thus allowing the estimation of the number of viable cells in the culture.
In addition, the IC50 of each liposomal formulation and free doxorubicin was assessed by performing a Crystal Violet assay on BT-474 cells treated for 24 h and incubated for additional 12 h in culture medium. For this experiment, cells were seeded in 96-well clear flat-bottom plates (5000 cells/well) and the treatments were performed in triplicate at different doxorubicin concentrations, namely 0.01 µM, 0.1 µM, 1 µM, 10 µM and 50 µM in DXR. The treatment with empty SL was performed by using the corresponding phospholipids equivalents to SL-DXR.

5.11.3.2 Activation of caspase 3-mediated apoptotic pathway by Western Blot

Western blot analysis was performed to evaluate the expression of Cleaved Caspase 3, which is considered to be the major executioner caspase in the apoptotic cascade, with respect to uncleaved Caspase 3 protein expression in BT-474 cells treated with each liposomal formulation and free doxorubicin, compared to untreated cells. BT-474 cells were cultured as in section 5.11.3.1, then 100000 cell/well where seeded in 6-well clear flat-bottom plates and let adhere overnight. Cells were treated for 6 h at 10 µM in doxorubicin at 37°C in a humidified incubator with 5% CO_2, then the medium was removed and replaced with fresh medium, followed by incubation at 37°C for additional 24 h.

At the end of the 24h of incubation the medium was removed, and cells were washed with PBS. Next, cells were treated on ice with a lysis buffer composed of 10 mM PMSF (phenylmethylsulfonyl fluoride; protease inhibitor) in isopropanol diluted with RIPA buffer 1X (containing Tris-HCl and sodium deoxycholate) for protein extraction. Cell lysates were collected and centrifuged for 30 minutes at 14000 rpm. The protein concentration of each supernatant was assessed by BCA assay (section 5.5.3.2). Briefly, this assay was performed in a 96-well clear flat-bottom plate by mixing 10 µl of protein solution with 190 µl of working reagent (bicinchoninic acid solution and

$CuSO_4$ 50:1 v/v). After 30 minutes of incubation at 37°C, absorbance measurement at λ = 562 nm was performed using a UV–visible microplate spectrophotometer. Protein quantification was performed exploiting a calibration curve of bovine serum albumin (BSA, Ɛ=0.664 $ml \cdot cm^{-1} \cdot mg^{-1}$) ranging from 0.025 to 2 mg/ml. At this point, 25 µg of proteins were loaded in each lane of a 10% polyacrylamide gel and subjected to SDS-PAGE electrophoresis. The bands were transferred to a 0.45 µm nitrocellulose membrane at 100V for 60 minutes in the presence of 25 mM Tris, 192 mM glycine and 10% MeOH. Following the transfer, the membrane was stained with ponceau solution for a preliminary evaluation of protein transfer, then it was blocked for 45 minutes at room temperature with 5% dry milk in PBST containing 0.1% Tween 20 in PBS-buffered saline 1X, and washed 3 times for 10 min with PBST. The membrane was then incubated overnight at 4°C with a rabbit polyclonal antibody against Cleaved Caspase 3 at 1:1000 dilution in PBST containing 5% BSA. At the end of the incubation, the membrane was rinsed with PBST and incubated for 1 h at room temperature with the secondary anti-rabbit antibody (1:10000 in 5% dry milk in PBST). Reactive proteins were stained with the Amersham ECL Plus Western Blotting Detection System (GE Healthcare Europe GmbH, Milan, Italy) and chemiluminescence was measured with a Fusion Solo S instrument (Vilber Lourmat).

The membrane was then stripped using 0.5 M NaOH and blocked again with 5% dry milk in PBST, followed by overnight incubation at 4°C with a rabbit polyclonal antibody against Caspase 3 at 1:1000 dilution in PBST containing 5% BSA. The membrane was then rinsed with PBST and incubated for 1 h at room temperature with the secondary anti-rabbit antibody (1:10000 in 5% dry milk in PBST). Reactive proteins were stained with ECL and visualized with Fusion Solo S instrument. Finally, the membrane was rinsed with PBST and incubated o/n at 4°C with a mouse monoclonal antibody against β-actin (used as a loading control) at 1:1000 dilution in PBST containing 5% BSA. After rinsing in PBST the membrane was incubated with the secondary anti-mouse antibody (1:10000 in 5% dry milk in PBST), followed by staining with ECL and chemiluminescence visualization. The bands relative to cleaved caspase 3 and caspase 3 were quantified by using ImageJ software and normalized to that of β-actin. The ratio Cleaved caspase3/Caspase 3 was also calculated.

5.12 *IN VIVO* EXPERIMENTS

5.12.1 Ethics statement

The study protocol was approved by the Ethics Committee of the University of Padova and the Italian Ministry of Health (938/2016 PR obtained on October 10, 2016), and animals were handled in compliance with national (Italian) Legislative Decree 26/2014 guidelines and with the “Guide for the Care and Use of Laboratory Animals” by the National Research Council of the National Academies.

5.12.2 Pharmacokinetics in rats

In vivo pharmacokinetic studies were carried out in female Sprague Dawley rats (140-190 g). The rats were randomly divided in four groups of 3 rats each. A dose of 2.5 mg/kg in DXR of either free drug or DXR-loaded liposomal formulation (SL, SIL, $SSIL_2$) was administered via tail vein to the rats previously anesthetized with isoflurane gas (mixed with O_2 in enclosed cages). At scheduled time points blood samples (~200 µl) were collected from the tail into heparin treated tubes and thereafter immediately centrifuged 15 min x 1500 g to separate plasma. DXR was extracted by treating 50 µl of plasma with 10 µl of 1M Triton X-100 (for liposome disruption) and 580 µl of 81 mM HCl in isopropanol to allow plasma proteins precipitation. After o/n incubation at 4°C, samples were centrifuged 3 min at 3000 rpm and the supernatants were analyzed by fluorometric measurements (λ_{ex}= 470nm; λ_{em}= 584nm). The concentration of DXR in each plasma sample was extrapolated through a calibration curve of standards solutions of either DXR (0.01 - 0.25 µg/ml) or DXR-loaded stealth liposomes (0.1 - 5 µg/ml) for the liposomal formulations.

The data were analyzed by applying a bicompartmental model using PKSolver 2.0 software.

5.12.3 Organ toxicity evaluation

The animals used for the pharmacokinetic studies (section 5.12.2), subjected to single tail vein injection of either DXR or DXR-loaded liposomal formulation, were sacrificed 48 hours after the drug administration. The main organs (liver, kidneys, heart, spleen, brain, lungs) were immediately excised, washed with 50 mM Tris, 150 mM KCl, 2 mM EDTA pH 7.4, cut into pieces, frozen in liquid N_2, and stored at -80°C until use. Furthermore, one piece of each organ was placed in 10% formalin for histological examination.
Quantification of the gene expression of three inflammatory cytokines and histological examination was performed on the collected tissues.

5.12.3.1 Gene expression quantification by qRT-PCR

The gene expression of three cytokines involved in the inflammatory response, namely interleukin 1β (IL-1β), interleukin 6 (IL-6) and tumor necrosis factor α (TNFα), was evaluated to assess and compare the inflammatory state of each collected organ after the administration of the liposomal formulations. This evaluation was performed by RNA extraction from the tissues and subsequent mRNA quantification.

5.12.3.1.1 mRNA extraction

mRNA extraction from tissues was performed using SV Total RNA Isolation System Promega kit.

According to the protocol, about 200 mg of tissue were homogenized though the probe of a T-25 digital ULTRA-TURRAX homogenizer in a sterile Eppendorf tube with 1 ml of RNA lysis buffer (4 M guanidine thiocyanate, 0.01 M Tris (pH 7.5), 0.97% β-mercaptoethanol). 175 µl of the final sample were transferred into a new tube and added of 350 µl of RNA dilution buffer, then mixed and incubated 3 minutes at 70°C. After centrifugation at 13000 g for 11 minutes, the supernatant was collected and transferred into a new tube, followed by addition of 300 µl of 95% v/v EtOH. The final mixture was properly mixed and purified by centrifugation (60 seconds x 13000 g) on a spin column, discharging the eluate. 600 µl of RNA wash solution (60 mM potassium acetate, 10 mM Tris-HCl (pH 7.5) in 60% v/v EtOH) were added, repeating the centrifugation for 60 seconds x 13000 g and throwing again the eluate.

50 µl of DNase incubation mix were added to the column to digest contaminating genomic DNA. This mix was composed of 40 µl of Yellow Core Buffer (0.0225 M Tris pH 7.5, 1.125 M NaCl, 0.0025 % w/v yellow dye), 5 µl of 0.09 M $MnCl_2$ and 5 µl of DNase I. After 15 minutes the DNase reaction was stopped by addition of 200 µl of DNase Stop Solution (2 M guanidine isothiocyanate, 4 mM Tris-HCl (pH 7.5) and 57% v/v EtOH) and centrifuging 60 seconds x 13000 g.

The column was washed twice with RNA Wash Solution, using different volumes: 600 µl the first time, centrifuging 60 seconds x 13000 g, and 250 µl the second time, centrifuging 2 minutes x 13000 g, discharging the eluates. Subsequently, the RNA was collected by elution with 100 µl of Nuclease-free water and centrifugation for 60 seconds at 13000 g, preserving the eluate which was stored at -80°C until use.

5.12.3.1.2 Determination of the mRNA concentration

The extracted mRNA samples were thawed and kept on ice.
Spectrophotometric analysis of the samples was performed to assess both the RNA concentration and the purity degree. In particular, 1 µl of each RNA sample solution was analyzed by a micro-volume UV-Vis spectrophotometer evaluating the following parameters:

- Abs_{260} / Abs_{230}, revealing the presence of any contaminants, like guanidine thiocyanate and other detergents contained in the RNA lysis buffer. After a successful RNA extraction, this value usually ranges from 1.8 to 2.2.

- Abs_{260} / Abs_{280}, indicating the purity of the RNA with respect to proteins and phenols. The value resulting from this ratio should be comprised between 1.7 and 2.1.

5.12.3.1.3 Quantitative Reverse Transcription-Polymerase Chain Reaction (qRT-PCR)

The evaluation of the gene expression was performed using the quantitative reverse transcription-polymerase chain reaction (qRT-PCR) technique, which is based on the amplification and quantification of the cDNA derived from the reverse transcription of the target mRNA.

One Step Solution SYBR PrimeScript RT-PCR kit II (Takara, Japan) was used for the amplification reaction, exploiting specific primers for the genes of interest, listed in Table 5.15.

Table 5.15: Primers used in the qRT-PCR analysis.

GENE	Forward primer (5'-3')	Reverse primer (5'-3')
IL-1β	*AAATGCCTCGTGCTGTCTGA*	*CAAGGCCACAGGGATTTTGTC*
IL 6	*AAGCCAGAGTCATTCAGAGCAA*	*GGTCCTTAGCCACTCCTTCT*
TNF α	*GATCGGTCCCAACAAGGAGG*	*GCTTGGTGGTTTGCTACGAC*
ACTIN	*GCCACCAGTTCGCCATGGA*	*TTCTGACCCATACCCACCAT*

RNA samples were properly diluted with nuclease-free water, depending on the concentration measured as in section 5.12.3.1.2, to obtain 180 ng of RNA in 1.8 µl.
3.2 µl of working reagent was added to each RNA sample, previously pipetted in a 48 wells plate, reaching a final volume of 5 µl. The working reagent was prepared with:

- 2.5 µl of *2X One Step SYBR® RT-PCR Buffer IV*, including dNTP mixture (deoxyribonucleotide triphosphate), Mg^{2+} and SYBR® Green (fluorophore able to intercalate DNA permitting the quantification of the amplified genes);
- 0.2 µl of *PrimeScript™ 1 step Enzyme Mix II*, including the enzymes required for the reverse transcription of RNA to DNA (PrimeScript RTase), for the amplification reaction (TaKaRa Ex Taq™ HS, thermosensitive enzyme) and RNase Inhibitor;
- 0.1 µl of *ROX™ Reference Dye/Dye II*, used for normalization of fluorescence intensity by background subtraction;
- 0.4 µl of *10 µM Primers (forward and reverse)*, specific for the genes of interest.

Each 48 wells plate was analyzed by Eco™ Real-Time PCR system, which performs a series of thermic cycles as illustrated in Figure 5.24. Briefly, the reverse transcription takes place during the initial incubation for 15 minutes at 50°C, followed by 2 minutes at 95°C needed for polymerase activation. Next, 40 cycles of amplifications were performed and at the end an interval at high temperature was used to obtain the melting curve and verify whether non-specific amplifications occurred.

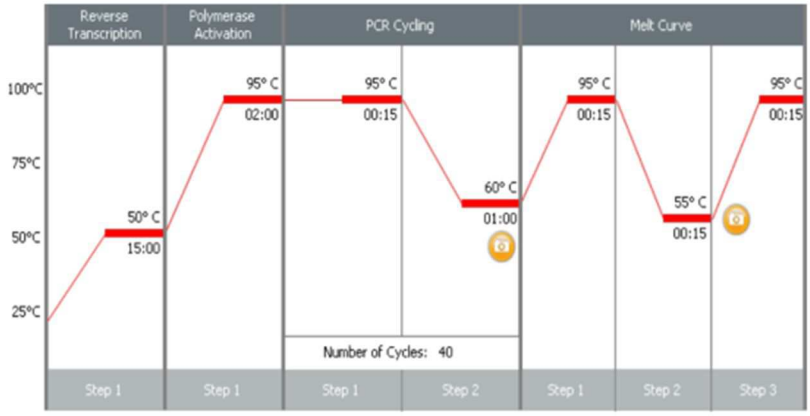

Figure 5.24: Thermal reaction cycle of qRT-PCR.

The relative mRNA expression was calculated according to the $\Delta\Delta C_t$ method [107], by determining the cycle threshold (C_t) values and using β-actin as the housekeeping gene.

Briefly, EcoStudy software was employed to derive for each well a C_t value, which represents the number of cycles necessary for the fluorescence value to rise above a predetermined threshold. This value is inversely proportional to the amount of RNA present, since the lower the number of cycles to reach the threshold value, the greater the amount of RNA present at the beginning of the process. All C_t values were normalized to the housekeeping gene (actin) by subtraction of the C_q value of actin, obtaining a ΔC_t:

$$\Delta C_{t\,=} C_{t\,GENE} - C_{t\,ACTIN}$$

Subsequently, the ΔC_t of the gene was normalized to the control sample, thus extrapolating the $\Delta\Delta C_t$:

$$\Delta\Delta C_t = \Delta C_{t\,SAMPLE} - \Delta C_{t\,CONTROL}$$

From this value, the expression of the gene of interest with respect to the housekeeping gene was quantified:

$$RQ = 2^{-\Delta\Delta C_t}$$

5.12.3.2 Histological analyses

Standard histological techniques were used to process the samples. Briefly, sections obtained from paraffin-embedded liver, spleen, heart, kidney, lungs and brain tissues were stained with haematoxylin and eosin (H&E). All histological examinations were conducted by the same pathologist (prof. Maria Guido, Department of Medicine, General Pathology and Cytopathology Unit, University of Padova), blinded to the study groups of origin of the sections.

5.12.4 Statistical analysis

Obtained data were analyzed with the software GraphPad Prism 7.0 and compared using one-way ANOVA. In the event of significant differences ($\alpha = 0.05$), the ANOVA was followed up with the Tukey post-hoc test. A p value <0.05 was considered statistically significant. Unless otherwise stated, data are presented as mean ± SD.

6. RESULTS

6.1 PRELIMINARY STUDIES

6.1.1 Liposomes characterization by Dynamic Light Scattering (DLS) measurements

Dimensional analysis of liposomes formulated during preliminary studies, involving the use of $mPEG_{2kda}$-lipid(s) derivatives, provided the results reported in Table 6.1.

Table 6.1: Liposome size distribution and polydispersity index (PdI).

	Size (nm)	PdI
CL (naked)	92.50 ± 1.20	0.080
SL (stealth)	87.03 ± 0.47	0.038
SSL_2 (super stealth $DSPE_2$)	90.87 ± 0.76	0.056
SSL_4 (super stealth $DSPE_4$)	93.87 ± 0.21	0.053

All liposomal formulations were characterized by vesicles with a mean hydrodynamic diameter of about 90 nm, so they can be classified as small unilamellar vesicles (SUV). Moreover, the suspensions were homogeneous since the polydispersity index was always lower than 0.1 and the instrument revealed the presence of only one population of particles of the same dimensions, represented as a single peak, with small standard deviations. In Figure 6.1 it is reported an example of dimensional analysis by DLS of a liposomal sample.

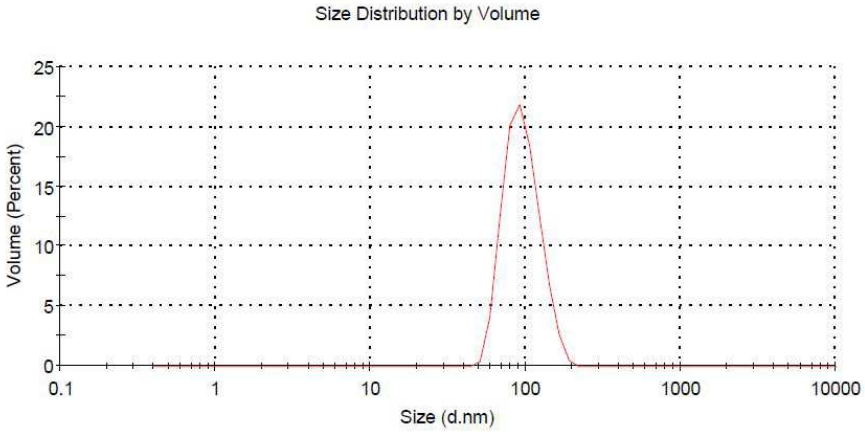

Figure 6.1: Example of dimensional analysis by DLS.

6.1.2 Long-term stability studies

Dimensional analysis over time was performed by DLS measurements of 3 mM samples of each liposomal formulation, containing 0.05% w/v NaN_3 and stored up to 5 months at 4°C.
Naked liposomes (CL) started to aggregate after 2 months of storage at 4°C since a second population (peak) of particles appeared around 5000 nm, accounting for 11% of the total population of liposomes. PEGylated liposomes, instead, maintained their dimensions for longer periods since aggregates appeared only after 4 months along with an increase of PdI.
Collected data are reported in Table 6.2 and Table 6.3.

Table 6.2: Mean size and PdI over time of naked liposomes.

	CL	
time	**mean size (nm)**	**PdI**
1 day	92.5 ± 1.2	0.080
2 days	92.9 ± 0.5	0.057
3 days	93.2 ± 1.1	0.041
5 days	92.9 ± 2.3	0.057
7 days	93.9 ± 1	0.044
11 days	93.4±0.5	0.070
15 days	92.9 ± 0.3	0.093
18 days	92.23 ± 2.3	0.076
22 days	93.4 ± 1.24	0.072
1 month	95.26 ± 0.3	0.052
2 months	106.4 ± 2.3 (89%) 4989.6 ± 175.8 (11%)	0.139

Table 6.3: Mean size and PdI over time of PEGylated liposomes.

	SL		SSL_2		SSL_4	
time	**mean size (nm)**	**PdI**	**mean size (nm)**	**PdI**	**mean size (nm)**	**PdI**
1 day	87.03 ± 0.47	0.04	90.87 ± 0.76	0.05	93.87 ± 0.21	0.05
5 days	87.75 ± 0.12	0.03	92.46 ± 0.57	0.03	94.61 ± 0.76	0.04
6 days	86.9 ± 0.30	0.04	91.36 ± 1.30	0.05	94.83 ± 0.10	0.04
7 days	87.09 ± 0.40	0.04	90.85 ± 0.86	0.05	93.31 ± 1.28	0.06
14 days	89.12 ± 2.12	0.04	93.42 ± 1.06	0.05	95.4 ± 0.55	0.05
21 days	88.11 ± 1.22	0.05	91.23 ± 0.78	0.04	93.26 ± 0.39	0.05
1 month	88.77 ± 0.68	0.05	92.88 ± 1.76	0.06	95.86 ± 0.88	0.05
2 months	89.86 ± 1.01	0.08	92.26 ± 1.06	0.06	97.04 ± 1.67	0.06
3 months	92.85 ± 0.50	0.09	96.38 ± 1.00	0.08	99.2 ± 0.70	0.08
4 months	93.8 ± 1.2(91%) 5220 ± 143.8(9%)	0.15	96.9 ± 0.50	0.08	100.3 ± 0.30	0.08
5 months			116.2 ± 2.1(92%) 5453.6 ± 165.7(8%)	0.32	122.8 ± 1.8(90%) 5324.9 ± 184.2(10%)	0.34

6.1.3 *In vitro* stability experiments in presence of a detergent

In Figure 6.2 and Figure 6.3 are represented the stability profiles of the liposomal formulations, respectively including 5% mol and 10% mol of $mPEG_{2kda}$-lipid(s) derivatives, in presence of increasing concentrations of detergent (Triton X-100).

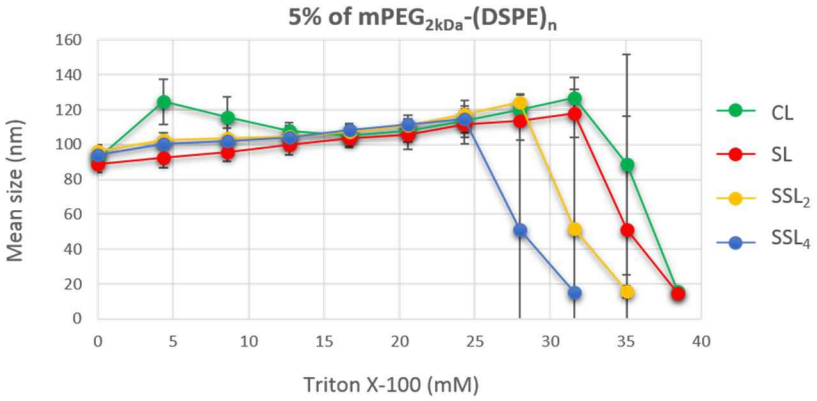

Figure 6.2: Stability profile of liposome with 5% mol of $mPEG_{2kDa}$-$(DSPE)_n$ compared to naked liposomes in the presence of increasing concentration of Triton X-100.

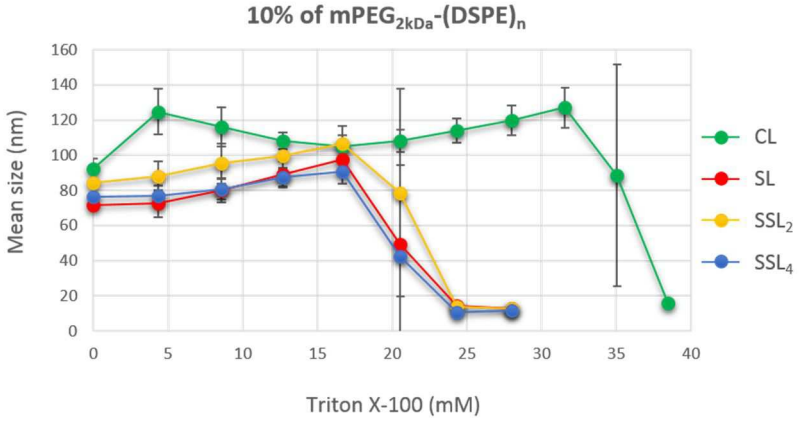

Figure 6.3: Stability profile of liposome with 10% mol of $mPEG_{2kDa}$-$(DSPE)_n$ compared to naked liposomes in the presence of increasing concentration of Triton X-100.

The general trend shown for all tested formulation was an initial progressive increase in vesicles size, followed by a sudden disruption when a certain concentration of detergent was reached, with formation of mixed micelles.

A negative trend of stability emerged with the increase of the hydrophobic anchor (PEG-DSPE > PEG-$DSPE_2$ > PEG-$DSPE_4$) in the formulations with 5% mol of $mPEG_{2kda}$-lipid(s) derivatives. On the other hand, formulations with 10% mol of polymer proved to be even less stable than those with 5% mol, since the required concentration of detergent for liposome disruption was respectively

25 mM and 30-40 mM. In addition, these formulations showed a similar stability behavior meaning that, above a certain polymer concentration, liposomes are intrinsically unstable.

6.1.4 Doxorubicin release experiments

Encapsulation efficiency was similar for both CL, SL and SSL_n (30-40%). The liposomal formulations were analyzed by fluorometer to assess the DXR fluorescence dequenching over time, thus evidencing the drug release profiles shown in Figure 6.4.

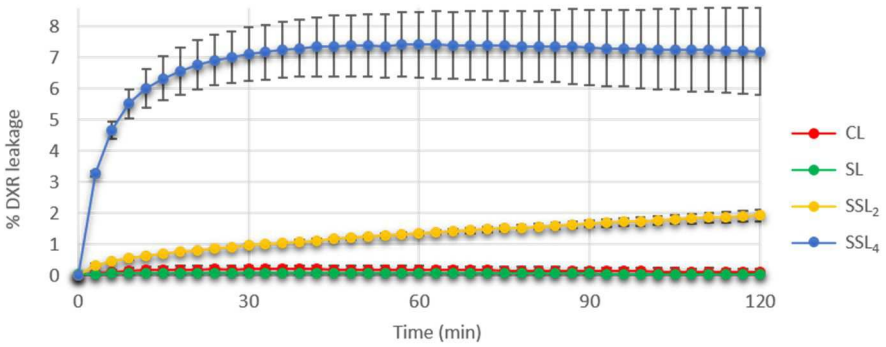

Figure 6.4: In vitro releasing profiles of doxorubicin from the liposomal formulations.

After 2 hours of incubation at 37°C the percentage of DXR release is lower than 0.3% for naked and stealth liposomes, whereas lower than 2% for super stealth liposomes SSL_2. Super stealth liposomes SSL_4, instead, were characterized by an initial burst release effect during the first few minutes, after which a plateau was reached, and the drug was not released significantly. The total DXR leakage from SSL_4 resulted lower than 8%.

Overall, the drug leakage was very slow for all formulations meaning that DXR is efficiently entrapped inside the nanocarrier. This depends on the drug molecules which, upon entrapment inside the aqueous acidic core, get protonated and associate to sulfate divalent anions forming DOX-sulfate aggregates as straight fiber bundles [101, 108, 109]. Therefore, in order to be released doxorubicin should first dissolve and then diffuse across the bilayer, process that requires longer times than the release of a drug in its soluble form.

6.1.5 Pharmacokinetics in rats

DXR quantification by fluorimetry of plasma samples allowed to obtain the pharmacokinetic profile (Figure 6.5Figure 6.5) and parameters of each liposomal formulation. In Table 6.4 are reported the pharmacokinetic parameters obtained using the software PK Solver 2.0 and applying a bicompartmental model.

According to data shown, stealth liposomes presented a prolonged half-life ($t_{½}$ ~22h) compared to SSL_2 ($t_{½}$ ~8h) and SSL_4 ($t_{½}$ ~7h), which were eliminated even faster from the bloodstream than naked liposomes ($t_{½}$ ~10h). Concordantly, the clearance rate of SSL_2 was comparable to that of naked liposomes (~2 µl/h), whereas the clearance rate of SSL_4 was increased of more than 2-fold (~5.6 µl/h), proving the destabilizing effect of $mPEG_{2kda}$-lipid(s) derivatives. Concurrently with the fast clearance from the bloodstream and decreased half-life of SSL_4, a lower AUC was also observed with respect to the other liposomal formulations.

These findings confirmed the trend observed in the stability tests with Triton X-100.

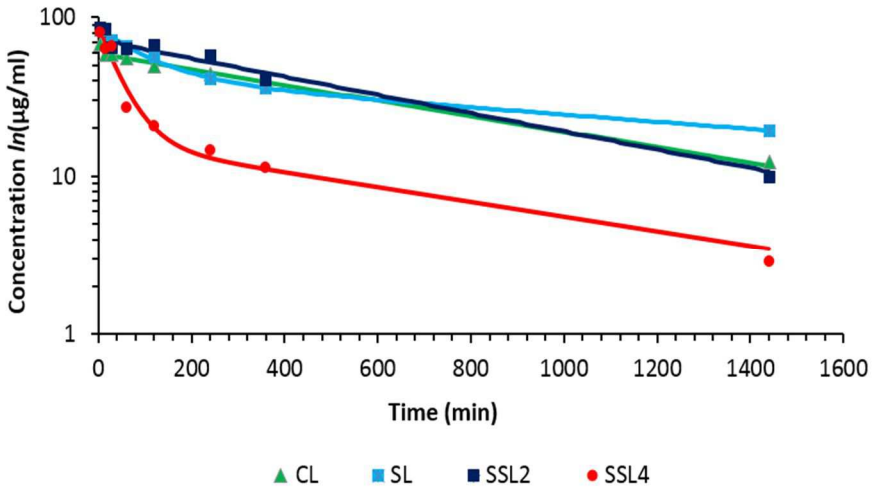

Figure 6.5: In vivo pharmacokinetic profiles of the liposomal formulations.

Table 6.4: Pharmacokinetic parameters calculated by PK Solver 2.0.

	$t_{1/2}$ α (h)	$t_{1/2}$ β (h)	Vd (ml)	AUC (µg/ml·h)	Cl_p (µl/h)
CL (naked)	0.046	10.30	0.040	872.57	1.994
SL (stealth)	1.316	22.14	0.027	1398.21	1.244
SSL_2 (super stealth $DSPE_2$)	0.655	8.76	0.042	910.67	1.911
SSL_4 (super stealth $DSPE_4$)	0.554	7.44	0.046	307.93	5.650

Due to the instability of SSL_2 and SSL_4 systems it was decided to further stabilize the liposomes using PEG 5kDa.

6.2 SYNTHESIS OF PEG DENDRON-LIPIDS DERIVATIVES

6.2.1 Synthesis of PEG dendrons

Dendrons are repetitively branched polymers which, thanks to the increased number of functionalizable peripheral groups, allow the conjugation of multiple molecules (depending on the branching degree). Therefore, different PEG dendrons were synthesized starting from either $mPEG_{5kDa}$-NHS or Boc-NH-PEG_{5kDa}-NHS with the purpose of conjugating 2 or 4 molecules of phospholipid.

The synthesis proceeded by derivatization at the NHS-activated carboxyl end with a symmetric dicarboxylic branching agent, namely β-glutamic acid (β-Glu), alternated to the consequently activation of the new carboxylic groups. This coupling/activation steps were repeated until the required branching degree was achieved to consent the coupling with 2 or 4 molecules of DSPE. The results of the synthesis were reported in Table 6.5.

Table 6.5: Results and yields of the synthesis steps of PEG dendrons.

Synthesis steps of *$mPEG_{5kDa}$-βGlu-$(βGlu)_2$-$(NHS)_4$*	**Yield (% w/w)**	**NHS activation degree (%)**	**βGlutamic acid coupling (%)**
mPEG-NHS		81	
mPEG-βGlu	98		80
mPEG-βGlu-$(NHS)_2$	93	76	
mPEG-βGlu-$(βGlu)_2$	93		81
mPEG-βGlu-$(βGlu)_2$-$(NHS)_4$	66	62	

Synthesis steps of *Boc-NH-PEG_{5kDa}-βGlu-$(βGlu)_2$-$(NHS)_4$*	**Yield (% w/w)**	**NHS activation degree (%)**	**βGlutamic acid coupling (%)**
Boc-NH-PEG-NHS		78	
Boc-NH-PEG-βGlu	98		99
Boc-NH-PEG-βGlu-$(NHS)_2$	95	71	
Boc-NH-PEG-βGlu-$(βGlu)_2$	85		66
Boc-NH-PEG-βGlu-$(βGlu)_2$-$(NHS)_4$	97	63	

Synthesis steps of *$mPEG_{5kDa}$-βGlu-$(βGlu)_2$-$(βGlu)_4$-$(NHS)_8$*	**Yield (% w/w)**	**NHS activation degree (%)**	**βGlutamic acid coupling (%)**
mPEG-NHS		81	
mPEG-βGlu	96		83
mPEG-βGlu-$(NHS)_2$	84	67	
mPEG-βGlu-$(βGlu)_2$	96		71
mPEG-βGlu-$(βGlu)_2$-$(NHS)_4$	87	65	
mPEG-βGlu-$(βGlu)_2$-$(βGlu)_4$	90		52
mPEG-βGlu-$(βGlu)_2$-$(βGlu)_4$-$(NHS)_8$	90	65	

Synthesis steps of *Boc-NH-PEG$_{5kDa}$-βGlu-(βGlu)$_2$-(βGlu)$_4$-(NHS)$_8$*	Yield (% w/w)	NHS activation degree (%)	βGlutamic acid coupling (%)
Boc-NH-PEG-NHS		78	
Boc-NH-PEG-βGlu	98		99
Boc-NH-PEG-βGlu-(NHS)$_2$	97	74	
Boc-NH-PEG-βGlu-(βGlu)$_2$	92		67
Boc-NH-PEG-βGlu-(βGlu)$_2$-(NHS)$_4$	93	66	
Boc-NH-PEG-βGlu-(βGlu)$_2$-(βGlu)$_4$	93		85
Boc-NH-PEG-βGlu-(βGlu)$_2$-(βGlu)$_4$-(NHS)$_8$	100	64	

6.2.2 Characterization of the synthesized PEG dendrons

After each step of β-Glutamic acid coupling to the polymer, for further increasing PEG branching, the degree of derivatization was assessed by ^{1}H NMR spectroscopy and the percentages are reported in Table 6.5. The values were calculated by integration of the signals of β-Glutamic acid with respect to a reference signal, namely the Boc protecting group (integrating for 9 H) for Boc-PEG dendrons and the methoxy group for mPEG dendrons (integrating for 3 H). In Figure 6.6 - Figure 6.9 are reported the ^{1}H NMR spectra of the final PEG dendrons, prior to the last activation of the distal carboxyl groups, with the corresponding signals integrations shown in Table 6.6 - Table 6.9.

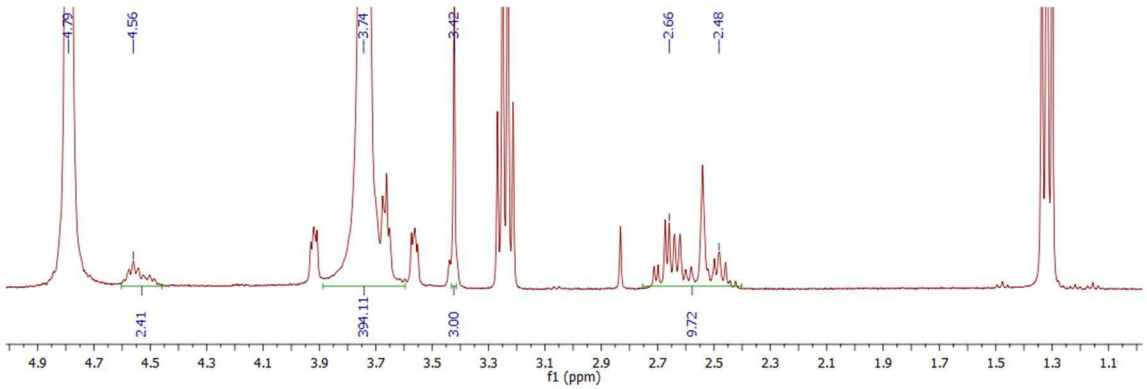

Figure 6.6: ^{1}H NMR spectroscopy of mPEG-βGlu(βGlu)$_2$ in D_2O (δ 4.79 ppm).

Table 6.6: Signals integration of mPEG-βGlu(βGlu)$_2$.

	Chemical shift, δ (ppm)	Multiplicity	Theoretical integration	Sperimental integration
-NHCH(**CH$_2$**)$_2$CONH-	2.48	m	4	9.72
-NHCH(**CH$_2$**)$_2$(COOH)$_2$	2.66	m	8	
-O**CH$_3$**	3.42	s	3	3
-(**CH$_2$CH$_2$**O)$_n$-	3.74	s	455	394.11
-NH**CH**(CH$_2$)$_2$-	4.56	m	3	2.41

According to data reported in Table 6.6 about 81% of β-Glutamic acid derivatization was achieved, corresponding to 3.24 mol COOH/mol of PEG. The presence of 3 carboxyl groups for each molecule of polymer was enough to allow the following conjugation with 2 molecules of DSPE to achieve $mPEG_{5kDa}$-$(DSPE)_2$.

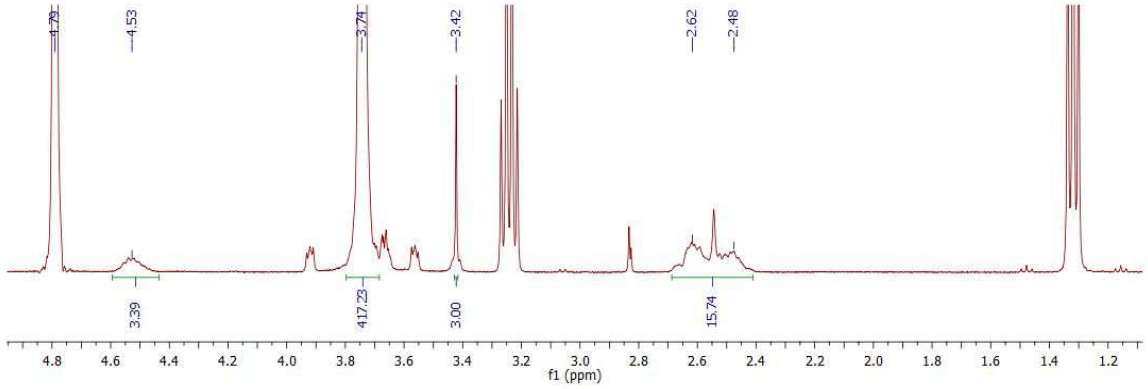

Figure 6.7: ^1H NMR spectroscopy of mPEG-βGlu(βGlu)$_2$(βGlu)$_4$ in D_2O (δ 4.79 ppm).

Table 6.7: Signals integration of mPEG-βGlu(βGlu)$_2$(βGlu)$_4$.

	Chemical shift, δ (ppm)	Multiplicity	Theoretical integration	Sperimental integration
-NHCH(**CH_2**)$_2$CONH-	2.48	m	12	15.74
-NHCH(**CH_2**)$_2$(COOH)$_2$	2.62	m	16	
-O**CH_3**	3.42	s	3	3
-(**CH_2CH_2**O)$_n$-	3.74	s	455	417.23
-NH**CH**(CH_2)$_2$-	4.53	m	7	3.39

In this case, an average of 4.16 mol COOH/mol PEG was achieved (roughly 52% of β-Glutamic acid derivatization), which was sufficient to permit the following coupling of 4 molecules of DSPE to obtain $mPEG_{5kDa}$-$(DSPE)_4$.

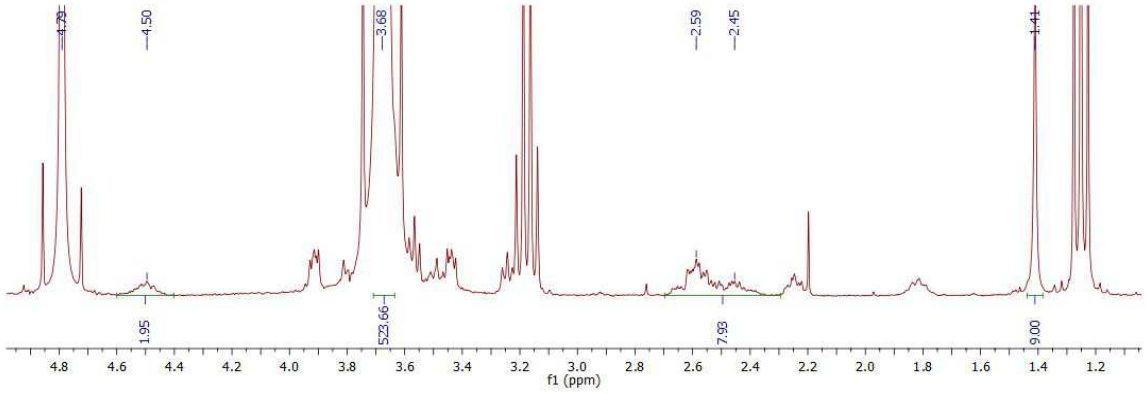

Figure 6.8: ^{1}H NMR spectroscopy of Boc-NH-PEG-ßGlu(ßGlu)$_2$ in D_2O (δ 4.79 ppm).

Table 6.8: Signals integration of Boc-NH-PEG-ßGlu(ßGlu)$_2$.

	Chemical shift, δ (ppm)	Multiplicity	Theoretical integration	Sperimental integration
-OC(**CH_3**)$_3$	1.41	s	9	9
-NHCH(**CH_2**)$_2$CONH-	2.45	m	4	7.93
-NHCH(**CH_2**)$_2$(COOH)$_2$	2.59	m	8	
-(**CH_2CH_2**O)$_n$-	3.68	s	455	523.66
-NH**CH**(CH_2)$_2$-	4.50	m	3	1.95

The data in Table 6.8 confirmed the average coupling of two molecules of β-Glutamic acid to each PEG molecule (2.64 mol of COOH/mol PEG). Such degree of derivatization was sufficient to consent the coupling of 2 DSPE and provide Boc-NH-PEG$_{5kDa}$-(DSPE)$_2$.

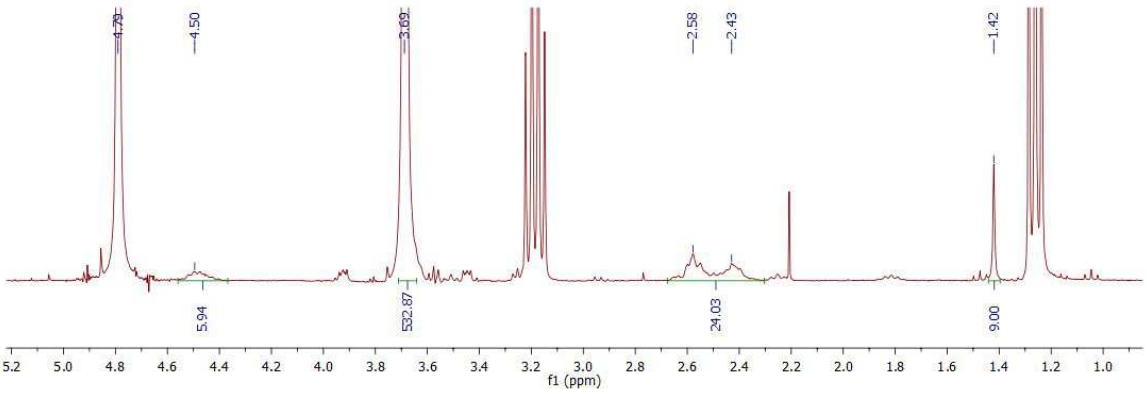

Figure 6.9: ^{1}H NMR spectroscopy of Boc-NH-PEG-ßGlu(ßGlu)$_2$(ßGlu)$_4$ in D_2O (δ 4.79 ppm).

Table 6.9: Signals integration of Boc-NH-PEG-ßGlu(ßGlu)$_2$(ßGlu)$_4$.

	Chemical shift, δ (ppm)	Multiplicity	Theoretical integration	Sperimental integration
-OC(**CH$_3$**)$_3$	1.42	s	9	9
-NHCH(**CH$_2$**)$_2$CONH-	2.43	m	12	24.03
-NHCH(**CH$_2$**)$_2$(COOH)$_2$	2.58	m	16	
-(**CH$_2$CH$_2$**O)$_n$-	3.69	s	455	532.87
-NH**CH**(CH$_2$)$_2$-	4.50	m	7	5.94

According to Table 6.9 about 85% of β-Glutamic acid derivatization was obtained, reflecting the presence of 6.8 mol COOH/mol PEG and allowing for the conjugation of 4 molecules of DSPE to yield the final Boc-NH-PEG$_{5kDa}$-(DSPE)$_4$.

Further characterization by MALDI-TOF mass spectroscopy of synthesized PEG dendrons permitted to assess the effective increment of molecular weight compared to the starting polymer. In Figure 6.10 are reported the mass spectroscopy analyses of Boc-NH-PEG$_{5kDa}$-NHS, Boc-NH-PEG$_{5kDa}$-βGlu-(βGlu)$_2$-(NHS)$_4$ and Boc-NH-PEG$_{5kDa}$-βGlu-(βGlu)$_2$-(βGlu)$_4$-(NHS)$_8$.

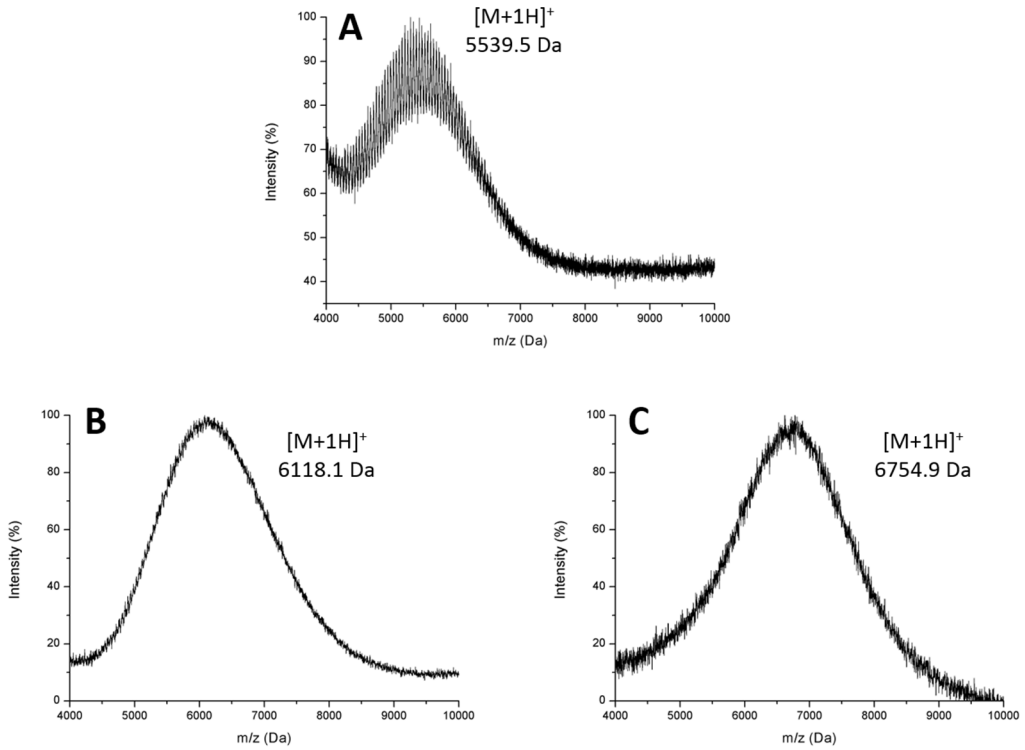

Figure 6.10: MALDI-TOF mass spectroscopy of (A) Boc-NH-PEG$_{5kDa}$-NHS, (B) Boc-NH-PEG$_{5kDa}$-ßGlu-(ßGlu)$_2$-(NHS)$_4$ and (C) Boc-NH-PEG$_{5kDa}$-ßGlu-(ßGlu)$_2$-(ßGlu)$_4$-(NHS)$_8$.

The observed molecular weight of Boc-NH-PEG_{5kDa}-NHS was 5539.5 Da. The molecular weight of Boc-NH-PEG_{5kDa}-βGlu-$(βGlu)_2$-$(NHS)_4$, instead, resulted as 6118.1 Da, confirming an average coupling of 2 molecules of β-Glutamic acid and 63% NHS activation. Boc-NH-PEG_{5kDa}-βGlu-$(βGlu)_2$-$(βGlu)_4$-$(NHS)_8$ showed a molecular weight of 6754.9 Da, justifying the conjugation of 6 β-Glutamic acid molecules and 64% NHS activation.

In Figure 6.11Figure 6.11 are reported the mass spectroscopy analyses of $mPEG_{5kDa}$-NHS, $mPEG_{5kDa}$-βGlu-$(βGlu)_2$-$(NHS)_4$ and $mPEG_{5kDa}$-βGlu-$(βGlu)_2$-$(βGlu)_4$-$(NHS)_8$. The obtained average masses of the synthesized mPEG dendrons were consistent with the integrations of ^1H NMR spectroscopy. $mPEG_{5kDa}$-NHS molecular weight resulted 5504.3 Da. The observed molecular weight of $mPEG_{5kDa}$-βGlu-$(βGlu)_2$-$(NHS)_4$, instead, was 5876.1 Da, justifying the attachment of 2 β-Glutamic acid molecules and 62% NHS activation. $mPEG_{5kDa}$-βGlu-$(βGlu)_2$-$(βGlu)_4$-$(NHS)_8$ resulted with a molecular weight of 6417.8 Da, corresponding to the derivatization with about 4 β-Glutamic acid molecules and 65% NHS activation.

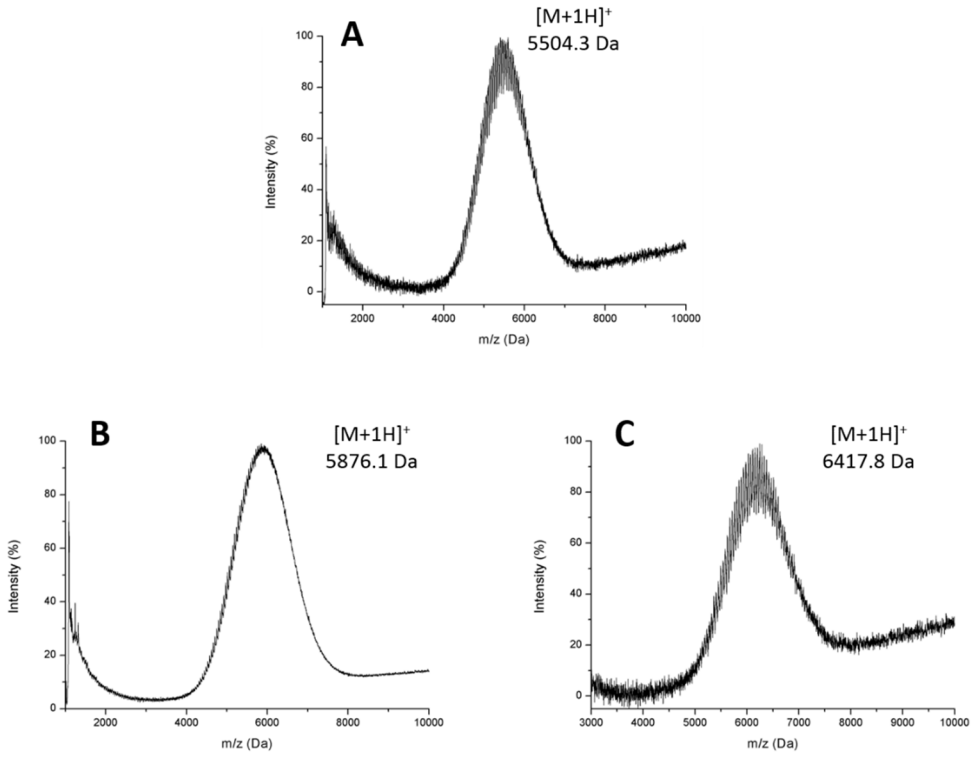

Figure 6.11: MALDI-TOF mass spectroscopy of (A) $mPEG_{5kDa}$-NHS, (B) $mPEG_{5kDa}$-βGlu-$(βGlu)_2$-$(NHS)_4$ and (C) $mPEG_{5kDa}$-βGlu-$(βGlu)_2$-$(βGlu)_4$-$(NHS)_8$.

6.2.3 Distearoylphosphatidylethanolamine (DSPE) conjugation and PEG dendron-lipids derivatives purification

The carboxyl groups of the synthesized PEG dendons were activated to succinimide esters and coupled to either 2 or 4 molecules of distearoylphosphatidylethanolamine (DSPE), leading to the corresponding PEG dendron-lipids derivatives. Several approaches were exploited to purify the final products from unreacted DSPE and other contaminants. The first method relied on the coupling of free DSPE to lauroyl chloride, which was added to the reaction mixture after reaction completion, to selectively remove DSPE upon precipitation in organic solvent. It was decided to conduct a preliminary test on a linear Boc-NH-PEG_{5kDa}-NHS reacted with an excess of DSPE. In Figure 6.12 and Figure 6.13 are reported the ^{1}H NMR spectra of the reaction mixture before and after purification, respectively. Table 6.10 refers to the signals integration of the reaction mixture before purification, taking as reference Boc (integrating for 9 H).

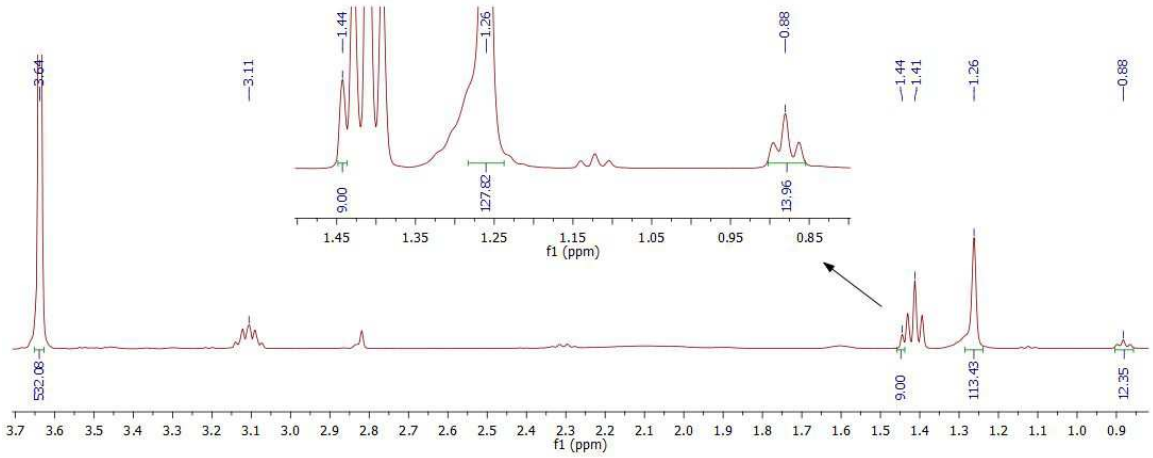

Figure 6.12: ^{1}H NMR spectroscopy of Boc-NH-PEG_{5kDa}-DSPE (reaction mixture) in $CDCl_3$ (δ 7.26 ppm).

Table 6.10: Signals integration of Boc-NH-PEG_{5kDa}-DSPE (reaction mixture).

	Chemical shift, δ (ppm)	Multiplicity	Theoretical integration	Sperimental integration
-**CH_3** [DSPE]	0.88	t	6	12.35
-(**CH_2**)$_n$-CH_3 [DSPE]	1.25	s	64	113.43
-OC(**CH_3**)$_3$	1.44	s	9	9
-(**CH_2CH_2**O)$_n$-	3.64	s	455	532.08

The integration values reported in Table 6.10 confirmed the presence of excess DSPE in the reaction mixture, therefore purification was needed. The signals at δ 1.41 ppm (t) and δ 3.11 ppm (q) are characteristic of triethylamine, reagent used to create basic conditions, in deuterated chloroform.

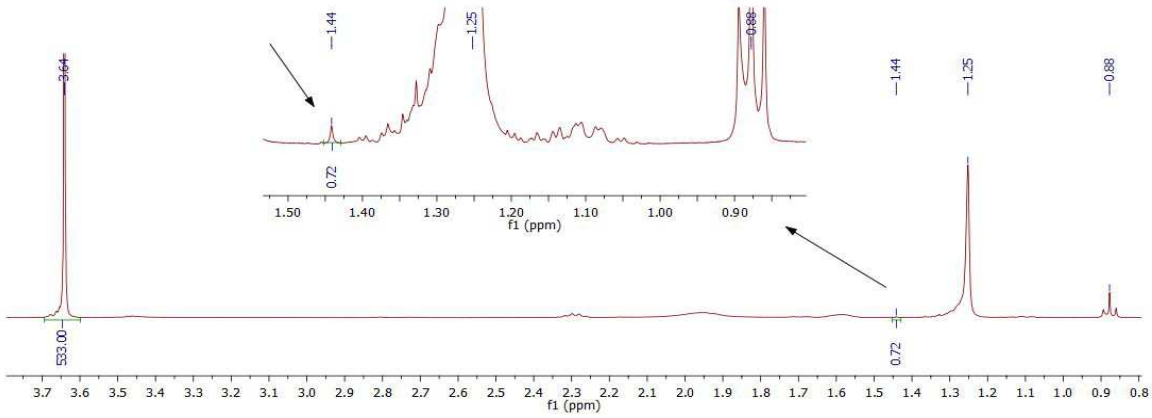

Figure 6.13: ^{1}H NMR spectroscopy in $CDCl_3$ (δ 7.26 ppm) of the reaction mixture after purification with lauroyl chloride.

The ^{1}H NMR spectrum shown in Figure 6.13 evidenced that the acidic conditions originated over time from the reaction between lauroyl chloride and unreacted DSPE led to the deprotection of the polymer (Boc cleavage). This side-reaction is not desired at this step because the primary amino group generated can also react with activated moieties. PEG protons were taken as reference and the integration of Boc signal resulted in 0.72 H, instead of the expected 9 H for each molecule of PEG, which means that only about 8% of PEG was still Boc-protected. For this reason, it was decided to exploit another method for DSPE purification without risking PEG deprotection for Boc-PEG dendron derivatives.

The second approach relied on the low solubility of DSPE in acetonitrile to remove the unreacted amount by selective precipitation with respect to PEG dendron-lipids derivative, since PEG increased the solubility of conjugated phospholipids. This method was firstly exploited to purify the reaction mixture containing Boc-NH-PEG_{5kDa}-$(DSPE)_2$. In Figure 6.14 is reported the ^{1}H NMR spectrum of the collected supernatants, with the corresponding signals integration shown in Table 6.11. Figure 6.15 and Table 6.12, instead, refer to the ^{1}H NMR spectroscopy of the recovered precipitate after 4 cycles of precipitation in ACN, storage at -4°C and subsequent centrifugation. The integration of the signals in the spectrum was performed taking as reference the Boc protecting group of PEG (integrating for 9 H).

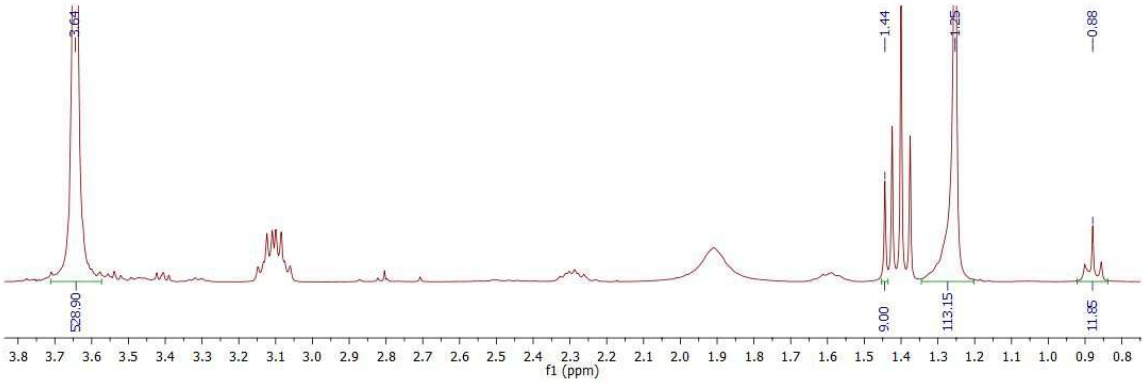

Figure 6.14: ^{1}H NMR spectroscopy of purified Boc-NH-PEG_{5kDa}-$(DSPE)_2$ in $CDCl_3$ (δ 7.26 ppm).

Table 6.11: Signals integration of purified Boc-NH-PEG_{5kDa}-$(DSPE)_2$.

	Chemical shift, δ (ppm)	Multiplicity	Theoretical integration	Sperimental integration
-**CH_3** [DSPE]	0.87	t	12	11.85
-(**CH_2**)$_n$-CH_3 [DSPE]	1.25	s	128	113.15
-OC(**CH_3**)$_3$	1.44	s	9	9
-(**CH_2CH_2**O)$_n$-	3.64	s	455	528.90

The result of the integrations was consistent with the conjugation of 2 molecules of DSPE.

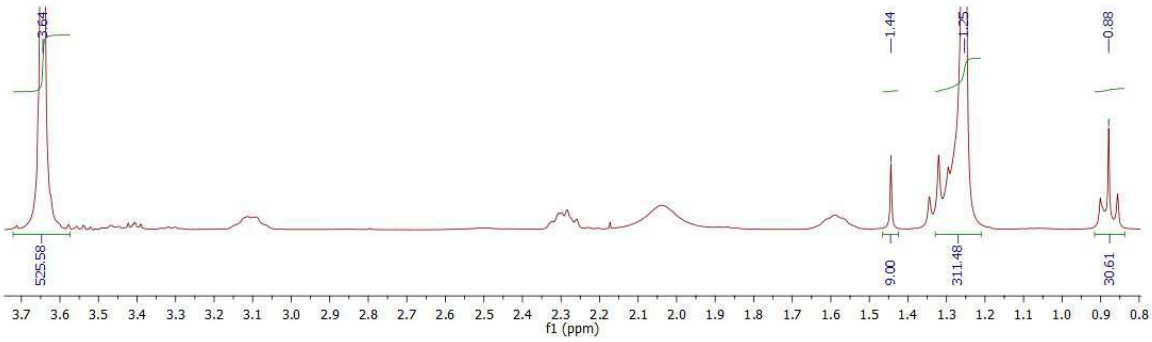

Figure 6.15: ^{1}H NMR spectroscopy in $CDCl_3$ (δ 7.26 ppm) of the precipitate recovered from DSPE purification.

Table 6.12: Signals integration of the precipitate recovered after purification.

	Chemical shift, δ (ppm)	Multiplicity	Theoretical integration	Sperimental integration
-**CH_3** [DSPE]	0.88	t	12	30.61
-(**CH_2**)$_n$-CH_3 [DSPE]	1.25	s	128	311.48
-OC(**CH_3**)$_3$	1.44	s	9	9
-(**CH_2CH_2**O)$_n$-	3.64	s	455	525.58

In the final recovered precipitate a large excess of DSPE was found, as shown by the integration values of Table 6.12, but also PEG was still present, despite 4 repeated cycles of purification by precipitation in ACN had been performed. This means that probably the difference in solubility between the PEG dendron-lipids derivative and free DSPE was not sufficient to provide complete purification by means of selective precipitation in organic solvent. In addition, only 334 mg of purified product were recovered out of the initial 600 mg of activated polymer used for the reaction, proving that this method was not as efficient as expected because a consistent amount of PEG co-precipitated with unreacted DSPE.

Hence, especially for the purification of the PEG dendron derivative coupled to 4 molecules of DSPE it was decided to resort to another technique. After the reaction of 500 mg of Boc-NH-PEG_{5kDa}-βGlu$(βGlu)_2(βGlu)_4(NHS)_8$ (64% NHS activation) with 1,1 equiv. DSPE (329 mg) with respect to the activated carboxyl groups, a first purification step by precipitation in ACN was performed and 506 mg of product were recovered. ^{1}H NMR spectroscopy couldn't be exploited to quantify the degree of DSPE derivatization since the reference signal of Boc was covered by the signals of triethylamine, so it was decided to perform an additional purification by flash column chromatography.

Therefore, thin layer chromatograph (TLC) was firstly carried out to assess the separation of the compounds in the reaction mixture. In Figure 6.16 are reported the best separation conditions achieved by elution with $CHCl_3$:MeOH 8:2 v/v (10 ml + 20 µl H_2O). On the left the reaction mixture (R) was compared to DSPE and 0.2% w/v ninhydrin in EtOH solution was used for DSPE visualization. On the right, instead, the comparison was made with the PEG_{5kDa}-βGlu$(βGlu)_2(βGlu)_4(NHS)_8$ using iodine vapors (I_2) for PEG visualization.

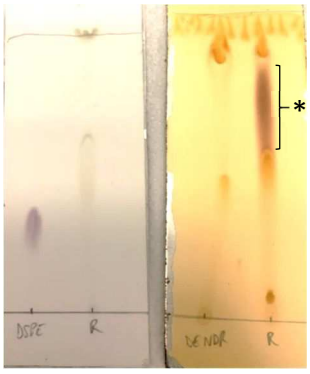

Figure 6.16: Thin layer chromatograph (TLC) of the reaction mixture. On the left ninhydrin staining was used for DSPE visualization, whereas on the right iodine vapors for PEG identification. The brownish red spot indicated with (*) corresponds to the product.

The purification by flash chromatography was performed on 100 mg of product, which were dissolved in the smallest possible volume of chloroform and loaded into the column. In Figure 6.17

are reported the fractions initially eluted: fractions 6-16 containing the product were gathered, concentrated, precipitated in cold diethyl ether and dried under vacuum to recover the product.

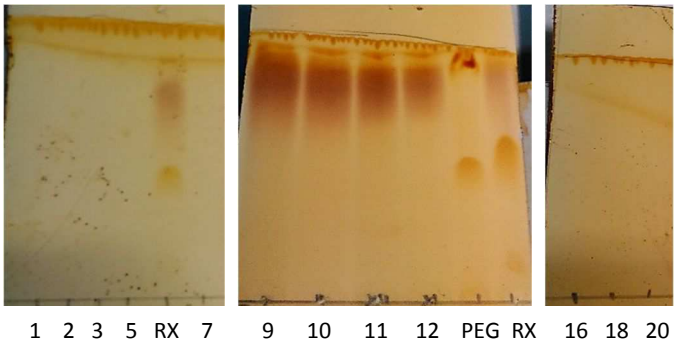

Figure 6.17: Fractions collected by flash column chromatography.

Only 32 mg of purified product were recovered out of the starting 100 mg and characterized by ^{1}H NMR spectroscopy (Figure 6.18, Table 6.13).

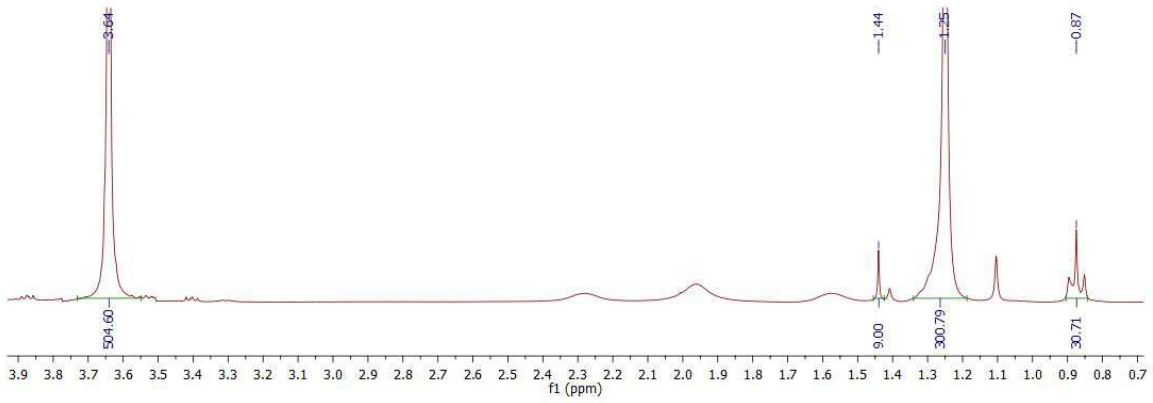

Figure 6.18: ^{1}H NMR spectroscopy of purified Boc-NH-PEG$_{5kDa}$-(DSPE)$_4$ in $CDCl_3$ (δ 7.26 ppm).

Table 6.13: Signals integration of purified Boc-NH-PEG$_{5kDa}$-(DSPE)$_4$.

	Chemical shift, δ (ppm)	Multiplicity	Theoretical integration	Sperimental integration
-**CH$_3$** [DSPE]	0.87	t	24	30.71
-(**CH$_2$**)$_n$-CH$_3$ [DSPE]	1.25	s	256	300.79
-OC(**CH$_3$**)$_3$	1.44	s	9	9
-(**CH$_2$CH$_2$**O)$_n$-	3.64	s	455	504.60

According to the integration values reported in Table 6. an average of 5 DSPE molecules were coupled to each molecule of PEG dendron. This result demonstrated that DSPE reacted quantitatively with the activated carboxyl groups since also in the previously TLC there weren't spots corresponding to unreacted DSPE in the reaction mixture.

Since the yield of product recovery was very low, all the remaining fractions were reunited, together with the eluate obtained after washing the column with 50 ml of methanol, concentrated and precipitated in cold diethyl ether. After drying under vacuum other 15 mg were recovered but ^{1}H NMR spectroscopy revealed the presence of an excess of DSPE. It can be concluded that probably a considerable amount of product remained stacked into the column.

Thus, it was decided to purify the synthesized PEG dendron-lipids derivatives simply by dialysis in 20% v/v MeOH, since DSPE is moderately soluble in MeOH. The final purified X-PEG$_{5kDa}$-(DSPE)$_n$ were characterized by ^{1}H NMR spectroscopy as shown in Figure 6.19- Figure 6.21. The integration of the signals (Table 6.14 - Table 6.16) was performed using the Boc protecting group as reference for Boc-NH-PEG$_{5kDa}$-(DSPE)$_n$ derivatives and the methoxy group for mPEG$_{5kDa}$-(DSPE)$_n$ derivatives. The only exception was made for Boc-NH-PEG$_{5kDa}$-(DSPE)$_2$ since a sufficient amount (334 mg) was already purified by precipitation in acetonitrile (Figure 6.14).

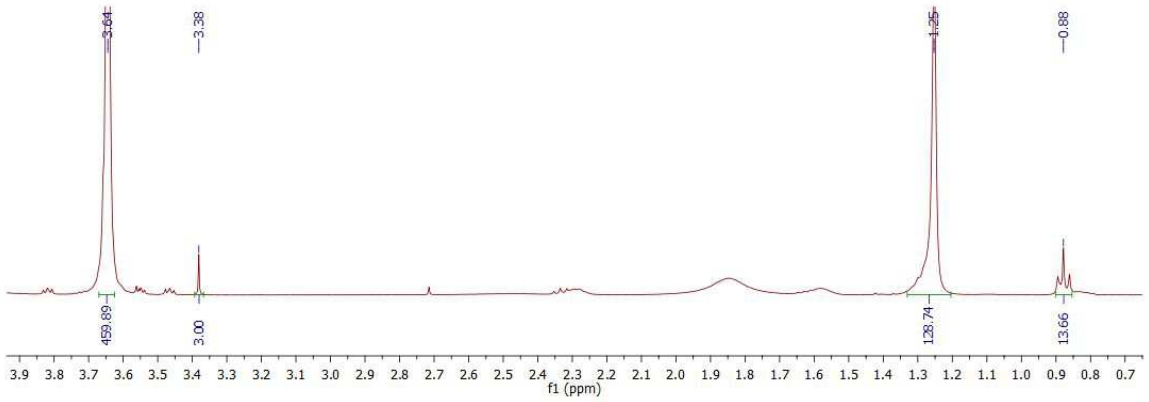

Figure 6.19: ^{1}H NMR spectroscopy of purified mPEG$_{5kDa}$-(DSPE)$_2$ in $CDCl_3$ (δ 7.26 ppm).

Table 6.14: Signals integration of purified mPEG$_{5kDa}$-(DSPE)$_2$.

	Chemical shift, δ (ppm)	Multiplicity	Theoretical integration	Sperimental integration
-**CH$_3$** [DSPE]	0.88	t	12	13.66
-(**CH$_2$**)$_n$-CH$_3$ [DSPE]	1.25	s	128	128.74
-O**CH$_3$**	3.38	s	3	3
-(**CH$_2$CH$_2$**O)$_n$-	3.64	s	455	459.89

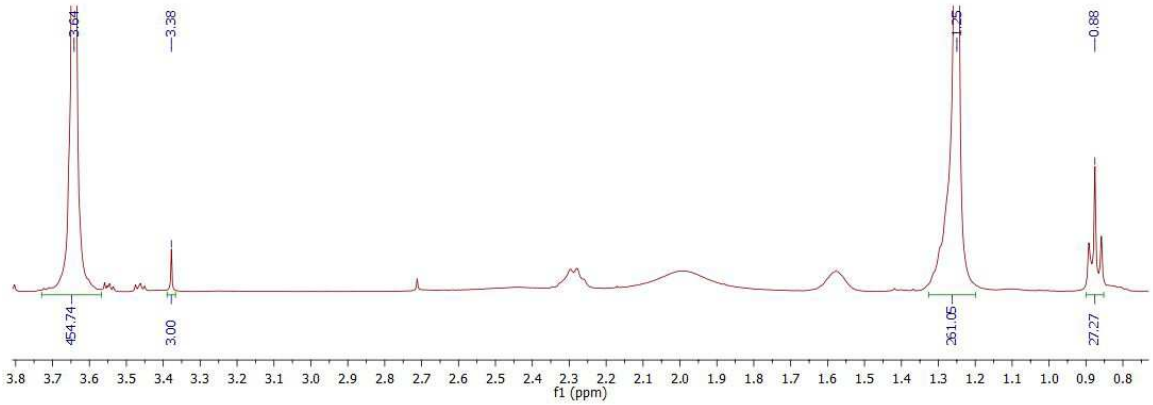

Figure 6.20: ^{1}H NMR spectroscopy of purified $mPEG_{5kDa}$-$(DSPE)_4$ in $CDCl_3$ (δ 7.26 ppm).

Table 6.15: Signals integration of purified $mPEG_{5kDa}$-$(DSPE)_4$.

	Chemical shift, δ (ppm)	Multiplicity	Theoretical integration	Sperimental integration
-**CH_3** [DSPE]	0.88	t	24	27.27
-(**CH_2**)$_n$-CH_3 [DSPE]	1.25	s	256	261.05
-O**CH_3**	3.38	s	3	3
-(**CH_2CH_2**O)$_n$-	3.64	s	455	504.60

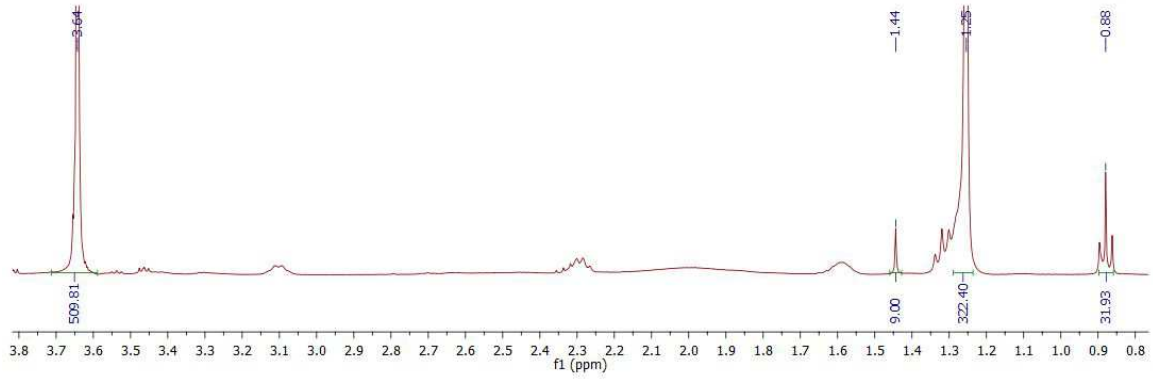

Figure 6.21: ^{1}H NMR spectroscopy of purified Boc-NH-PEG_{5kDa}-$(DSPE)_4$ in $CDCl_3$ (δ 7.26 ppm).

Table 6.16: Signals integration of purified Boc-NH-PEG_{5kDa}-$(DSPE)_4$.

	Chemical shift, δ (ppm)	Multiplicity	Theoretical integration	Sperimental integration
-**CH_3** [DSPE]	0.88	t	24	31.93
-(**CH_2**)$_n$-CH_3 [DSPE]	1.25	s	256	322.40
-OC(**CH_3**)$_3$	1.44	s	9	9
-(**CH_2CH_2**O)$_n$-	3.64	s	455	509.81

The purification by dialysis of Boc-NH-PEG_{5kDa}-$(DSPE)_4$ confirmed the results obtained by flash column chromatography purification, since the signals integration of the ^1H NMR spectrum in Figure 6.21 evidenced the derivatization of the polymer with 5 DSPE molecules.

Diffusion ordered NMR spectroscopy (DOSY) relates the chemical shifts of NMR resonances from a given molecular species to the translational diffusion coefficient of that species. DOSY has been utilized as a powerful tool in recent years to investigate solution state structures and interactions of small organic molecules, organometallic aggregates, and macromolecules [110].
Characterization of the purified products by ^1H DOSY NMR spectroscopy (Figure 6.22 - Figure 6.24) confirmed that the molecule of DSPE were effectively covalently attached to the polymer backbone since all the chemical shifts of the molecules have the same diffusion coefficient. $CDCl_3$ and other residual solvents (e.g. triethylamine) presented different diffusion coefficients, as expected.

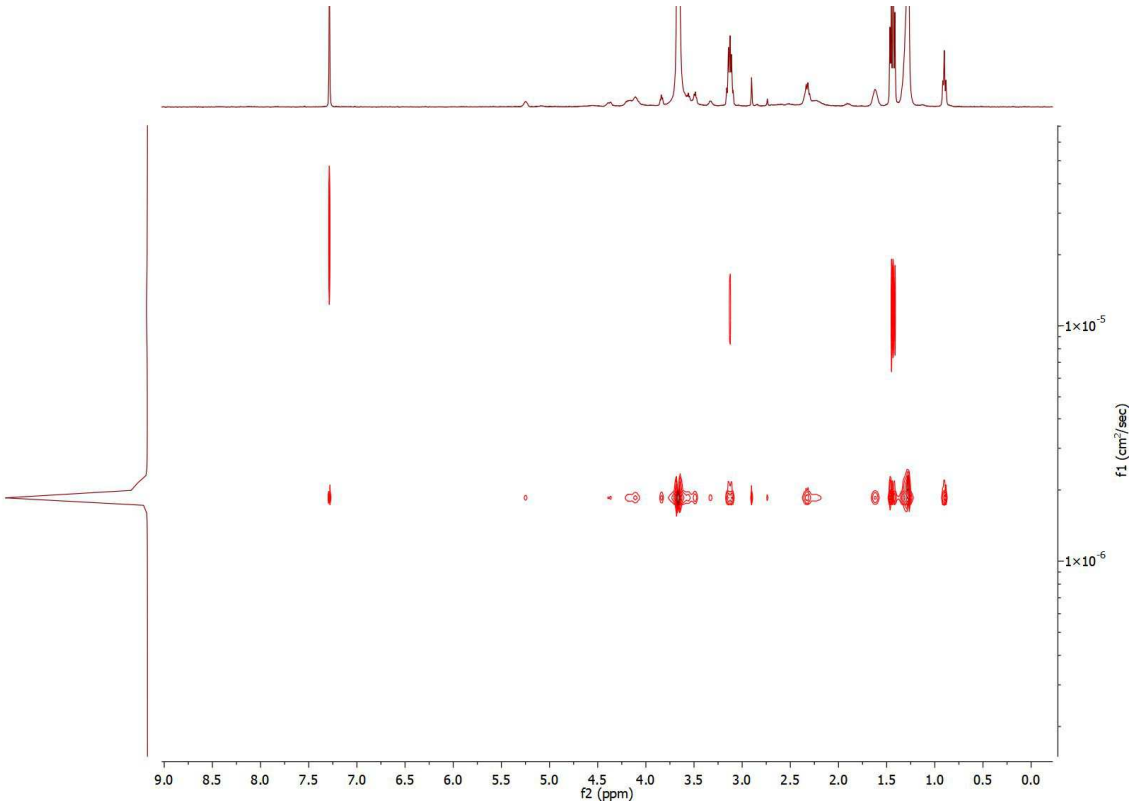

Figure 6.22: ^1H DOSY NMR spectrum of Boc-NH-PEG_{5kDa}-$(DSPE)_2$ in $CDCl_3$ at room temperature.

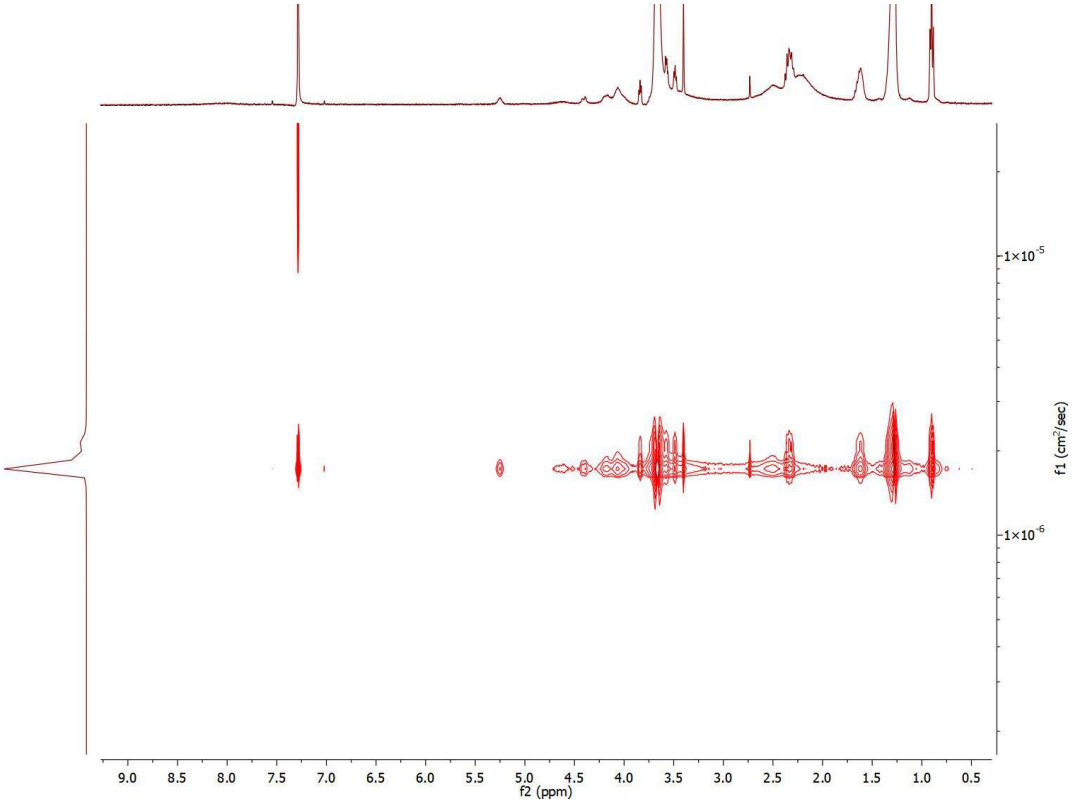

Figure 6.23: ^{1}H DOSY NMR spectrum of $mPEG_{5kDa}$-$(DSPE)_2$ in $CDCl_3$ at room temperature.

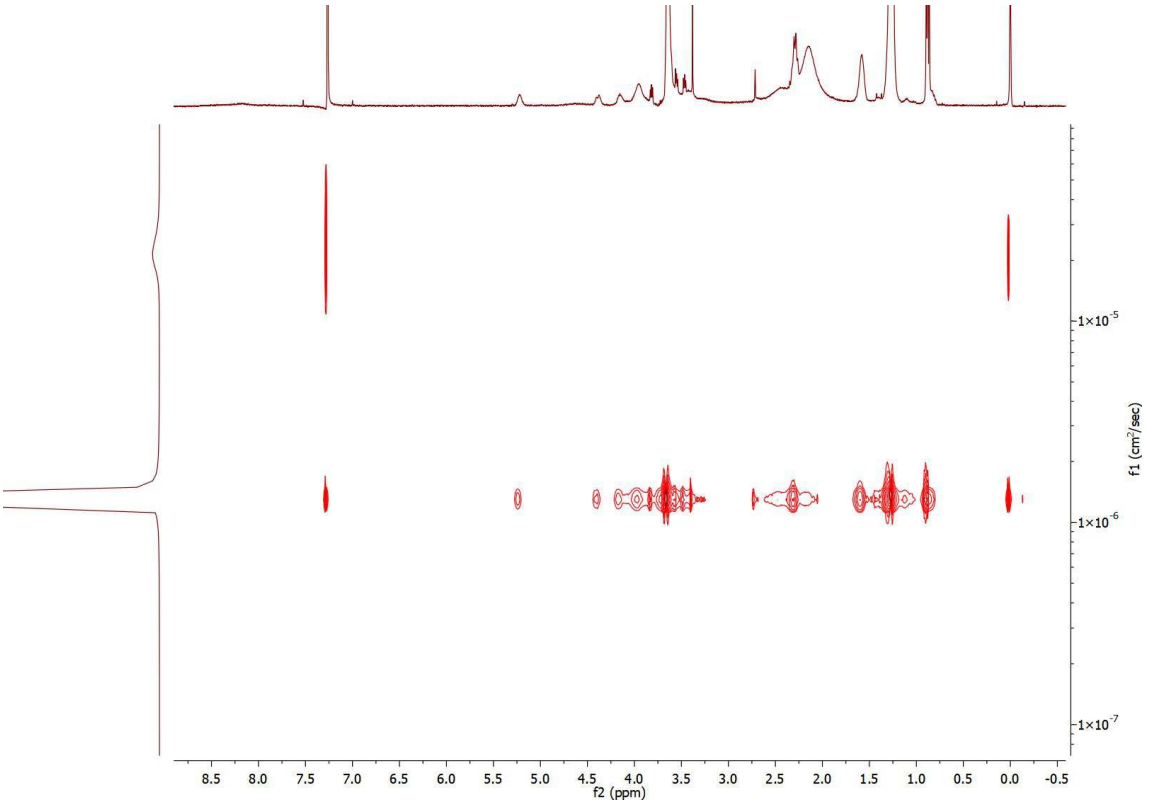

Figure 6.24: ^{1}H DOSY NMR spectrum of $mPEG_{5kDa}$-$(DSPE)_4$ in $CDCl_3$ at room temperature.

6.3 BOC-PEG DENDRON-LIPIDS DERIVATIVES MODIFICATION FOR LIGAND COUPLING

6.3.1 Removal of protecting group t-Boc from Boc-NH-PEG dendron-lipids derivatives

Boc protecting group was cleaved in acidic conditions from Boc-NH-PEG_{5kDa}-$(DSPE)_n$ to free the primary amino group of PEG. The removal was confirmed by the absence of corresponding signal in the ^1H NMR spectrum, as shown in Figure 6.25 and Figure 6.26 respectively.

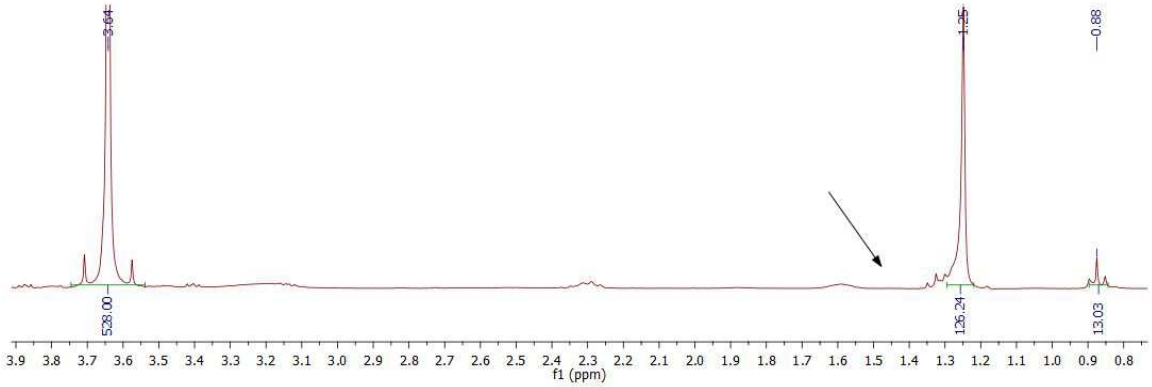

Figure 6.25: ^1H NMR spectroscopy of H_2N-PEG_{5kDa}-$(DSPE)_2$ in $CDCl_3$ (δ 7.26 ppm).

The percentage of free amino groups was calculated by Snyder and Sobocinski assay, resulting in 82% of deprotected polymer.

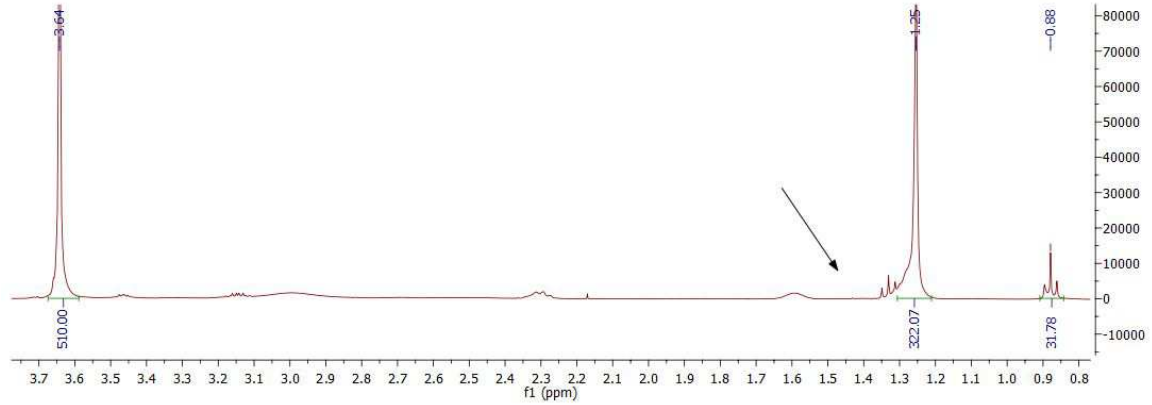

Figure 6.26: ^1H NMR spectroscopy of H_2N-PEG_{5kDa}-$(DSPE)_4$ in $CDCl_3$ (δ 7.26 ppm).

Snyder and Sobocinski assay was performed to assess the degree of Boc-cleavage, resulting in 93% of free amino goups.

6.3.2 SPDP coupling to NH_2-PEG_{5kDa}-$(DSPE)_n$

N-Succinimidyl 3-[2-pyridyldithio]-propionate ester (SPDP) was coupled to PEG dendron-lipids derivatives with the aim of introducing a reversible disulphide bond that can be exploited for the following coupling of the targeting ligand.

After o/n reaction in basic conditions of H_2N-PEG_{5kDa}-$(DSPE)_2$ with SPDP, Snyder and Sobocinski assay was performed to quantify PEG free amino groups and, thus, the degree of SPDP derivatization, resulting as 5.7%. This result confirmed that the reaction took place successfully, with a yield of reaction corresponding to 88% w/w. The product was characterized by ^{1}H NMR spectroscopy analysis and compared to the NMR spectrum of SPDP (Figure 6.27, Table 6.17 and Table 6.18), resulting in about 80% of SPDP derivatization. This value might be underestimated since the signal of PEG protons was taken as reference.

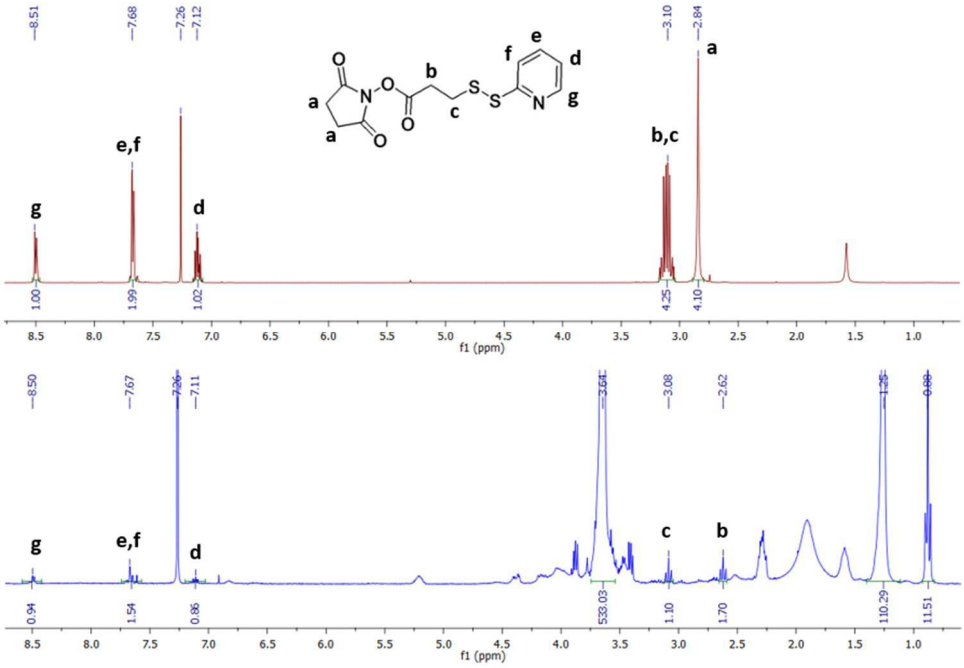

Figure 6.27: ^{1}H NMR spectroscopy of SPDP (in red) and PDP-NH-PEG_{5kDa}-$(DSPE)_2$ (in blue) in $CDCl_3$ (δ 7.26 ppm).

Table 6.17: Signals integration of SPDP.

	Chemical shift, δ (ppm)	Multiplicity	Theoretical integration	Sperimental integration
-**CH_2**CON- (a)	2.84	s	4	4.10
-**CH_2**COO- (b)	3.10	m	2	4.25
-**CH_2**S- (c)	3.10	m	2	
-C=NCH=**CH**- (d)	7.12	m	1	1.02
-S-C-**CH**=CH- (e)	7.68	m	1	1.99
-S-C-CH=**CH**- (f)	7.68	m	1	
-C=N**CH**=CH- (g)	8.51	dt	1	1

Table 6.18: Signals integration of PDP-NH-PEG$_{5kDa}$-(DSPE)$_2$.

	Chemical shift, δ (ppm)	Multiplicity	Theoretical integration	Sperimental integration
-**CH$_3$** [DSPE]	0.88	t	12	11.51
-(**CH$_2$**)$_n$-CH$_3$ [DSPE]	1.25	s	128	110.29
-**CH$_2$**COO- (b)	2.62	t	2	1.70
-**CH$_2$**S- (c)	3.08	t	2	1.10
-(**CH$_2$CH$_2$**O)$_n$-	3.64	s	455	533.03
-C=NCH=**CH**- (d)	7.11	m	1	0.86
-S-C-**CH**=CH- (e)	7.67	m	1	1.54
-S-C-CH=**CH**- (f)	7.67	m	1	
-C=N**CH**=CH- (g)	8.50	dt	1	0.94

6.3.3 BMPS coupling to NH$_2$-PEG$_{5kDa}$-(DSPE)$_n$

N-(β-maleimidopropyloxy)succinimide ester (BMPS) was conjugated to PEG dendron-lipids derivatives to provide a terminal maleimide reactive moiety which can be further exploited for the coupling of the targeting ligand, by formation of a non-cleavable thioether bond.

H$_2$N-PEG$_{5kDa}$-(DSPE)$_2$ was first reacted with BMPS in basic conditions at pH 8.0. Snyder and Sobocinski assay was performed to assess the amount of free amino groups in the reaction mixture and, thus, of unreacted PEG, resulting as 1% so the coupling reaction took place successfully (yield: 92% w/w). The product was characterized by ^{1}H NMR spectroscopy analysis and compared to the spectrum of BMPS (Figure 6.28, Table 6.19).

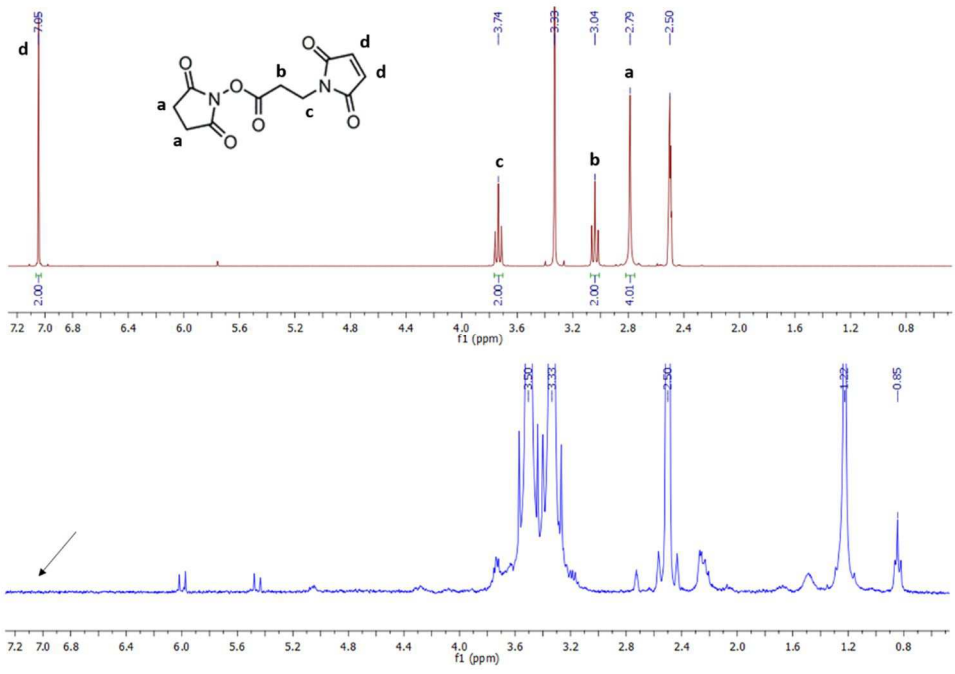

Figure 6.28: ^{1}H NMR spectroscopy of BMPS (red) and BMP-NH-PEG$_{5kDa}$-(DSPE)$_2$ (blue) in DMSO-d6 (δ 2.5-3.33 ppm).

Table 6.19: Signals integration of BMPS.

	Chemical shift, δ (ppm)	Multiplicity	Theoretical integration	Sperimental integration
-**CH_2**CON- (a)	2.79	s	4	4.01
-**CH_2**COO- (b)	3.04	t	2	2.00
-**CH_2**NCO- (c)	3.74	t	2	2.00
-**CH**=**CH**- (d)	7.05	s	2	2.00

As shown in Figure 6.28 by the arrow in the ^{1}H NMR spectrum of BMP-NH-PEG_{5kDa}-$(DSPE)_2$ the signal of the maleimide protons was missing, so it was hypothesized that excessive maleimide hydrolysis occurred in these conditions. The confirmation was given by the ^{1}H NMR spectrum of BMPS in D_2O in presence of a small percentage of NaOD to provide basic environment (Figure 6.29).

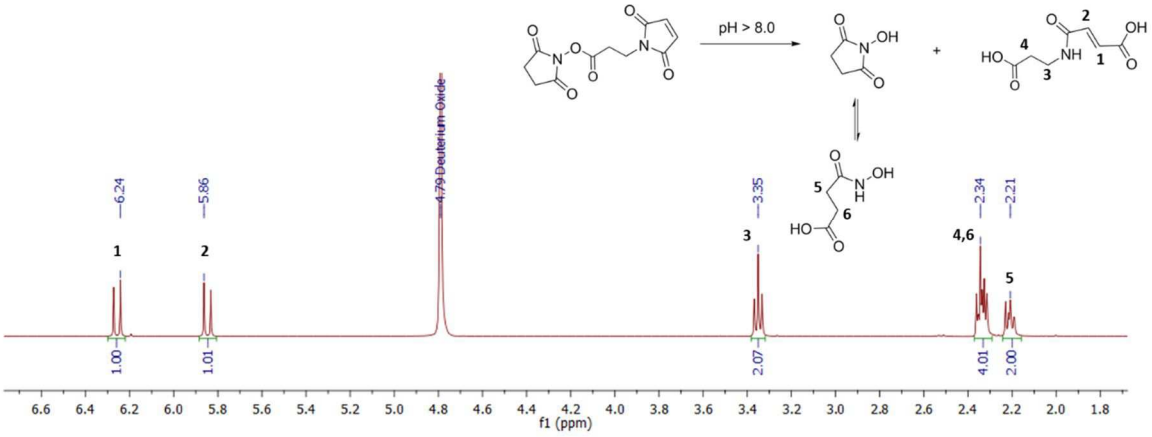

Figure 6.29: ^{1}H NMR spectroscopy of hydrolyzed BMPS in D_20 added of NaOD.

This hypothesis was confirmed by the presence of the two signals at δ 5.86 ppm and δ 6.24 ppm, formed upon maleimide ring opening, also in the previously reported (Figure 6.28) 1H NMR spectrum (the difference in chemical shift was due to the different deuterated solvent used).

The reaction was therefore repeated lowering the pH at 7.2 to slow the hydrolysis reaction. In Figure 6.30 and Figure 6.31 is shown the 1H NMR spectroscopy analysis of the achieved product, with the corresponding signals integrations in Table 6.20 and Table 6.21.

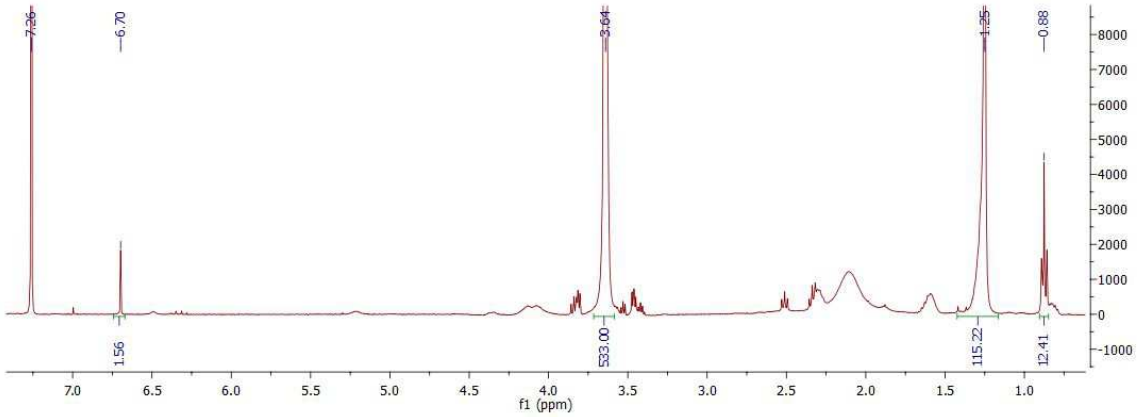

Figure 6.30: ^{1}H NMR spectroscopy of BMP-NH-PEG_{5kDa}-$(DSPE)_2$ in $CDCl_3$ (δ 7.26 ppm).

Table 6.20: Signals integration of BMP-NH-PEG_{5kDa}-$(DSPE)_2$.

	Chemical shift, δ (ppm)	Multiplicity	Theoretical integration	Sperimental integration
-**CH_3** [DSPE]	0.88	t	12	12.41
-(**CH_2**)$_n$-CH_3 [DSPE]	1.25	s	128	115.22
-(**CH_2CH_2**O)$_n$-	3.64	s	455	533.00
--**CH**=**CH**-	6.70	s	2	1.56

According to the integration value of the maleimide protons, roughly 78% of BMPS coupling was achieved in for BMP-NH-PEG_{5kDa}-$(DSPE)_2$. An underestimation is expected since the integration was calculated with respect to PEG protons.

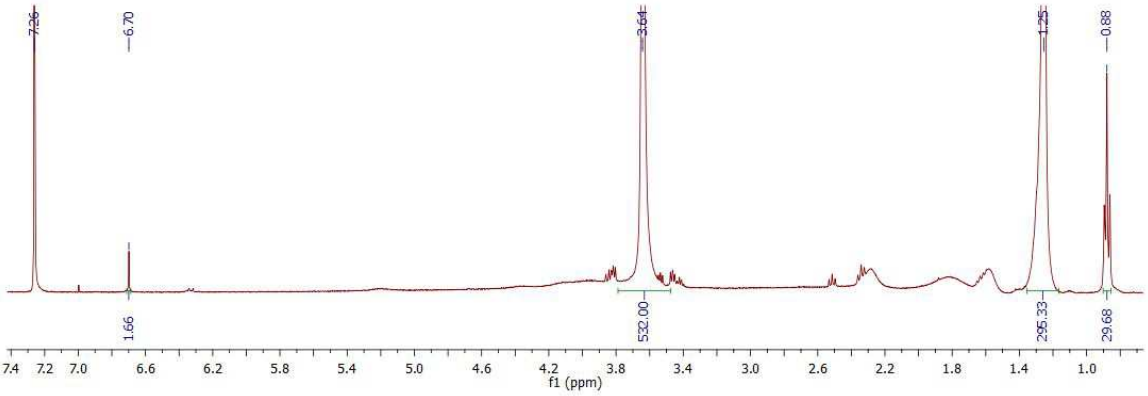

Figure 6.31: ^{1}H NMR spectroscopy of BMP-NH-PEG_{5kDa}-$(DSPE)_4$ in $CDCl_3$ (δ 7.26 ppm).

Table 6.21: Signals integrations of BMP-NH-PEG$_{5kDa}$-(DSPE)$_4$.

	Chemical shift, δ (ppm)	Multiplicity	Theoretical integration	Sperimental integration
-**CH$_3$** [DSPE]	0.88	t	24	29.68
-(**CH$_2$**)$_n$-CH$_3$ [DSPE]	1.25	s	256	295.33
-(**CH$_2$CH$_2$**O)$_n$-	3.64	s	455	532.00
--**CH**=**CH**-	6.70	s	2	1.66

A similar value of BMPS derivatization was obtained for BMP-NH-PEG$_{5kDa}$-(DSPE)$_4$ (83%). Underestimation is expected also in this case.

6.4 PREPARATION OF Fab'

The whole antibody Trastuzumab was firstly characterized by two distinct mass spectrometry analyses, MALDI-TOF and ESI-TOF, to determine its molecular weight, resulting in 148720.69 Da and 148061.00 Da, respectively (Figure 6.32 and Figure 6.33).

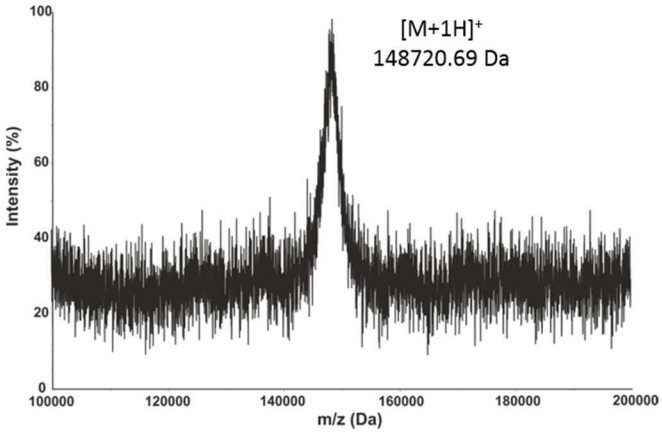

Figure 6.32: Determination of Trastuzumab molecular weight by MALDI-TOF mass analysis.

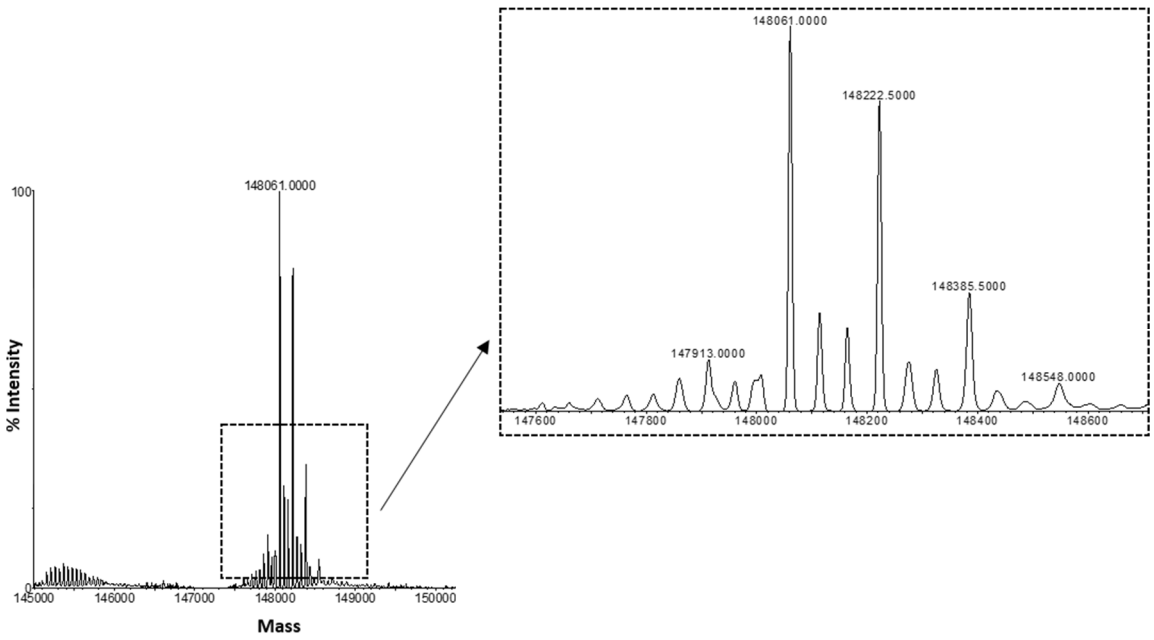

Figure 6.33: Determination of Trastuzumab molecular weight by ESI-TOF mass analysis.

The difference in molecular weight is attributable to the heterogeneous glycosylation pattern of Trastuzumab, shown in the zoomed mass spectrum reported in the squared box in Figure 6.33.

Proteolytic digestion of Trastuzumab with pepsin provided the $F(ab')_2$ which was purified by gel filtration. The corresponding chromatographic profile, eluted at 13 ml, is reported in Figure 6.34.

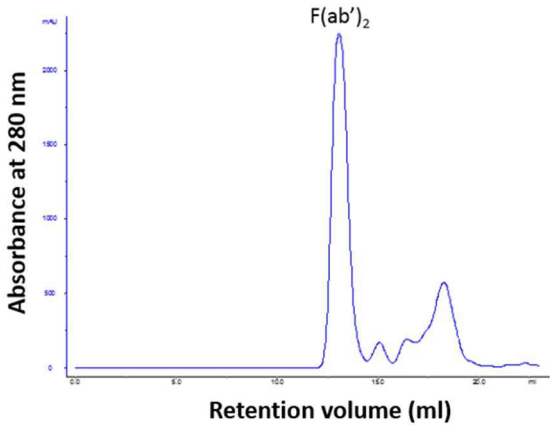

Figure 6.34: Chromatographic profile of $F(ab')_2$ purification by gel filtration chromatography on a Superose 12 10/300 GL column eluting with PBS 1X pH 7.4, in isocratic conditions, at a flow rate of 0.5 ml/min (λ=280 nm).

The collected peak was characterized by mass spectroscopy, as shown in Figure 6.35, to assess the molecular weight of $F(ab')_2$. MALDI-TOF mass spectroscopy provided 97628.0 Da and ESI-TOF mass analysis 97290.5 Da.

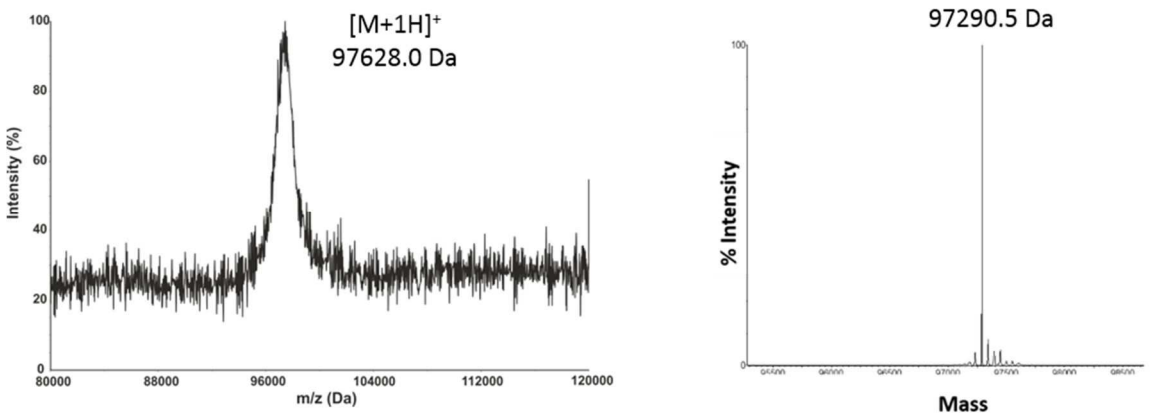

Figure 6.35: Determination of $F(ab')_2$ molecular weight by MALDI-TOF (on the left) and ESI-TOF (on the right) mass analysis.

Fab' was obtained by the reduction of $F(ab')_2$ with cysteamine and was purified from the reducing agent by gel filtration chromatography (Figure 6.36). The corresponding peak was eluted at 14.5 ml.

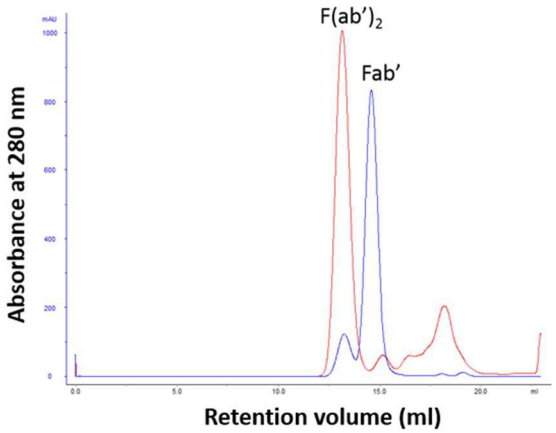

Figure 6.36: Chromatographic profile of Fab' (blue line) purification by gel filtration chromatography on a Superose 12 10/300 GL column eluting with 50 mM sodium phosphate, 150 mM sodium chloride, 10 mM EDTA pH 5.0, in isocratic conditions, at a flow rate of 0.5 ml/min (λ=280 nm). $F(ab')_2$ chromatogram (red line) was superimposed to Fab' help identification.

As expected, Fab' was eluted later than F(ab')$_2$ due to its lower hydrodynamic volume. The collected peak was analyzed by mass spectrometry to evaluate the molecular weight (Figure 6.37). MALDI-TOF mass spectroscopy provided 48772.2 Da and ESI-TOF mass analysis 48648.5 Da.

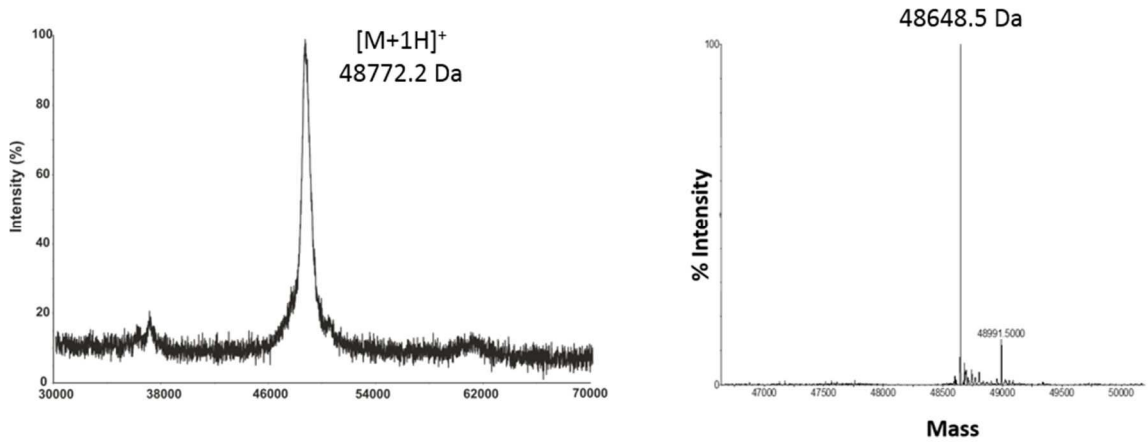

Figure 6.37: Determination of Fab' molecular weight by MALDI-TOF (on the left) and ESI-TOF (on the right) mass analysis.

All purified proteins were characterized by SDS-PAGE analysis (Figure 6.38). Trastuzumab appeared as a band at ~150 kDa, whereas F(ab')$_2$ at ~100 kDa and Fab' at ~50 kDa, confirming the results obtained by mass spectroscopy analysis.

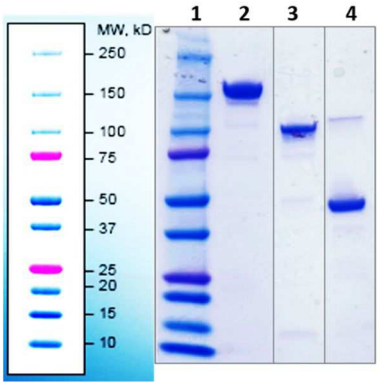

Figure 6.38: Characterization by SDS-PAGE (4-15%) in non-reducing conditions of (1) markers, (2) Trastuzumab, (3) F(ab')$_2$, (4) Fab'. Proteins were stained with Coomassie blue.

6.5 PEGYLATION OF Fab'

6.5.1 Fab' PEGylation with MAL-PEG$_{5kDa}$-FITC

Fab' PEGylation was performed immediately after Fab' purification. Preliminary studies were performed using MAL-PEG$_{5kDa}$-FITC and the reaction mixture was purified by gel filtration as shown in Figure 6.39. The collected peaks were characterized by SDS-PAGE analysis (Figure 6.40).

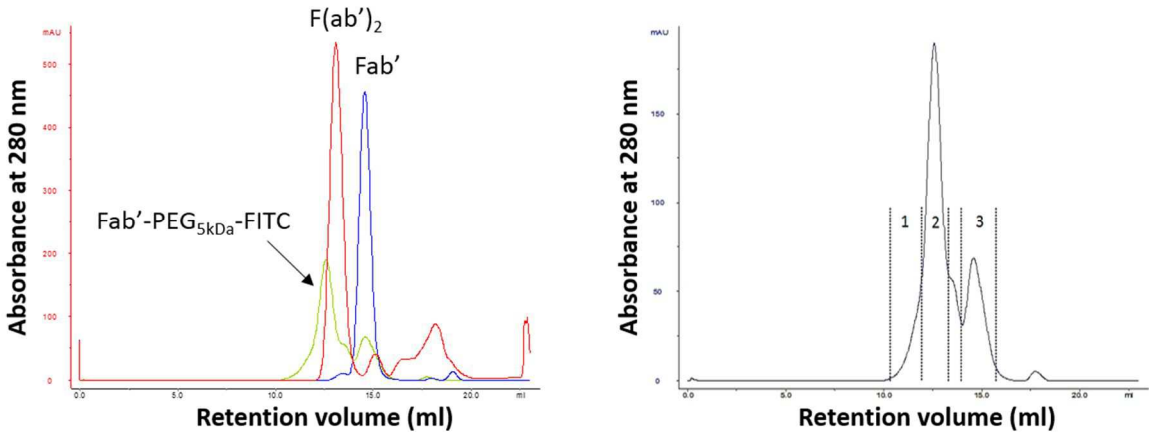

Figure 6.39: On the left is shown the comparison between the chromatographic profiles of Fab'-PEG$_{5kDa}$-FITC (green line), Fab' (blue line) and F(ab')$_2$ (red line). On the right is reported the chromatographic profile of the reaction mixture of PEGylated Fab': fractions 1, 2 and 3 were collected and analysed by SDS-PAGE. The purification was carried out on a Superose 12 10/300 GL column in isocratic conditions (flow rate: 0.5ml/min) eluting with PBS 1X pH 7.4.

Due to the higher hydrodynamic volume provided by PEG, the PEGylated protein was eluted before the unconjugated Fab'.

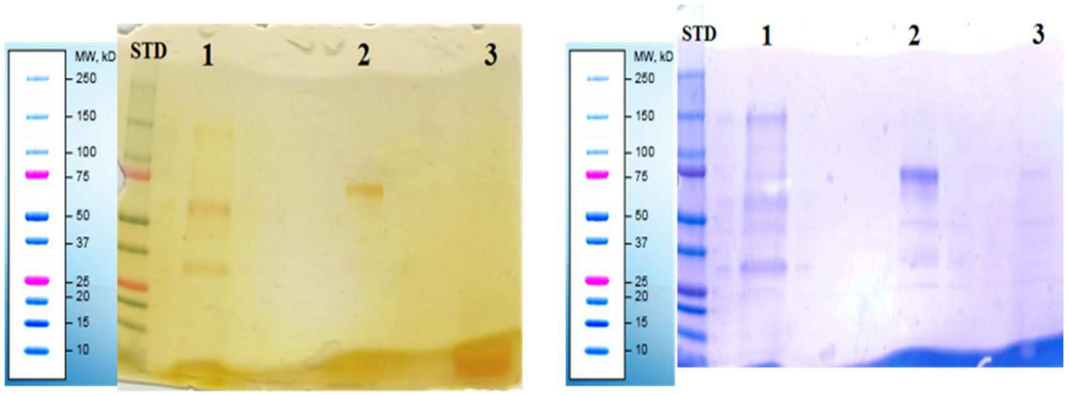

Figure 6.40: Characterization by SDS-PAGE (4-15%) in non-reducing conditions of (STD) protein standards, fractions 1 (1), 2 (2) and 3 (3) collected by gel filtration chromatography. On the left the gel was stained with iodine for PEG visualization, on the right with Coomassie blue to visualize the proteins.

The product was successfully purified since in fraction 2 only one band at ~75 kDa was observed (both at the iodine and Coomassie staining), corresponding to the monoconjugate Fab'-PEG5kDa-FITC. The higher apparent molecular weight of PEGylated Fab' is due to PEG which has a high hydrodynamic volume.

6.5.2 Fab' PEGylation with PDP-NH-PEG$_{5kDa}$-(DSPE)$_n$

PEGylation of Fab' was performed also with PDP-NH-PEG$_{5kDa}$-(DSPE)$_2$ as soon as Fab' was purified to prevent thiols re-oxidation. The first reaction was stirred o/n at 4°C with 9 equiv. of PDP-PEG$_{5kDa}$-(DSPE)$_2$ and the reaction mixture was purified by gel filtration (Figure 6.41). The collected peaks were characterized by SDS-PAGE analysis (Figure 6.42).

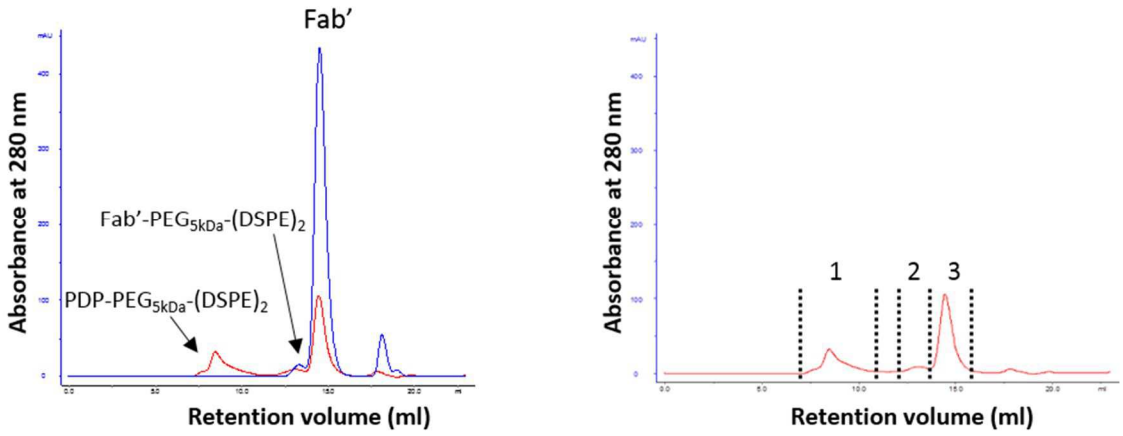

Figure 6.41: On the left is shown the comparison between the chromatographic profiles of Fab'-PEG$_{5kDa}$-(DSPE)$_2$ (red line) and Fab' (blue line). On the right is reported the chromatographic profile of the reaction mixture of PEGylated Fab': fractions 1, 2 and 3 were collected and analysed by SDS-PAGE. The purification was carried out on a Superose 12 10/300 GL column in isocratic conditions (flow rate: 0.5ml/min) eluting with PBS 1X pH 7.4.

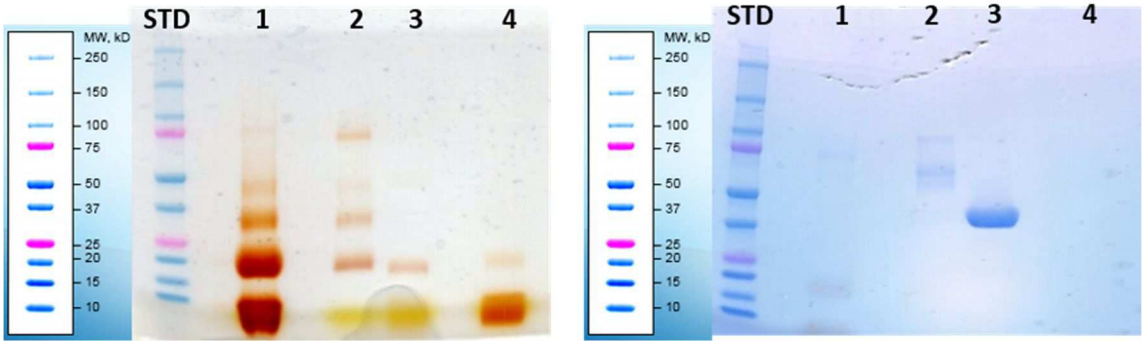

Figure 6.42: Characterization by SDS-PAGE (4-15%) in non-reducing conditions of (STD) protein standards, fractions 1 (1), 2 (2) and 3 (3) collected by gel filtration chromatography. PDP-NH-PEG$_{5kDa}$-(DSPE)$_2$ was used as reference (4). On the left the gel was stained with iodine for PEG visualization, on the right with Coomassie blue to visualize the proteins.

SDS-PAGE analysis revealed by iodine staining that fraction 1 corresponded to the unreacted PEG dendron-lipids derivative forming micelles in aqueous solutions. The expected product, instead, corresponded to fraction 2 in which a band at ~75 kDa was observed both at the iodine and Coomassie staining. The intensity of the band was not strong also because the protein concentration of fraction 2, detected by UV-Vis spectrophotometric measurement, was too low to permit the loading of the same amount of protein of the other lanes (only 2.5 µg were used instead of 10 µg). Fraction 3 corresponded to unreacted Fab'.

Reacting Fab' with a mixture of $mPEG_{5kDa}$-$(DSPE)_2$:PDP-PEG_{5kDa}-$(DSPE)_2$ 4:1 mol/mol seemed to increase the yield of PEGylated Fab' as shown in Figure 6.43 by characterization through SDS-PAGE analysis of the reaction mixture.

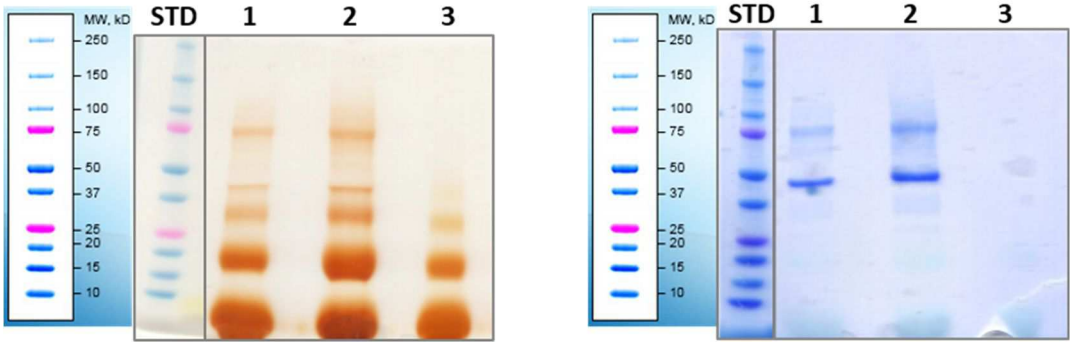

Figure 6.43: Characterization by SDS-PAGE (4-15%) in non-reducing conditions of (STD) protein standards, reaction mixture of Fab' with $mPEG_{5kDa}$-$(DSPE)_2$:PDP-PEG_{5kDa}-$(DSPE)_2$ 4:1 mol/mol. (1) 10 µg and (2) 20 µg of total protein in the reaction mixture. PEG micelles of $mPEG_{5kDa}$-$(DSPE)_2$:PDP-PEG_{5kDa}-$(DSPE)_2$ 4:1 mol/mol were loaded as reference (3). On the left the gel was stained with iodine for PEG visualization, on the right with Coomassie blue to visualize the proteins.

The bands in lane 2 corresponding to unreacted Fab' (~50 kDa) and monoconjugate Fab'-PEG_{5kDa}-(DSPE)2 (~75 kDa) were quantified using ImageJ software to assess the amount of PEGylated Fab' within the reaction mixture, resulting in about 41% of Fab'-PEG_{5kDa}-$(DSPE)_2$.

6.5.3 Fab' PEGylation with BMP-NH-PEG_{5kDa}-$(DSPE)_n$

Fab' was reacted also with BMP-PEG_{5kDa}-$(DSPE)_n$, referred to as MAL-PEG_{5kDa}-$(DSPE)_n$ for simplicity, and the reaction mixture was characterized by SDS-PAGE analysis and compared to the reaction mixture of Fab' PEGylation with commercial MAL-PEG_{5kDa}-DSPE (Figure 6.44).

The monoconjugate Fab'-PEG_{5kDa}-$(DSPE)_n$ run as a globular protein of ~75 kDa due to the high molecular weight of PEG. Unreacted Fab' corresponded to the band at ~50 kDa. The bands observed at ~37 kDa, instead, can be attributed to the PEGylated heavy and light chain of Fab', obtained upon excessive reduction of $F(ab')_2$ by cysteamine that occur at a certain extent, leading to the formation of this by-products as impurities.

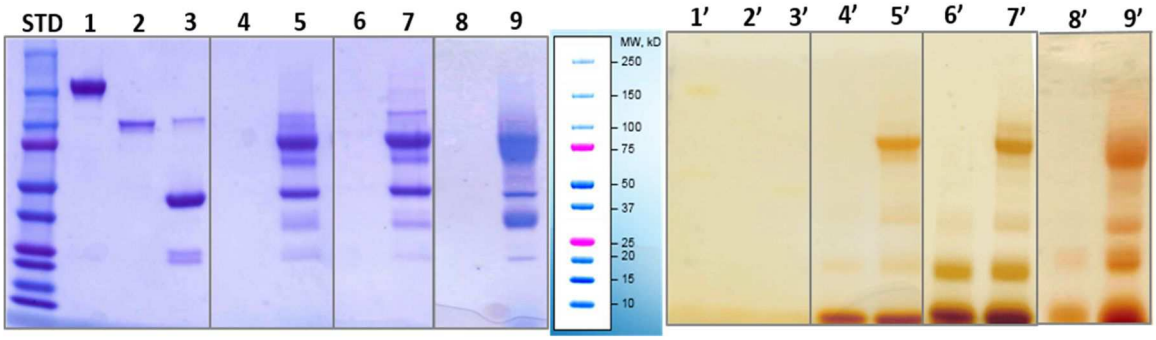

Figure 6.44: Characterization by SDS-PAGE (4-15%) in non-reducing conditions of (STD) protein standards, (1-1') Trastuzumab, (2-2') F(ab')$_2$, (3-3') Fab', (4-4') commercial MAL-PEG$_{5kDa}$-DSPE, (5-5') reaction mixture of Fab' PEGylated with MAL-PEG$_{5kDa}$-DSPE, (6-6') MAL-PEG$_{5kDa}$-(DSPE)$_2$, (7-7') reaction mixture of Fab' PEGylated with MAL-PEG$_{5kDa}$-(DSPE)$_2$, (8-8') MAL-PEG$_{5kDa}$-(DSPE)$_4$, (9-9') reaction mixture of Fab' PEGylated with MAL-PEG$_{5kDa}$-(DSPE)$_4$. On the left the gel was stained with iodine for PEG visualization, on the right with Coomassie blue to visualize the proteins.

6.6 OPTIMIZATION Fab' PRODUCTION

Scale-up of Fab' production by reaction of 17.3 mg/ml of F(ab')$_2$ with 10 mM cysteamine led to excessive reduction of Fab', resulting in the formation of two bands at ~20-25 kDa (corresponding to the heavy and light chains of Fab'), as shown by SDS-PAGE analysis reported in Figure 6.45.

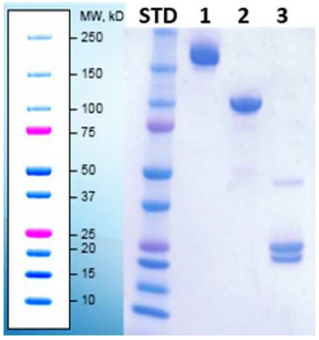

Figure 6.45: Characterization by SDS-PAGE (4-15%) in non-reducing conditions of (STD) protein standards, (1) Trastuzumab, (2) F(ab')$_2$, (3) Fab'. Staining with Coomassie blue was used for proteins visualization.

Therefore, different reaction conditions were tested with the aim of optimizing the yield of Fab' and preventing its excessive reduction. The characterizations were performed by SDS-PAGE analysis.

6.6.1 Fixed F(ab')$_2$ concentration

The first attempt was performed by keeping F(ab')$_2$ concentration constant at 17.3 mg/ml and varying cysteamine concentration in the range of 50 to 5 mM. SDS-PAGE characterization is reported in Figure 6.46.

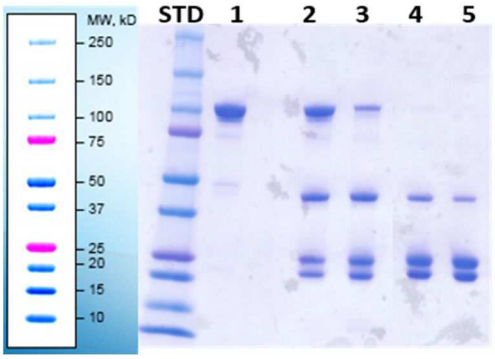

Figure 6.46: Characterization by SDS-PAGE (4-15%) in non-reducing conditions of (STD) protein standards, F(ab')$_2$ (1); F(ab')$_2$ (17.3 mg/ml) reduction with cysteamine 5 mM (2), 10 mM (3), 25 mM (4), and 50 mM (5). Proteins were stained with Coomassie blue.

Excessive reduction of Fab' was still observed when using either 50 or 25 mM cysteamine, whereas 10 and 25 mM cysteamine provided incomplete reduction of F(ab')$_2$.
Therefore, the experiment was repeated decreasing F(ab')$_2$ concentration to 2 mg/ml and using 0.5-1-3 mM cysteamine. Figure 6.47 evidenced that reducing both F(ab')$_2$ and cysteamine concentration couldn't prevent excessive reduction and, in addition, very low yield of Fab' was achieved, whilst F(ab')$_2$ was still the predominant species in almost all cases.

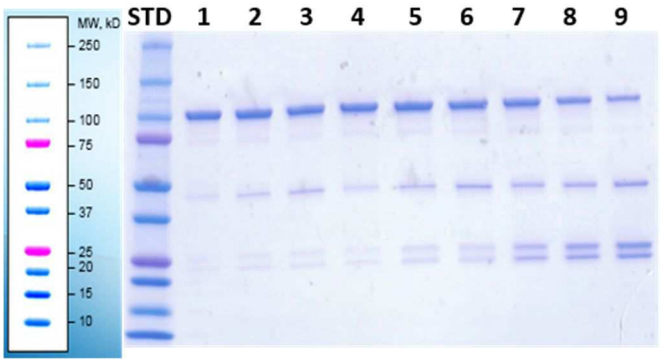

Figure 6.47: Characterization by SDS-PAGE (4-15%) in non-reducing conditions of (STD) protein standards, 2 mg/ml F(ab')$_2$ reduction with cysteamine 0.5 mM (1) 15 min, (2) 30 min, (3) 60 min; cysteamine 1 mM (4) 15 min, (5) 30 min, (6) 60 min; cysteamine 3 mM (7) 15 min, (8) 30 min, (9) 60 min. Coomassie blue was used for proteins staining.

6.6.2 Fixed cysteamine concentration

Another tested approach implied keeping constant cysteamine concentration (10 mM) whilst varying $F(ab')_2$ concentration from 2 mg/ml to 10 mg/ml. Characterization by SDS-PAGE is reported in Figure 6.48.

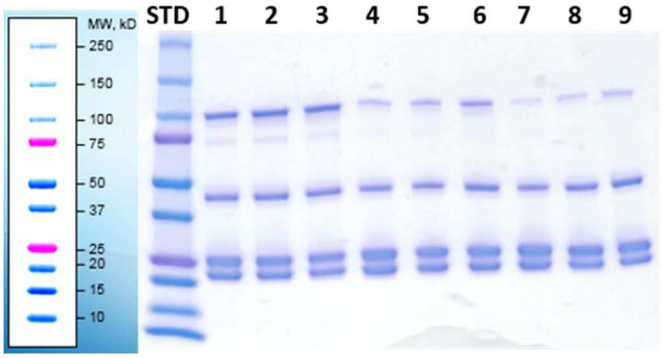

Figure 6.48: Characterization by SDS-PAGE (4-15%) in non-reducing conditions of (STD) protein standards, $F(ab')_2$ reduction using 10 mM cysteamine: (1) 2 mg/ml $F(ab')_2$ – 10 min; (2) 5 mg/ml $F(ab')_2$ – 10 min; (3) 10 mg/ml $F(ab')_2$ – 10 min; (4) 2 mg/ml $F(ab')_2$ – 20 min; (5) 5 mg/ml $F(ab')_2$ – 20 min; (6) 10 mg/ml $F(ab')_2$ – 20 min; (7) 2 mg/ml $F(ab')_2$ – 30 min; (8) 5 mg/ml $F(ab')_2$ – 30 min; (9) 10 mg/ml $F(ab')_2$ – 30 min. Proteins were stained with Coomassie blue.

None of these conditions provided just the desired Fab' because in all cases relevant reduction of the interchain disulphide bond was observed (two bands at ~20-25 kDa), as well as non-reduced $F(ab')_2$.

6.6.3 Other conditions

Other conditions (according to section 5.7.3) were tested to assess whether changes in temperature, pH and buffer could affect the yield of reaction. Characterization by SDS-PAGE analysis of each tested condition is shown in Figure 6.49 and Figure 6.50.

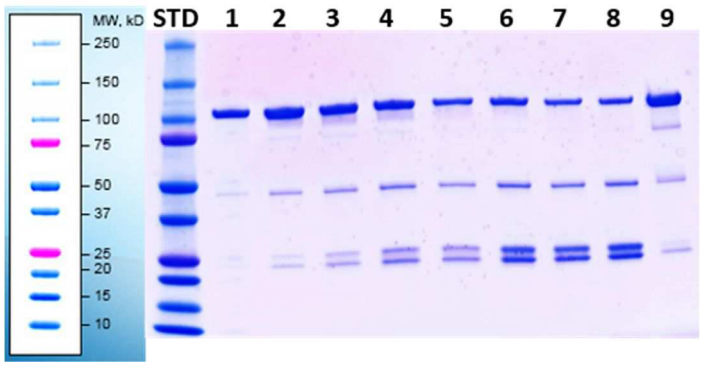

Figure 6.49: Characterization by SDS-PAGE (4-15%) in non-reducing conditions of (STD) protein standards, 2 mg/ml $F(ab')_2$ reduced with 5 mM cysteamine in 0.1 M phosphate buffer, 2 mM EDTA pH 6.0 after (1) 15 min, (2) 30 min, (3) 1 h, (4) 2 h, (5) 3 h, (6) 4 h, (7) 5 h, (8) 6 h; (9) 0.5 mg/ml $F(ab')_2$ reduced with 10 mM cysteamine in PBS, 5 mM EDTA pH 5.0. Proteins were stained with Coomassie blue.

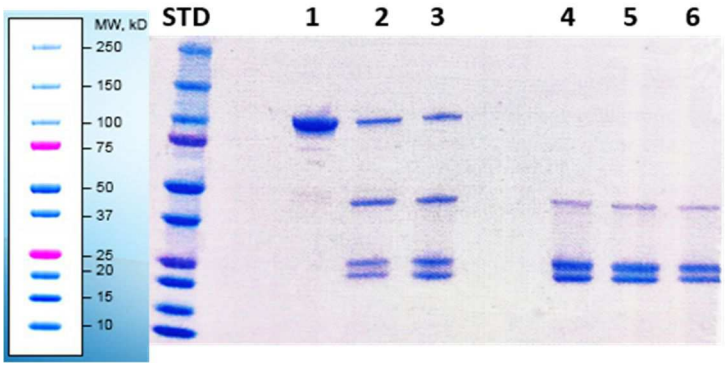

Figure 6.50: Characterization by SDS-PAGE (4-15%) in non-reducing conditions of (STD) protein standards, (1) F(ab')$_2$; (2) 0.5 mg/ml F(ab')$_2$ reduced with 10 mM cysteamine 30 min rt in in 20 mM sodium acetate, 100 mM Na_2SO_4 pH 5.0, 5 mM EDTA pH 5.0; (3) 2 mg/ml F(ab')$_2$ reacted for 16 h at 20°C with 5 mM cysteamine in 0.1 M phosphate buffer, 2 mM EDTA pH 6.0; 10 mg/ml F(ab')$_2$ reduced at 37°C in 150 mM NaCl, 50 mM NaH_2PO_4, 10 mM EDTA pH 7.2 with 50 mM cysteamine after (4) 30 min, (5) 60 min, (6) 90 min. Proteins are stained with Coomassie blue.

None of the tested conditions could provide a good yield of Fab' fragment as prevalent species since at the same time a consistent amount of either F(ab')$_2$ or Fab' heavy and light chains were obtained. Thus, it was decided to change strategy, trying to selectively re-oxidize just the free thiols of heavy and light chains, thus reforming the disulphide interchain bond.

6.7 SELECTIVE RE-OXIDATION Fab'

Mild re-oxidation of interchain disulphide bond between heavy and light chain the Fab' fragment was attempted by means of 1 µM $CuSO_4$. SDS-PAGE analysis characterization of each reaction is reported in Figure 6.51.

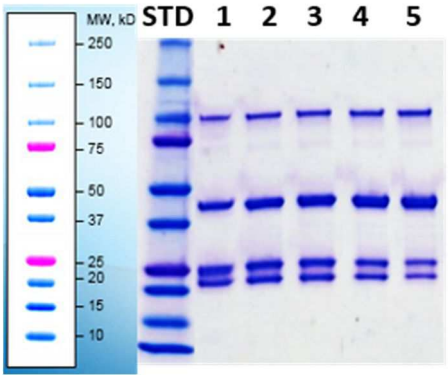

Figure 6.51: Characterization by SDS-PAGE (4-15%) in non-reducing conditions of (STD) protein standards, (1) reaction mixture of 17.3 mg/ml F(ab')$_2$ reduction with cysteamine; Fab' re-oxidation with 1 µM $CuSO_4$ after (2) 30 min, (3) 1 h, (4) 2 h, (5) 3 h. Coomassie blue was used for protein visualization.

None of the tested conditions could provide efficient re-oxidation, so the amount of $CuSO_4$ was increased to 0.01-1 mM and the reaction was monitored by SDS-PAGE analysis (Figure 6.52).

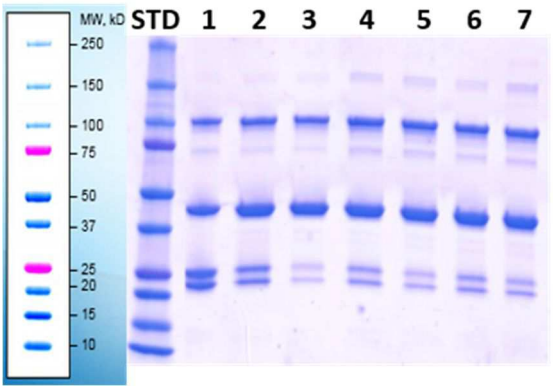

Figure 6.52: Characterization by SDS-PAGE (4-15%) in non-reducing conditions of (STD) protein standards, (1) reaction mixture of 17.3 mg/ml F(ab')$_2$ reduction with 10 mM cysteamine; Fab' re-oxidation with 0.01 mM $CuSO_4$ after (2) 1 h, (3) 3 h; with 0.1 mM $CuSO_4$ after (4) 1 h, (5) 3 h; with 1 mM $CuSO_4$ after (6) 1 h, (7) 3h. Proteins were stained with Coomassie blue.

Incubation with 0.01 mM $CuSO_4$ for 3 h proved to be the best condition since the intensity of the two bands referring to the heavy and light chain of Fab' sensibly decreased in correspondence to an increased intensity of the band of Fab'. In addition, the formation of undesired higher MW aggregates was observed when $CuSO_4$ concentration was increased to 0.1-1 mM.

In both gels, F(ab')$_2$ band at ~100 kDa appeared since cysteamine removal by centrifugation through 10 k MWCO PES concentrators could not purify also non-reduced F(ab')$_2$. However, since F(ab')$_2$ doesn't present any reactive moiety PEGylation can't occur at this fragment and purification can be achieved in a following step.

6.7.1 Selective re-oxidation followed by Fab' PEGylation

Since the re-oxidation step might affect also the vicinal sulfhydryl groups used for PEG coupling, re-oxidized Fab' was reacted with MAL-PEG$_{5kDa}$-DSPE to assess whether its reactivity toward the maleimide group of PEG was maintained or not.

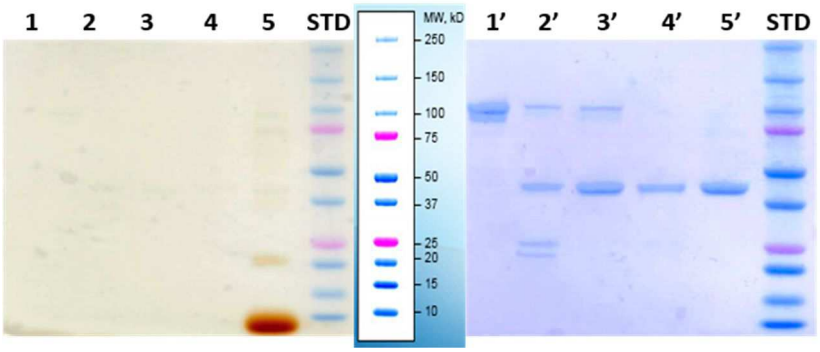

Figure 6.53: Characterization by SDS-PAGE (4-15%) in non-reducing conditions of protein standards (STD), F(ab')$_2$ (1), F(ab')$_2$ reduction with 25 mM cysteamine (2), Fab' re-oxidation with 10 µM $CuSO_4$ after 3 h incubation (3), Fab' purified by gel filtration chromatography (4), reaction mixture of Fab' PEGylation with MAL-PEG$_{5kDa}$-DSPE (5). On the left the gel was stained with iodine for PEG visualization, on the right with Coomassie blue to visualize the proteins.

As shown in Figure 6.53, PEGylation after Fab' re-oxidation didn't occur since iodine staining didn't reveal bands at ~75 kDa (monoconjugate), probably because the re-oxidation involved also the two vicinal sulfhydryl in the hinge region of the Fab'.

6.7.2 Fab' PEGylation followed by selective re-oxidation

Fab' PEGylation followed by bland and selective re-oxidation of the sulfhydryl groups of the heavy and light chains of Fab' provided the expected results. SDS-PAGE analysis reported in Figure 6.54, indeed, evidenced that Fab' PEGylation successfully occurred since a band at ~75 kDa was visible both with iodine and Coomassie blue staining, corresponding to the monoconjugate. Furthermore, the intensity of the two bands of Fab' heavy and light chains (~20-25 kDa) and the corresponding PEGylated forms (~37 kDa) was not consistent.

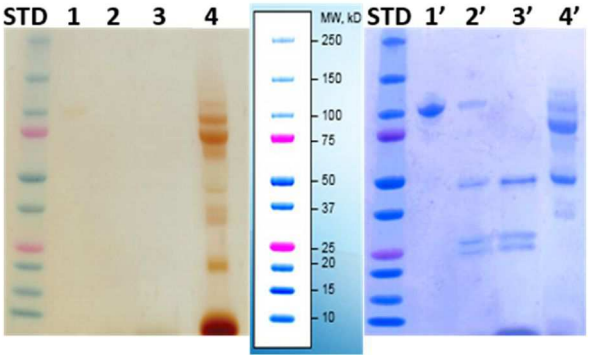

Figure 6.54: Characterization by SDS-PAGE (4-15%) in non-reducing conditions of (STD) protein standards, (1-1') F(ab')$_2$, (2-2') F(ab')$_2$ reduction with 10 mM cysteamine, (3-3') Fab' purified by gel filtration chromatography, (4-4') reaction mixture of Fab' PEGylation with MAL-PEG$_{5kDa}$-DSPE after 3 h incubation 10 µM $CuSO_4$. On the left the gel was stained with iodine for PEG visualization, on the right with Coomassie blue to visualize the proteins.

6.8 EVALUATION OF STORAGE CONDITIONS

As shown by the SDS-PAGE analysis in Figure 6.55, using water instead of 150 mM NaCl, 50 mM NaH_2PO_4, 10 mM EDTA pH 5.0 buffer for cysteamine purification by means of PES concentrators devices, drastically reduced the excessive reduction of Fab' fragment. In addition, significant differences among the tested storage conditions (to verify the effect on protein integrity) were not observed. To ensure that Fab' reactivity towards PEG maleimide group was still preserved, even in absence of EDTA, reduced and purified Fab' was reacted with MAL-PEG_{5kDa}-DSPE and the PEGylation occurred successfully, ad demonstrated in Figure 6.56.

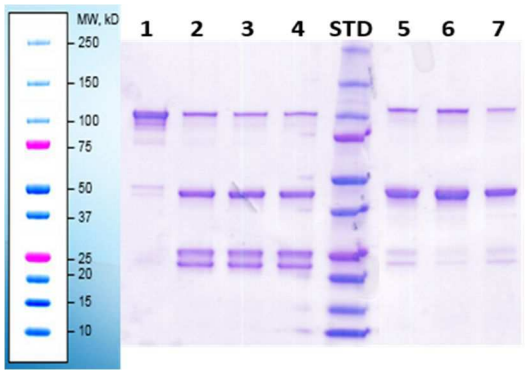

Figure 6.55: Characterization by SDS-PAGE (4-15%) in non-reducing conditions of (STD) protein standards, $F(ab')_2$ (1), Fab' purification from cysteamine through 10k MWCO PES concentrators using 150 mM NaCl, 50 mM NaH_2PO_4, 10 mM EDTA pH 5.0 buffer, followed by storage by N_2 freezing (2), at -20°C (3) and at 4°C (4). Cysteamine purification using water, instead of buffered solution, and storage by freezing in N_2 (5), at -20°C (6) and at 4°C (7).

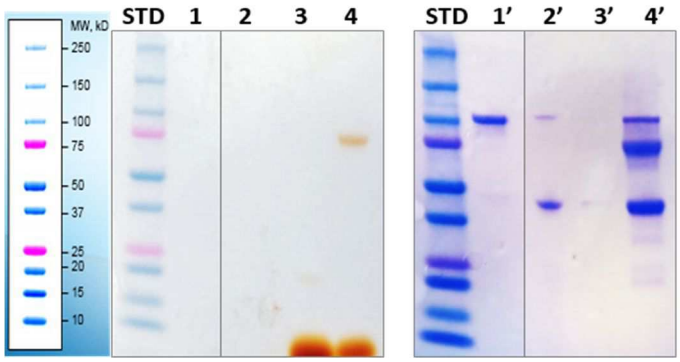

Figure 6.56: Characterization by SDS-PAGE (4-15%) in non-reducing conditions of (STD) protein standards, (1-1') $F(ab')_2$, (2-2') $F(ab')_2$ reduced with 10 mM cysteamine and buffer exchanged in water using PES 10k MWCO; (3-3') MAL-PEG_{5kDa}-DSPE; (4-4') reaction mixture of Fab' PEGylation with MAL-PEG_{5kDa}-DSPE.

6.9 IMMUNOLIPOSOMES FORMULATION

6.9.1 Liposomes preparation

An example of dimensional analysis of conventional (CL), stealth (SL) and super stealth (SSL_n) liposomes formulated including 4% mol of $mPEG_{5kDa}$-$(DSPE)_n$, is reported in Table 6.22.

Table 6.22: Example of liposome size distribution and polydispersity index (PdI).

	Size (nm)	PdI
CL (naked)	79.24 ± 1.82	0.06 ± 0.00
SL (stealth)	87.70 ± 2.37	0.05 ± 0.01
SSL_2 (super stealth $DSPE_2$)	97.27 ± 0.65	0.07 ± 0.01
SSL_4 (super stealth $DSPE_4$)	96.06 ± 1.20	0.05 ± 0.01

All formulated liposomes were characterized by a mean diameter of about 90-100 nm, except for conventional liposomes (CL) which were smaller and measured about 80 nm. This slight different in hydrodynamic volume can be attributed to the presence or absence of PEG on liposomes surface. The suspensions were homogeneous, with a very low polydispersity index (PdI < 0.1), since the instrument revealed the presence of only one population of particles of the same dimensions, represented as a single peak, with small standard deviations. In Figure 6.57 is reported an example of dimensional analysis by DLS of a liposomal sample.

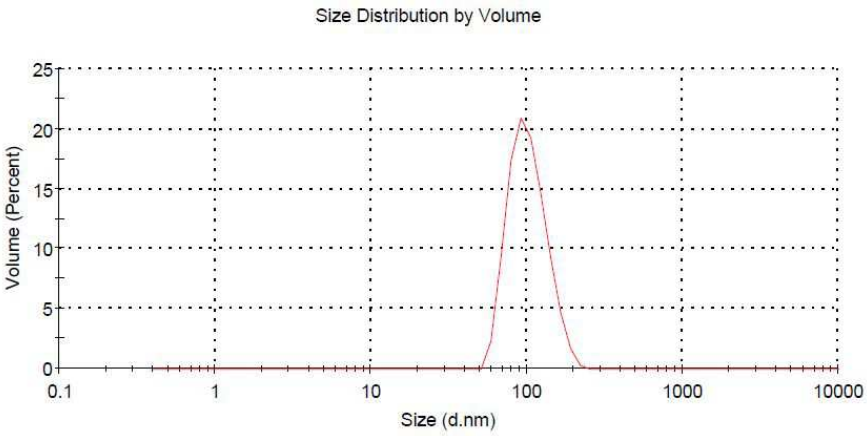

Figure 6.57: Example of dimensional analysis by DLS.

Doxorubicin was successfully loaded into liposomes, achieving a high encapsulation efficiency in all formulations: EE% > 95% for conventional (CL) and stealth liposome (SL), whereas EE% > 80% for super stealth formulations (SSL_n).

6.9.2 Post-insertion of PEG-lipid(s) derivatives

6.9.2.1 1st approach

In the 1st approach the post-insertion of PEG dendron-lipids derivatives was performed on doxorubicin-loaded pre-formed naked liposomes (CL) to obtain super stealth immunoliposomes ($SSIL_n$). $mPEG_{5kDa}$-$(DSPE)_n$ and Fab'-PEG_{5kDa}-$(DSPE)_n$ were either transferred separately and sequentially or simultaneously as a mixture.

$SSIL_2$ were successfully formulated by sequential post-insertion of $mPEG_{5kDa}$-$(DSPE)_2$ and Fab'-PEG_{5kDa}-$(DSPE)_2$ as demonstrated by SDS-PAGE analyses (Figure 6.58). The hydrodynamic volume assessed by DLS measurements after post-insertion also showed an increase of about 20 nm, from 96.65 ± 2.13 nm (PdI 0.06) for CL liposomes to a final mean size of 114.9 ± 0.82 nm (PdI 0.08) for $SSIL_2$. In addition, micro BCA-assay, performed on the final purified liposomal suspension, confirmed the transfer of the ligand-coupled PEG dendron-lipids derivatives into the bilayer at a final ratio of 131 µg Fab'/µmol HSPC.

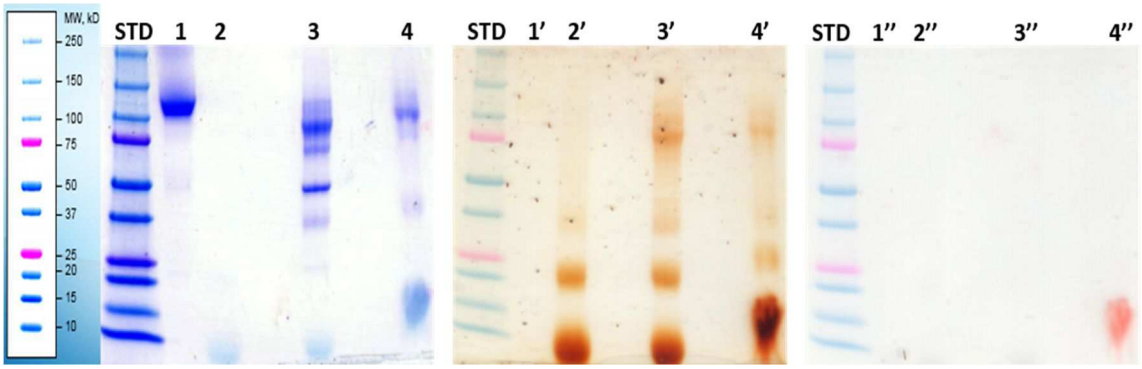

Figure 6.58: Characterization by SDS-PAGE (4-15%) in non-reducing conditions of (STD) protein standards, (1-1'-1'') F(ab')$_2$, (2-2'-2'') MAL-PEG$_{5kDa}$-DSPE$_2$, (3-3'-3'') Fab' PEGylation reaction mixture, (4-4'-4'') SSIL$_2$ after purification by gel filtration chromatography on a CL-4B column. [1-4] Coomassie blue staining for protein visualization, [1'-4'] iodine staining for PEG visualization and [1''-4''] unstained gel reported to show the red spot corresponding to DXR encapsulated in SSIL$_2$.

SDS-PAGE analysis evidenced that after purification by gel chromatography on a CL-4B column unreacted Fab' (~50 kDa) was removed and the transfer of Fab'-PEG_{5kDa}-$(DSPE)_2$ successfully occurred since Coomassie blue staining revealed a band at ~75 kDa.

Characterization of $SSIL_4$ formulated by sequential post-insertion of $mPEG_{5kDa}$-$(DSPE)_4$ and Fab'-PEG_{5kDa}-$(DSPE)_4$, instead, couldn't be completed since, after purification by gel chromatography on a CL-4B column, liposomes aggregated upon concentration in 50k MWCO Amicon devices. In Figure 6.59 is reported the dimensional analysis by DLS measurement of $SSIL_4$ after concentration, showing the formation of a second population (~20 %) of particles at higher hydrodynamic volume and polydispersity index (PdI > 0.15).

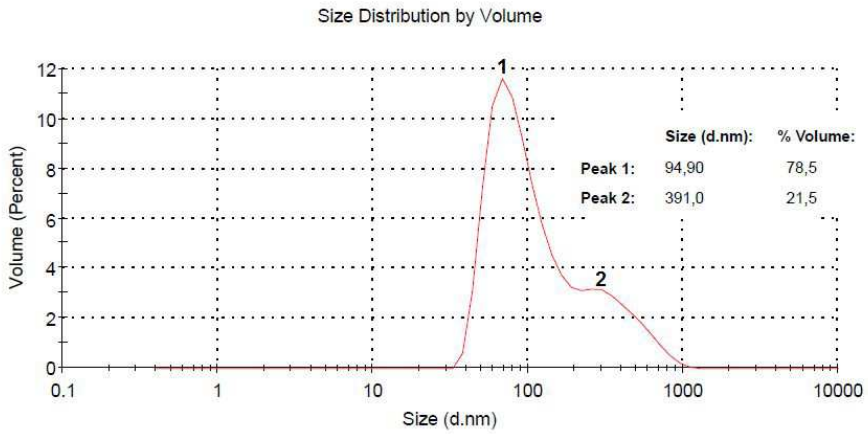

Figure 6.59: Evaluation of $SSIL_4$ mean size after purification and concentration.

Unfortunately, also simultaneous post-insertion of $mPEG_{5kDa}$-$(DSPE)_4$ and Fab'-PEG_{5kDa}-$(DSPE)_4$ couldn't provide $SSIL_4$ because the transfer of ligand-coupled PEG dendron-lipids derivative didn't occur. Dimensional evaluation through DLS measurements confirmed that liposomes mean diameter didn't significantly increase after post-insertion. The failed transfer was evidenced by SDS-PAGE analysis (Figure 6.60), since Coomassie blue staining didn't reveal bands at ~75 kDa corresponding to the monoconjugate Fab'-PEG_{5kDa}-$(DSPE)_4$.

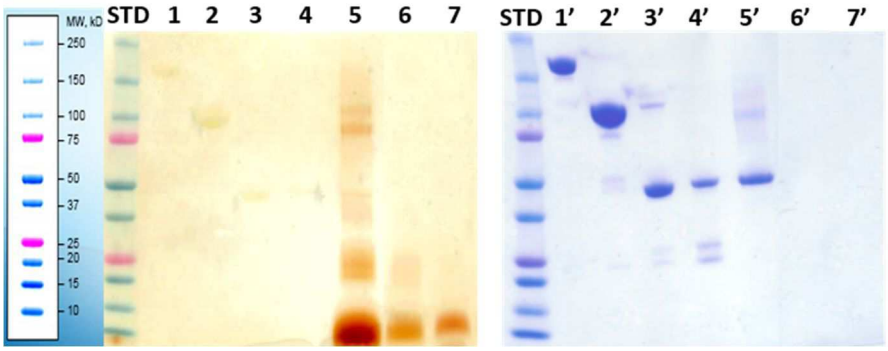

Figure 6.60: SDS-PAGE (4-15%) characterization in non-reducing conditions of (STD) protein standards, (1-1') Trastuzumab, (2-2') $F(ab')_2$, (3-3') $F(ab')_2$ reduced by cysteamine (reaction mixture), (4-4') Fab' purified by gel filtration chromatography, (5-5') reaction mixture of Fab' PEGylation with MAL-PEG-$DSPE_4$ after re-oxidation with $CuSO_4$, (6-6') MAL-PEG-$DSPE_4$, (7-7') $SSIL_4$ after purification by CL-4B. On the left the gel was stained with iodine for PEG visualization, on the right with Coomassie blue to visualize the proteins.

SIL were formulated by simultaneous post-insertion of $mPEG_{5kDa}$-DSPE and Fab'-PEG_{5kDa}-DSPE to assess whether the failure of transfer depended on the formulation approach itself or, perhaps, on the synthesized polymer. Figure 6.61 evidenced that also in this case the ligand-coupled PEG-lipid derivative failed to transfer from the micelles solution into the liposome bilayer because of the lack of bands at ~75 kDa, corresponding to the monoconjugate Fab'-PEG_{5kDa}-DSPE, after purification.

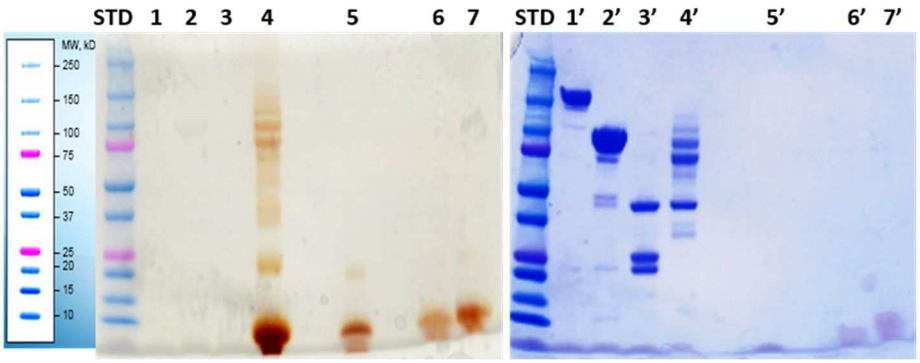

Figure 6.61: SDS-PAGE (4-15%) characterization in non-reducing conditions of (STD) protein standards, (1-1') Trastuzumab, (2-2') F(ab')$_2$, (3-3') F(ab')$_2$ reduced by cysteamine (reaction mixture), (4-4') reaction mixture of Fab' PEGylation with MAL-PEG-DSPE after re-oxidation with $CuSO_4$, (5-5') MAL-PEG-DSPE, (6-6') and (7-7') SIL after purification by CL-4B at increasing amount. On the left the gel was stained with iodine for PEG visualization, on the right with Coomassie blue to visualize the proteins.

Further characterization of the obtained liposomes was performed by transmission electron microscopy (TEM). The acquired images showed that super stealth immunoliposomes formulated either by sequential or simultaneous post-insertion of both mPEG$_{5kDa}$-(DSPE)$_n$ and Fab'-PEG$_{5kDa}$-(DSPE)$_n$ where characterized by the presence of vesicles with a jagged and discontinuous surface, in particular SSIL$_4$ (Figure 6.62). This might explain the physical instability of the formulations.

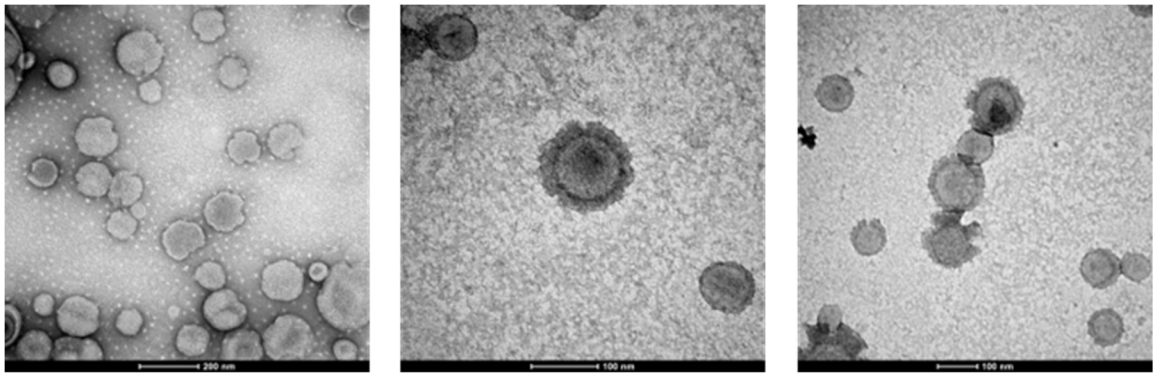

Figure 6.62: SSIL$_4$ characterization by transmission electron microscopy (TEM).

6.9.2.2 2nd approach

Post-insertion of PEG dendron-lipids derivatives was performed on doxorubicin-loaded pre-formed stealth (SL) and super stealth liposomes (SSL$_n$) to obtain the corresponding super stealth immunoliposomes (SSIL$_n$).

As shown in Table 6.23Table 6.23 and Figure 6.63, dimensional analysis through DLS measurements on the final liposomal suspension of $SSIL_2$ and SIL evidenced the presence of a single population of particles of the same dimensions, represented as a single peak, with small standard deviations. In addition, both the suspensions were homogeneous since the polydispersity index was very low (PdI < 0.1).

Table 6.23: Immunoliposomes size distribution and polydispersity index (PdI).

	Size (nm)	**PdI**
SIL (stealth immunoliposomes)	128.23 ± 1.02	0.04 ± 0.03
$SSIL_2$ (super stealth immunoliposomes $DSPE_2$)	102.11 ± 3.68	0.05 ± 0.02

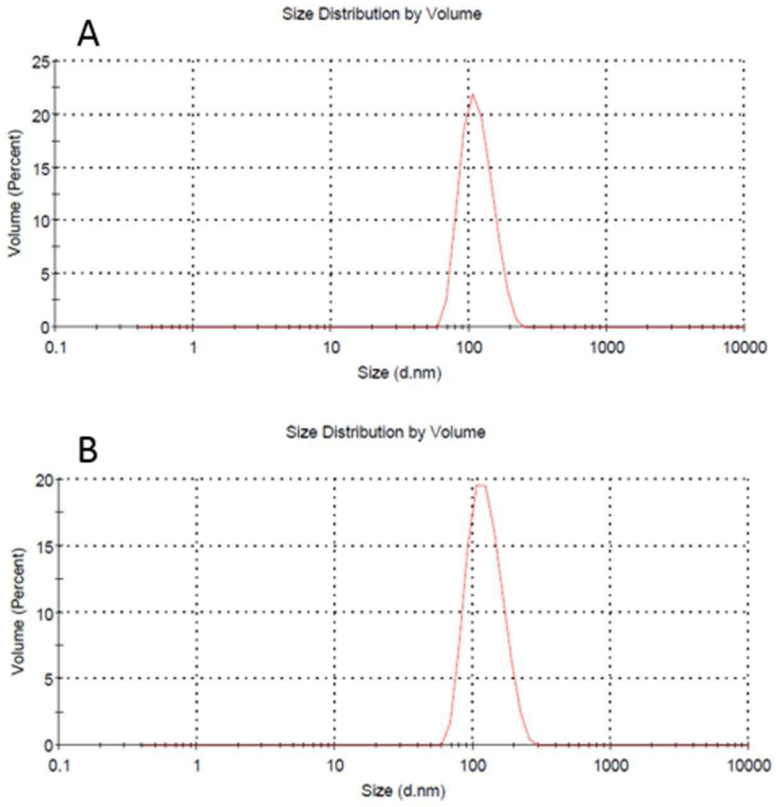

Figure 6.63: Dimensional analysis by DLS of (A) $SSIL_2$ and (B) SIL.

SDS-PAGE analysis confirmed that the post-insertion of ligand-coupled PEG-lipid(s) derivatives successfully took place as demonstrated by (Figure 6.64 and Figure 6.65). Moreover, quantification by micro BCA-assay on the final purified liposomal suspension resulted in 79.8 µg Fab'/µmol HSPC for SIL and 23.63 µg Fab'/µmol HSPC for $SSIL_2$.

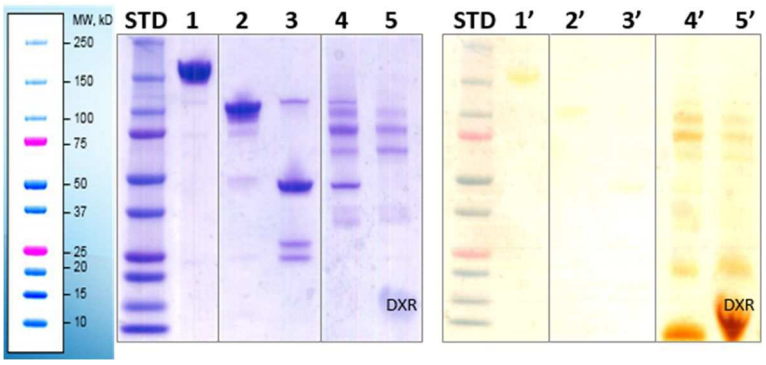

Figure 6.64: SDS-PAGE (4-15%) characterization in non-reducing conditions of (STD) protein standards, (1-1') Trastuzumab, (2-2') F(ab')$_2$, (3-3') reaction mixture of F(ab')$_2$ reduction with cysteamine 10 mM purified by 10k MWCO PES, (4-4') Fab' PEGylation with MAL-PEG$_{5kDa}$-DSPE, after re-oxidation with 10 µM $CuSO_4$ (reaction mixture), (5-5') SIL after purification by gel filtration chromatography through CL-4B column. On the left the gel was stained with iodine for PEG visualization, on the right with Coomassie blue to visualize the proteins.

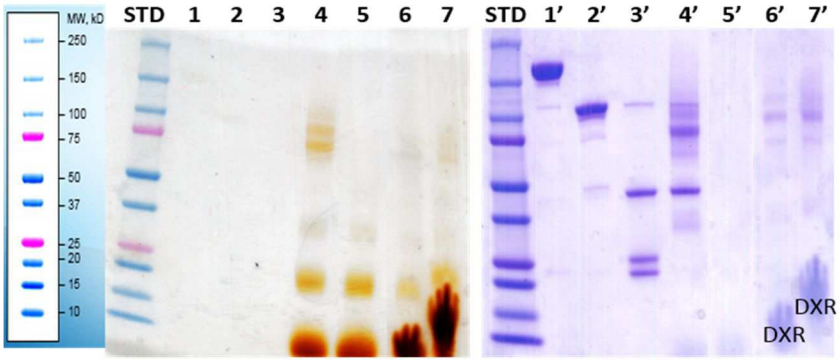

Figure 6.65: SDS-PAGE (4-15%) characterization in non-reducing conditions of (STD) protein standards, (1-1') Trastuzumab, (2-2') F(ab')$_2$, (3-3') reaction mixture of F(ab')$_2$ reduction with cysteamine 10 mM purified by 10k MWCO PES, (4-4') Fab' PEGylation with MAL-PEG$_{5kDa}$-DSPE$_2$, after re-oxidation with 10 µM $CuSO_4$ (reaction mixture), (5-5') MAL-PEG$_{5kDa}$-DSPE$_2$; (6-6')-(7-7') 2,5 and 5µl respectively of SSIL$_2$ after purification by gel filtration chromatography on a CL-4B column. On the left the gel was stained with iodine for PEG visualization, on the right with Coomassie blue to visualize the proteins.

In both SIL and SSIL$_2$, unreacted Fab' and F(ab')$_2$ were successfully removed from the final liposome suspension by gel filtration chromatography through a CL-4B column. Fab'-PEG-(DSPE)$_n$, instead, was transferred to the lipid bilayer since a band at ~75 kDa (monoconjugated Fab') and at ~85-90 kDa (biconjugated Fab') were revealed. Di-PEGylated Fab' formed upon excessive reduction of Fab' by cysteamine.

In Figure 6.66 are reported the images acquired by TEM analysis of the final liposomal suspension of SIL and SSIL$_2$. Doxorubicin is visible as crystals inside the vesicles.

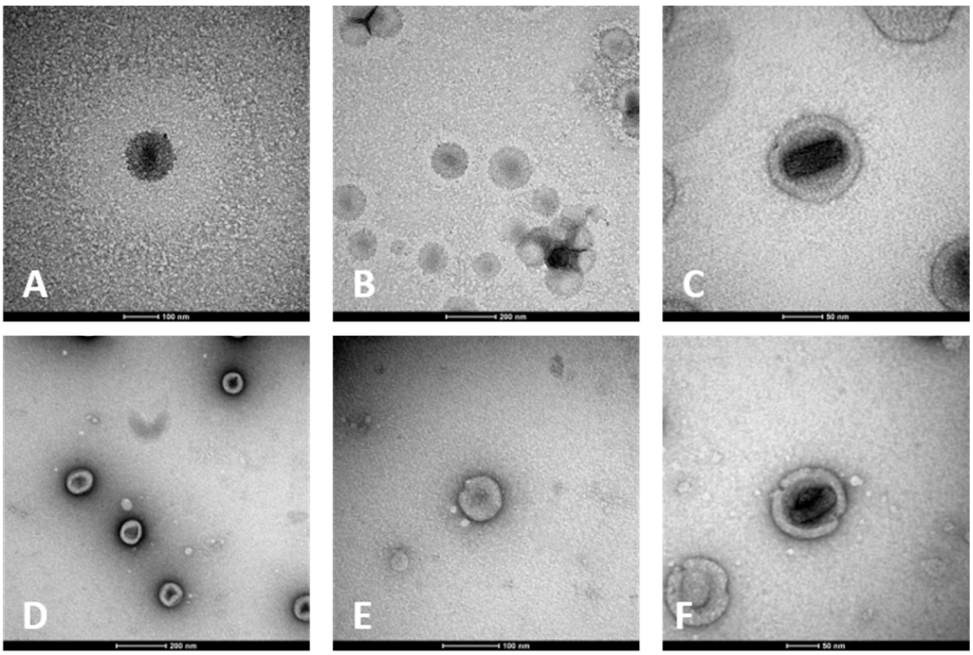

Figure 6.66: Transmission electron microscopy (TEM) characterization of SIL (A, B, C) and $SSIL_2$ (D, E, F).

$SSIL_4$ formulation resulted the most challenging also using this post-insertion approach. Following doxorubicin loading and removal through PD-10 desalting columns of non-encapsulated drug, the suspension was concentrated by centrifugation on 50k MWCO Amicon devices and characterized by DLS. Liposomes resulted either increased in mean size and polydispersity index (e.g. 185.00 ± 4.38 nm, PdI > 0.1) or presented a small percentage of aggregates, clear sign of physical instability. It was concluded that probably this instability was due to the $mPEG_{5kDa}$-$DSPE_4$ included in the initial lipid mixture.

6.10 *IN VITRO* EXPERIMENTS

6.10.1 Long-term stability studies

Samples of each liposomal formulation (300 µl, 3 mM) containing 0.05% w/v NaN_3 were incubated at 4-25-37°Cover time. Vesicles mean size and polydispersity (PdI) were assessed by DLS measurements at predetermined time points as shown in Table 6.24 – Table 6.27. After about 2 months of incubation at 4°C and 25 °C all tested formulations were still stable and homogeneous (PdI <0.1), whereas at 37°C all liposomal formulations started to aggregate after 14 days of incubation, showing also increased PdI (> 0.1).

Table 6.24: Mean size and PdI over time of stealth liposomes incubated at 4-25-37°C.

STEALTH LIPOSOMES (SL)						
	4°C		25°C		37°C	
time	**mean size (nm)**	**PdI**	**mean size (nm)**	**PdI**	**mean size (nm)**	**PdI**
T=0	99.6 ± 2.1	0.05	99.6 ± 2.1	0.05	99.6 ± 2.1	0.05
1 day	102.8 ± 1.1	0.04	103.1 ± 1.0	0.05	99.8 ± 3.9	0.05
3 days	103.2 ± 0.8	0.05	102.0 ± 0.9	0.03	103.9 ± 0.4	0.09
1 week	103.6 ± 1.5	0.04	102.0 ± 1.0	0.04	103.1 ± 2.6	0.13
2 weeks	102.4 ± 0.8	0.05	101.1 ± 2.8	0.06	Aggregates	> 0.3
3 weeks	102.7 ± 0.8	0.05	103.3 ± 1.1	0.05	(> 4600 nm)	
4 weeks	103.0 ± 0.5	0.06	102.4 ± 3.1	0.06		
5 weeks	102.6 ± 0.6	0.06	101.2 ± 1.7	0.06		
6 weeks	101.0 ± 2.1	0.06	99.8 ± 1.8	0.10		
7 weeks	103.8 ± 0.3	0.05	101.9 ± 3.3	0.08		
8 weeks	101.3 ± 1.5	0.05	103.6 ± 1.7	0.11		
9 weeks	104.8 ± 1.0	0.06	102.9 ± 3.6	0.08		
11 weeks	104.3 ± 0.3	0.04	103.8 ± 1.8	0.10		

Table 6.25: Mean size and PdI over time of stealth immunoliposomes incubated at 4-25-37°C.

STEALTH IMMUNOLIPOSOMES (SIL)						
	4°C		25°C		37°C	
time	**mean size (nm)**	**PdI**	**mean size (nm)**	**PdI**	**mean size (nm)**	**PdI**
T=0	124.2 ± 0.5	0.05	124.2 ± 0.5	0.05	124.2 ± 0.5	0.05
1 day	129.0 ± 0.3	0.05	126.6 ± 1.6	0.05	122.9 ± 3.3	0.02
3 days	127.6 ± 1.8	0.02	123.1 ± 1.1	0.03	124.3 ± 2.9	0.08
1 week	128.2 ± 0.6	0.05	124.1 ± 3.4	0.07	122.3 ± 4.4	0.10
2 weeks	126.2 ± 2.3	0.06	122.0 ± 5.6	0.07	123.2 ± 3.2 (83%)	0.15
3 weeks	128.1 ± 0.8	0.04	125.2 ± 1.9	0.05	Aggregates	
4 weeks	127.0 ± 1.3	0.04	122.9 ± 3.0	0.05		
5 weeks	126.2 ± 2.1	0.04	124.0 ± 2.8	0.06		
6 weeks	125.8 ± 3.5	0.07	124.0 ± 4.1	0.06		
7 weeks	128.5 ± 2.4	0.06	125.7 ± 6.0	0.07		
8 weeks	126.0 ± 2.0	0.07	129.7 ± 2.9	0.07		
9 weeks	127.7 ± 2.8	0.05	126.3 ± 4.7	0.09		
11 weeks	132.1 ± 0.1	0.07	130.2 ± 1.9	0.1		

Table 6.26: Mean size and PdI over time of stealth liposomes SSL_2 incubated at 4-25-37°C.

SUPER STEALTH LIPOSOMES (SSL_2)						
	4°C		25°C		37°C	
time	**mean size (nm)**	**PdI**	**mean size (nm)**	**PdI**	**mean size (nm)**	**PdI**
T=0	97.7 ± 3.4	0.04	97.7 ± 3.4	0.04	97.7 ± 3.4	0.04
1 day	99.2 ± 0.9	0.03	97.4 ± 2.7	0.04	97.3 ± 3.5	0.05
3 days	102.3 ± 0.9	0.05	98.5 ± 2.7	0.04	94.6 ± 4.0	0.06
1 week	100.8 ± 0.5	0.05	99.5 ± 0.9	0.03	98.0 ± 1.9	0.12
2 weeks	98.1 ± 3.3	0.05	98.5 ± 2.6	0.04	Aggregates	>0.9
3 weeks	100.0 ± 2.0	0.04	98.3 ± 2.2	0.04	(> 2100 nm)	
4 weeks	98.1 ± 2.2	0.06	97.2 ± 2.7	0.04		
5 weeks	102.6 ± 0.9	0.04	98.7 ± 1.6	0.04		
6 weeks	102.5 ± 0.4	0.05	97.1 ± 2.6	0.05		
7 weeks	104.2 ± 2.0	0.05	97.7 ± 0.7	0.07		

Table 6.27: Mean size and PdI over time of super stealth immunoliposomes ($SSIL_2$) incubated at 4-25-37°C.

SUPER STEALTH IMMUNOLIPOSOMES ($SSIL_2$)						
	4°C		25°C		37°C	
time	**mean size (nm)**	**PdI**	**mean size (nm)**	**PdI**	**mean size (nm)**	**PdI**
T=0	101.7 ± 0.7	0.05	101.7 ± 0.7	0.05	101.7 ± 0.7	0.05
1 day	103.2 ± 1.0	0.04	100.0 ± 1.3	0.06	100.0 ± 4.2	0.05
3 days	101.5 ± 1.0	0.05	101.8 ± 1.2	0.03	99.9 ± 3.5	0.08
1 week	102.5 ± 2.4	0.03	100.0 ± 3.2	0.06	99.6 ± 2.7	0.07
2 weeks	103.5 ± 1.3	0.05	101.1 ± 1.3	0.03	103.7 ± 0.7 (82.8%)	0.18
3 weeks	102.4 ± 2.6	0.05	98.4 ± 2.9	0.03		
4 weeks	103.4 ± 1.8	0.06	99.0 ± 2.8	0.02		
5 weeks	103.7 ± 1.6	0.09	99.8 ± 1.4	0.06		
6 weeks	102.7 ± 2.5	0.06	99.6 ± 1.8	0.05		
7 weeks	104.3 ± 0.9	0.08	100.4 ± 0.8	0.06		
8 weeks	104.8 ± 0.7	0.07	98.4 ± 1.3	0.08		

6.10.2 Drug release experiments

The formulated liposomes were analyzed by fluorometer to assess the DXR fluorescence dequenching over time, thus evidencing the drug release profiles shown in Figure 6.67. In all tested formulation there wasn't drug leakage up to 16 h, meaning that doxorubicin is efficiently entrapped inside the nanocarrier.

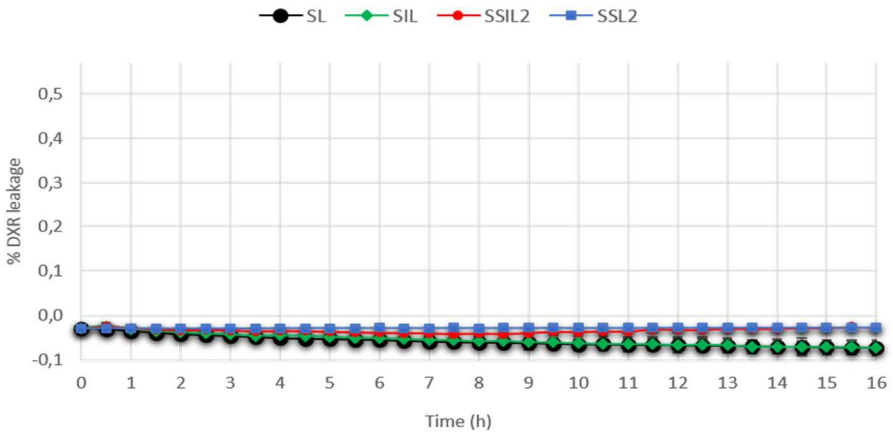

Figure 6.67: In vitro releasing profiles of doxorubicin from the liposomal formulations.

6.10.3 Cytotoxicity studies

6.10.3.1 Effect of the liposomal formulations on cell viability

Crystal Violet Assay on human breast ductal carcinoma cell line (BT-474) overexpressing HER-2, treated with liposomal formulation at different doxorubicin concentrations, provided the results reported in Figure 6.68. As expected, the free drug was the most potent, since the cell viability was reduced to 20-30 % after a 24h-treatment, even at the lowest tested concentration (1 µM). By increasing the concentration to 10 µM, the cell viability was reduced of more than 50% by all treatments, except for 1 h treatment followed by a short incubation (72 h) period.

As expected, empty stealth liposomes (SL) proved to be non-cytotoxic at all the tested conditions, since the cell viability was preserved. Differences between non-targeted (SL-DXR) and target (SIL-DXR and $SSIL_2$-DXR) liposomal formulations were emphasized at 10 µM DXR. In fact, SL-DXR could not reduce the cell viability below 50% after a 24 h-treatment with 10 µM DXR, whereas both SIL-DXR and $SSIL_2$-DXR reduced cell viability to about 40% in the same experimental conditions.

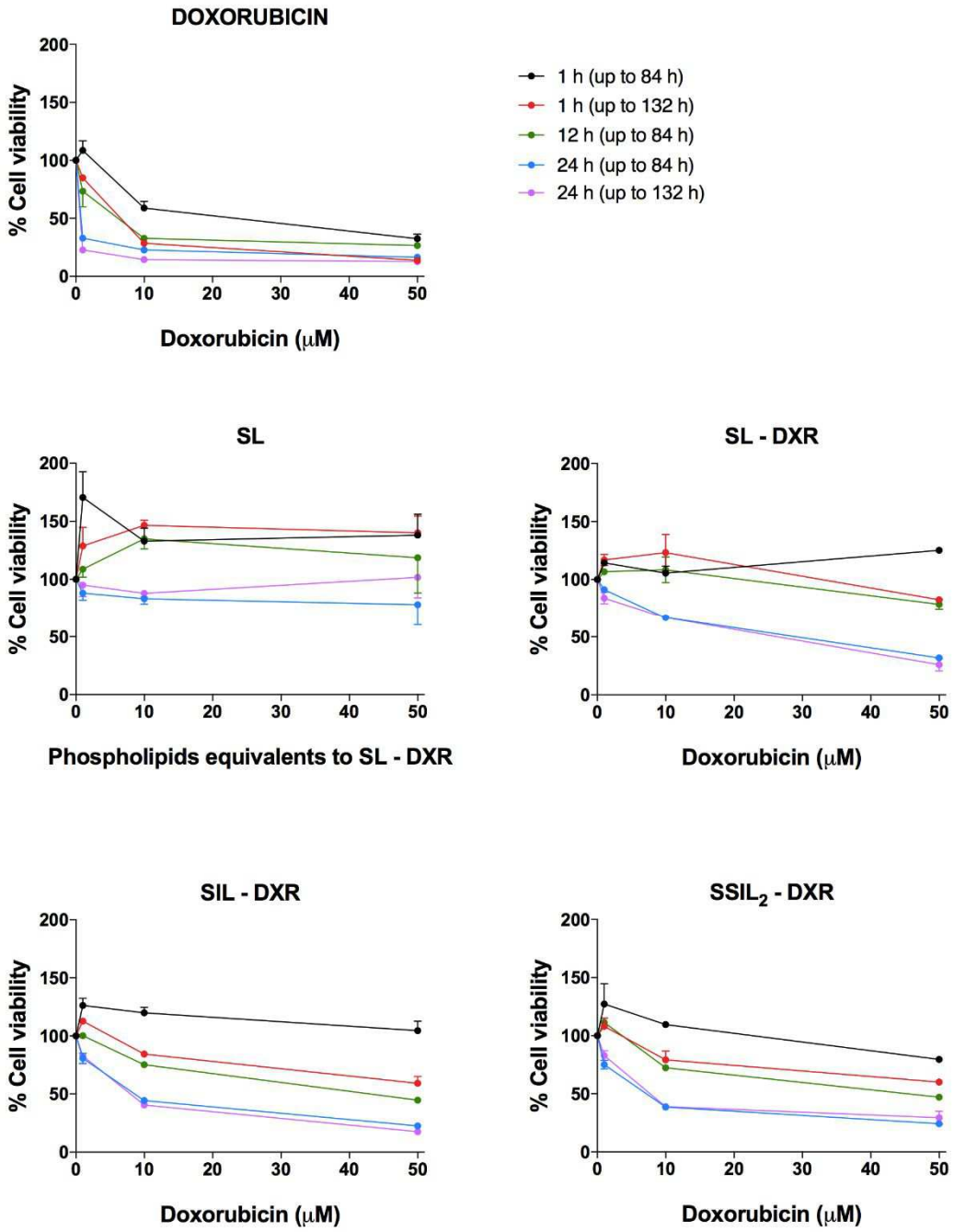

Figure 6.68: Cell viability (%) of BT-474 cells treated for 1 h, 12 h, 24 h with free doxorubicin, doxorubicin-loaded stealth liposomes (SL), doxorubicin-loaded stealth immunoliposomes (SIL-DXR) and doxorubicin-loaded super stealth immunoliposomes ($SSIL_2$) at a final DXR concentration of 1 μM, 10 μM and 50μM. Cells were also treated with empty stealth liposomes (SL), used as control, at the same lipid concentration of SL-DXR. After treatment, cells were washed and incubated with culture medium up to 84 h (short incubation) or 132 h (long incubation).

Since the treatments at 10 μM in doxorubicin best evidenced the differences between targeted and non-targeted formulations, statistical analysis was conducted on the data obtained at this concentration, to ascertain whether SIL-DXR and $SSIL_2$-DXR show significant differences in their effect with respect to SL-DXR (Figure 6.69).

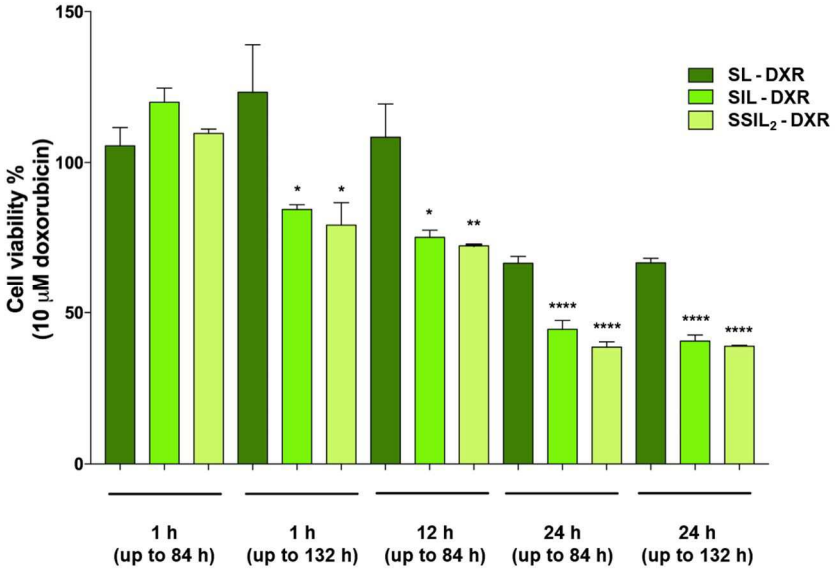

*Figure 6.69: Significance of cell viability (%) differences at 10 μM doxorubicin between SL, SIL and $SSIL_2$ with different length of treatment. * p<0.05, ** p<0.01, **** p<0.0001 vs SL-DXR.*

Cell viability of BT-474 cells treated with SL-DXR, SIL-DXR and $SSIL_2$-DXR was significantly different with respect to cells treated with free doxorubicin or empty SL (data not shown).
As demonstrated by Figure 6.69, statistically significant differences among the formulations couldn't be observed after 1 h treatment at 10 μM in DXR and additional incubation in culture medium up to 84 h. Cell viability became significantly different (*p <0.05) between targeted (SIL-DXR and $SSIL_2$-DXR) and non-targeted (SL-DXR) formulations after 1h treatment followed by long incubation in culture medium (up to 132 h) and the difference between SL-DXR and $SSIL_2$-DXR was further stressed (**p <0.01) after the 12 h treatment. However, the greatest statistical difference among targeted and non-targeted liposomes was observed after the 24 h treatments (****p <0.0001).

In Figure 6.70 IC50 calculation is reported for each liposomal formulation and free doxorubicin. This experiment was performed on BT-474 cells treated for 24 h and incubated for additional 12 h in culture medium. It was clearly evidenced that, at the tested conditions, all the doxorubicin-loaded liposomal formulations possessed the same potency in inducing cell death, since the IC50 values where virtually identical (Table 6.28). Small differences were observed taking into consideration the efficacy of each formulation (SL-DXR < SIL-DXR < $SSIL_2$-DXR) and, interestingly, $SSIL_2$-DXR possessed the same efficacy of free doxorubicin.

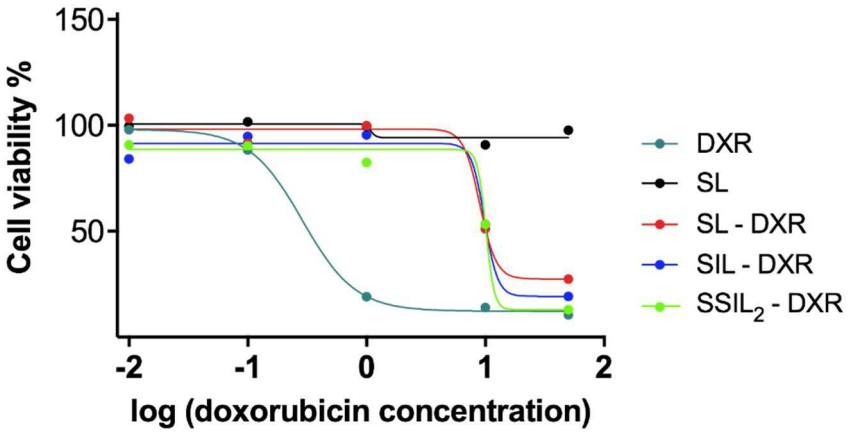

Figure 6.70: IC50 calculation of the liposomal formulations and free doxorubicin.

Table 6.28: IC50 values of the liposomal formulations and free doxorubicin.

	IC50 (μM)
DXR	0.288
SL-DXR	8.973
SIL-DXR	9.848
$SSIL_2$-DXR	10.100

6.10.3.2 Effect of the liposomal formulations on cell apoptosis

A preliminary evaluation of the effect of the three formulations on apoptotic pathways was obtained through a western blot analysis aiming to assess the expression of Cleaved Caspase 3 and Caspase 3 upon treatment of BT-474 cells with each liposomal formulation and free doxorubicin, compared to untreated cells. Cleaved caspase 3 and caspase 3 were quantified using ImageJ software and normalized to β-actin (Figure 6.71). The ratio between Cleaved Caspase 3 and Caspase 3 expression was also evaluated [111].

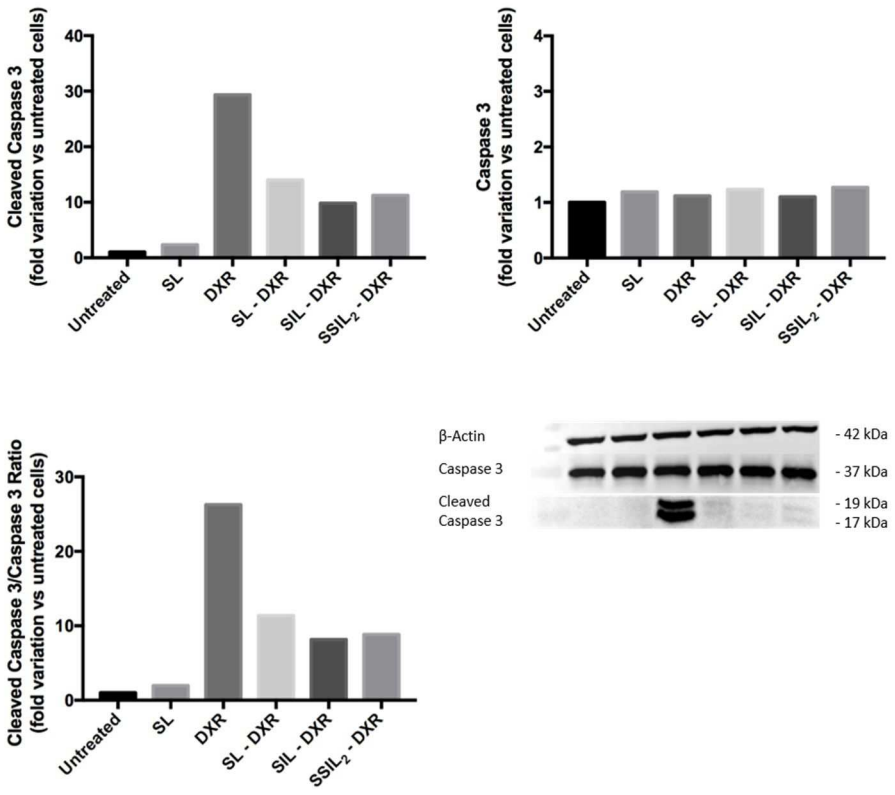

Figure 6.71: Cleaved caspase 3 and Caspase 3 protein expression variation versus untreated cells. The ratio between Cleaved Caspase 3 and Caspase 3 is also reported.

This preliminary test evidenced that after 6 h treatment, followed by 24 h of incubation with culture medium, the expression levels of Cleaved Caspase 3 (marker of apoptosis) were increased by almost 30-fold in cells treated with DXR, as expected, with respect to the untreated cells. A 10-fold increment was observed in cells treated with the three doxorubicin-loaded liposomal formulations with respect to untreated cells.
Empty SL didn't affect the expression of Cleaved Caspase 3 with respect to untreated cells, since they didn't induce apoptosis.

6.11 *IN VIVO* EXPERIMENTS

6.11.1 Pharmacokinetics in rats

Fluorometric analysis of the collected plasma samples allowed the quantification of DXR. The obtained data were elaborated using the software PK Solver 2.0 and applying a bicompartmental model to get the pharmacokinetic profile (Figure 6.72 and Figure 6.73) and the corresponding pharmacokinetic parameters of each liposomal formulation (Table 6.29).

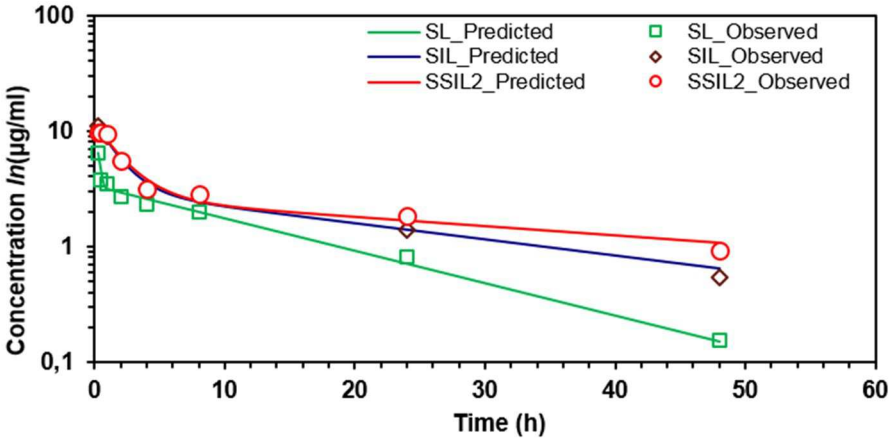

Figure 6.72: In vivo pharmacokinetic profiles of SL, SIL, $SSIL_2$.

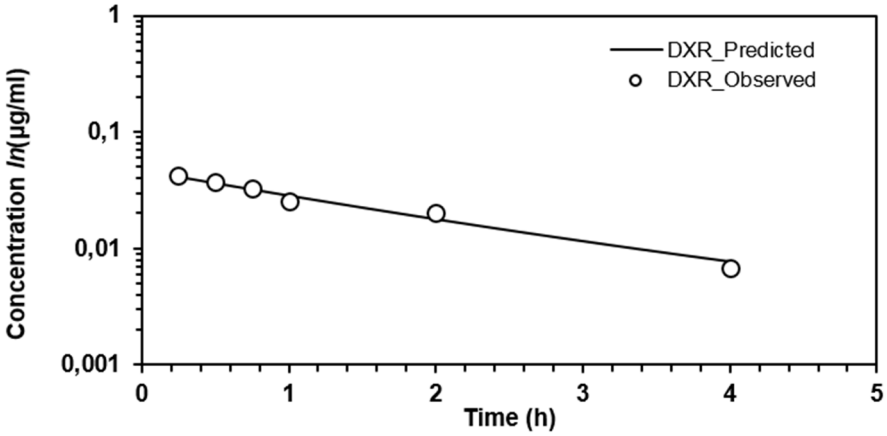

Figure 6.73: In vivo pharmacokinetic profiles of doxorubicin.

Table 6.29: Pharmacokinetic parameters calculated by PK Solver 2.0.

Parameter	Unit	DXR	SL	SIL	$SSIL_2$
$t_{1/2\,\alpha}$	*h*	1.09	0.11	1.19	1.50
$t_{1/2\,\beta}$	*h*	2.52	10.77	21.43	37.80
V_d	*ml*	52.85	1.39	2.03	2.20
CL	*ml/h*	23.43	0.47	0.23	0.16
$AUC_{0\text{-}inf}$	*µg/ml*h*	0.11	53.49	108.84	161.07

Data in Table 6.29 confirmed the increased stability provided by PEG dendron-lipids derivatives over PEG-single phospholipid, since $SSIL_2$ showed prolonged half-life ($t_{½}$), almost 4-fold with respect to SL. Interestingly, also SIL $t_{½}$ resulted 2-fold prolonged compared to SL, even though it is expected to be similar, so further investigation might be required. As expected, all liposomal

formulation presented an increased half-life with respect to the free doxorubicin. A reduction in clearance rate was also observed, from ~0.5 ml/h for SL to ~0.2 ml/h for $SSIL_2$, demonstrating that the formulation containing PEG dendron-lipids derivatives were eliminated more slowly and, thus, circulate longer in the bloodstream. On the other hand, free doxorubicin is promptly eliminated (~23 ml/h). $SSIL_2$ were also characterized by higher bioavailability (AUC) and distribution volume (Vd) compared to all the other tested formulations.

Overall, $SSIL_2$ proved to be endowed with the best *in vivo* behavior.

6.11.2 *In vivo* toxicity evaluation

6.11.2.1 Gene expression quantification by qRT-PCR

The gene expression of interleukin 1β (IL-1β), interleukin 6 (IL-6) and tumor necrosis factor α (TNFα), was evaluated in liver, kidney, spleen and heart tissues to assess and compare the toxicity of the liposomal formulations toward these organs after single dose administration.

In Figure 6.74 the gene expression of the pro-inflammatory cytokines in the liver is reported.

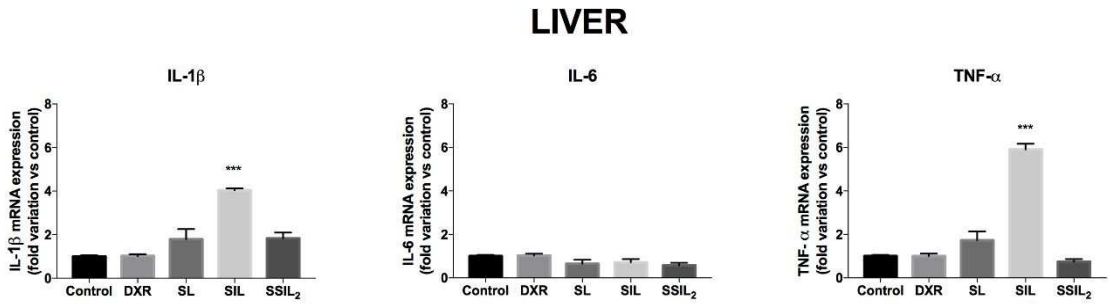

*Figure 6.74: Gene expression of the three pro-inflammatory cytokines IL-1β, IL-6 and TNFα in the liver. *** p<0.001 vs control.*

IL-1β and TNFα expression was significantly increased in rats treated with SIL (***p <0.001), whereas SL and $SSIL_2$ didn't provoke significant changes in the gene expression with respect to the control group. Constant levels of IL-6 expression were observed in all the study groups, and gene expression levels of all the three cytokines was not affected by free doxorubicin in the liver with respect to the control group.

Figure 6.75 shows the gene expression of the three cytokines in the kidneys.

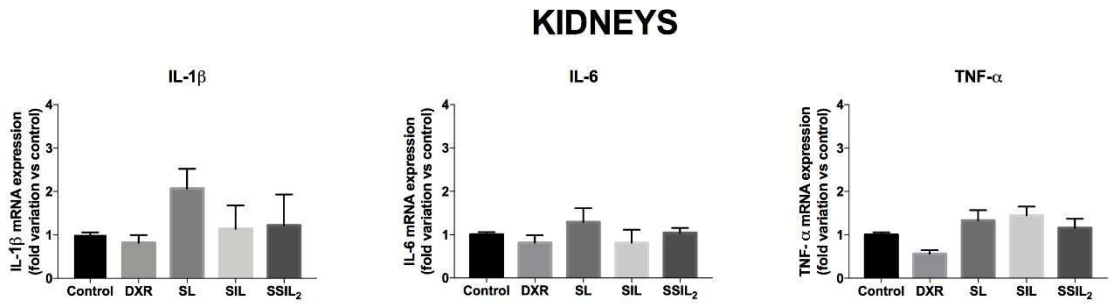

Figure 6.75: Gene expression of the three pro-inflammatory cytokines IL-1β, IL-6 and TNFα in the kidneys.

IL-1β expression in animals treated with SIL tended to increase also in the kidneys but this difference was not statistically significant, due probably to the high inter-individual variability. Overall, no statistically significant differences in gene expression could be evidenced in the animal groups treated with the different formulations with the respect to the control group.

In Figure 6.76 the variation of IL-1β, IL-6 and TNFα gene expression in the heart is reported.

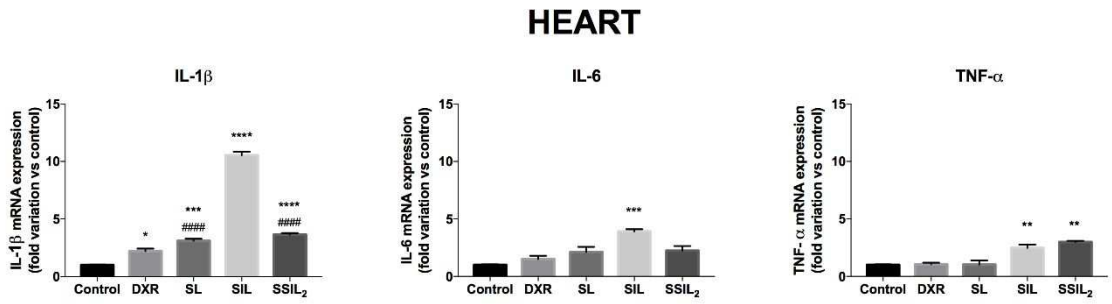

Figure 6.76: Gene expression of the three pro-inflammatory cytokines IL-1β, IL-6 and TNFα in the heart.
** p<0.05, ** p<0.01, *** p<0.001, **** p<0.0001 vs control; #### p<0.0001 vs SIL.*

Since the most prominent side-effect of doxorubicin therapy is cardiotoxicity, it was important to evaluate the inflammatory state of heart tissue. Since cardiotoxicity is dose-dependent, a low single dose cannot probably induce cardiotoxicity. However, a 2-fold increase in IL-1β expression could be observed in DXR-treated animals. In these experimental conditions, the animals treated with the three liposomal formulations showed a significantly relevant increase of IL-1β expression (10-fold for SIL-treated animals and about 3-fold for SL and $SSIL_2$) compared to the control group. However, IL-1β gene expression was significantly lower in the heart of SL and $SSIL_2$-treated animals with respect to SIL-treated rats. The gene expression of IL-6 show a trend similar to that of IL-1β, whereas TNFα increased significantly in both SIL and $SSIL_2$-treated rats.

Figure 6.77 shows the levels of gene expression variation of the three cytokines in the spleen.

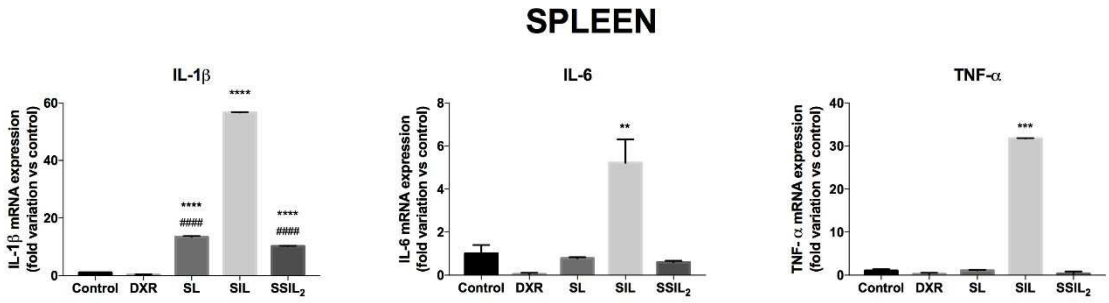

*Figure 6.77: Gene expression of the three pro-inflammatory cytokines IL-1β, IL-6 and TNFα in the spleen. ** p<0.01, *** p<0.001, **** p<0.0001 vs control; #### p<0.0001 vs SIL.*

Results shown in Figure 6.77 are in accordance with the finding obtained in the other organs. The rats treated with SL, SIL and $SSIL_2$ evidenced a significant increase of IL-1β, IL-6 and TNFα expression compared to the control group. In particular, IL-1β expression increased dramatically (55-fold) in SIL treated rats, whereas an increase of about 10-fold was observed in animals treated with SL and $SSIL_2$. It should also be noticed that the gene expression of IL-1β in SL and $SSIL_2$-treated rats was significantly lower than that of SIL-treated animals. Gene expression of IL-6 and TNFα was significantly increased only in SIL treated rats with respect to the control group.

6.11.2.2 Histological analyses

The histological analyses performed on liver and spleen sections are reported below. The other organs (i.e. heart, lungs, brain) didn't show any pathological alteration in all the groups of rats examined (data not shown). The liver of rat treated with free DXR (Figure 6.79 a) where undistinguishable from that of control animals (Figure 6.78 a), whereas rats treated with free DXR showed an extremely slight increase in hematopoiesis in the splenic tissue (Figure 6.79 b) when compared to untreated rats (Figure 6.78 b).

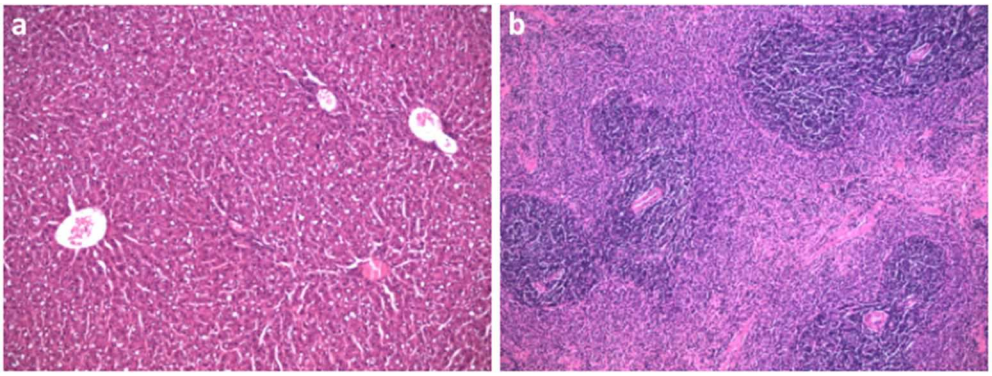

Figure 6.78: Representative photomicrographs of a control rat. No histological alterations could be observed in the liver (a) and spleen (b).

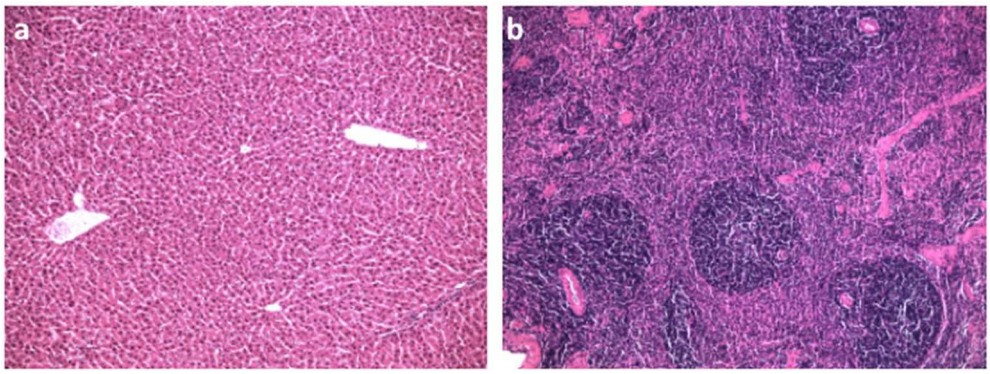

Figure 6.79: Representative photomicrographs of a rat treated with free DXR. No histological alterations in the liver (a) and a slight increased hematopoiesis in the splenic tissue (b) could be observed.

Animals treated with SL-DXR and SIL-DXR showed similar histological alterations in liver and spleen, i.e. numerous granulomatous lesions, sometimes associated with apoptotic bodies, in the liver (Figure 6.80 a), and variable degree of histiocytosis associated with marked increase in extramedullary hematopoiesis (megakaryocytosis in particular) in the spleen (Figure 6.80 b).

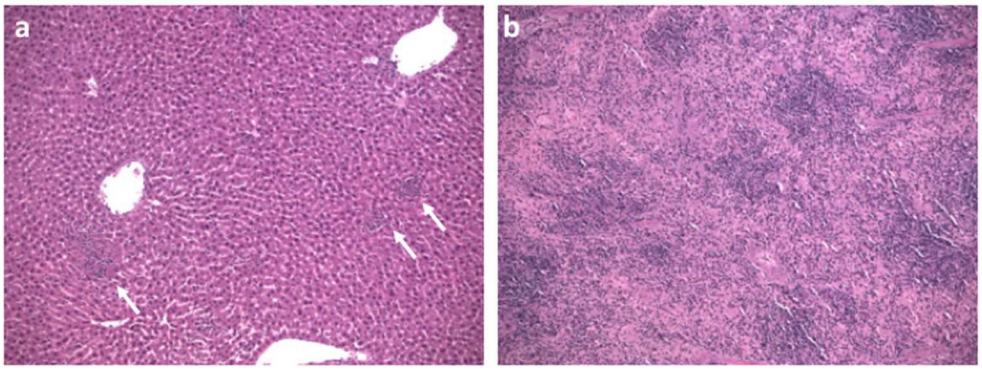

Figure 6.80: Representative photomicrographs of a rat treated with SL – DXR and SIL – DXR. Multiple granulomatous lesions in the liver (a, indicated by arrows) and extensive fibrosis associated with increased hematopoiesis in the splenic tissue (b) could be observed.

Interestingly, in rats treated with $SSIL_2$-DXR only one isolated granuloma was observed in the otherwise healthy livers (Figure 6.81 a), and only a slight increase of hematopoiesis could be observed in the splenic tissue (Figure 6.81 b).

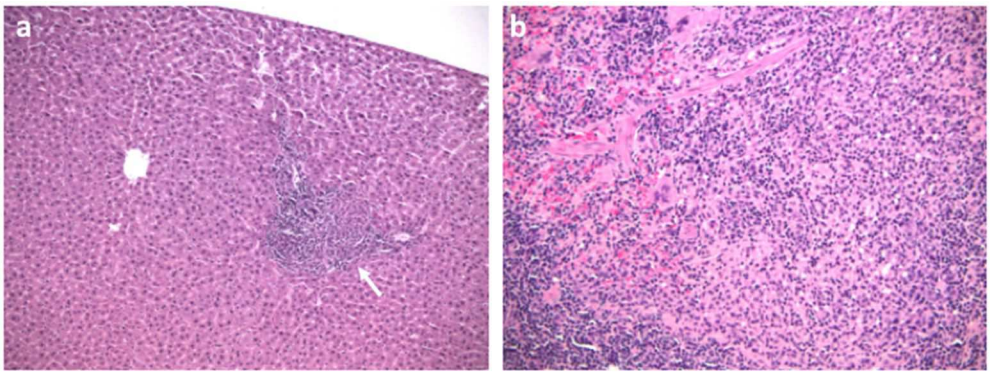

Figure 6.81: Representative photomicrographs of a rat treated with $SSIL_2$ – DXR. An isolated granulomatous lesion in the liver (a, indicated by the arrow) and slightly increased hematopoiesis in the splenic tissue (b) could be observed.

7. DISCUSSION

Modern pharmaceutical technology is aiming at overcoming the limitations imposed by classical anticancer therapy and, therefore, improving the pharmacokinetic profile of molecules endowed with good biological activity but presenting low therapeutic index and remarkable side effects. The present work focuses on doxorubicin, an anthracycline antibiotic commonly used in the treatment of a wide range of hematological malignancies and solid tumors. Despite being highly potent (IC50: 4 nM – 32 µM depending on the cell line [112]), its clinical use is limited by several side effects, such as acute vomiting and nausea, mucositis, gastrointestinal problems, alopecia, etc., and the most prominent being cardiotoxicity. These side effects are attributable to the lack of selectivity of doxorubicin toward cancer cells. Therefore, the research has been focusing through the years on the development of Drug Delivery Systems (DDSs) to achieve a selective delivery to the tumor site exploiting specific targeting agents.

Nowadays, liposomes are considered amongst the most useful and versatile of all DDSs. An important turning point in the field of drug delivery was achieved with stealth liposomes, obtained by surface modification with hydrophilic polymers, usually polyethylene glycol (PEG). This strategy confers "stealth" properties, allowing to avoid the recognition and subsequent clearance by the mononuclear phagocyte system, thereby increasing their circulation half-life. In such way, an increased dose of anticancer drug can passively accumulate in the tumor site exploiting the enhanced permeation and retention (EPR) effect [1]. The polymer is attached to the bilayer by means of conjugation to a natural phospholipid like distearoylphosphatidylethanolamine (DSPE), obtaining a PEG-single phospholipid derivative which is included in lipid mixture during the formulation process. Doxyl®/Caelyx®, containing $mPEG_{2kDa}$-DSPE, was the first stealth liposomal doxorubicin formulation reaching the market. However, it was reported in literature [57] that the beneficial effect of PEG shielding might be lost upon PEG-phospholipid detachment in biological liquids, leaving the carrier vulnerable to opsonization. To solve this problem Super Stealth Liposomes (SSLs) were developed [2] in which a molecule of PEG dendron 5 kDa is linked to 2 or 4 molecules of DSPE (PEG dendron-lipids derivative) allowing to increase the hydrophobic interactions with the bilayer, thereby reducing the detachment.

Further advancement in liposomes development was achieved with the introduction of stealth immunoliposomes (SILs). In fact, the use of monoclonal antibodies (mAbs) or their fragments (Fab', scFv, ect.) as targeting agents, conjugated at the distal end of PEG-single phospholipid derivatives, has shown to promote the specific delivery to solid tumor cells, by binding with high affinity to tumor-associated internalizing agents, overexpressed on the surface of these cells.

The goal of the present work was to generate a new formulation of *Super Stealth Immunoliposomes* (SSILs) which should be both stable in the bloodstream and able to reach selectively the target by conjugation of PEG dendron-lipids derivatives to the Fab' moiety (fragment, antigen-binding) of a monoclonal antibody. In this case, the selected Fab' derived from

Trastuzumab that targets, with high affinity, the human epidermal growth factor receptor 2 (HER2), which is overexpressed on the surface of certain tumor cells.

Since commercial Doxyl® contains $mPEG_{2kDa}$-DSPE, the initial idea was to formulate super stealth immunoliposomes using as well PEG_{2kDa} dendron-lipids derivatives. Firstly, preliminary *in vitro* and *in vivo* studies were carried out with SSLs prepared with $mPEG_{2kDa}$-$(DSPE)_n$ to assess whether the physico-chemical properties and half-life were improved compared to the corresponding SLs. Small unilamellar vesicles (SUV) with a mean hydrodynamic diameter of about 90 nm were obtained, according to dimensional analysis by dynamic light scattering (DLS). In addition, the suspensions were homogeneous, with a very low polydispersity index (PdI <0.1). *In vitro* stability studies over time evidenced, as expected, that conventional naked liposomes were less stable compare to PEGylated formulations since after two months of storage at 4°C a second population of particles (aggregates) appeared at 4989.6 ± 175.8 nm, accounting for 11% of the total liposomes population. SL, indeed, resulted homogeneous and stable up to 4 months of storage, whereas SSLs started to aggregate after almost 5 months, confirmed by the increased PdI (SL: 5220 ± 143.8 nm [9%]; SSL_2: 5453.6 ± 165.7 nm [8%]; SSL_4: 5324.9 ± 184.2 nm [10%]). The trend proved the stabilizing effect provided by PEG, which prevents aggregation by forming a hydrophilic shield on liposomes surface that provides steric hindrance. The liposomal formulations were then treated with increasing concentration of a detergent, Triton X-100, to evaluate and compare their stability profile. All tested formulations showed a progressive increase in mean diameter, followed by a sudden disruption, with formation of mixed micelles in solution, once the critical concentration of detergent was reached, at which saturation of the liposome bilayer is achieved. Comparing the profiles of the formulations with 5% mol of $mPEG_{2kda}$-$(DSPE)_n$, a negative trend of stability emerged with the increase of the hydrophobic anchor (PEG-DSPE > PEG-$DSPE_2$ > PEG-$DSPE_4$) and the liposome disruption was achieved at 30-40 mM Triton X-100. However, the differences were not relevant, even compared to naked liposomes, therefore the *in vitro* stability in presence of a detergent might not derive exclusively by the effect of a more stable attachment of PEG to the bilayer but also by the presence of hydrogenated soybean phosphatidylcholine (HSPC) which forms packed and stable bilayers. In this case, indeed, when the hydrophobic anchor of PEG is increased liposomes disrupted at slightly lower detergent concentrations, indicating minor stability. In the formulations with 10% mol of polymer a similar stability trend was observed meaning that, above a certain polymer concentration, liposomes are intrinsically unstable and 25 mM Triton X-100 was sufficient to induce vesicles disruption. It should be notice that all these formulations were less stable with respect to conventional liposomes.

Doxorubicin encapsulation was performed by remote loading technique [99-101] and the calculated encapsulation efficiency resulted about 30-40% for both CL, SL and SSL_n. The drug was efficiently entrapped inside the nanocarrier and the leakage was very low since upon entrapment inside the aqueous acidic core, it gets protonated and associates to sulfate divalent anions forming DOX-sulfate aggregates as straight fiber bundles [101, 108, 109]. Therefore, doxorubicin should first dissolve and then diffuse across the bilayer, requiring longer times than the release of a drug in its soluble form. Consequently, the *in vivo* half-life of entrapped doxorubicin is strictly related to that of the nanocarrier, acquiring increased probability to reach the tumor site by enhanced

permeability and retention (EPR) effect. After 2 hours of incubation at 37°C the percentage of DXR release was <0.3% for CL and SL, whereas <2% for super stealth liposomes SSL_2. SSL_4, instead, presented a burst release at the beginning, reaching in few minutes a plateau at which doxorubicin leakage is almost insignificant. The total DXR leakage from SSL_4 resulted <8%.

Pharmacokinetics in female Sprague Dawley rats confirmed that stealth liposomes were the most stable, presenting a prolonged half-life ($t_{½}$~22h) compared to SSL_2 ($t_{½}$~8h) and SSL_4 ($t_{½}$~7h), which were eliminated even faster from the bloodstream than naked liposomes ($t_{½}$ ~10h). Similarly, the clearance rate of SSL_2 was comparable to that of naked liposomes (1.91 µl/h and 1.99 µl/h respectively), whereas a 2-fold increment of the clearance rate was observed for SSL_4 (5.65 µl/h), proving the destabilizing effect of $mPEG_{2kda}$-lipid(s) derivatives. As a result, a lower AUC was detected for SSL_4 compared to the other liposomal formulations. Overall, pharmacokinetic studies evidenced the decreased stability of the formulations upon increment of the hydrophobic anchor of PEG. It was hypothesized that probably less molecules of $mPEG_{2kDa}$-$(DSPE)_n$ could fit in the bilayer due to the increased dimensions of the phospholipid portion, thus reducing the number of PEG chains, as well, protruding from the liposomes surface. This might result in incomplete surface shielding, leaving the nanocarrier vulnerable to opsonization during the circulation in the bloodstream. Previous studies with super stealth liposomes formulated with $mPEG_{5kDa}$-$(DSPE)_n$ showed the opposite trend, with increased stability of the formulated liposomes upon increment of the number of DSPE attached to the polymer. Considering this fact, it is also possible that PEG 2kDa couldn't provide the same "stealth" effect observed with PEG 5kDa. For this reason, it was decided to formulate super stealth immunoliposomes using PEG 5kDa.

PEG_{5kDa} dendron-lipids derivatives were successfully synthesized, starting either from $mPEG_{5kDa}$-NHS or Boc-PEG_{5kDa}-NHS for the following coupling to targeting agent. According to MALDI-TOF mass spectroscopy and ^{1}H NMR spectroscopy characterization, an average of coupling of 2 β-Glutamic acid molecules was achieved in both $mPEG_{5kDa}$-$\beta Glu(\beta Glu)_2$ and Boc-NH-PEG_{5kDa}-$\beta Glu(\beta Glu)_2$. Such degree of derivatization was considered sufficient to consent the coupling of 2 DSPE to both synthesized polymers. An average of 4 and 6 coupled β-Glutamic acid molecules was assessed, instead, for $mPEG_{5kDa}$-$\beta Glu(\beta Glu)_2(\beta Glu)_4$ and Boc-NH-PEG_{5kDa}-$\beta Glu(\beta Glu)_2(\beta Glu)_4$, respectively, allowing in both cases the coupling of 4 DSPE. After DSPE conjugation, several approaches were exploited to purify the final products from unreacted DSPE and other contaminants. The first method, relying on the coupling of free DSPE to lauroyl chloride to selectively remove DSPE upon precipitation in organic solvent, led to Boc deprotection as proved by ^{1}H NMR spectroscopy. The second approach, relied instead on the low solubility of DSPE in acetonitrile to remove the unreacted amount by selective precipitation with respect to PEG dendron-lipids derivative, since PEG should increase the solubility of conjugated phospholipids. After several cycles of purification of the reaction mixtures by precipitation in acetonitrile, a certain amount of PEG was still present in the precipitate as detected by ^{1}H NMR spectroscopy and, in addition, the yield of purified product was modest (about 55%). The difference in solubility between the PEG dendron-lipids derivative and free DSPE was probably not sufficient to provide complete purification by means of selective precipitation in organic solvent, leading to co-precipitation of PEG dendron-lipids derivatives with unreacted DSPE. Hence, purification by flash

column chromatography was attempted with Boc-NH-PEG_{5kDa}-$(DSPE)_4$ but also in this case the yield of purified product was very low (about 32%). Therefore, it was decided to perform a simple purification by dialysis in 20% v/v MeOH since DSPE is moderately soluble in MeOH and ^{1}H NMR spectroscopy characterization of the final purified mPEG_{5kDa}-$(DSPE)_2$ and Boc-NH-PEG_{5kDa}-$(DSPE)_2$ confirmed the effective coupling of 2 DSPE molecules. Purified mPEG_{5kDa}-$(DSPE)_4$ presented, instead, 4 coupled DSPE molecules, whereas the corresponding Boc-PEG dendron resulted conjugated to 5 DSPE molecules. Boc removal from the final purified Boc-NH-PEG_{5kDa}-$(DSPE)_n$ derivatives was confirmed by the disappearance of the relative signal in the ^{1}H NMR spectrum, allowing to free the distal amino group of PEG.

Fab' (Fragment antigen-binding) of Trastuzumab, chosen as targeting agent, was successfully obtained by proteolytic digestion by pepsin, yielding $F(ab')_2$, and further reduction of the disulfide bonds in the hinge region by cysteamine. SDS-PAGE analysis showed that $F(ab')_2$ and Fab' fragments collected by gel filtration chromatography were pure and the molecular weight assessed by MALDI-TOF and ESI-TOF mass spectrometry also corresponded. Two different strategies of Fab' conjugation to Boc-PEG dendron-lipids derivatives were explored, including either the formation of a non-cleavable thioether bond or the creation of a reversible disulphide bond. Even though non-cleavable bonds possess higher blood stability, disulphide bonds are also relatively stable in circulation and are reduced only inside the cells where higher concentration of thiols, such as glutathione, is present. The reversible disulphide bond was introduced by previous modification of PEG with the heterobifunctional cross-linker N-Succinimidyl 3-[2-pyridyldithio]-propionate ester (SPDP) and further reaction with the sulfhydryls group of Fab'. According to ^{1}H NMR spectroscopy 80% of SPDP derivatization was achieved. SDS-PAGE characterization of the purified reaction mixture revealed that the best reaction yields of monoPEGylated Fab' (band at ~75 kDa) were obtained by reacting Fab' with a mixture of 4:1 mol/mol mPEG_{5kDa}-$(DSPE)_2$:PDP-PEG_{5kDa}-$(DSPE)_2$. The formation of the non-cleavable thioether bond, instead, was obtained by derivatization at the primary amino group of PEG with N-(ß-maleimidopropyloxy)succinimide ester (BMPS) and further reaction with the sulfhydryls group of Fab'. ^{1}H NMR spectroscopy revealed that BMPS coupling to PEG amino group in basic conditions (pH 8.0) occurred successfully, but such conditions provoked the hydrolysis of the maleimide group of the cross-linker, toward which Fab' coupling is addressed. SDS-PAGE analysis confirmed the absence of PEGylated derivatives. Maleimide degradation was prevented by lowering the pH to 7.2 (neutral conditions) and 78% of BMPS derivatization was achieved and monoPEGylated Fab'- PEG_{5kDa}-DSPE, Fab'-PEG_{5kDa}-$(DSPE)_2$ and PEG_{5kDa}-$(DSPE)_4$ were successfully obtained and characterized by SDS-PAGE analysis. These ligand-coupled PEG_{5kDa} dendron-lipid(s) derivatives were used in stealth immunoliposomes (SILs) and super stealth immunoliposomes (SSILs) formulation.

SDS-PAGE analysis evidenced that, upon scale-up of Fab' production, excessive reduction of Fab' occurred, resulting in the formation of two bands at ~20-25 kDa, corresponding to the heavy and light chains of Fab'. The presence of other available thiols might become a problem during the PEGylation step, since PEG coupling might occur also at these additional reactive sites, generating undesired by-products. The need for optimization led to extensive analysis of the reaction conditions (Fab' and cysteamine concentrations, buffer, pH, temperature) but also of the

purification process and storage conditions. None of the tested conditions could provide a good yield of Fab' fragment as prevalent species since at the same time a consistent amount of either $F(ab')_2$ (band at about 100 kDa) or Fab' heavy and light chains were obtained. Thus, it was decided to attempt a selective re-oxidation of the free thiols of heavy and light chains, aiming at reforming the disulphide interchain bond. Mild re-oxidation for 3 hours with 10 µM $CuSO_4$ provided the best results, since SDS-PAGE analysis evidenced that the two bands at ~20-25 kDa were almost disappeared with respect to the initial reaction mixture, meaning that the disulphide bond was recreated. At lower concentrations of $CuSO_4$ the disulphide bond between heavy and light chains was still reduced, whereas at higher $CuSO_4$ concentrations undesired higher molecular weight aggregates were originated. Unfortunately, the re-oxidation reaction affected also the vicinal sulfhydryl groups of the hinge region, toward which the PEGylation reaction is addressed, thereby preventing their reactivity and the lack of Fab' PEGylation was evidenced by SDS-PAGE analysis. Therefore, Fab' PEGylation should be necessarily performed prior to re-oxidation. Indeed, Fab' PEGylation followed by bland and selective re-oxidation of the sulfhydryl groups of the heavy and light chains provided the expected monoPEGylated Fab' (band at ~75 kDa) and the diPEGylated Fab' in a smaller percentage (band at ~90 kDa). Furthermore, the intensity of the two bands of Fab' heavy and light chains (~20-25 kDa) and the corresponding PEGylated forms (~37 kDa) was not consistent. The latest achievement regarding $F(ab')_2$ reduction evidenced that the excessive reduction of Fab' fragment is drastically reduced when cysteamine purification is performed in water instead of 150 mM NaCl, 50 mM NaH_2PO_4, 10 mM EDTA pH 5.0 buffer solution. Fab' reactivity towards PEG maleimide group was still preserved and, additionally, only the monoPEGylated species was formed. At the same time, different overnight storage conditions (4°C, –20°C, freezing in liquid N_2) were tested to verify the effect on the integrity of purified Fab' but significant differences were not observed with SDS-PAGE analysis. This evidenced that probably the excessive Fab' reduction was more correlated to pH and salts concentration in the reaction mixture solution rather than storage conditions. During the process of cysteamine purification probably some regions of oversaturation are generated, and this might affect the protein integrity in a certain way.

Different approaches of liposomes preparation were exploited to assess the best formulation conditions to obtain super stealth immunoliposomes. mPEG-lipid(s) derivatives or/and ligand-coupled PEG-lipid(s) derivatives were included in the formulation following the post-insertion technique [68], either into drug-loaded pre-formed naked liposomes or into drug-loaded pre-formed stealth/super stealth liposomes. Prior to post-insertion, dimensional analysis by DLS of the starting liposomal suspensions confirmed that all the prepared formulations were homogeneous, with a very low polydispersity index (PdI < 0.1). The mean diameter of the PEGylated formulations (SL, SSL_2, SSL_4) ranged from about 85 nm to 100 nm, whereas conventional liposomes (CL) measured about 80 nm. The slightly different hydrodynamic volume can be attributed to the absence of PEG-coating on liposomes surface. Doxorubicin encapsulation was performed by remote loading technique and a high encapsulation efficiency was achieved in all formulations: EE% > 95% for conventional (CL) and stealth liposome (SL), whereas EE% > 80% for super stealth formulations (SSL_n). In the 1st post-insertional approach $mPEG_{5kDa}$-$(DSPE)_n$ and Fab'-PEG_{5kDa}-

$(DSPE)_n$ were either transferred separately and sequentially or simultaneously (mixture) on doxorubicin-loaded pre-formed naked liposomes (CL) to obtain super stealth immunoliposomes ($SSIL_n$). Even though $SSIL_2$ were successfully formulated and characterized by DLS and SDS-PAGE analyses and micro-BCA assay for Fab' quantification, this method failed to produce stable $SSIL_4$. As soon as they were purified by gel chromatography, liposomes aggregated upon concentration in 50k MWCO Amicon devices, confirmed by DLS measurement in which is reported the formation of a second population (~20 %) of particles at higher hydrodynamic volume and increased polydispersity index (PdI > 0.15). Otherwise, SDS-PAGE analysis also evidenced after purification the failure of ligand-coupled PEG-lipid derivative transfer into the liposome bilayer because of the lack of bands at ~75 kDa, corresponding to the monoconjugate Fab'-PEG_{5kDa}-DSPE. Further characterization by transmission electron microscopy (TEM) demonstrated that liposomes where characterized by jagged and discontinuous surfaces, justifying the physical instability of the formulated vesicles. Therefore, several hypotheses were formulated, starting from the first assumption that probably a certain initial amount of PEG in the starting formulation might be required to provide a certain degree of stability and rigidity to the bilayer. Accordingly, the increased hydrophobic anchor of PEG might somehow destabilize liposomes bilayer leading to aggregation. SIL were, thus, formulated by simultaneous post-insertion of $mPEG_{5kDa}$-DSPE and Fab'-PEG_{5kDa}-DSPE to assess whether the failure of transfer depended on the formulation approach itself or, perhaps, on the synthesized polymer. SDS-PAGE analysis demonstrated that the transfer of Fab'-PEG_{5kDa}-DSPE also failed, thus it was concluded that this approach was not efficient enough to permit the formulation of SSILs. Post-insertion of PEG dendron-lipids derivatives was, thus, performed on doxorubicin-loaded pre-formed stealth (SL) and super stealth liposomes (SSL_n) to obtain the corresponding super stealth immunoliposomes ($SSIL_n$). Dimensional analysis through DLS measurements on the final liposomal suspension of $SSIL_2$ (102.11 ± 3.68 nm) and SIL (128.23 ± 1.02 nm) evidenced that the homogeneity of the suspensions was maintained (PdI <0.1). SDS-PAGE analysis confirmed that the post-insertion of ligand-coupled PEG-lipid(s) derivatives successfully took place in both formulations and unreacted Fab' and $F(ab')_2$ were purified by gel filtration chromatography. Fab' quantification was performed by micro BCA-assay on the final purified liposomal suspension, resulting in 79.8 µg Fab'/µmol HSPC for SIL and 23.63 µg Fab'/µmol HSPC for $SSIL_2$. Unfortunately, $SSIL_4$ formulation resulted the most challenging also in this post-insertion approach. Following doxorubicin loading and removal through PD-10 desalting columns of non-encapsulated drug, problems of aggregation still occurred, so it was concluded that this instability might depend on $mPEG_{5kDa}$-$DSPE_4$ included in the initial lipid mixture. Thereby, the following *in vitro* and *in vivo* studies were focused on the previous formulations and further investigations might be required to assess if $mPEG_{5kDa}$-$DSPE_4$ needs to be re-synthesized.

Dimensional evaluation by DLS measurement over time of liposomes stored at different temperatures to assess and compare their *in vitro* stability revealed that after about 2 months of incubation at 4°C and 25 °C all tested formulations were still stable and homogeneous (PdI <0.1), whereas at 37°C all liposomal formulations started to aggregate after 14 days of incubation, showing also increased PdI (> 0.1). The trend at 4°C and 25°C confirmed the stabilizing effect

provided by PEG by steric hindrance. Drug release experiments evidenced that in all tested formulations doxorubicin was efficiently entrapped inside the nanocarrier and drug leakage was not observed within the 16 h of incubation. This is attributable to the formation of DOX-sulfate aggregates as straight fiber bundles in the aqueous core of the nanocarrier, visible also in the TEM images of the final liposomal suspensions, as discussed with preliminary liposomal formulations with PEG 2kDa. Preliminary *in vitro* cytotoxicity studies were performed on human breast ductal carcinoma cell line (BT-474) overexpressing HER-2, aiming at evaluating both the effect of the targeted liposomal formulations on cell viability and apoptosis compared to the non-targeted ones. As expected, empty stealth liposomes (SL) proved to be non-cytotoxic at all the tested conditions, since the cell viability was entirely preserved, whereas free doxorubicin resulted the most potent treatment, since the cell viability was reduced to 20-30 % after a 24h-treatment, even at the lowest tested concentration (1 µM). By increasing the concentration (10 µM), the cell viability was reduced of more than 50% by all treatments, except for 1 h treatment followed by a short incubation (72 h) period. Regarding the doxorubicin liposomal formulations, our data clearly demonstrated that a 24 h-treatment with SL-DXR (10 µM DXR) could not reduce the cell viability below 50%, whereas both SIL-DXR and $SSIL_2$-DXR reduced cell viability to about 40% in the same experimental conditions. The increased cytotoxic effect of target liposomal formulations compared to non-targeted liposomes is attributable to the presence of the targeting agent, the Fab' fragment of Trastuzumab, which selectively binds to the HER2 receptors, known to be overexpressed on the surface of BT-474 cells. Thus, after cell washing with fresh complete medium upon treatment completion, only the targeted nanocarriers remain stuck on the cell surface, facilitating the internalization by the cells over time. This effect should be emphasized in short-term treatment and prolonged incubation periods and at lower doxorubicin concentration. In the 24h-treatment at the highest doxorubicin concentration tested (50 µM), indeed, both SL-DXR and SIL-DXR/$SSIL_2$-DXR induced the same reduction of cell viability. The highest potency shown by doxorubicin depends on the small dimensions of the free drug versus the liposomal formulations, allowing for easier diffusion through the cell membrane and access into the intracellular compartments. Statistical analysis conducted on the data obtained at 10 µM DXR, concentration at which the differences between the liposomal formulations were emphasized, ascertained that the cell viability of BT-474 cells treated with SL-DXR, SIL-DXR and $SSIL_2$-DXR was significantly different with respect to cells treated either with free doxorubicin or empty SL. Cell viability became significantly different (*p <0.05) between targeted (SIL-DXR and $SSIL_2$-DXR) and non-targeted (SL-DXR) formulations after 1h treatment followed by long incubation in culture medium (up to 132 h) and the difference between SL-DXR and $SSIL_2$-DXR was further stressed (**p <0.01) after the 12 h treatment. However, the greatest statistical difference among targeted and non-targeted liposomes was observed after the 24 h treatments (****p <0.0001), indicating that a 24 hour-treatment is the best experimental protocol to use for an *in vitro* evaluation of DXR activity. Preliminary IC50 calculation evidenced that, at the tested conditions, all the doxorubicin-loaded liposomal formulations possessed the same potency in inducing cell death, since the IC50 values for SL-DXR, SIL-DXR and $SSIL_2$-DXR were very similar, whereas small differences were observed taking into consideration the efficacy (maximum effect) of each formulation (SL-DXR < SIL-DXR <

$SSIL_2$-DXR). Interestingly, $SSIL_2$-DXR possessed the same efficacy of free doxorubicin. However, it should be stressed that these are preliminary results and further investigations are needed to effectively assess the real potency of each formulation, since the choice of the correct doxorubicin concentration, as well as the time of treatment and incubation, is a fundamental parameter. It would be also interesting to test different cell lines, both HER2+ and HER2- to further confirm the efficacy of this targeted formulations compared to non-targeted liposomes. Evaluation of the effect of the three formulations on apoptotic pathways, which are unfortunately based on a single preliminary experiment, evidenced a sharp increment (30-fold) of the expression levels of Cleaved Caspase 3 (marker of apoptosis) after 6 h treatment with DXR followed by 24 h of incubation with cell medium, with respect to the untreated cells. At the tested conditions, the three liposomal formulations also started to activate the apoptotic pathways, since they led to the overexpression of Cleaved Caspase 3, although the extent of the increase was very low when compared to free DXR. Therefore, better treatment conditions must be assessed.

In vivo pharmacokinetic studies in rats confirmed the increased stability of all liposomal formulation compared to free doxorubicin, proving the stabilizing effect provided by PEG dendron-lipids derivatives over PEG-single phospholipid. $SSIL_2$ showed almost a 4-fold prolonged half-life ($t_{½}$ = 37.80 h) with respect to SL ($t_{½}$ = 10.77 h). Interestingly, also SIL caused a 2-fold prolongation of half-life ($t_{½}$ = 21.43 h) compared to SL, even though the half-lives of these two formulations were expected to be similar, since the presence of the targeting agent shouldn't significantly affect the pharmacokinetic parameters. Further investigation on the pharmacokinetic determinants of SIL might therefore be required. In addition, the clearance rate of $SSIL_2$ (~0.2 ml/h) was reduced with respect to SL (~0.5 ml/h), confirming that the formulation containing PEG dendron-lipids derivatives were eliminated more slowly and, thus, circulate longer in the bloodstream. Concordantly, $SSIL_2$ bioavailability (AUC) and distribution volume (Vd) resulted increased compared to all the other tested formulations. Overall, $SSIL_2$ proved to be endowed with the best *in vivo* behavior. *In vivo* organ toxicity evaluation after single dose administration of 2.5 mg/kg in DXR evidenced that the gene expression of the three pro-inflammatory cytokines interleukin β1 (IL-1β), interleukin 6 (IL-6) and tumor necrosis factor α (TNFα) was increased in rats, especially when treated with SIL-DXR. In particular, this formulation significantly enhanced IL-1β gene expression in liver, spleen and heart tissues, as well as TNFα expression in liver and spleen and IL-6 expression in the spleen. As far as histological analysis is concerned, no significant differences could be observed between SL and SIL, since both these formulations were able to induce dramatic alterations of liver and spleen, organs particularly rich of cells of the reticuloendothelial system (RES). This is probably due to the hepatic and splenic deposition of a fraction of the administered dose of these two formulations, as already suggested by previous studies with similar liposomal formulations [113]. Conversely, $SSIL_2$ caused only limited histological alterations in these organs, further confirming their increased stability and lower uptake in RES organs when compared to SL [2]. The partial discrepancies in histological and molecular findings (i.e. the significant difference between SL and SIL in sustaining an inflammatory state, although being able to cause morphological changes in hepatic and splenic tissues) need to be further investigated. Other studies [114] indicate that assessing gene expression of

inflammatory cytokines could add novel information on the toxicity of nanocarriers, which cannot be obtained by histology and hematology. Future studies will include the evaluation of hematological and biochemical parameters of rats and of circulating inflammatory cytokines, as well as *in vitro* toxicological analysis in order to unravel the mechanism(s) by which SL and SIL formulations induce an increase of inflammatory cytokines in some organs.

Taken together, our data lead to the conclusion that $SSIL_2$ proved to be the safest formulation in terms of cytokines expression and histological analysis of RES organs, and also, as expected, this is the formulation with the best pharmacokinetic profile, representing a promising system to improve conventional cancer therapy by enhancing drug delivery and antitumor efficacy.

8. REFERENCES

[1] H. Maeda, "The enhanced permeability and retention (EPR) effect in tumor vasculature: the key role of tumor-selective macromolecular drug targeting," (in eng), *Adv Enzyme Regul,* vol. 41, pp. 189-207, 2001.

[2] G. Pasut *et al.*, "Polyethylene glycol (PEG)-dendron phospholipids as innovative constructs for the preparation of super stealth liposomes for anticancer therapy," *Journal of Controlled Release,* vol. 199, pp. 106-113, 2015/02/10/ 2015.

[3] "Cancer", in http://www.who.int/news-room/fact-sheets/detail/cancer, ed: World Healt Organization (WHO), 01 February 2018.

[4] Stewart, BW, and W. CP, *World cancer report 2014* Lyon: International Agency for Research on Cancer, 2014.

[5] R. L. Siegel, K. D. Miller, and A. Jemal, "Cancer statistics, 2018," (in eng), *CA Cancer J Clin,* vol. 68, no. 1, pp. 7-30, Jan 2018.

[6] Noone *et al.*, " SEER Cancer Statistics Review, 1975-2015," ed. Bethesda, MD: National Cancer Institute., 2018.

[7] "Cancer", "World Healt Organization (WHO)," ed, 01 February 2018.

[8] K. V. A. A. K. and A. J. C., "Robbins basic pathology," 10th ed, 28th March 2017.

[9] P. Anand *et al.*, "Cancer is a preventable disease that requires major lifestyle changes," (in eng), *Pharm Res,* vol. 25, no. 9, pp. 2097-116, Sep 2008.

[10] G. Danaei, S. Vander Hoorn, A. D. Lopez, C. J. L. Murray, and M. Ezzati, "Causes of cancer in the world: comparative risk assessment of nine behavioural and environmental risk factors," *The Lancet,* vol. 366, no. 9499, pp. 1784-1793, 2005.

[11] P. Vineis and C. P. Wild, "Global cancer patterns: causes and prevention," *The Lancet,* vol. 383, no. 9916, pp. 549-557, 2014.

[12] V. Malhotra and M. C. Perry, "Classical Chemotherapy: Mechanisms, Toxicities and the Therapeutc Window," *Cancer Biology & Therapy,* vol. 2, no. sup1, pp. 1-3, 2003/03/01 2003.

[13] "Targeted cancer therapies," in https://www.cancer.gov/about-cancer/treatment/types/targeted-therapies/targeted-therapies-fact-sheet, ed: National Cancer Institute.

[14] R. Bayat Mokhtari *et al.*, "Combination therapy in combating cancer," (in eng), *Oncotarget,* vol. 8, no. 23, pp. 38022-38043, Jun 6 2017.

[15] P. D. Q. A. T. E. Board, "Breast Cancer Treatment (PDQ(R)): Patient Version," in *PDQ Cancer Information Summaries*Bethesda (MD): National Cancer Institute (US), 2002.

[16] P. D. Q. A. T. E. Board, "Male Breast Cancer Treatment (PDQ(R)): Patient Version," in *PDQ Cancer Information Summaries*Bethesda (MD): National Cancer Institute (US), 2002.

[17] J. V. Lacey, Jr. *et al.*, "Breast cancer epidemiology according to recognized breast cancer risk factors in the Prostate, Lung, Colorectal and Ovarian (PLCO) Cancer Screening Trial Cohort," (in eng), *BMC Cancer,* vol. 9, p. 84, Mar 17 2009.

[18] K. C. Johnson *et al.*, "Active smoking and secondhand smoke increase breast cancer risk: the report of the Canadian Expert Panel on Tobacco Smoke and Breast Cancer Risk (2009)," (in eng), *Tob Control,* vol. 20, no. 1, p. e2, Jan 2011.

[19] M. Gage, D. Wattendorf, and L. R. Henry, "Translational advances regarding hereditary breast cancer syndromes," (in eng), *J Surg Oncol,* vol. 105, no. 5, pp. 444-51, Apr 1 2012.

[20] B. O. Anderson *et al.*, "Guideline implementation for breast healthcare in low-income and middle-income countries: overview of the Breast Health Global Initiative Global Summit 2007," (in eng), *Cancer,* vol. 113, no. 8 Suppl, pp. 2221-43, Oct 15 2008.

[21] P. C. Gotzsche and M. Nielsen, "Screening for breast cancer with mammography," (in eng), *Cochrane Database Syst Rev,* no. 1, p. Cd001877, Jan 19 2011.

[22] R. W. Carlson, C. A. Hudis, and K. I. Pritchard, "Adjuvant endocrine therapy in hormone receptor-positive postmenopausal breast cancer: evolution of NCCN, ASCO, and St Gallen recommendations," (in eng), *J Natl Compr Canc Netw,* vol. 4, no. 10, pp. 971-9, Nov 2006.

[23] M. Jahanzeb, "Adjuvant Trastuzumab Therapy for HER2-Positive Breast Cancer," *Clinical Breast Cancer,* vol. 8, no. 4, pp. 324-333, 2008.

[24] S. K. Singh, S. Singh, J. W. Lillard, and R. Singh, "Drug delivery approaches for breast cancer," *International Journal of Nanomedicine,* vol. 12, pp. 6205-6218, 08/24 2017.

[25] K. K. Jain, "Current status and future prospects of drug delivery systems," (in eng), *Methods Mol Biol,* vol. 1141, pp. 1-56, 2014.

[26] T. M. Allen and P. R. Cullis, "Drug delivery systems: entering the mainstream," (in eng), *Science,* vol. 303, no. 5665, pp. 1818-22, Mar 19 2004.

[27] S. Bamrungsap *et al.*, "Nanotechnology in therapeutics: a focus on nanoparticles as a drug delivery system," (in eng), *Nanomedicine (Lond),* vol. 7, no. 8, pp. 1253-71, Aug 2012.

[28] V. Wagner, A. Dullaart, A. K. Bock, and A. Zweck, "The emerging nanomedicine landscape," (in eng), *Nat Biotechnol,* vol. 24, no. 10, pp. 1211-7, Oct 2006.

[29] M. L. Etheridge, S. A. Campbell, A. G. Erdman, C. L. Haynes, S. M. Wolf, and J. McCullough, "The big picture on nanomedicine: the state of investigational and approved nanomedicine products," (in eng), *Nanomedicine,* vol. 9, no. 1, pp. 1-14, Jan 2013.

[30] D. Peer, J. M. Karp, S. Hong, O. C. Farokhzad, R. Margalit, and R. Langer, "Nanocarriers as an emerging platform for cancer therapy," (in eng), *Nat Nanotechnol,* vol. 2, no. 12, pp. 751-60, Dec 2007.

[31] D. A. Scheinberg, C. H. Villa, F. E. Escorcia, and M. R. McDevitt, "Conscripts of the infinite armada: systemic cancer therapy using nanomaterials," (in eng), *Nat Rev Clin Oncol,* vol. 7, no. 5, pp. 266-76, May 2010.

[32] A. D. Bangham and R. W. Horne, "NEGATIVE STAINING OF PHOSPHOLIPIDS AND THEIR STRUCTURAL MODIFICATION BY SURFACE-ACTIVE AGENTS AS OBSERVED IN THE ELECTRON MICROSCOPE," (in eng), *J Mol Biol,* vol. 8, pp. 660-8, May 1964.

[33] Y. P. Patil and S. Jadhav, "Novel methods for liposome preparation," (in eng), *Chem Phys Lipids,* vol. 177, pp. 8-18, Jan 2014.

[34] C. Huang, D. Quinn, Y. Sadovsky, S. Suresh, and K. J. Hsia, "Formation and size distribution of self-assembled vesicles," *Proceedings of the National Academy of Sciences,* 10.1073/pnas.1702065114 vol. 114, no. 11, p. 2910, 2017.

[35] M. Antonietti and S. Förster, *Vesicles and Liposomes: A Self-Assembly Principle Beyond Lipids*. 2003, pp. 1323-1333.

[36] G. Battaglia and A. Ryan, *The evolution of vesicles from bulk lamellar gels*. 2005, pp. 869-76.

[37] G. Bozzuto and A. Molinari, "Liposomes as nanomedical devices," (in eng), *Int J Nanomedicine,* vol. 10, pp. 975-99, 2015.

[38] A. Akbarzadeh *et al.*, "Liposome: classification, preparation, and applications," (in eng), *Nanoscale Res Lett,* vol. 8, no. 1, p. 102, Feb 22 2013.

[39] J. Fang, H. Nakamura, and H. Maeda, "The EPR effect: Unique features of tumor blood vessels for drug delivery, factors involved, and limitations and augmentation of the effect," (in eng), *Adv Drug Deliv Rev,* vol. 63, no. 3, pp. 136-51, Mar 18 2011.

[40] J. D. Byrne, T. Betancourt, and L. Brannon-Peppas, "Active targeting schemes for nanoparticle systems in cancer therapeutics," (in eng), *Adv Drug Deliv Rev,* vol. 60, no. 15, pp. 1615-26, Dec 14 2008.

[41] M. Grit and D. J. Crommelin, "Chemical stability of liposomes: implications for their physical stability," (in eng), *Chem Phys Lipids,* vol. 64, no. 1-3, pp. 3-18, Sep 1993.

[42] V. Weissig, T. K. Pettinger, and N. Murdock, "Nanopharmaceuticals (part 1): products on the market," *International Journal of Nanomedicine,* vol. 9, pp. 4357-4373, 09/15 2014.

[43] N. Monteiro, A. Martins, R. L. Reis, and N. M. Neves, "Liposomes in tissue engineering and regenerative medicine," *Journal of The Royal Society Interface,* 10.1098/rsif.2014.0459 vol. 11, no. 101, 2014.

[44] J. Senior, G. Gregoriadis, and K. A. Mitropoulos, "Stability and clearance of small unilamellar liposomes studies with normal and lipoprotein-deficient mice," *Biochimica et Biophysica Acta (BBA) - General Subjects,* vol. 760, no. 1, pp. 111-118, 1983/10/04/ 1983.

[45] X. Yan, G. L. Scherphof, and J. A. A. M. Kamps, "Liposome Opsonization," *Journal of Liposome Research,* vol. 15, no. 1-2, pp. 109-139, 2005/01/01 2005.

[46] A. Gabizon and D. Papahadjopoulos, "Liposome formulations with prolonged circulation time in blood and enhanced uptake by tumors," (in eng), *Proc Natl Acad Sci U S A,* vol. 85, no. 18, pp. 6949-53, Sep 1988.

[47] T. M. Allen and P. R. Cullis, "Liposomal drug delivery systems: from concept to clinical applications," (in eng), *Adv Drug Deliv Rev,* vol. 65, no. 1, pp. 36-48, Jan 2013.

[48] V. P. Torchilin, "Recent advances with liposomes as pharmaceutical carriers," (in eng), *Nat Rev Drug Discov,* vol. 4, no. 2, pp. 145-60, Feb 2005.

[49] S. Bibi, E. Lattmann, A. R. Mohammed, and Y. Perrie, "Trigger release liposome systems: local and remote controlled delivery?," (in eng), *J Microencapsul,* vol. 29, no. 3, pp. 262-76, 2012.

[50] K. Knop, R. Hoogenboom, D. Fischer, and U. S. Schubert, "Poly(ethylene glycol) in drug delivery: pros and cons as well as potential alternatives," (in eng), *Angew Chem Int Ed Engl,* vol. 49, no. 36, pp. 6288-308, Aug 23 2010.

[51] S. Dreborg and E. B. Akerblom, "Immunotherapy with monomethoxypolyethylene glycol modified allergens," (in eng), *Crit Rev Ther Drug Carrier Syst,* vol. 6, no. 4, pp. 315-65, 1990.

[52] T. Yamaoka, Y. Tabata, and Y. Ikada, "Distribution and tissue uptake of poly(ethylene glycol) with different molecular weights after intravenous administration to mice," (in eng), *J Pharm Sci,* vol. 83, no. 4, pp. 601-6, Apr 1994.

[53] M. L. Immordino, F. Dosio, and L. Cattel, "Stealth liposomes: review of the basic science, rationale, and clinical applications, existing and potential," (in eng), *Int J Nanomedicine,* vol. 1, no. 3, pp. 297-315, 2006.

[54] C. Allen *et al.*, "Controlling the physical behavior and biological performance of liposome formulations through use of surface grafted poly(ethylene glycol)," (in eng), *Biosci Rep,* vol. 22, no. 2, pp. 225-50, Apr 2002.

[55] S. M. Moghimi *et al.*, "Complement activation cascade triggered by PEG–PL engineered nanomedicines and carbon nanotubes: The challenges ahead," *Journal of Controlled Release,* vol. 146, no. 2, pp. 175-181, 2010/09/01/ 2010.

[56] T. Ishida and H. Kiwada, "Accelerated blood clearance (ABC) phenomenon upon repeated injection of PEGylated liposomes," (in eng), *Int J Pharm,* vol. 354, no. 1-2, pp. 56-62, Apr 16 2008.

[57] M. J. Parr, S. M. Ansell, L. S. Choi, and P. R. Cullis, "Factors influencing the retention and chemical stability of poly(ethylene glycol)-lipid conjugates incorporated into large unilamellar vesicles," (in eng), *Biochim Biophys Acta,* vol. 1195, no. 1, pp. 21-30, Oct 12 1994.

[58] R. E. Kontermann, "Immunoliposomes for cancer therapy," (in eng), *Curr Opin Mol Ther,* vol. 8, no. 1, pp. 39-45, Feb 2006.

[59] T. D. Heath, R. T. Fraley, and D. Papahdjopoulos, "Antibody targeting of liposomes: cell specificity obtained by conjugation of F(ab')2 to vesicle surface," (in eng), *Science,* vol. 210, no. 4469, pp. 539-41, Oct 31 1980.

[60] L. D. Leserman, J. Barbet, F. Kourilsky, and J. N. Weinstein, "Targeting to cells of fluorescent liposomes covalently coupled with monoclonal antibody or protein A," (in eng), *Nature,* vol. 288, no. 5791, pp. 602-4, Dec 11 1980.

[61] V. P. Torchilin, V. S. Goldmacher, and V. N. Smirnov, "Comparative studies on covalent and noncovalent immobilization of protein molecules on the surface of liposomes," *Biochemical and Biophysical Research Communications,* vol. 85, no. 3, pp. 983-990, 1978/12/14/ 1978.

[62] V. P. Torchilin, B. A. Khaw, V. N. Smirnov, and E. Haber, "Preservation of antimyosin antibody activity after covalent coupling to liposomes," *Biochemical and Biophysical Research Communications,* vol. 89, no. 4, pp. 1114-1119, 1979/08/28/ 1979.

[63] V. P. Torchilin, V. G. Omel'yanenko, A. L. Klibanov, A. I. Mikhailov, V. I. Gol'danskii, and V. N. Smirnov, "Incorporation of hydrophilic protein modified with hydrophobic agent into liposome membrane," (in eng), *Biochim Biophys Acta,* vol. 602, no. 3, pp. 511-21, Nov 18 1980.

[64] A. A. Bogdanov, A. L. Klibanov, and V. P. Torchilin, "Immobilization of alpha-chymotrypsin on sucrose stearate--palmitate containing liposomes," (in eng), *FEBS Lett,* vol. 175, no. 1, pp. 178-82, Sep 17 1984.

[65] A. L. Klibanov, K. Maruyama, A. M. Beckerleg, V. P. Torchilin, and L. Huang, "Activity of amphipathic poly(ethylene glycol) 5000 to prolong the circulation time of liposomes depends on the liposome size and is unfavorable for immunoliposome binding to target," (in eng), *Biochim Biophys Acta,* vol. 1062, no. 2, pp. 142-8, Feb 25 1991.

[66] C. B. Hansen, G. Y. Kao, E. H. Moase, S. Zalipsky, and T. M. Allen, "Attachment of antibodies to sterically stabilized liposomes: evaluation, comparison and optimization of coupling procedures," (in eng), *Biochim Biophys Acta,* vol. 1239, no. 2, pp. 133-44, Nov 1 1995.

[67] J. O. Eloy, R. Petrilli, L. N. F. Trevizan, and M. Chorilli, "Immunoliposomes: A review on functionalization strategies and targets for drug delivery," (in eng), *Colloids Surf B Biointerfaces,* vol. 159, pp. 454-467, Nov 1 2017.

[68] T. Ishida, D. L. Iden, and T. M. Allen, "A combinatorial approach to producing sterically stabilized (Stealth) immunoliposomal drugs," (in eng), *FEBS Lett,* vol. 460, no. 1, pp. 129-33, Oct 22 1999.

[69] J. A. Harding, C. M. Engbers, M. S. Newman, N. I. Goldstein, and S. Zalipsky, "Immunogenicity and pharmacokinetic attributes of poly(ethylene glycol)-grafted immunoliposomes," *Biochimica et Biophysica Acta (BBA) - Biomembranes,* vol. 1327, no. 2, pp. 181-192, 1997/07/25/ 1997.

[70] K. Maruyama, N. Takahashi, T. Tagawa, K. Nagaike, and M. Iwatsuru, "Immunoliposomes bearing polyethyleneglycol-coupled Fab' fragment show prolonged circulation time and high extravasation into targeted solid tumors in vivo," (in eng), *FEBS Lett,* vol. 413, no. 1, pp. 177-80, Aug 11 1997.

[71] D. B. Kirpotin *et al.*, "Antibody targeting of long-circulating lipidic nanoparticles does not increase tumor localization but does increase internalization in animal models," (in eng), *Cancer Res,* vol. 66, no. 13, pp. 6732-40, Jul 1 2006.

[72] S. Hosokawa, T. Tagawa, H. Niki, Y. Hirakawa, K. Nohga, and K. Nagaike, "Efficacy of immunoliposomes on cancer models in a cell-surface-antigen-density-dependent manner," (in eng), *Br J Cancer,* vol. 89, no. 8, pp. 1545-51, Oct 20 2003.

[73] W. Wang, S. Singh, D. L. Zeng, K. King, and S. Nema, "Antibody structure, instability, and formulation," (in eng), *J Pharm Sci,* vol. 96, no. 1, pp. 1-26, Jan 2007.

[74] G. Vidarsson, G. Dekkers, and T. Rispens, "IgG Subclasses and Allotypes: From Structure to Effector Functions," *Frontiers in Immunology,* vol. 5, p. 520, 10/2008/31/received10/06/accepted 2014.

[75] J. Harris Reed, J. Shire Steven, and C. Winter, "Commercial manufacturing scale formulation and analytical characterization of therapeutic recombinant antibodies," *Drug Development Research,* vol. 61, no. 3, pp. 137-154, 2004/03/01 2004.

[76] G. Kohler and C. Milstein, "Continuous cultures of fused cells secreting antibody of predefined specificity. 1975," (in eng), *J Immunol,* vol. 174, no. 5, pp. 2453-5, Mar 1 2005.

[77] S. L. Morrison, M. J. Johnson, L. A. Herzenberg, and V. T. Oi, "Chimeric human antibody molecules: mouse antigen-binding domains with human constant region domains," (in eng), *Proc Natl Acad Sci U S A,* vol. 81, no. 21, pp. 6851-5, Nov 1984.

[78] A. S. Manjappa *et al.*, "Antibody derivatization and conjugation strategies: application in preparation of stealth immunoliposome to target chemotherapeutics to tumor," (in eng), *J Control Release,* vol. 150, no. 1, pp. 2-22, Feb 28 2011.

[79] S. M. Andrew and J. A. Titus, "Fragmentation of immunoglobulin G," (in eng), *Curr Protoc Cell Biol,* vol. Chapter 16, p. Unit 16.4, Feb 2003.

[80] V. Crivianu-Gaita, A. Romaschin, and M. Thompson, "High efficiency reduction capability for the formation of Fab antibody fragments from F(ab)2 units," (in eng), *Biochem Biophys Rep,* vol. 2, pp. 23-28, Jul 2015.

[81] W. W. Cheng and T. M. Allen, "The use of single chain Fv as targeting agents for immunoliposomes: an update on immunoliposomal drugs for cancer treatment," *Expert opinion on drug delivery,* vol. 7, no. 4, pp. 461-478, 2010.

[82] P. Sapra, E. H. Moase, J. Ma, and T. M. Allen, "Improved therapeutic responses in a xenograft model of human B lymphoma (Namalwa) for liposomal vincristine versus liposomal doxorubicin targeted via anti-CD19 IgG2a or Fab' fragments," (in eng), *Clin Cancer Res,* vol. 10, no. 3, pp. 1100-11, Feb 1 2004.

[83] F. Pastorino *et al.*, "Doxorubicin-loaded Fab' fragments of anti-disialoganglioside immunoliposomes selectively inhibit the growth and dissemination of human neuroblastoma in nude mice," (in eng), *Cancer Res,* vol. 63, no. 1, pp. 86-92, Jan 1 2003.

[84] P. Carter *et al.*, *Humanization of an anti-p185HER2 antibody for human cancer therapy*. 1992, pp. 4285-9.

[85] P. Holliger and P. J. Hudson, "Engineered antibody fragments and the rise of single domains," (in eng), *Nat Biotechnol,* vol. 23, no. 9, pp. 1126-36, Sep 2005.

[86] S. Maximiano, P. Magalhaes, M. P. Guerreiro, and M. Morgado, "Trastuzumab in the Treatment of Breast Cancer," (in eng), *BioDrugs,* vol. 30, no. 2, pp. 75-86, Apr 2016.

[87] Y. Yarden, "The EGFR family and its ligands in human cancer. signalling mechanisms and therapeutic opportunities," (in eng), *Eur J Cancer,* vol. 37 Suppl 4, pp. S3-8, Sep 2001.

[88] T. Khoury *et al.*, "ERBB2 juxtamembrane domain (trastuzumab binding site) gene mutation is a rare event in invasive breast cancers overexpressing the ERBB2 gene," (in eng), *Mod Pathol,* vol. 24, no. 8, pp. 1055-9, Aug 2011.

[89] C. A. Hudis, "Trastuzumab--mechanism of action and use in clinical practice," (in eng), *N Engl J Med,* vol. 357, no. 1, pp. 39-51, Jul 5 2007.

[90] P. De, M. Hasmann, and B. Leyland-Jones, "Molecular determinants of trastuzumab efficacy: What is their clinical relevance?," (in eng), *Cancer Treat Rev,* vol. 39, no. 8, pp. 925-34, Dec 2013.

[91] R. Thirumaran, G. C. Prendergast, and P. B. Gilman, "Chapter 7 - Cytotoxic Chemotherapy in Clinical Treatment of Cancer," in *Cancer Immunotherapy*, G. C. Prendergast and E. M. Jaffee, Eds. Burlington: Academic Press, 2007, pp. 101-116.

[92] O. Tacar, P. Sriamornsak, and C. R. Dass, "Doxorubicin: an update on anticancer molecular action, toxicity and novel drug delivery systems," (in eng), *J Pharm Pharmacol,* vol. 65, no. 2, pp. 157-70, Feb 2013.

[93] Y. L. Lyu and L. F. Liu, "13 - Doxorubicin Cardiotoxicity Revisited: ROS Versus Top2," in *Recent Advances in Cancer Research and Therapy*, X.-Y. Liu, S. Pestka, and Y.-F. Shi, Eds. Oxford: Elsevier, 2012, pp. 351-369.

[94] Y. Fan and Q. Zhang, "Development of liposomal formulations: From concept to clinical investigations," *Asian Journal of Pharmaceutical Sciences,* vol. 8, no. 2, pp. 81-87, 2013/04/01/ 2013.

[95] "Liposome-encapsulated doxorubicin compared with conventional doxorubicin in a randomized multicenter trial as first-line therapy of metastatic breast carcinoma," *Cancer,* vol. 94, no. 1, pp. 25-36, 2002/01/01 2001.

[96] M. E. R. O'Brien *et al.*, "Reduced cardiotoxicity and comparable efficacy in a phase III trial of pegylated liposomal doxorubicin HCl (CAELYX™/Doxil®) versus conventional doxorubicin for first-line treatment of metastatic breast cancer," *Annals of Oncology,* vol. 15, no. 3, pp. 440-449, 2004.

[97] U. Bulbake, S. Doppalapudi, N. Kommineni, and W. Khan, "Liposomal Formulations in Clinical Use: An Updated Review," (in eng), *Pharmaceutics,* vol. 9, no. 2, Mar 27 2017.

[98] J. C. Stewart, "Colorimetric determination of phospholipids with ammonium ferrothiocyanate," (in eng), *Anal Biochem,* vol. 104, no. 1, pp. 10-4, May 1 1980.

[99] Y. Barenholz, "Doxil® — The first FDA-approved nano-drug: Lessons learned," *Journal of Controlled Release,* vol. 160, no. 2, pp. 117-134, 2012/06/10/ 2012.

[100] A. Fritze, F. Hens, A. Kimpfler, R. Schubert, and R. Peschka-Süss, "Remote loading of doxorubicin into liposomes driven by a transmembrane phosphate gradient," *Biochimica et Biophysica Acta (BBA) - Biomembranes,* vol. 1758, no. 10, pp. 1633-1640, 2006/10/01/ 2006.

[101] G. Haran, R. Cohen, L. K. Bar, and Y. Barenholz, "Transmembrane ammonium sulfate gradients in liposomes produce efficient and stable entrapment of amphipathic weak bases," (in eng), *Biochim Biophys Acta,* vol. 1151, no. 2, pp. 201-15, Sep 19 1993.

[102] S. L. Snyder and P. Z. Sobocinski, "An improved 2,4,6-trinitrobenzenesulfonic acid method for the determination of amines," (in eng), *Anal Biochem,* vol. 64, no. 1, pp. 284-8, Mar 1975.

[103] S. Zalipsky, E. Brandeis, M. S. Newman, and M. C. Woodle, "Long circulating, cationic liposomes containing amino-PEG-phosphatidylethanolamine," *FEBS Letters,* vol. 353, no. 1, pp. 71-74, 1994/10/10/ 1994.

[104] U. K. Laemmli, "Cleavage of Structural Proteins during the Assembly of the Head of Bacteriophage T4," *Nature,* vol. 227, p. 680, 08/15/online 1970.

[105] K. Shimura and B. L. Karger, "Affinity probe capillary electrophoresis: analysis of recombinant human growth hormone with a fluorescent labeled antibody fragment," (in eng), *Anal Chem,* vol. 66, no. 1, pp. 9-15, Jan 1 1994.

[106] J. R. Junutula *et al.*, "Site-specific conjugation of a cytotoxic drug to an antibody improves the therapeutic index," (in eng), *Nat Biotechnol,* vol. 26, no. 8, pp. 925-32, Aug 2008.

[107] S. Fleige, V. Walf, S. Huch, C. Prgomet, J. Sehm, and M. W. Pfaffl, "Comparison of relative mRNA quantification models and the impact of RNA integrity in quantitative real-time RT-PCR," (in eng), *Biotechnol Lett,* vol. 28, no. 19, pp. 1601-13, Oct 2006.

[108] D. D. Lasic, P. M. Frederik, M. C. Stuart, Y. Barenholz, and T. J. McIntosh, "Gelation of liposome interior. A novel method for drug encapsulation," (in eng), *FEBS Lett,* vol. 312, no. 2-3, pp. 255-8, Nov 9 1992.

[109] X. Li *et al.*, "Doxorubicin physical state in solution and inside liposomes loaded via a pH gradient," (in eng), *Biochim Biophys Acta,* vol. 1415, no. 1, pp. 23-40, Dec 9 1998.

[110] W. Li, H. Chung, C. Daeffler, J. A. Johnson, and R. H. Grubbs, "Application of 1H DOSY for Facile Measurement of Polymer Molecular Weights," *Macromolecules,* vol. 45, no. 24, pp. 9595-9603, 2012/12/21 2012.

[111] F. Yang, L. Song, H. Wang, J. Wang, Z. Xu, and N. Xing, "Combination of Quercetin and 2-Methoxyestradiol Enhances Inhibition of Human Prostate Cancer LNCaP and PC-3 Cells Xenograft Tumor Growth," (in eng), *PLoS One,* vol. 10, no. 5, p. e0128277, 2015.

[112] W. Yang *et al.*, "Genomics of Drug Sensitivity in Cancer (GDSC): a resource for therapeutic biomarker discovery in cancer cells," *Nucleic Acids Research,* vol. 41, no. D1, pp. D955-D961, 2013.

[113] M. L. Schipper *et al.*, "Particle Size, Surface Coating, and PEGylation Influence the Biodistribution of Quantum Dots in Living Mice," *Small (Weinheim an der Bergstrasse, Germany),* vol. 5, no. 1, pp. 126-134, 2009.

[114] K. B. Knudsen *et al.*, "In vivo toxicity of cationic micelles and liposomes," (in eng), *Nanomedicine,* vol. 11, no. 2, pp. 467-77, Feb 2015.